



Characterization of the role of lpaA on the cytoskeletal anchorage of *Shigella flexneri*

Daniel-Isui Aguilar-Salvador

► To cite this version:

Daniel-Isui Aguilar-Salvador. Characterization of the role of lpaA on the cytoskeletal anchorage of *Shigella flexneri*. Microbiology and Parasitology. Université Paris Cité, 2019. English. NNT : 2019UNIP7144 . tel-03127237

HAL Id: tel-03127237

<https://theses.hal.science/tel-03127237>

Submitted on 1 Feb 2021

HAL is a multi-disciplinary open access archive for the deposit and dissemination of scientific research documents, whether they are published or not. The documents may come from teaching and research institutions in France or abroad, or from public or private research centers.

L'archive ouverte pluridisciplinaire **HAL**, est destinée au dépôt et à la diffusion de documents scientifiques de niveau recherche, publiés ou non, émanant des établissements d'enseignement et de recherche français ou étrangers, des laboratoires publics ou privés.

Université de Paris

Ecole doctorale BioSPC ED562

Unité de Communications Intercellulaires et Infections

Microbiennes.

CIRB. CNRS UMR 7241/ INSERM 1050

Characterization of the role of IpaA on the cytoskeletal anchorage of *Shigella flexneri*

Par Daniel Isui AGUILAR SALVADOR

Thèse de doctorat de Microbiologie Procaryote et Eucaryote

Dirigée par Guy TRAN VAN NHIEU

Présentée et soutenue publiquement le 07/11/2019

Devant un jury composé de :

Agathe SUBTIL, DR2/CNRS, Institut Pasteur, Rapportrice

Christophe LE CLAINCHE, DR2/CNRS, Institut de Biologie Intégrative de la Cellule, Rapporteur

Sandrine BOURDOULOUS, DR2/CNRS, Institut Cochin, Examinatrice, Présidente

Fabrizia STAVRU, CR/CNRS, Institut Pasteur, Examinatrice

Guy TRAN VAN NHIEU, DR2 / INSERM, Collège de France, Directeur de thèse



Except where otherwise noted, this is work licensed under
<https://creativecommons.org/licenses/by-nc-nd/3.0/fr/>

Titre :

Caractérisation du rôle de la protéine IpaA sur l'ancrage cytosquelettique de *Shigella flexneri*

Résumé :

Shigella envahit les cellules de l'épithélium intestinal en injectant des protéines effectrices via un système de sécrétion de type III (T3SS). L'effecteur de type III IpaA se lie à la taline et à la vinculine par l'intermédiaire de trois sites de liaison à la vinculine (VBS), favorisant ainsi l'ancrage cytosquelettique ainsi que l'internalisation des bactéries. Contrairement à d'autres bactéries invasives, *Shigella* ne montre pas d'activité de liaison cellulaire constitutive mais déclenche une adhésion transitoire par l'activation de T3SS. IpaA VBS3 s'est avéré être structurellement analogue à l'hélice de la taline H5, qui, avec H1-H4, forme le faisceau de taline R1. L'analyse fonctionnelle identifiée IpaA VBS3 est nécessaire au recrutement de la taline dans les foyers d'entrée de *Shigella* et à la formation d'adhérences naissantes et de filopodes. IpaA VBS3 stimule également la capture filopodiale des bactéries et stabilise les adhérences cellulaires dans les cellules envahies. D'autre part, les modèles structurels des interactions IpaA VBS / Vinculin indiquent un nouveau mode d'activation de la vinculine, impliquant des changements conformationnels dans le domaine de la tête de la vinculine, conduisant à la trimérisation et à la stabilisation des adhérences focales. IpaA a également été observé comme étant injecté par une bactérie "s'embrassant et courant", facilitant des événements supplémentaires de liaison bactérienne et d'invasion. Cet amorçage dépendant d'IpaA dépendait d'IpaA VBS3 mais pas d'IpaA VBS1-2. Une fois injecté, IpaA, forme des grappes apposées sur le côté apical de la cellule pour induire une grappe d'intégrines. Globalement, les résultats indiquent que l'IpaA provoque des modifications générales des propriétés adhésives des cellules et favorise un mécanisme coopératif d'invasion de *Shigella*.

Mots clefs :

Shigella, Sécrétion Type III, invasion, IpaA, vinculine, taline

Title :

Characterization of the role of IpaA on the cytoskeletal anchorage of *Shigella flexneri*

Abstract :

Shigella invades cells of the intestinal epithelium by injecting effector proteins through a Type III Secretion System (T3SS). The type III effector IpaA binds to talin and vinculin through three Vinculin Binding Sites (VBSs), promoting cytoskeletal anchorage to promote bacterial internalization. As opposed to other invasive bacteria, *Shigella* does not show constitutive cell binding activity but triggers transient adhesion through T3SS activation. IpaA VBS3 was found to be structurally analogous to talin H5 helix, which, together with H1-H4, forms the R1 talin bundle. Functional analysis identified IpaA VBS3 is necessary for talin recruitment to *Shigella* entry foci and formation of nascent adhesions and filopodia. IpaA VBS3 also stimulates filopodial capture of bacteria and stabilizes cell adhesions in invaded cells. On the other hand, structural models of IpaA VBSs/Vinculin interactions indicate a novel mode of vinculin activation, involving conformational changes in vinculin head domain that leads to trimerization and stabilization of focal adhesions. IpaA was also observed to be injected by "kissing-and-running" bacteria, facilitating additional bacterial binding and invasion events. This IpaA-dependent priming was dependent on IpaA VBS3 but not on IpaA VBS1-2. Injected IpaA was observed to form clusters apposed to the cell apical side and to induce integrin clustering. Overall, the results indicate that IpaA triggers general changes in cell adhesive properties and promotes a cooperative mechanism of *Shigella* invasion.

Keywords :

Shigella, Type III secretion, invasion, IpaA, vinculin, talin

Qui zuuyu' naa gate'	No me verás morir	You will not see me die	Tu ne me verras pas mourir
Qui zuuyu' naa gate'	No me verás morir	You will not see me die	Tu ne me verras pas mourir
qui zanda gusiaandu' naa	no podrás olvidarme	you will not forget me	tu ne pourras pas m'oublier
Naa nga jñou'	Soy tu madre	I am your mother	je suis ta mère
bixhozelu'	tu padre	your father	ton père
diidxa' yooxho' bixhozegolalu'	la vieja palabra de tu abuelo	the word from your grndfather	l'ancien mot de votre grand-père
guira' ni ma bisiaa ca dxi ca lii	la costumbre de los tiempos	the habitude of times	la coutume des temps
nisa ruuna ti guesa ma stale dxi bibani	la lágrima que brota de un anciano sauce	the tear welling from an old willow	La larme qui jaillit d'un vieux saule
ti na' yaga ni jmá nabana'	la más triste de las ramas	the saddest branch	la plus triste des branches
biniti lade bandaga	perdida entre las hojas	lost among the leaves	perdue entre les feuilles
Qui zuuyu' naa gate'	No me verás morir	You will not see me die	Tu ne me verras pas mourir
ti naa nga	porque soy	because I am	parce que je suis
ti dxumi su	un cesto de carrizo	a reed-woven basket	un panier de roseaux
ra canibi ru' na'	donde aún se mueven las tenazas	where the old spiny lobster	où les pincas bougent encore
bixhoze bendabua'	del papá del camarón	still waves his pincers	du papa crevette
benda ni gudó diuxi	el pescado que Dios comió	the fish eaten by God	le poisson que Dieu a mangé
beenda ni bichá ruua ti lexu	la serpiente que devoró un conejo	the snake that gulped a rabbit	le serpent qui a dévoré un lapin
lexu ni gudxite gueu'	el conejo que siempre se burló del coyote	the rabbit that always teased the coyote	le lapin qui s'est toujours moqué du coyote
gueu' ni gubi lidxi bizu	el coyote que tragó un panal de avispa	the coyote that swallowed a wasps' nest	le coyote qui a avalé un nid de guêpes
dxia bizu ni rindani lu xidxe'	la miel que brota de mis senos	the honey that wells from my breasts	le miel qui jaillit de mes seins
xquipilu' nga naa	tu ombligo soy	your navel I am	ton nombril je suis
ne qui zuuyu' gate'	y no me verás morir	and you will not see me die	et tu ne me verras pas mourir
Neca zacuxhou' ma guirá tu zé	Aunque creas que todos se han marchado	You may think everyone has gone away	Même si tu penses que tout le monde est parti
qui zuuyu naa gate'	no me verás morir	but you will not see me die	tu ne me verras pas mourir
ziuu ti xuba'	Habrà una semilla	There will be a seed	Il y aura une graine
ga'chi' lade gui'xhi' nuu lu neza	escondida entre los matorrales del camino	hidden in the scrub by the path	caché dans les fourrés de la route
ndaani' guidxi di' zabigueta'	que a esta tierra ha de volver	that to this land will return	que sur cette terre reviendra
ne laa gusindani guendanabani	y sembrará el futuro	and will seed the future	et semera l'avenir
ne laa gaca gueta xquendanu	y será alimento de nuestras almas	and will feed our souls	et nourrira nos âmes
ne laa gusibani stiidxanu	y renacerá nuestra palabra	and our stories will be reborn	et notre parole renaîtra
ne qui zuuyu' naa gate'	y no me verás morir	and you will not see me die	et tu ne me verras pas mourir
ti zăcanu nadipa'	porque seremos fuertes	because we will stay strong	parce que nous serons forts
ti zabaninu xadxi	porque seremos siempre vivos	because we will always be alive	parce que nous serons toujours vivants
ti riuunda stinu qui zati	porque nuestro canto será eterno	because our song will be eternal	parce que notre chanson sera éternelle
ti zăcanu laanu ne lii	porque seremos nosotros y tu	because we will be us and you	parce qu'on sera nous et vous
ne ca xiiñi' xiiñinu	y los hijos de nuestros hijos	and our children's children	et les enfants de nos enfants
ne xu guidxilayú	y el temblor de la tierra	and the earth's quaking	et le tremblement de terre
ni gunibidxacha nisado'	que sacudirá el mar	that will shake the sea	qui secouera la mer
ne zăcanu stale lădxidó'	y seremos muchos corazones	and we will be many hearts	et nous serons beaucoup de coeurs
naaze dxiichi' xquenda binnizá	aferrados a la esencia de los <i>binnizá</i>	anchored to the essence of the <i>binnizá</i>	accrochés à l'essence des <i>binnizá</i>
ne qui zuuyu' gate'	y no me verás morir	and you will not see me die	et tu ne me verras pas mourir
qui zuuyu' naa gate'	no me verás morir	you will not see me die	tu ne me verras pas mourir
qui zuuyudio'	no me verás	you will not see me	tu ne me verras pas
naa gate'	morir	die	mourir

Irma Pineda

List of abbreviations

PAI	Pathogenicity Island
LPS	Lipopolysaccharide
ORF	Open Reading Frame
T3SS	Type III Secretion System
T3SA	type III Secretion Apparatus
ADF	Actin Depolymerization Factor
ABD	Actin Binding Domain
VBS	Vinculin Binding Site
VD	Vinculin Domain
Vt	Vinculin Tail Domain
ROCK	Rho Associated Protein Kinase
FAK	Focal Adhesion Kinase
EPEC	Enteropathogenic E. coli
EHEC	Enterohemorrhagic E. coli
GEF	Guanin Exchange Factor
SEC/MALS	Size exclusion chromatography-Multi Angle Light Scattering

List of Figures

FIGURE 1. SHIGELLA DIARRHEA MORTALITY RATE.....	10
FIGURE 2. SHIGELLA WHOLE-GENOME PHYLOGENETIC TREE	14
FIGURE 3. COMPARATIVE MAP OF THE SHIGELLA VIRULENCE PLASMID	17
FIGURE 4. STRUCTURE OF THE INTESTINAL MUCOSA.....	19
FIGURE 5. STRUCTURE OF THE SHIGELLA T3SS	22
FIGURE 6. REGULATION OF THE SECOND WAVE OF EFFECTORS	26
FIGURE 7. DYNAMICS OF ACTIN FILAMENTS.....	29
FIGURE 8. MYOSIN II AND A-ACTININ IN ACTIN FILAMENT CONTRACTION	31
FIGURE 9. INTEGRINS LIGANDS AND INTRACELLULAR DYNAMICS	33
FIGURE 10. MATURATION OF ADHESION STRUCTURES.....	35
FIGURE 11. MODEL OF THE MOLECULAR CLUTCH HYPOTHESIS	36
FIGURE 12. STRUCTURAL MODEL OF TALIN	37
FIGURE 13. VINCULIN STRUCTURE AND ACTIVATION	39
FIGURE 14. FOCAL ADHESION ORGANIZATION.....	40
FIGURE 15. CATCH-BOND MECHANISM SCHEME	44
FIGURE 16. PEDESTALS FORMED BY EPEC AND EHEC	46
FIGURE 17. FILOPODIAL CAPTURE	48
FIGURE 18. IPAA VINCULIN BINDING SITES.....	51
FIGURE 19. MODEL OF IPAA VBSS INTERACTION WITH FOCAL ADHESION PROTEINS	151
FIGURE 20. MODEL FOR IPAA ACTION ON TALIN AND VINCULIN	155

List of Tables

TABLE 1. SHIGELLA EFFECTOR PROTEINS	23
TABLE 2. PILI/FIMBRIAE OF PATHOGENIC GRAM-NEGATIVE BACTERIA	41
TABLE 3. NON-EXHAUSTIVE LIST OF ADHESION FACTORS AND HOST RECEPTORS OF PATHOGENIC BACTERIA ..	42

Table of contents

TABLE OF CONTENTS	7
1 INTRODUCTION	9
1.1 BACILLARY DYSENTERY	9
1.1.1 CLINICAL MANIFESTATIONS, COMPLICATIONS AND TRANSMISSION	9
1.1.2 EPIDEMIOLOGY	10
1.2 SHIGELLA SPP.	11
1.2.1 SHIGELLA CLASSIFICATION	11
1.2.2 EVOLUTION OF SHIGELLA	12
1.2.3 SHIGELLA VIRULENCE PLASMID	15
1.3 OVERVIEW OF SHIGELLA INVASION	18
1.3.1 ANATOMY OF THE INTESTINAL EPITHELIUM	18
1.3.2 SHIGELLA INVASION ROUTES OF THE INTESTINAL EPITHELIUM	20
1.4 THE SHIGELLA TYPE III SECRETION SYSTEM	21
1.4.1 THE SHIGELLA T3SS STRUCTURE	21
1.4.2 SHIGELLA T3SS EFFECTOR PROTEINS	22
1.5 MAIN PLAYERS OF THE CYTOSKELETON	26
1.5.1 ACTIN MONOMERS	26
1.5.2 ACTIN SEQUESTERING PROTEINS	27
1.5.3 SEVERING PROTEINS	27
1.5.4 ACTIN NUCLEATORS	30
1.5.5 CAPPING PROTEINS	30
1.5.6 CROSS-LINKING PROTEINS	31
1.6 ADHESION STRUCTURES	32
1.6.1 INTEGRINS	32
1.6.2 ADHESION FORMATION AND MATURATION	34
1.6.3 TALIN AND VINCULIN MOLECULAR CLUTCH	35
1.6.4 FORCE GENERATION AND MATURATION	39
1.7 ACTIN CYTOSKELETON REORGANIZATION BY BACTERIAL PATHOGENS	40
1.7.1 BACTERIAL ADHESION AND INTERNALIZATION STRATEGIES	41
1.7.2 E. COLI FIMH CATCH-BOND ADHESION	43
1.7.3 ZIPPERING: LISTERIA MONOCYTOGENES INVASION MECHANISM	44
1.7.4 ATTACHING AND EFFACING LESION PATHOGENS	45
1.7.5 SALMONELLA “TRIGGERED” INTERNALIZATION	46
1.7.6 SHIGELLA INVASION AND CYTOSKELETON REMODELLING	47
1.8 IPAA	49
1.8.1 IPAA VINCULIN BINDING SITES	50
2 RATIONALE OF THE PHD PROJECT	52
3 ARTICLE 1	54
3.1 OVERVIEW	54
4 ARTICLE 2	75

4.1 OVERVIEW	75
5 ARTICLE 3	124
5.1 OVERVIEW	124
6 DISCUSSION	146
6.1 IPAA VBS3 BINDING TO TALIN	147
6.2 VINCULIN SUPRA-ACTIVATION: A NOVEL INTERACTION MODE	149
6.3 FUNCTIONAL IMPLICATIONS OF VINCULIN SUPRA-ACTIVATION ON CELL ADHESION	152
6.4 IPAA VBSs ROLE DURING <i>SHIGELLA</i> INVASION	153
6.5 GENERAL CONCLUSION	155
7 REFERENCES	158

1 Introduction

1.1 Bacillary dysentery

1.1.1 Clinical manifestations, complications and transmission

Dysentery is a disease characterized by fever, abdominal pain, cramps, and diarrhea with bloody and mucoid stools. This disease is commonly caused by *Entamoeba histolytica* or by *Shigella* species, which are respectively termed amoebic dysentery and bacillary dysentery (“WHO | Dysentery” 2010). Although both diseases cause a similar set of symptoms, the underlying mechanisms are different.

Specifically, the symptoms caused by *Shigella* spp. reflect the pathogen ability to invade and multiply inside the colonic mucosa, triggering an intense inflammatory reaction, which eventually leads to destruction of infected tissue and is rarely followed by a systemic infection. The first symptoms are usually fever, headache, malaise, anorexia and vomiting, followed by watery diarrhea. In healthy individuals the symptoms recede in a few days. However, in some individuals, infection can lead to excretion of stools containing blood and mucus with abdominal cramps and tenesmus and in young infants can also lead to necrotising enterocolitis. In rare cases it can lead to meningitis, osteomyelitis, arthritis, splenic abscess, rectal prolapse, intestinal obstruction, toxic megacolon and perforation (Kotloff et al. 2018).

Humans are the only known natural host for *Shigella*, which is predominantly transmitted by faecal-oral contact favored by inadequate sanitation and hygiene. In rare cases, transmission has also been correlated with houseflies presence (Frag et al. 2013). In a study carried out in volunteers from a correctional facility, it was determined that around 100 colony-forming units suffice to produce a symptomatic infection (DuPont et al. 1989). Case reports of asymptomatic long-term carriage exist, but the prevalence at the population level is unknown (Levine et al. 1973)

1.1.2 Epidemiology

It is estimated that *Shigella* causes 269 million cases yearly worldwide, leading to ~210 thousand deaths. The global distribution of *Shigella* is strongly correlated with income levels, being the lower-income regions, such as sub-saharan Africa and south Asia (Figure 1), where incidence and mortality rates are higher (Khalil et al. 2018).

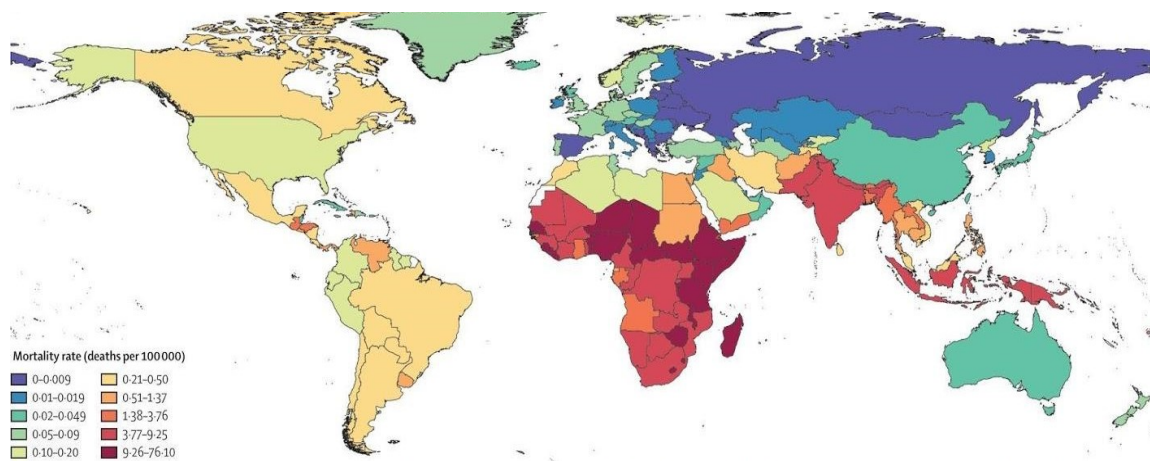


Figure 1. *Shigella* diarrhea mortality rate per 100 000 people in 2016 (Modified from (Khalil et al. 2018)).

In particular, infants under five years are highly vulnerable. In this population the incidence is estimated in 116 episodes per 1000 child-years. Elderly people are also at high risk of mortality. *Shigella* is the most common cause of diarrhea in adults older than 70 years, leading to 74 thousand deaths (Khalil et al. 2018). In high-income countries, *Shigella* is associated with travellers who visit regions where the incidence is high. It is estimated that 2-9% of the cases of traveller's diarrhea is due to these bacterial species (Shah, Ramsey, and DuPont 2009). Other relevant and

recent outbreaks in Europe have occurred among refugees from the Middle East living under poor sanitation conditions, where antibiotic-resistant strains of *Shigella* have been detected (Georgakopoulou et al. 2016).

1.2 *Shigella* spp.

Shigella discovery is attributed to Kiyoshi Shiga in 1898, who cultured the bacillus from a patient during an epidemic in Japan (Shiga 1901). Originally named *Bacillus dysenteriae*, the strain was subsequently called *Shigella dysenteriae* serotype 1. Discovered soon after *E. coli*, *Shigella* was placed in a different genus although it can also be considered as an *E. coli* sub-species. Absence of flagellum-based motility and lack of lactose fermentation were the main diagnostic criteria for its identification.

A different strain of *Shigella* was isolated by Simon Flexner, which is now known as *Shigella flexneri*. Yet another group was observed by Boyd, who undertook a project that resulted in several thousands cultures from different cases with different antiserum agglutination properties. Based on this collection he proposed a classification that forms the backbone of the current classification system (Boyd 1938), further improved by Ewing (Ewing 1949).

1.2.1 *Shigella* classification

Shigella is a Gram negative, non-motile, non-pigmented and facultatively anaerobic bacteria. It belongs to the *Enterobacteraceae* family and it has a morphology of straight rods of 1-3 x 0.7-1 µm (Strockbine and Maurelli 2015).

The existing classification of the *Shigella* genus has mainly historical reasons, and it has been kept as a separate genus from *E. coli* mainly due to the seriousness of the disease. There are 4 validated species within the *Shigella* genus, and within each species several serotypes have been classified: *S. dysenteriae* (with 15 serotypes), *S. boydii* (19 serotypes), *S. flexneri* (14 serotypes and subserotypes) and *S. sonnei* (Strockbine and Maurelli 2015). *S. dysenteriae* and *S. flexneri* are the main cause of bacillary dysentery epidemics.

The division of each species into serotypes is based on the lipopolysaccharide O antigen. *S. flexneri* serotypes share a common basic lipopolysaccharide structure and differ by the addition of glucosyl and/or O-acetyl residues (Simmons and Romanowska 1987). *S. boydii* and *S. dysenteriae* have well differentiated serotypes from other *Shigella* species, although they are highly related to *E. coli* O antigen (P. R. Edwards and Ewing 1986). *S. sonnei* has only one serotype, which reflects its clonal origin and low variation level (Karaolis, Lan, and Reeves 1994)

1.2.2 Evolution of *Shigella*

Despite being categorized as a separate genus, current evidence indicates that *Shigella* species are biotypes or clones of *Escherichia coli*. Early studies using Multi Locus Enzyme Electrophoresis to compare 1600 *E. coli* strains with 123 strains of the four species of *Shigella* clustered into *E. coli* groups, rather than clustering in a separate group (Ochman et al. 1983). Phylogenetic analysis of the 16S ribosomal DNA also placed *Shigella* species and *E. coli* in the same phylogenetic group (Cilia, Lafay, and Christen 1996).

Analysis of polymorphisms in housekeeping genes of *Shigella* and *E. coli* also suggests that different *Shigella* species are the result of convergent evolution rather than a single speciation event, with up to 8 separate divergence events happening within a time frame of 35,000 to 270,000 years from the present (Pupo, Lan, and Reeves 2000), although more recent analysis indicate that the number of divergence event could be as low as four (Sahl et al. 2015). Convergent evolution is further stressed by the fact that phenotypic characteristics such as lack of motility and lactose fermentation have different genetic basis in different strains across the genus (Pupo, Lan, and Reeves 2000; Al Mamun, Tominaga, and Enomoto 1997; Ito et al. 1991). Also, the high diversity of the O antigen come from different mechanisms of acquisition; *S. flexneri* variations come mostly from phage-encoded enzymes (Simmons and Romanowska 1987), while several other unique antigens are identical to other *E. coli* strains (P. R. Edwards and Ewing 1986). *S. sonnei* O antigen synthesis gene is encoded on a plasmid, presumably acquired by lateral transfer (Kopecko, Washington, and Formal 1980). Furthermore, a whole-genome-alignment-phylogeny classifies *Shigella* serotypes in 5 distinct clades, differing from their current classification and reflecting its multiple origin (Figure 2). *S. sonnei* also

encodes a Type VI Secretion System that contributes to killing of other microbiota competitors like *E. coli*, which can prevent pathogenic infections (Anderson et al. 2017). This advantage may be relevant for its increasing prevalence in developed countries, where *S. sonnei* is the most common *Shigella* serotype (Kotloff et al. 2018).

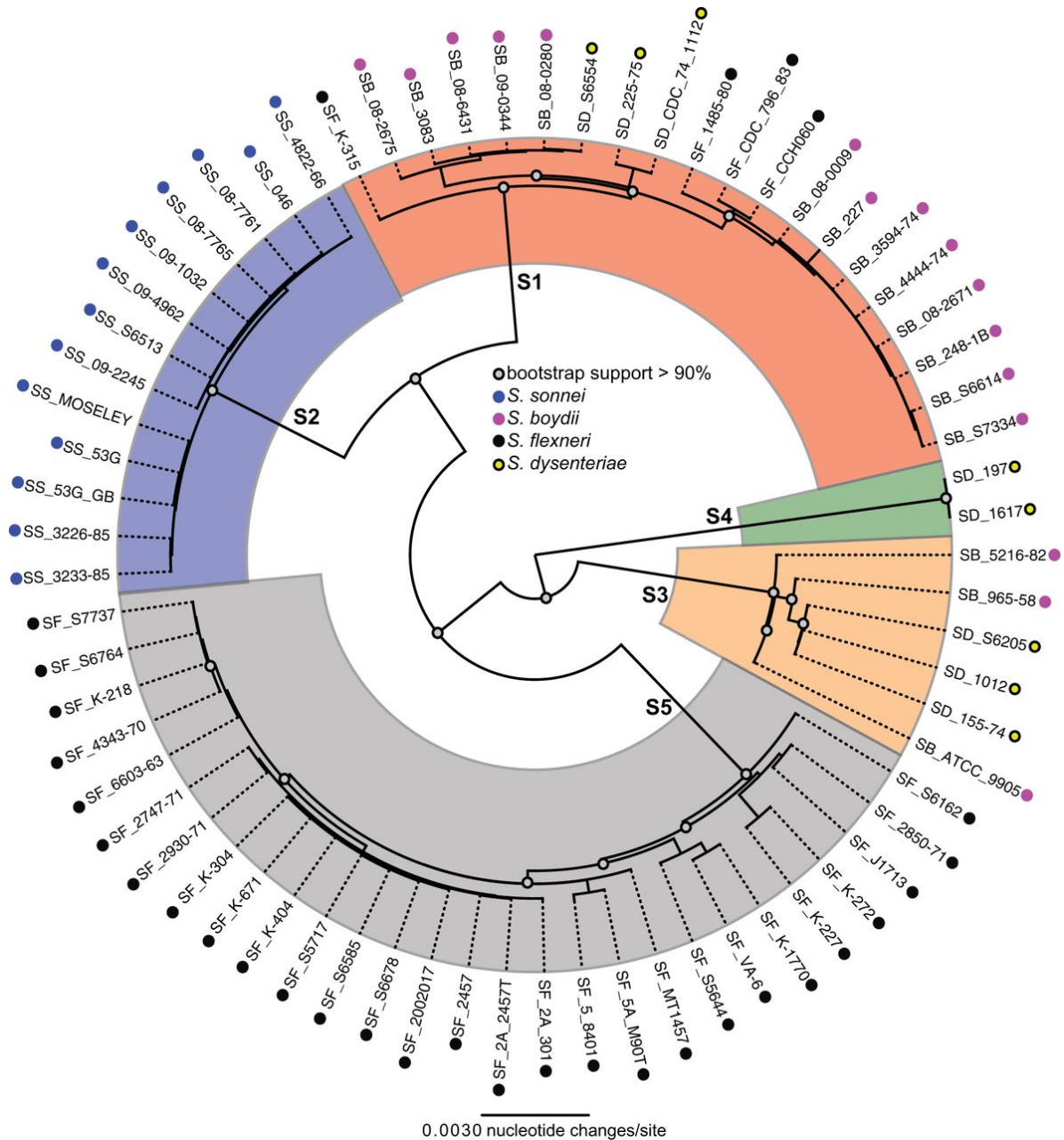


Figure 2. *Shigella* whole-genome phylogenetic tree. Strains from *S. flexneri* (SF), *S. sonnei* (SS), *S. boydii* (SB) and *S. dysenteriae* (SD) are clustered in 5 different monophyletic lineages (S1-S5). Reproduced from (Sahl et al. 2015).

One of the most relevant evolutionary events in the *Shigella* species is the appearance of a large virulence plasmid pINV, which will be further discussed in more detail. In addition to this event, other plasmids with different functions have also

been acquired by different species, including the plasmid pHS-2, which control the O antigen chain-length and the plasmids pDPT1 and pSSE3, which encode the production of colicins (Calcuttawala et al. 2015). Most recently, acquisition of plasmids encoding antibiotic resistance have been found, including resistance to sulfonamide, streptomycin and tetracycline (Holt et al. 2012), fluoroquinolones (Gu et al. 2012) and azithromycin (Baker et al. 2015).

At the genomic level, *Shigella* spp. has incorporated pathogenesis-associated genomic regions, or Pathogenicity Islands (PAI), which enhance its virulence and adaptation to its niche. Three PAIs have been identified in *S. flexneri*, with the role of some encoded proteins identified. LPS modification enzymes (Allison and Verma 2000) allow the evasion of the humoral immune response, which targets mainly the O antigen; enterotoxins ShET1 and ShET2 play a role in the watery diarrhea (Fasano et al. 1995) Proteases (Rajakumar, Sasakawa, and Adler 1997) play different roles, Pic plays a role in the degradation of the extracellular environment in the gut and in the host (Henderson et al. 1999; Al-Hasani et al. 2009); iron acquisition genes in the aerobactin operon allow *Shigella* to counteract the iron-deficient environment (Moss et al. 1999; Nassif et al. 1987); colicin resistance genes may play a role in its survival in the intestinal lumen (Vokes et al. 1999). *S. dysenteriae* type 1 also produces the Shiga toxin, which inhibits host protein synthesis. This leads to fluid accumulation, paralysis and cell death. Because the kidney highly expresses the toxin receptor Gb3, this toxin can also lead to hemorrhagic uremic syndrome (Johannes and Römer 2010).

1.2.3 *Shigella* virulence plasmid

The *Shigella* large virulence plasmid varies in size, being as large as 220 kb (Figure 3). This plasmid is sufficient to confer invasion in eukaryotic cells by otherwise non-invasive *E. coli* strains (Sansonetti et al. 1983). This plasmid contains around 280 open reading frames (ORFs), of which half are associated with insertion sequence elements suggesting a highly polyphyletic origin. For example, *Yersinia* low-calcium-response plasmid harbors a sequence homologous to a region in the *ipa-mxi-spa*

gene cluster. Other ORFs homologous to genes of *M. tuberculosis*, *S. typhimurium*, *M. bovis*, *E. coli*, and *V. cholerae* have also been reported (Venkatesan et al. 2001).

Importantly, the virulence plasmid harbors a 32 kb gene cluster that encodes the Mxi-Spa Type III Secretion System (Figure 3), which structure and role in invasion will be further described. In the same cluster, there are also a series of effector proteins, termed “Invasion Plasmid Antigens”, or Ipas, that mediate bacterial invasion and manipulate the immune response. The transcriptional regulation of this region is controlled by temperature, osmolarity and pH, with optimal conditions being 37°C, physiological saline concentration and pH 7.4 (Maurelli, Blackmon, and Curtiss 1984; Porter and Dorman 1994; Nakayama and Watanabe 1995). The *virF* regulatory gene is normally silenced by the chromosomally encoded H-NS protein until a shift in temperature to 37°C releases the transcriptional silencing by adjusting the DNA structure at the *virF* promoter (Maurelli and Sansonetti 1988; Stoebel, Free, and Dorman 2008).

VirF promotes the transcription of VirB, which antagonizes H-NS repression.

Specifically, VirB activates the *mxl* and *spa* genes that encode the T3SS, chaperon and protein effector genes and the regulator gene *mxlE* (Schroeder and Hilbi 2008).

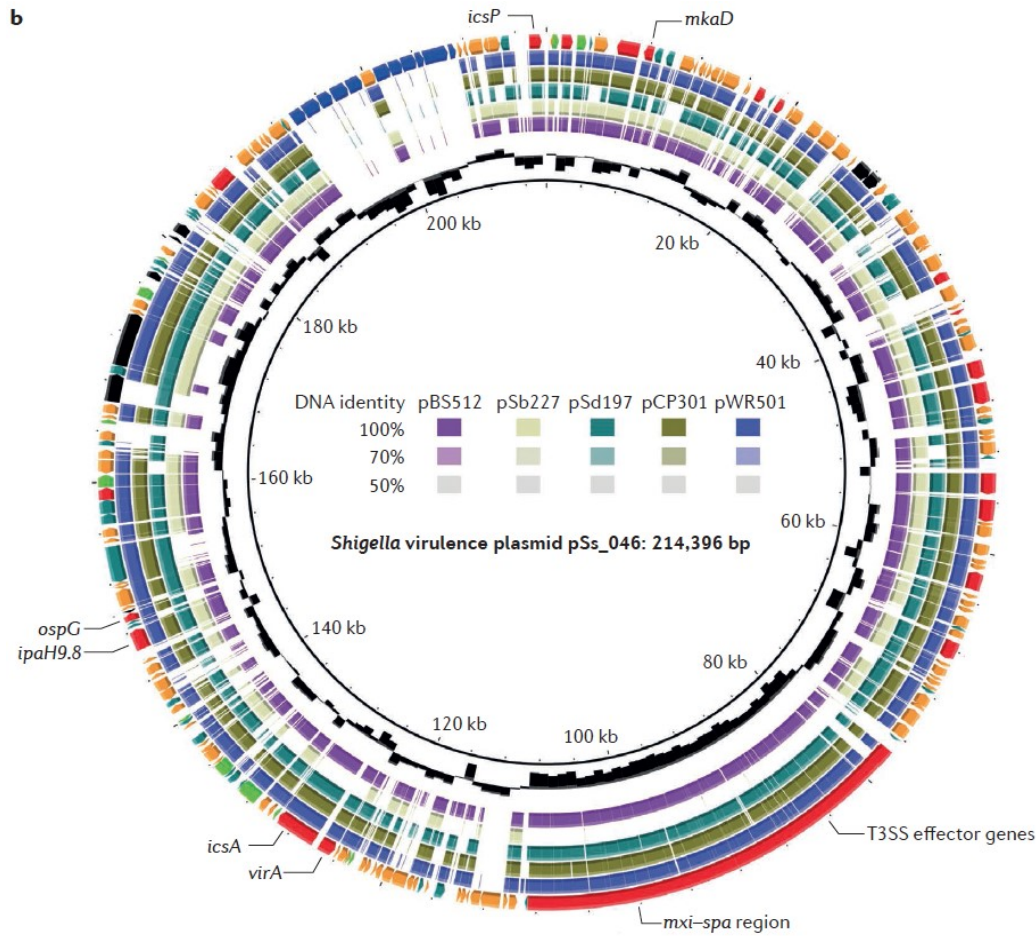


Figure 3. A comparative gene map of the *Shigella* virulence plasmid. Black ring shows the GC content of the reference pSs_046 sequence. The following purple, pale green, teal, khaki, and blue rings show comparisons between pSs_046 and the virulence plasmids of *S. boydii* str. BS512, *S. boydii* str. Sb227, *S. dysenteriae* str. Sd197, *S. flexneri* F2a str. 301 (pCP301) and *S. flexneri* F5a (pWR501), respectively. Outer ring represents annotations of genes or genetic clusters based on function: known virulence factor genes (red); plasmid replication, transfer and maintenance genes (black); transposon, phage-borne and insertion sequence elements (orange); genes encoding hypothetical proteins (teal); *S. sonnei*-specific O antigen biosynthesis cluster (blue); genes encoding proteins with other known functions (green). ipa, invasion plasmid antigen gene; icsP, also known as sopA; T3SS, type III secretion system. Modified from (The et al. 2016).

1.3 Overview of *Shigella* invasion

Before reaching the intestinal epithelium, *Shigella* needs to overcome physiological barriers throughout the digestive tract. *Shigella* spp. are resistant to acidic environments, presumably through glutamate-dependent acid-resistance pathway which allows them to survive the passage through the stomach (Jennison and Verma 2007). Afterwards, its primary sites of infection are the terminal ileum, colon and rectum. Another barrier *Shigella* has to overcome is the mucin layer that covers the intestinal epithelium. This layer consists of a heterogeneous meshwork of proteins including the large glycoproteins mucins ($>2 \times 10^6$ Da). All four species of *Shigella* produce mucinase and neuraminidase (Haider et al. 1993), which may allow them to degrade this barrier and get access to the intestinal epithelial cells.

1.3.1 Anatomy of the intestinal epithelium

The intestinal epithelium is a single-cell layer that extends across the 4 regions of the intestine (jejunum, ileum, caecum and colon). Its structure differs between regions. The small intestine is rich in villi, protrusions that extend into the lumen and maximize the contact area and therefore the nutrient adsorption. In opposition, villi are absent in the colon. The epithelium also forms invaginations named “crypts of Lieberkühn”.

Figure 4 depicts the spatial segregation of epithelial cell types. Stem cells are located at the depth of the crypts and as daughter cells are produced and differentiate, they migrate upwards. Four distinct cell types are produced from this stem cell population: absorptive, goblet, enteroendocrine and Paneth cells. Absorptive cells, or enterocytes, are the most abundant population of cells and have microvilli on their apical side; Goblet cells secrete mucus; Enteroendocrine cells secrete peptides and catecholamines, whilst Paneth cells secrete antibacterial proteins. As the intestinal epithelium is renewed, the old cells are extruded into the intestinal lumen at the villi apical extremities or the crypts' mouth. (For a review on the mechanisms of cell renewal see (Crosnier, Stamataki, and Lewis 2006)).

Enterocytes are polarized and form a highly tight barrier through tight junctions, adherens junctions and desmosomes. This barrier is permeable to ions, nutrients and water, while restricting the passage of proteins, lipids and microorganisms from the lumen to the lamina propria (Takuya Suzuki 2013).

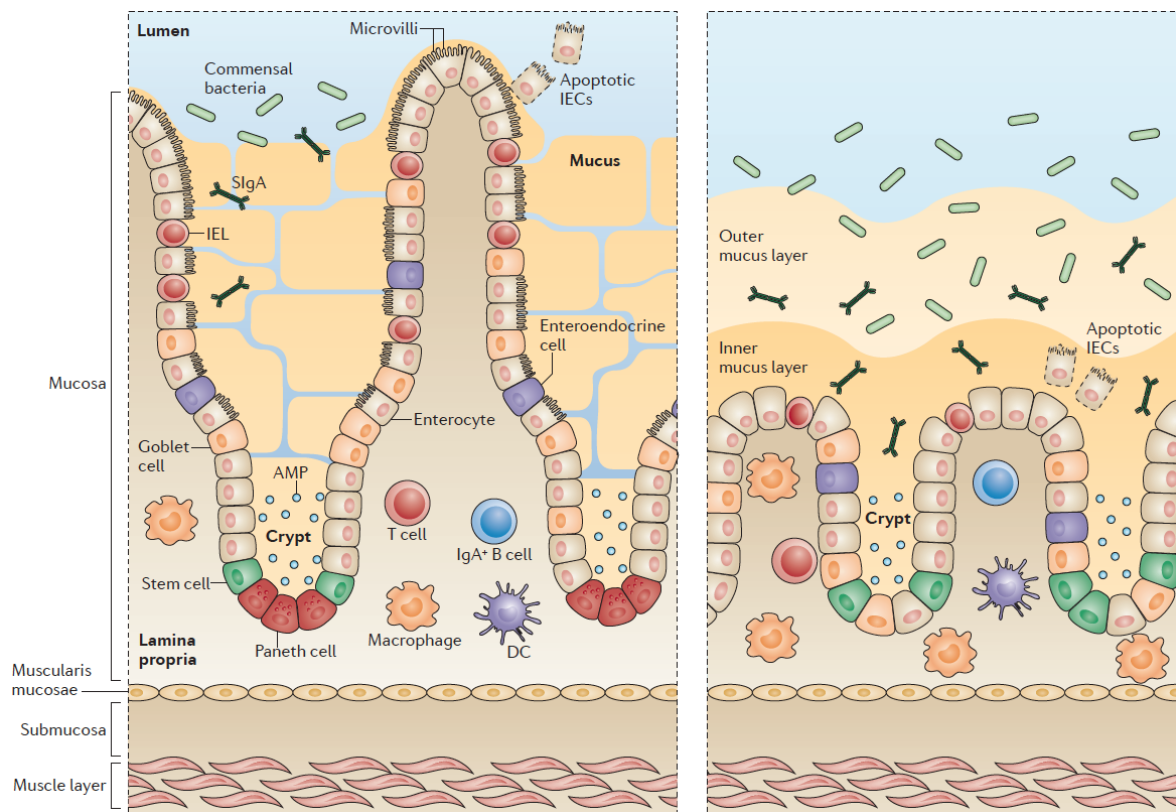


Figure 4. Structure of the intestinal mucosa in the jejunum (left) and in the colon (right). IEL: Intraepithelial lymphocytes; IEC: Intraepithelial cells; AMP: Antimicrobial peptides. Modified from (Mowat and Agace 2014)

In addition to epithelial cells, there is also an abundant population of immune cells interspaced with epithelial cells. Tuft cells detect the presence of helminths (Gerbe et al. 2016) and M cells perform uptake and presentation of luminal antigens to immune cells (Ohno 2016).

M cells are associated to subepithelial lymphoid aggregates, termed gut-associated lymphoid tissue, which prime adaptive immune cell responses in the intestine by

presenting antigens to dendritic cells. The best characterized of these aggregates are the Peyer's patches in the small intestine (Cornes 1965), which consists of B cell lymphoid follicles and T cell areas. Also, in the large intestine, there are structures termed cecal patches in the ileocaecal valve and colonic patches in the colon and rectum. Both patches resemble in function and structure to Peyer patches, albeit smaller in size (Owen, Piazza, and Ermak 1991).

In the lamina propria, there are also CD4+ and CD8+ T cells, with an effector memory phenotype. There is also a large population of IgA and IgM producing B cells and macrophages. These antibodies are shed into the lumen of the intestine and prevent bacterial adhesion to the epithelium. Eosinophils and mast cells are also present along the intestinal tract and contribute to the regulation of the inflammatory response (for a review see (Mowat and Agace 2014)).

1.3.2 *Shigella* invasion routes of the intestinal epithelium

The initial routes of invasion are not entirely clear and will be further discussed in detail. Early observation of biopsies from *Shigella*-infected patients suggested the gut-associated lymphoid tissue as one of the primary sites targeted (Mathan and Mathan 1991). In the rabbit ileal loop model, M cells were reported as the initial route of entry (Wassef, Keren, and Mailloux 1989). However, a guinea pig model that recapitulates several clinical features of the human infection shows that epithelial cells are invaded as early as 2-6 hours post-administration (Shim et al. 2007).

Using a guinea pig intra-rectal inoculation model, it was observed that enterocytes at the colonic crypts mouths were targeted at the onset of colonization and bacteria spread by cell-to-cell transmission into the crypts along the infection (Arena et al. 2015). In the rabbit ileal loop model, there is evidence that *Shigella* traverses the cell monolayer through M cells (Sansonetti et al. 1996), a step that would allow it to infect macrophages in the M cell pouch. According to this model, after inducing the pyroptotic death of macrophages, *Shigella* would invade epithelial cells from the basal side. Pyroptosis also leads to the release of pro-inflammatory cytokines IL-1 β

and IL-18, and invasion of epithelial release of IL-8. This causes a strong inflammatory response that recruits polymorphonuclear leukocytes and destabilizes the intestinal epithelium, hence facilitating invasion from lumenal bacteria.

1.4 The *Shigella* Type III Secretion System

1.4.1 The *Shigella* T3SS structure

A key element for the pathogenesis of *Shigella* is its T3SS. This apparatus functions as a needle, translocating effector proteins from the bacterial cytoplasm to the host cell cytosol (Figure 5). Assembly of fully functional T3SS apparatus is regulated by temperature but the injection of T3 effectors is dependent on host membrane contact (Veenendaal et al. 2007).

The T3SS is generally divided in three parts: the basal body, the needle and the tip complex. The basal body anchors the apparatus to the bacterial membranes (Figure 5). MxiD and MxiM form a ring in the outer membrane. On the cytoplasmic side, a C-ring formed by the proteins Spa33, MxiK and MxiN mediates the recognition, sorting and secretion of effectors, where the ATPase activity of Spa47 is involved (B. Hu et al. 2015; Burgess et al. 2016; Morita-Ishihara et al. 2006). Spa32 interacts with Spa40 and controls the length of the needle (Botteaux et al. 2010; Tamano et al. 2002). Other proteins are also present, but their roles remain unclear.

The needle is composed of the major MxiH and the minor MxiI subunits. MxiH assembles in a helical fashion and constitutes the needle rod with a 2-3 nm inner diameter (Blocker et al. 2001), while MxiI is proposed to be involved, together with MxiC, in the secretion activation upon contact of the host membrane (El Hajjami et al. 2018; Cherradi et al. 2013).

Before contact with the host membrane the needle tip complex composed of IpaD and perhaps IpaB remains in a closed conformation (Veenendaal et al. 2007; Cheung et al. 2015). IpaB and IpaC are translocated upon contact with host cells,

likely by interacting with membrane enriched in cholesterol and sphingolipids-containing membranes (Goot et al. 2004). IpaB and IpaC form the translocon allowing the translocation of effector proteins.

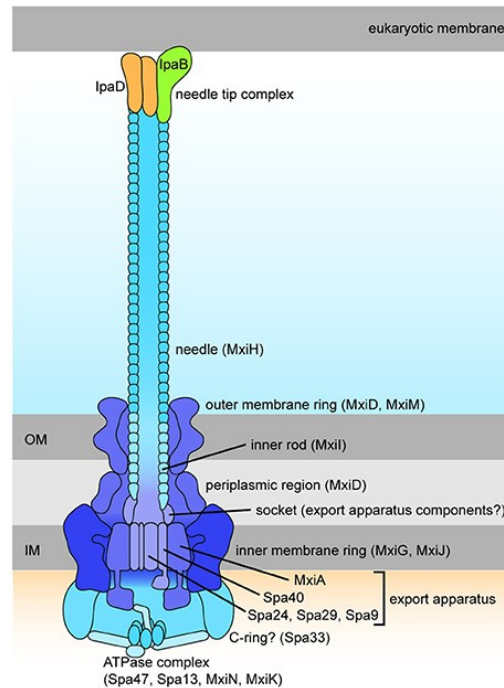


Figure 5. Structure of the *Shigella* T3SS. Tip components shown in yellow and green. Needle components in blue-greens, transmembrane base dark purple, inner membrane export apparatus light purple, C-ring and ATPase complex in light blues. OM, outer membrane. IM, inner membrane

1.4.2 *Shigella* T3SS effector proteins

At 37°C the transcriptional activator VirF is expressed and activates *virB* expression. VirB is also a transcriptional activator that activates the *ipa* (Invasion Plasmid Antigens) operon and the *mxi* (Membrane Expression of Ipa) - *spa* (Surface Presentation of Ipa) operon. Expression of these operons triggers bacterial entry mediated by the T3SS (Du et al. 2016), along with other effector genes. Injection of effector proteins is temporarily divided into two waves. After initial host cell contact,

the injection of the first wave of effectors happens within minutes (Enninga et al. 2005).

Shigella T3SS uses chaperons to prevent degradation and to target effector proteins to the secretion apparatus. The IpgC chaperone also regulates the expression of the second wave of T3S effectors. Prior to activation of T3 secretion, the IpgC chaperone associates with IpaB and IpaC and prevents their premature interaction in the bacterial cytosol (Parsot 2003; Pilonieta and Munson 2008). After activation of T3 secretion, IpaB and IpaC are secreted, releasing IpgC, which may then interact with the MxiE transcriptional activator. This allows the formation of the complex IpgC-MxiE that promotes triggering the transcription of genes harboring a MxiE box, (Figure 6) corresponding to genes of the second wave of effectors (Kane et al. 2002). Genes belonging to the second wave of effectors are mainly involved in high-jacking host signaling, apoptosis inhibition and regulation of long-term effects on the host immune response (For review, see Mattock and Blocker 2017).

Table 1. <i>Shigella</i> effector proteins. Modified from (Killackey, Sorbara, and Girardin 2016)		
<i>Shigella</i> effector (wave)	Host targets	Effect on host process
IpgB1 (1st)	Acts as GEF for Rac	Induces actin remodeling to facilitate invasion (Z. Huang et al. 2009)
IpgB2 (1st)	Acts as GEF for RhoA	Induces actin remodeling to facilitate invasion (Z. Huang et al. 2009)
IpgD (1st)	Acts as PI(4, 5)P ₂ -4-phosphatase to generate PI5P Diverts host cell recycling endosome machinery Increases levels of PI5P leading to p53 degradation	Induces actin remodelling to facilitate invasion. (Niebuhr et al. 2002) Allows rapid escape from the entry vacuole. (Mellouk et al. 2014) Induces PI3K/Akt-dependent survival pathways. (Pendaries et al. 2006)

IpaC (1st)	Activates Src Kinase and Cdc42 Inserts into vacuole membrane	Mediates invasion (T. Suzuki et al. 2000; Mounier et al. 2009)
IpaA (1st)	Targets Host-cell focal adhesion components vinculin and talin. Promotes RhoA activation	Promotes anchoring at the site of membrane ruffling (Tran Van Nhieu, Ben-Ze'ev, and Sansonetti 1997; Izard, Tran Van Nhieu, and Bois 2006; C. Valencia-Gallardo et al. 2019) Promotes actin rearrangement (Demali, Jue, and Burridge 2006)
IpaB (1st)	Binds to cholesterol on the host cell surface Inserts into vacuole membrane Reduces and disrupt balanced levels of cholesterol and lipids	Promotes bacterial adhesion (Romero et al. 2011; Lafont et al. 2002) Interferes with proper Golgi function (Mounier et al. 2012)
VirA (1st)	Catalyzes GTP hydrolysis in Rab1 Induces p53 degradation	Disrupts ER-to-Golgi trafficking and autophagy (Selyunin et al. 2014) Blocks apoptosis (Bergounioux et al. 2012)
IcsB (1st)	Blocks autophagy targeting by binding Atg5 Binds cholesterol	Reduces autophagy (Kayath et al. 2010; Ogawa et al. 2005)
OspB (2nd)	Induces mTOR signaling through IQGAP1	Inhibits autophagy (Lu et al. 2015)
IpaJ (2nd)	Cleaves N-myristoylated glycine from ARF1 to disrupt its localization	Disrupts autophagosome maturation and host membrane trafficking (Dobbs et al. 2015)
IpaH9.8 (2nd)	Targets and degrade NEMO/IKK γ	Disrupts NF- κ B signaling (Ashida et al. 2010)
IpaH4.5 (2nd)	Targets and degrades p65 subunit of NF- κ B Targets and degrades TBK1	Disrupts NF- κ B signaling (Wang et al. 2013) (Wang et al. 2013) (Zheng et al. 2016)
IpaH072 2 (2nd)	Targets and degrade TRAF2	Disrupts NF- κ B signaling (Ashida, Nakano, and Sasakawa 2013)
OspZ (2nd)	Prevents nuclear translocation of p65	Disrupts NF- κ B signaling (Newton et al. 2010)
OspI (2nd)	Deamidates UBC13 E2 enzyme needed for activation of TRAF6	Disrupts NF- κ B signaling (Sanada et al. 2012)

OspG (2nd)	Interferes with ubiquitin proteasomal degradation of I κ B- α	Disrupts NF- κ B signaling (Kim et al. 2005)
OspF (2nd)	Inactivates the ERK and p38 MAP kinases using its phosphothreonine lyase activity	Disrupts MAPK signaling (Reiterer et al. 2011)
OspC3 (2nd)	Interacts with caspase-4-p19 subunit and inhibits its heterodimerization and activation	Inhibits pyroptosis within epithelial cells (Kobayashi et al. 2013)
IpaH1.4/ 2.5	Induces proteosomal degradation of HOIP	Suppression of NF- κ B activation (de Jong et al. 2016)

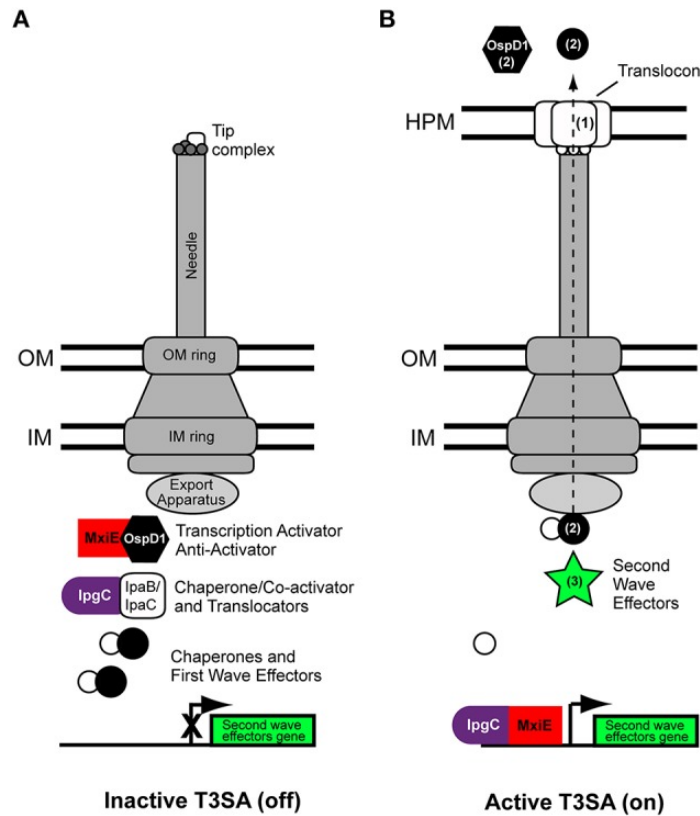


Figure 6. Regulation of the second wave of effectors. A. Inactive T3SA. B. Active T3SA. Prior to activation of T3 secretion, the IpgC chaperone associates with IpaB and IpaC. After activation, IpaB and IpaC are secreted, releasing IpgC, which may then interact with the MxiE transcriptional activator. This allows the transcription of genes harboring a MxiE box. Modified from (Campbell-Valois and Pontier 2016)

1.5 Main players of the cytoskeleton

1.5.1 Actin monomers

The actin cytoskeleton is commonly targeted by pathogens, being highly conserved among animals and a central element in various cellular processes. Actin monomer, termed G-actin, can polymerize into actin filaments, or F-actin. ATP-G-actin

polymerizes into ATP-F-actin, which has an intrinsic ATPase activity leading to ADP F-actin. ADP F-actin is less stable than ATP G-actin, rendering ADP F-actin filaments prone to disassembly (Dominguez and Holmes 2011).

The incorporation of actin monomers is asymmetrical. The barbed end (or plus end) of actin filaments incorporates ATP-actin monomers, while the pointed end (or minus end) is more prone to be disassembled (Figure 7A). Simultaneous incorporation of monomers at one end and disassembly on the other gives rise to treadmilling.

1.5.2 Actin sequestering proteins

In the intracellular milieu, actin binds to profilin. This complex represents the main source of monomers for polymerization. Profilin catalyzes the ADP/ATP exchange in actin monomers, while inhibiting the spontaneous filament nucleation property of actin monomers (Dominguez and Holmes 2011). Profilin-actin also binds to other proteins involved in actin polymerization, such as formins and Ena/VASP proteins (Kovar et al. 2006) (Figure 7).

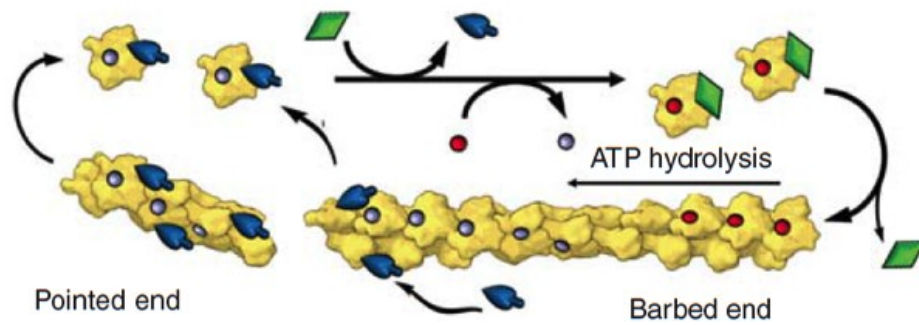
Thymosin- β 4 is a peptide of 43 residues. In its N-terminus it has short helix that binds the actin barbed end and the rest of the helix, forms an extended region that binds the front surface of actin and a second helix that caps actin pointed end (Xue et al. 2014). This results in the blockage of engagement of actin monomers into polymerization. However, profilin and thymosin- β 4 are constantly exchanging actin monomers, allowing elongation of actin filaments (Pantaloni and Carlier 1993).

1.5.3 Severing proteins

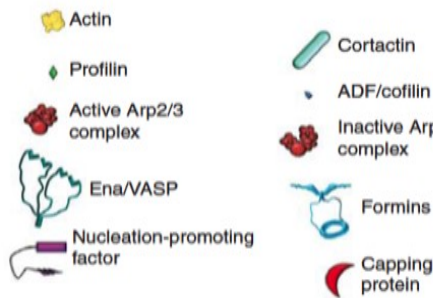
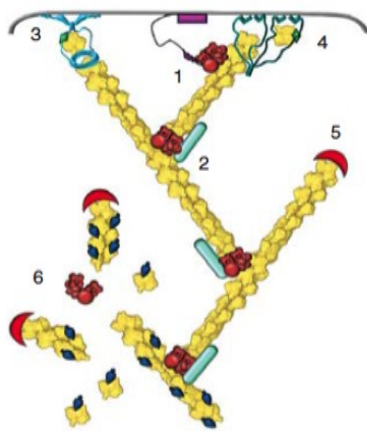
Depolymerization in cells is enhanced by proteins of the ADF/Cofilin family, which includes Actin Depolymerization Factor (ADF), cofilin-1, cofilin-2 and twinfilin. This family of proteins have a higher affinity for ADP-actin than for ATP-actin, and therefore bind to ADP-actin fiber stretches and promote the severing of these filaments (Barbara W. Bernstein 2010).

Gelsolin proteins also sever actin filaments and cap their barbed ends. Most of its family members' activity is regulated by calcium binding. Mutants of this protein have defects in cellular motility and decreased blood clotting.

A



B



C

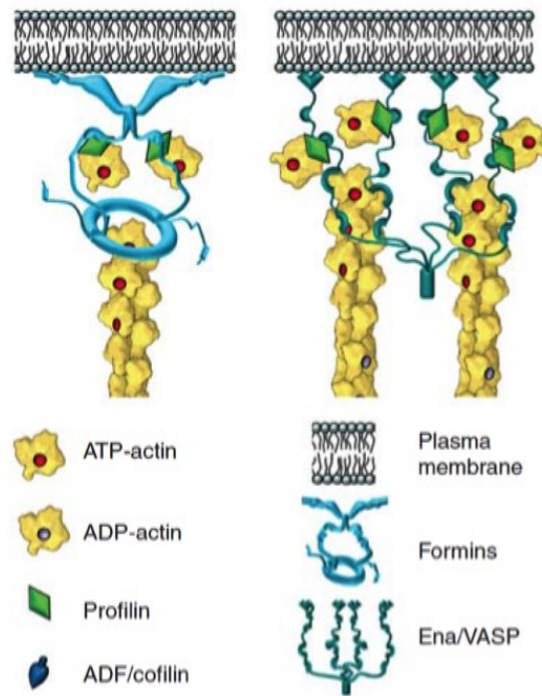


Figure 7. Dynamics of actin filaments. A. Actin polymerization. B. Actin regulation. (1) Arp2/3 recruitment (2) Actin branching (3) Formin elongation of actin fibers (4) Ena/VASP elongation of actin fibers (5) Filament capping (6) Depolymerization of actin filaments. C. Formin and Ena/VASP nucleation and elongation activity. Modified from (Svitkina 2018).

1.5.4 Actin nucleators

Actin nucleators initiate the *de novo* polymerization of actin filaments. The Arp2/3 complex is one of the best characterized actin nucleators. It is composed of a core of 7 proteins. Upon the interaction of Nucleation Promoting Factors (members of the Wiskott-Aldrich Syndrome Protein family, WAVE, among others), actin filaments and actin monomers, Arp2/3 is recruited and activated by Arf1 and Rac1 (Koronakis et al. 2011). Through the VCA domains of the Nucleation Promoting Factors, Arp2/3 is connected to the mother actin filament and nucleates the polymerization of a new branched actin filament (Pollard 2007). Given the Arp2/3 structure, the daughter filament elongates at an angle of 70° from the mother filament (Amann and Pollard 2001). At a large scale, polymerization of new branched filaments upon existing filaments give rise to branched actin networks, which are enriched in lamellipodia (Figure 7B).

In opposition to Arp2/3, formins nucleate and elongate unbranched actin filaments in filopodia, stress fibers and actin cables. They are characterized by the presence of the Formin Homology Domains 1 and 2, which mediate their interaction with profilin and their nucleation activity, respectively. Their ATP-dependent activity results in a highly processive actin polymerization (Romero et al. 2004). In a similar fashion, Ena/VASP proteins also promote the nucleation and elongation of actin filaments (Figure 7C), and works in neurons show that they are particularly important for filopodial formation (Lebrand et al. 2004).

1.5.5 Capping proteins

Capping protein and CapZ bind to the barbed end of actin filaments, blocking both the addition and loss of actin subunits (Isenberg, Aebi, and Pollard 1980; J. Xu, Casella, and Pollard 1999), therefore preventing the assembly/disassembly of filaments. In conjunction with the branching activity of Arp2/3, a network of short and highly branched actin filaments can be formed (Figure 7B) (M. Edwards et al. 2014).

1.5.6 Cross-linking proteins

Individual actin filaments can be bundled together through the action of actin cross-linkers, such as α -actinin isoforms 1 and 4 or fimbrin. These proteins contain Actin-Binding Domains (ABD) that connects two separate actin fibers. α -actinin has also the ability to associate with other cytoskeletal, signaling and membrane molecules (Sjöblom, Salmazo, and Djinoić-Carugo 2008).

The organization into bundles by filament bundling facilitates the mechanical contraction exerted by myosins molecular motors. In particular, Myosin II transforms the chemical energy released by ATP hydrolysis into mechanical work that results in pulling of actin filaments (Figure 8). The pulling activity is the result of the myosin II polymerization into bipolar filaments, with the motor domains walking in opposing cross-linked actin filaments (Figure 8) (Sweeney and Holzbaaur 2018).

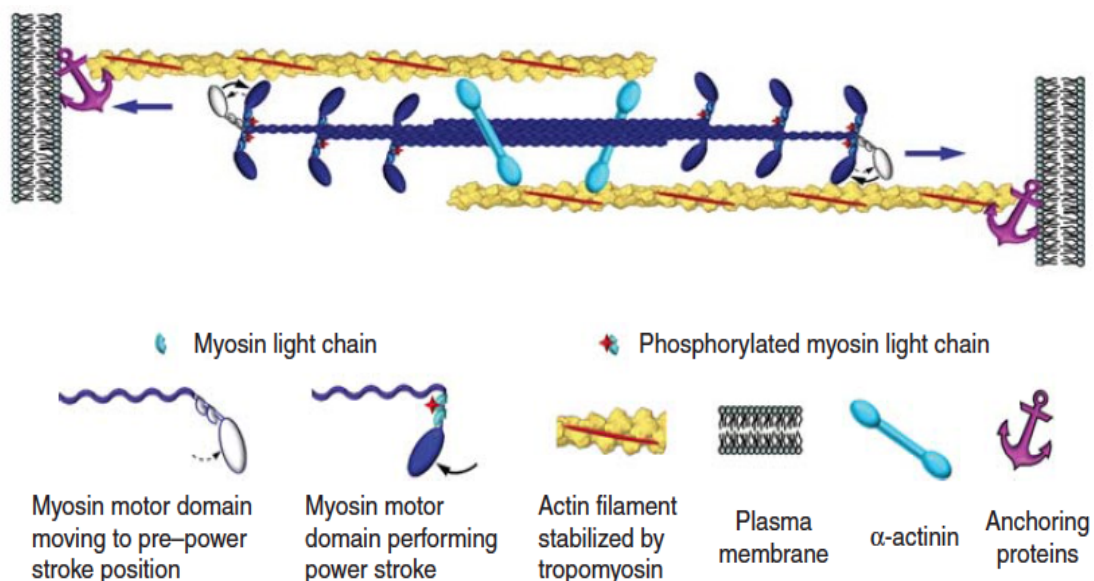


Figure 8. Myosin II and α -actinin in actin filament contraction. Myosin II polymerizes into bipolar filaments, with the motor domains walking in opposing actin filaments cross-linked by α -actinin. Modified from (Svitkina 2018).

1.6 Adhesion structures

1.6.1 Integrins

The intracellular actomyosin cytoskeleton dynamically interacts with the extracellular environment through linker molecules anchoring transmembrane receptors that connect with the extracellular environment. Integrins and cadherins are two of the main receptors that connect the actomyosin cytoskeleton with the outer environment and to respond to mechanical and biochemical cues.

Integrins are cell adhesion receptors, and its super-family is composed of 18 types of α subunits and 8 types of β subunits, which can associate into 24 different $\alpha\beta$ heterodimers, the β subunit determining the family. The α and β subunits are non-covalently associated transmembrane proteins. Different pairs can bind to different ligands, such as RGD motif (present in fibronectin and vitronectin), collagen, laminin, or ligands in leukocytes (Kechagia, Ivaska, and Roca-Cusachs 2019; Hynes 2002) (Figure 9).

Although not proven for all $\alpha\beta$ pairs, some integrins can transition from a “bent closed” or inactive form, to an extended closed and finally to an extended open. This transition is associated with an increase in the affinity of the integrin for its substrate.

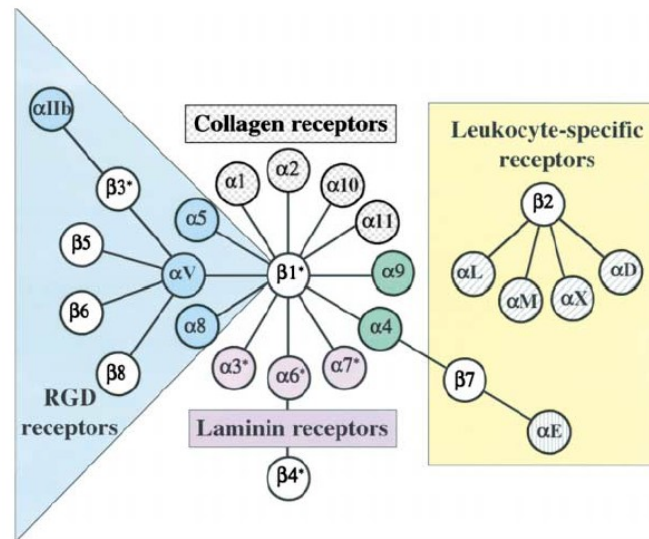


Figure 9. Integrins ligands and intracellular dynamics. Different $\alpha\beta$ pairs and their ligands (Modified from Hynes 2002).

Integrin transition from closed bent to open extended is enhanced by the binding of kindlin, and notably talin, which binds to the cytoplasmic tail of the β subunit, a process termed “inside-out activation”, as opposed to “outside-in signaling” implicating the activation of integrins through the binding of their extracellular ligand.

Talin recruitment to the membrane is presumably achieved through its interaction with Rap1-GTP-Interacting-Adaptor-Molecule (RIAM), which links membrane associated Rap1 with cytoplasmic talin (Lee et al. 2009) and concentrates it at the tip of actin growing filaments in lamellipodial and filopodial protrusions (Lagarrigue et al. 2015).

Integrins display catch-slip bonds with RGD-ligands (Kong et al. 2009), ICAM (W. Chen, Lou, and Zhu 2010) and VCAM (Choi et al. 2014). In an ideal bond between molecules, the lifetime of the interaction would not depend on force. However, bonds usually behave under non-ideal regimes. Under a slip regime, the bond between two molecules will decrease its lifetime as force is applied. Counter-intuitively, catch-slip bonds undergo first a catch regime where application of force will increase the

lifetime of the bond, therefore strengthening the interaction. This catch regime is followed by a slip regime until detachment (Rakshit and Sivasankar 2014).

In order for the force to be effectively transmitted between the actomyosin cytoskeleton and the extracellular environment, integrin molecules need to be connected to the actin cytoskeleton. This task is performed by linker proteins such as talin, tensin, filamin and α -actinin, which bind simultaneously to integrins and F-actin. This force-enhanced process leads to the maturation of adhesion structures through the recruitment of additional scaffolding and signaling molecules.

1.6.2 Adhesion formation and maturation

Filopodia are finger-like structures that protrude out of the cells' edge. Its extension is driven by actin polymerization mediated by formins and regulated by Rho GTPases, capping proteins and Ena/VASP (Gupton and Gertler 2007; Lagarrigue et al. 2015; Albuschies and Vogel 2013). Deeper into the cell edge, short-lived adhesions (~60 seconds turnover) can be found in the lamellipodium, termed “nascent adhesions”. Larger adhesions, known as “focal complexes” with a persistence of several minutes can be found further back from the leading edge. These focal complexes can mature into large focal adhesions (3-10 μ m long) located at the extremes of stress fibers, with a persistence time of 30-60 min (Zimerman, Volberg, and Geiger 2004).

There is evidence that adhesions at the shaft of the filopodia and nascent adhesions mature into focal adhesions upon the advancement of lamellipodia (Figure 10) (Wong, Guo, and Wang 2014). Nascent adhesion formation is independent of myosin II and contain integrins, talin, kindlin, vinculin, α -actinin, paxilin and FAK. These adhesions can either disassemble or further mature into focal adhesions in a process largely driven by tension and crosslinking exerted by myosin II.

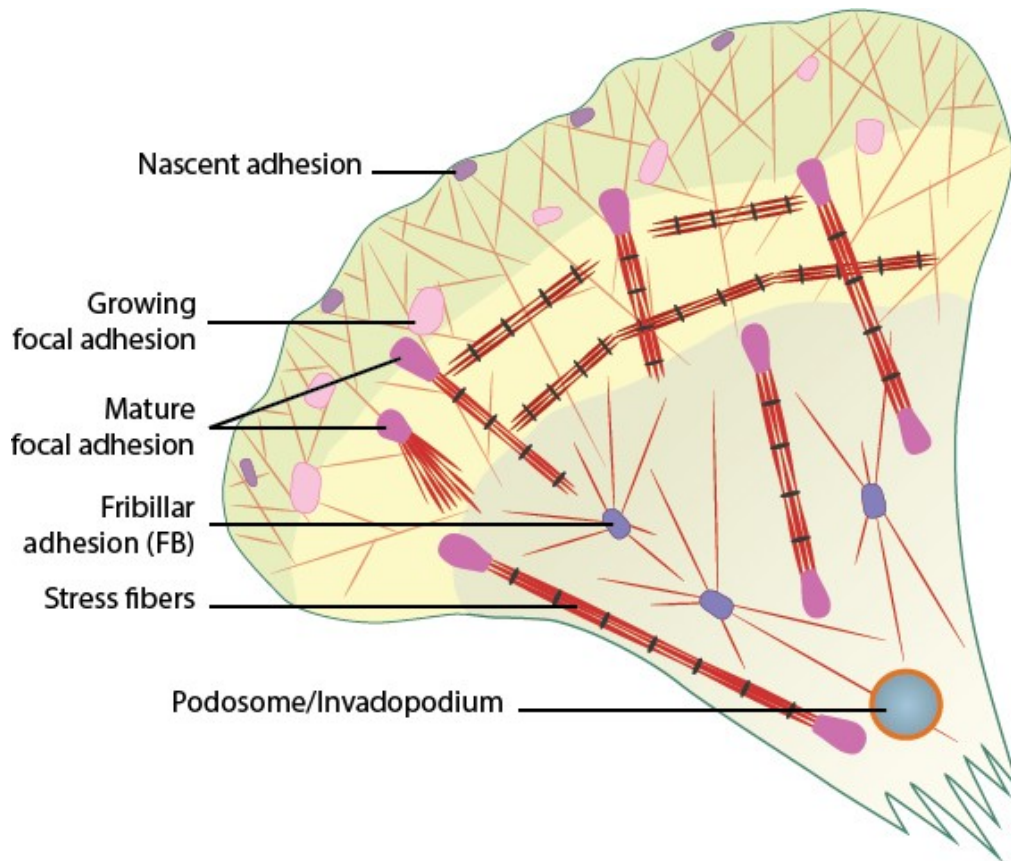


Figure 10. Maturation of adhesion structures. Modified from (www.mechanobio.info)

1.6.3 Talin and Vinculin molecular clutch

The molecular clutch hypothesis postulates that focal adhesions mediate the interactions between the retrograde-moving actin and ligand-bounded cytoskeleton. This interaction regulates the protrusive activity of the actin cytoskeleton. In adherent migrating cells, the cortical actin cytoskeleton is organized into two structurally and functionally distinct regions: the lamellipodium and the lamellum. In the lamellipodium Arp2/3-driven actin polymerization generates pushing force. However, when the molecular clutch is not engaged (i.e. when actin fibers are not tethered to the extracellular matrix), actin movement results in treadmilling behaviour towards the interior of the cell due to the resistance from the plasma membrane, generating rearward movement. When the clutch is engaged, on the other hand, forces required

to counteract membrane resistance are transmitted to the matrix and protrusions at the cell edge are generated (Figure 11).

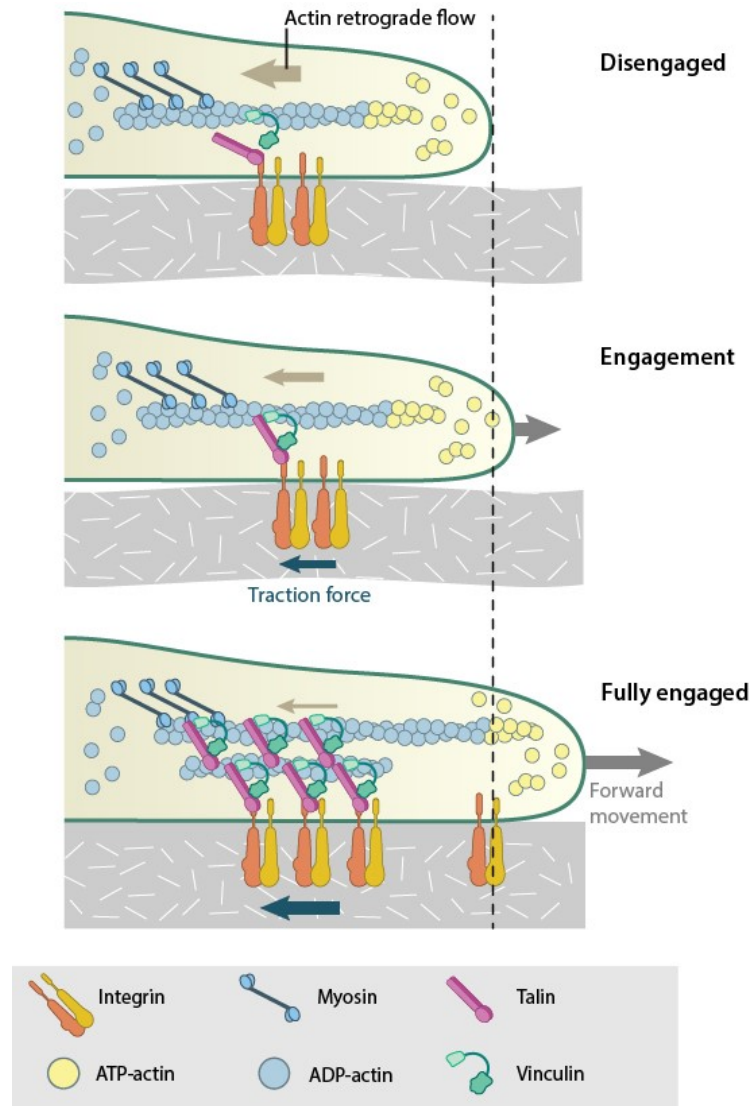


Figure 11. Model of the molecular clutch hypothesis. Disengaged molecular clutch results in actin treadmilling behaviour towards the interior of the cell, generating rearward movement. Engagement, forces required to counteract membrane resistance are transmitted to the matrix and protrusions at the cell edge are generated.

Interaction between actin cytoskeleton and the extracellular matrix involves transmembrane proteins and linker molecules. In focal adhesions, the linker integrins bind to the extracellular matrix. In addition, the role of talin as an integrin-actin linker molecule is remarkable, because it possesses structural characteristics of a molecular mechanosensor regulated by force. One characteristic is its ability to scaffold vinculin in a force-dependent manner (Figure 12). Talin is organized in two domains, the N-terminal FERM domain can bind phospholipids and integrin, responsible for the inside-out signaling activity through integrins (Anthis et al. 2009). The C-terminal domain contains 13 helical bundles (designated R1-R13) that contain two actin binding sites on the rod domain and one in the FERM domain at least 11 putative Vinculin Binding sites (VBSs), each one constituted by a single amphipathic α -helix (Gingras et al. 2005). However, all of the VBSs helices are buried within α -helix bundles until they become exposed, which happens only upon force-dependent stretching of talin and bundle unfolding (Figure 12B) (Hytönen and Vogel 2008); (del Rio et al. 2009).

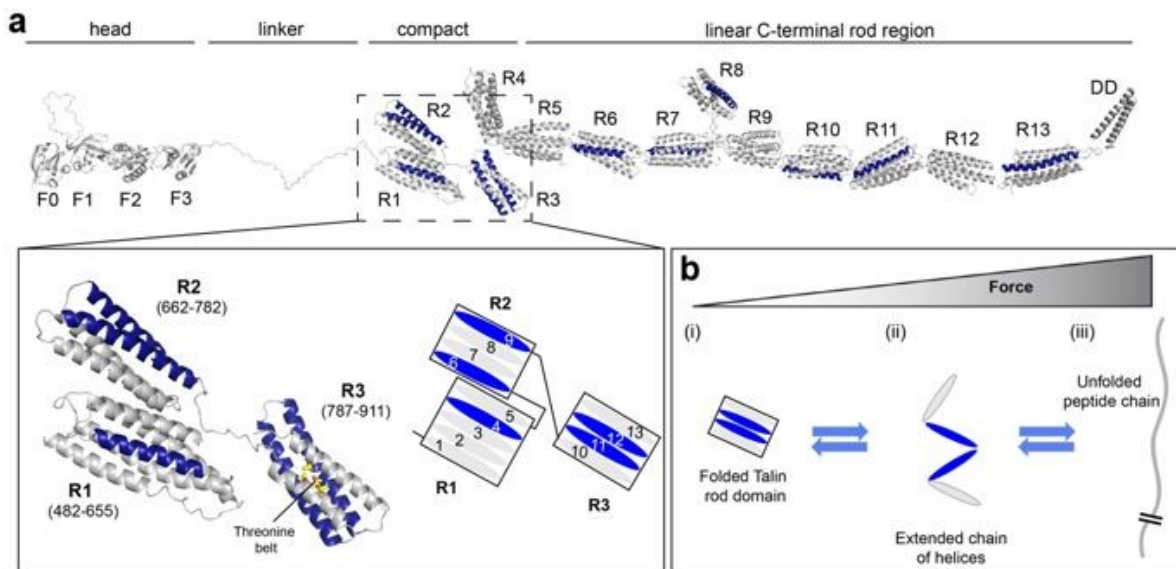


Figure 12. A. Structural model of Talin. Depicted in blue are the Vinculin Binding sites. B. Unfolding of helix bundle. Talin bundles unfolding leads to unveiling VBSs. Modified from (Yao et al. 2015)

Talin bundles unfold in a hierarchical manner, depending on the force required for their unfolding. It has been shown that all bundles, at least *in vitro*, are susceptible to be unfolded by stretching forces ranging from 5 to 30 pN (Haining et al. 2016; Yao et al. 2015). In its inactive form, vinculin has a globular structure consisting of two domains: a head domain and a tail domain connected by an unstructured linker (Figure 13). Both head and tail domains consist of α -helix bundles, the head is organized in four subdomains (named VD1-VD4), while the tail domain contains a single bundle (termed Vt) (Borgon et al. 2004). The vinculin intra-molecular interaction occurs between the Vt and head subdomains VD1 and VD4 (Izard et al. 2004; Cohen et al. 2005). When these interactions are disrupted, the actin binding site on Vt is free to interact with F-actin under a catch-bond regime (D. L. Huang et al. 2017). Reported VBSs from talin and α -actinin bind to the VD1 domain (Izard et al. 2004). However, whether talin VBSs exposure alone is sufficient for vinculin activation *in vivo* is a matter of debate. There are observations that phosphorylation on vinculin tyrosine residues 100 and 1065 by Src (Auernheimer et al. 2015) and F-actin binding (H. Chen, Choudhury, and Craig 2006) facilitates vinculin activation. Also, PI(4, 5)P₂ is required for vinculin sequestration at FAs and contributes to their stabilization (Chinthalapudi et al. 2014).

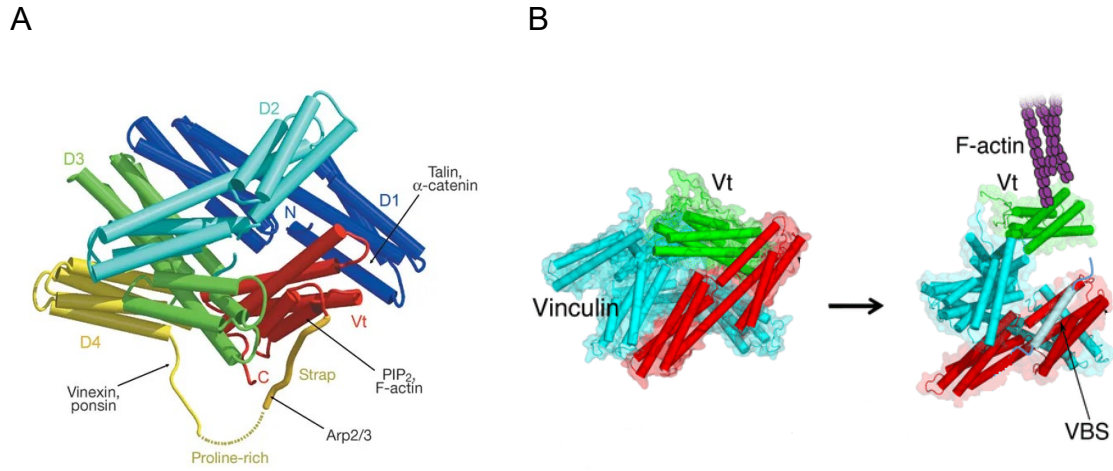


Figure 13. A. Vinculin structure and activation. Vinculin subdomains are indicated in colors (D1, blue; D2, cyan; D3, green; D4, yellow; Tail domain, red). Binding sites for Talin, α -catenin, PIP₂, F-actin, Arp2/3, vinexin and Ponsin are indicated. B. Vinculin activation by VBSs. Vinculin head domain is colored in cyan, VD1 is indicated in red, Tail domain in green. VBS (light cyan) interaction with VD1 disrupts heat-tail interaction and leads to interaction with F-actin (purple). Modified from (Bakolitsa et al. 2004 and Park et al. 2014).

1.6.4 Force generation and maturation

Initial nascent adhesion formation is dependent on actin polymerization, in which Rac1 activation and Arp2/3 have been implicated (Wu et al. 2012).

This is in contrast to nascent adhesions that mature into focal adhesions in a process that requires stress fibre assembly and myosin II activity (Oakes et al. 2012). Myosin II activity is sustained by Rho through the action of Rho associated protein kinase (ROCK). As adhesion structures mature, its composition changes and generates a complex 3D organization (Figure 14). Signalling proteins like FAK and Paxilin localize next to the integrin cytoplasmic tails, together with the Talin head. However, talin rod

protrudes inwards, colocalizing with vinculin, which is initially recruited to the plasma membrane, but relocalizes as the adhesion matures and talin VBS are unveiled by force. Talin tail, which binds to F-actin colocalizes with proteins like zyxin, VASP and α -actinin (Case and Waterman 2015).

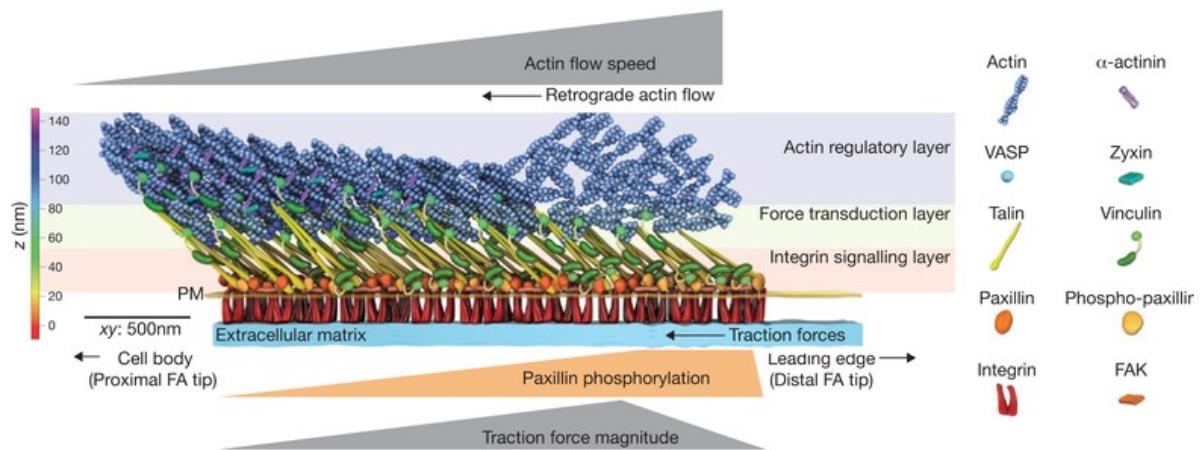


Figure 14. Focal adhesion organization. Internal organization changes with respect to traction forces and protein composition follow a layered organization. Modified from (Case and Waterman 2015)

1.7 Actin cytoskeleton reorganization by bacterial pathogens

1.7.1 Bacterial adhesion and internalization strategies

Shigella, as other bacterial pathogens, has evolved different ways to target and manipulate host cells. As a first step, pathogens must adhere to host cells. Several pathogens express pili- or fimbriae-associated adhesins. Pili are adhesive peritrichous, non-flagellar, filamentous organelles that stick out of the bacterial surface. They allow the bacteria to attach to host cell receptors, targeting glycolipids, glycoproteins, mannose residues or mucus. There are four types of pili: type I, type IV, P pili, bundle-forming pili and Curli and they are widespread among pathogenic Gram-negative bacteria, as described in Table 2.

Table 2. Pili/fimbriae of pathogenic Gram-negative bacteria

Table 2. Pili/fimbriae of pathogenic Gram-negative bacteria (modified from Bhunia 2018)	
Type of pili	Present in
Type I	<i>E. coli</i> , <i>H. influenzae</i> , <i>Y. pestis</i>
Type IV	<i>Pseudomonas</i> spp., <i>Vibrio</i> spp., Enteropathogenic <i>E. coli</i> , <i>N. meningitidis</i>
P pili	<i>E. coli</i> , <i>H. influenzae</i> , <i>Y. pestis</i>
Bundle-forming pili	Enteropathogenic <i>E. coli</i>
Curli	<i>S. enterica</i> , <i>E. coli</i>

Bacteria also express adhesion proteins at their surface that promote a tight binding to host cells that are relevant for attachment and invasion. These proteins commonly target host surface molecules or the extracellular matrix, as can be seen in table 3.

Table 3. Non-exhaustive list of adhesion factors and host receptors of pathogenic bacteria

Table 3. Non-exhaustive list of adhesion factors and host receptors of pathogenic bacteria (modified from Bhunia 2018; Solanki, Tiwari, and Tiwari 2018)		
Pathogen	Adhesion factors	Host receptor
<i>L. monocytogenes</i>	Internalin A	E-cadherin
	Internalin B	c-Met, gC1q-R/p32
	Virulence invasion protein	Gp90
	Listeria adhesion protein	Hsp60
<i>Campylobacter spp.</i>	CadF	Fibronectin
<i>Arcobacter</i>	Hemagglutinin	Glycan receptor
Enteropathogenic, enterohemorrhagic E.coli	Intimin	Translocated intimin receptor
<i>Y. enterocolitica</i>	YadA	Collagen/fibronectin/laminin/ β 1-integrin
<i>S. aureus</i>	Fibronectin-binding protein	Fibronectin
<i>V. cholerae</i>	Toxin-coregulated pili	Glycoprotein
<i>N. meningitides</i>	OpcA	Vitronectins, proteoglycans
<i>E. coli</i>	OmpA	Ecgp glycoprotein
<i>B. pertussis</i>	Pertactin	Not identified
<i>Y. pseudotuberculosis</i>	Invasin	β 1-integrin

In addition to classically described adhesin-receptor interactions, some bacteria have evolved more sophisticated forms of targeting their niche, which in some cases include the manipulation of the cell intracellular machinery, notably the cell cytoskeleton.

1.7.2 *E. coli* FimH catch-bond adhesion

Uropathogenic *E. coli*, a bacterial species that colonizes the urinary tract, expresses a variant of the type 1 fimbriae whose affinity for its receptor is enhanced under high flow velocity conditions (high shear-stress) (Thomas et al. 2002).

Type I fimbriae are assembled via the chaperone/usher pathway, which consists of: a chaperon protein which interacts with the pilus and usher proteins including an usher protein, which forms the translocation pore in the outer membrane. Around 1000 copies of the subunit FimA forms the fimbriae's rod, while a single copy of the FimF, FimG and FimH subunits constitute the adhesive tip. FimH, located at the fimbriae distal part, is highly variable, which reflects different specificities for different targets (Mortezaei et al. 2015). FimH from the uropathogenic *E.coli* strain J96 contains three aminoacid substitutions relative to the gene encoded by the intestinal *E. coli* strain F18 that confer its catch-bond binding properties for the mannose receptor (Thomas et al. 2002). Conformational changes between the pilin domain and the lectin domain mediate this process. The physical separation of these domains induced by force removes the allosteric inhibition exerted by the pilin domain upon the binding of the lectin domain for its target (Figure 15), increasing the affinity of the lectin for the mannose residue (Sauer et al. 2016).

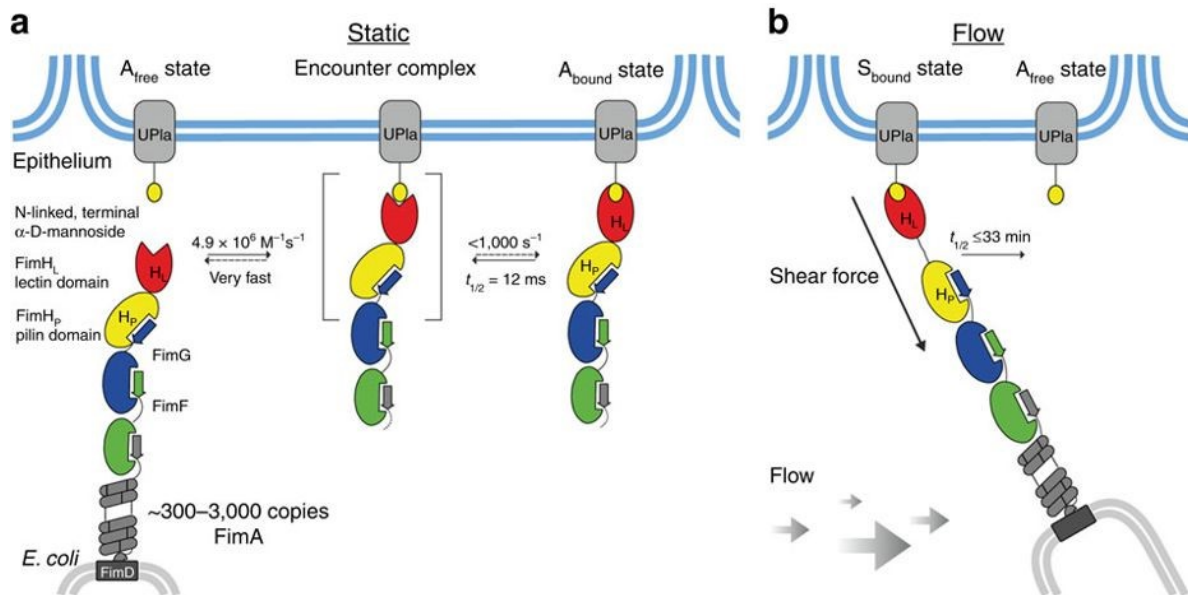


Figure 15. Catch-bond mechanism scheme. On low force, FimH binds transiently to its receptor. Upon flow application, lectin and pilin domains are separated and the high-affinity state for the lectin domain is stabilized after release of the allosteric-inhibitory pilin domain.

1.7.3 Zippering: *Listeria monocytogenes* invasion mechanism

Invasive bacteria have developed mechanisms that allow them to induce their internalization by host cells. Such is the case of *L. monocytogenes*, a Gram-positive pathogen. Following ingestion of contaminated food, *Listeria* can invade the intestinal epithelium and disseminate to the liver, spleen, cross the blood-brain- and the fetoplacental barriers. *Listeria* causes a potentially lethal disease when associated with sepsis, bacterial meningitis, infection of the fetus and pregnancy complications (Radoshevich and Cossart 2018).

Listeria entry in non-phagocytic cells is mediated by two surface-expressed proteins: Internalin A (InIA) and Internalin B (InIB), which bind to their eukaryotic receptors E-

cadherin (Gaillard et al. 1991; Mengaud et al. 1996) and c-Met (Pentecost et al. 2010), respectively.

E-cadherin is part of adherens junctions that mediate cell-to-cell adhesions in the intestinal epithelium. This transmembrane protein mediates homotypic interactions between cells and are connected to the actomyosin cytoskeleton mainly through α -catenin, β -catenin and p120-catenin. Both cadherin-cadherin interactions and the cadherin-catenin complex (E-cadherin/ α -catenin/ β -catenin) interaction with F-actin display a catch-bond behaviour (Buckley et al. 2014; Rakshit et al. 2012). p120 phosphorylation state is also able to allosterically regulate the affinity of homophilic cadherin interactions (Shashikanth et al. 2015).

Targeting E-cadherin by InIA is sufficient to promote internalization (Lecuit et al. 1997). InIA affinity for E-cadherin, however, is low, and is thought to be compensated by the high amount of molecules throughout the bacterial surface, and might allow it to dissociate from E-cadherin once internalized (Wollert, Heinz, and -D. Schubert 2007).

Initial interaction of InIA with E-cadherin requires its presence in lipid rafts and leads to the recruitment of α -catenin, β -catenin and p120-catenin (Lecuit et al. 2000). *Listeria* internalization involves the recruitment of Src kinase (Sousa et al. 2007), which phosphorylates E-cadherin and triggers its ubiquitination by Hakai, thus marking E-cadherin molecules for endocytosis (Bonazzi et al. 2008). Src kinase, together with Rac1 promote the recruitment of cortactin, an activator of Arp2/3. This cascade leads to a local and transient actin polymerization event that is essential for internalization. Molecular motor myosin VIIa and vezatin are also recruited by α -catenin to bacterial entry sites and might play a role in the generation of force for *Listeria* internalization (Sousa et al. 2004).

1.7.4 Attaching and Effacing Lesion Pathogens

Pathogens in this category include Enteropathogenic *E. coli* (EPEC), Enterohemorrhagic *E. coli* (EHEC) and *C. rodentium*. These bacterial pathogens

remain extracellular and remodel the enterocyte cell surface by effacing the microvilli and create a novel structure termed “pedestal” underneath them (Figure 16).

The pedestal formation depends on a T3SS, which inserts the bacterial Tir effector in the host membrane. In EPEC, Tir serves as a receptor for the bacterial surface protein Intimin (Kenny et al. 1997). Tir triggers Intimin clustering and phosphorylation by host kinases of the families Abl/Arg, Src, and Tec families (Kenny 1999). This phosphorylation results in the binding of the adaptor proteins Nck1 and 2 through their SH domains (Gruenheid et al. 2001). This leads to the further recruitment of N-WASP and ultimately to the activation of the Arp2/3 complex (Kalman et al. 1999), resulting in actin polymerization. In EHEC, Arp2/3 is activated upon the multimerization induced by the translocated bacterial protein EspFU (Campellone, Robbins, and Leong 2004).

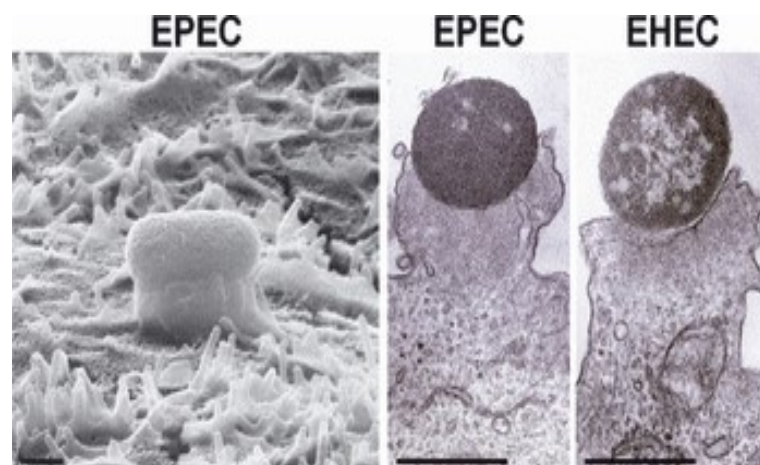


Figure 16. Pedestals formed by EPEC and EHEC. Scanning electron micrographs (left) and transmission electron microscopy (center and right) from EPEC and EHEC apposed to pedestals in intestinal cells. Modified from (Campellone et al. 2008)

1.7.5 *Salmonella* “triggered” internalization

Salmonella enterica species encompass a group of bacterial enteropathogenic strains that cause diseases in animals and humans. *S. Typhi* and a few other non-

Typhoidal serotypes can cause serious systemic disease in humans. All strains share the ability to invade intestinal epithelial cells. *S. Typhi* can also invade the spleen, liver and gallbladder (Dougan and Baker 2014). Invasion of *Salmonella* is associated with the generation of membrane ruffles around its entry site, generated by the action of injected effector proteins, by a so-called “trigger mechanism”.

Salmonella expresses a T3SS in its Pathogenicity Island 1 (SPI-1) that translocates protein effectors that manipulate the host cytoskeleton. The SopB, SopE and SopE2 effectors promote *Salmonella* uptake by host cells and a triple mutant prevents cytoskeletal remodeling and entry (Zhou et al. 2001). SopB activity as a phosphatidylinositol 4, 5 bisphosphate phosphatase leads to ruffle formation. Its activity causes the accumulation of PI3P, PI(3,4)P₂ and PI(3,4,5)P₃ (Mallo et al. 2008) which, among other effects lead to the activation of RhoG (Patel and Galán 2006).

The SopE2 and SopE effectors are GEF mimics. The former activates Cdc42 (Stender et al. 2000) and the latter activates both Cdc42 and Rac1 (Hardt et al. 1998; Friebel et al. 2001). RhoG and Rac1 activation contributes to ruffle formation and bacteria uptake, while Cdc42 activation is important for downstream signal transduction (Patel and Galán 2006). Actin is also directly targeted by *Salmonella* through SipA and SipC. SipA prevents actin depolymerization by binding to and stabilizing actin filaments (McGhie, Hayward, and Koronakis 2004) SipC, which is also part of the T3SS translocon, nucleates and bundles actin filaments (Hayward and Koronakis 1999).

1.7.6 *Shigella* Invasion and Cytoskeleton remodeling

At initial stages of the invasion process, binding of bile salts to IpaD favors exposure of IpaB at the tip complex (Epler et al. 2012). IpaB binds to the extracellular portion of the host receptor CD44 (Skoudy et al. 2000; Lafont et al. 2002). *Shigella* interacts with filopodia through the tip complex proteins IpaB and IpaD and is pulled towards the cell body (Figure 17A) (Romero et al. 2011). This interaction is mediated by a limited number of T3SS apparatus in the bacterial surface, which can withstand stall

forces exerted by retracting filopodia in the ranges of tens of picoNewtons. (Romero et al. 2012).

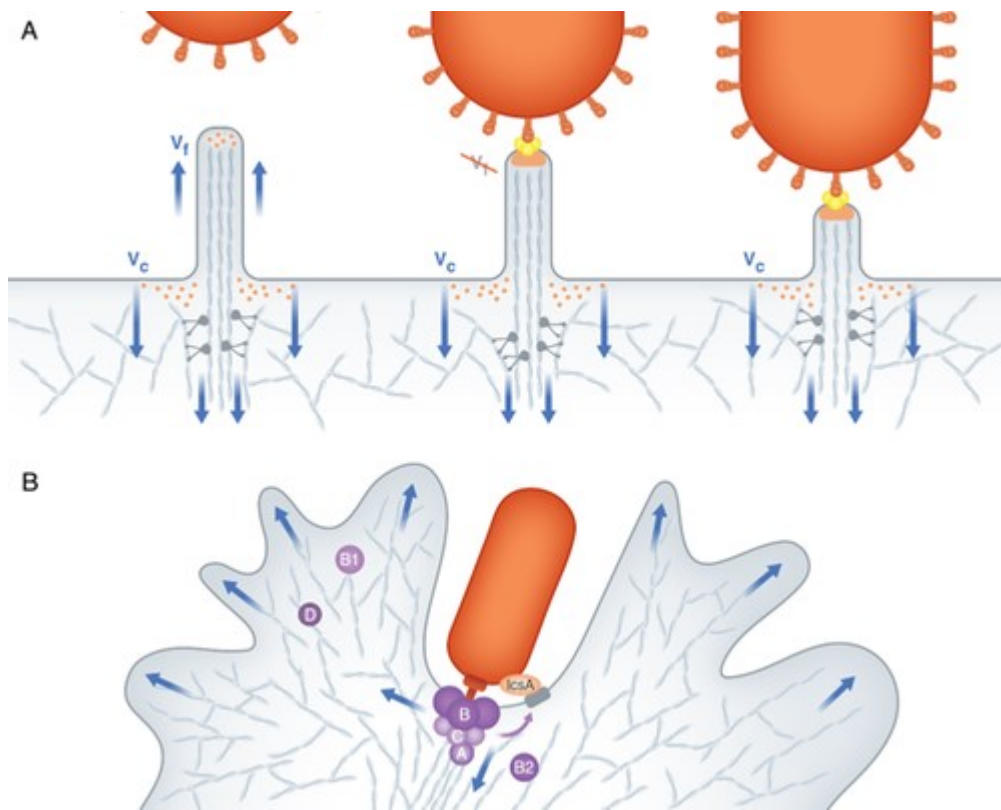


Figure 17. A. Filopodial capture. B. Effector proteins during invasion (C. M. Valencia-Gallardo, Carayol, and Van Nhieu 2015)

Although *Shigella* does not express any known adhesins, it has been reported that lcsA, an outer membrane protein involved in intracellular actin-based motility can function as an inducible adhesin under bile salts presence and dependent of the activation of the T3SS (Brotcke Zumsteg et al. 2014). Human α -defensin 5 has also been reported to enhance bacterial adhesion (D. Xu et al. 2018).

Bacterial invasion is achieved by the interplay of proteins from the first wave (Figure 16B). In addition to its role as part of the translocon, lpaC also possesses the ability to induce actin polymerization through Src (Mounier et al. 2009) and Rac (Tran Van Nhieu et al. 1999). lpgB1 and lpgB2 are GEFs that target and activate Rac1 and

RhoA, respectively (Z. Huang et al. 2009), contributing to the formation of Arp2/3-dependent membrane ruffles. IpgD has a phosphatidylinositol 4, 5 bisphosphate 4-phosphatase activity, this decreases the tethering force between the plasma membrane and the actin cytoskeleton (Niebuhr et al. 2002). IpgD also inhibits calcium signaling leading to the preservation of cell adhesion structures (Sun et al. 2017). Furthermore, its activity leads to a positive feedback loop that promotes ARF6 activation, leading to a Rac1-dependent actin remodelling (Garza-Mayers et al. 2015). IpaA role will be further discussed in detail.

Once *Shigella* is internalized inside a vacuole, it escapes into the host cytosol. The *Shigella* T3 apparatus activity has been shown to trigger vacuolar lysis (Du et al. 2016), IpgD-mediated interaction of Rab-11 containing vacuoles and macropinosomes with the bacterial vacuole might also affect the stability of the vacuole (Mellouk et al. 2014; Weiner et al. 2016).

Shigella does not express a flagellum and is non-motile in the extracellular environment. However, once free in the cytosol, *Shigella* exhibits intracellular motility. The above-mentioned outer membrane protein IcsA is expressed at one pole of the bacteria and binds N-WASP, which activates Arp2/3, leading to the formation of an actin comet tail (Egile et al. 1999). This activity is further enhanced by the T3SS-dependent recruitment of the N-WASP activator, TOCA-1 (Egile et al. 1999; Leung, Ally, and Goldberg 2008). During cell-to-cell spreading, the type 3 effectors OspE1 and OspE2 interact with PDLIM to activate protein kinase C involved in cell spreading (Defilippi et al. 1997; Yi et al. 2014). Actin polymerization by formin Dia1, which is recruited around intracellular *Shigella* by IpgB2, drives intercellular spread. (Alto et al. 2006; Heindl et al. 2010). Myosin X has also been observed to be involved in the formation of *Shigella*-containing protrusions into neighbouring cells (Bishai et al. 2013).

1.8 IpaA

IpaA is a 633 aminoacid multi-domain protein (Venkatesan and Buysse 1990). A fragment of IpaA consisting of its first 500 aminoacids activates RhoA and competes with the talin binding to the integrin $\beta 1$ subunit. This fragment inhibits $\beta 1$ integrin

anchoring to stress fibers and, together with the stimulation of actomyosin contraction, results in their disassembly (Demali, Jue, and Burridge 2006).

Early studies identified IpaA-dependent vinculin recruitment in bacterial entry foci. Of note, *ipaA* mutants display a 10-fold decrease in invasion ability (Tran Van Nhieu, Ben-Ze'ev, and Sansonetti 1997), indicating a crucial role for IpaA during *Shigella* invasion. IpaA association with vinculin N-terminal head domain was also shown to activate vinculin binding to F-actin (Bourdet-Sicard et al. 1999)

1.8.1 IpaA Vinculin Binding Sites

The region responsible in IpaA for vinculin binding and F-actin capping was mapped to the C-terminal domain (Ramarao et al. 2007), where three vinculin binding sites were identified (Figure 18A) (Park, Valencia-Gallardo, et al. 2011). These VBSs consist of amphipathic α -helices similar to the talin VBSs and were shown to be responsible for the previously observed vinculin recruitment to bacterial foci (Figure 17B) (Izard, Tran Van Nhieu, and Bois 2006). IpaA VBS1 dissociation constant (K_d) for vinculin is in the picomolar range, and is at least 10-fold lower than that reported for α -actinin VBS (P. R. J. Bois et al. 2005). VBS1 interaction with vinculin occurs through the first helical bundle of vinculin D1 domain and promotes the helical-bundle conversion associated with vinculin activation. IpaA VBS2 was shown to be able to interact with the second bundle of D1 in an additive manner (Tran Van Nhieu and Izard 2007), thereby stabilizing IpaA VBS1-2-vinculin interaction, with K_d in the femtomolar range (Izard, Tran Van Nhieu, and Bois 2006). IpaA VBS 1-2 interaction with vinculin leads to its activation and is necessary for efficient bacterial entry and cell-cell spreading.

A third VBS (VBS3) was also identified. As for IpaA VBS1, the IpaA VBS3 peptide binds to and activates vinculin (Park, Valencia-Gallardo, et al. 2011). In addition to this, it was recently shown to promote filopodial capture by targeting a partially-stretched conformer of talin (Valencia-Gallardo et al. 2019). IpaA VBS3 may stabilize filopodial tip adhesion upon bacterial capture. When filopodia retracts, IpaA VBS3 may cooperate with VBS1-2 to trigger vinculin activation and anchor the bacteria to

the cytoskeleton. In addition, IpaA might function as a scaffolding molecule, bridging vinculin through VBS1-2 and semi-stretched talin through VBS3.

A



B

VBS3 492-**I**FE**A**SKK**V**TNS**L**SN**L**IS**L**I-510
 VBS2 566-**I**Y**E**KA**K**E**V**SS**A**LS**K**VL**S**K**I**-584
 VBS1 612-**I**Y**K**AA**K**D**V**TT**S**LS**K**VL**K**NI-630
 ::: :,*:::***:::*

C

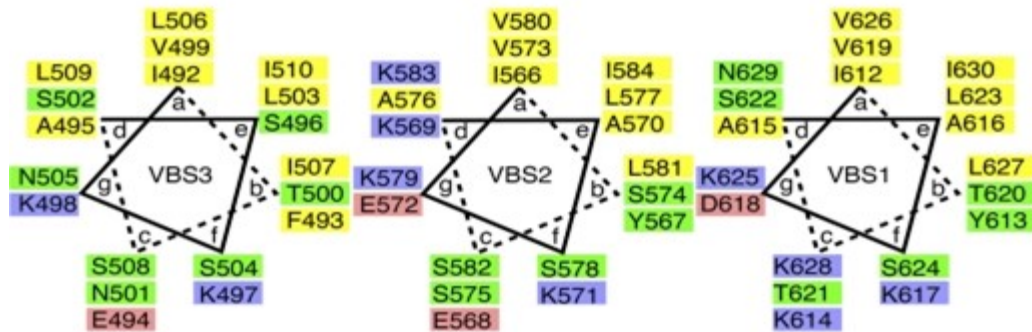


Figure 18. IpaA Vinculin Binding Sites. A. Scheme of the location of VBSs along IpaA and their aminoacid sequence. B. Alignment of the three IpaA VBSs. C. Helical wheel view of the three VBSs. Hydrophobic residues (yellow), charged residues (red and blue), polar residues (green) Modified from (Park, Valencia-Gallardo, et al. 2011)

2 Rationale of the PhD project

My PhD project aims to further understand the role of *Shigella* T3SS protein effector IpaA during *Shigella* invasion and its mechanism of action. The host laboratory has previously identified three Vinculin Binding Sites in the C-terminal extreme of IpaA, which were reported to bind to and to activate the host cell protein Vinculin (Tran Van Nhieu, Ben-Ze'ev, and Sansonetti 1997; Izard, Tran Van Nhieu, and Bois 2006; Park, Valencia-Gallardo, et al. 2011). IpaA VBS1 interacts with the first helical bundle of the D1 domain promoting conformational changes that lead to the disruption of vinculin head-tail interaction. IpaA VBS2, interacts with the second bundle of the D1 domain and, in conjunction with IpaA VBS1 results in a femtomolar affinity IpaAVBS1-2/D1 complex. IpaA VBS3, when isolated, acts as IpaA VBS1.

The team has obtained evidence of novel mechanisms of action for IpaA VBSs. First of all, IpaA VBS3 was identified to interact with talin in a two-hybrid assay. Also, structural modeling based on cross-link maps obtained from IpaVBSs subdomains interacting with vinculin indicated that IpaA interacts with vinculin in a previously undescribed manner. An IpaA subdomain containing VBSs 1 to 3 (IpaA VBS1-3) induces conformational changes on vinculin head subdomains VD1 and VD2. Further biochemical assays also indicate the formation of homotrimers induced by IpaA VBS1-3.

The main goal of my thesis consisted in describing the effects of IpaA VBSs on host cell and during *Shigella* invasion. We therefore performed microscopy analysis of mammalian cells' adhesion structures transfected with different IpaA VBSs constructions in order to characterize its impact in the cell's cytoskeleton, with emphasis on the focal adhesion proteins vinculin and talin. We also implemented a microfluidics-based adhesion assay in order to characterize the functional impact of IpaA VBSs on the host's adhesion properties.

Together with biochemical evidence, invasion assays and structural modelling, we propose that IpaA VBS3 binds to a semi stretched conformer of talin, which stabilizes filopodial tip adhesions. In addition, IpaA VBS1-3 induces conformational changes in vinculin that lead to the unfolding of the vinculin head domain. This yet unreported mode of vinculin activation likely correspond to a mode occurring during mechanotransduction, that *Shigella* bypasses through the action of IpaA. The targeting of adhesion proteins to bacterial foci would stimulate the capture of additional bacteria and modify the susceptibility of the host membrane to prime it for bacterial adhesion and anchoring. This process would be further enhanced by the injection of protein effectors by kiss-and-run bacteria.

3 Article 1

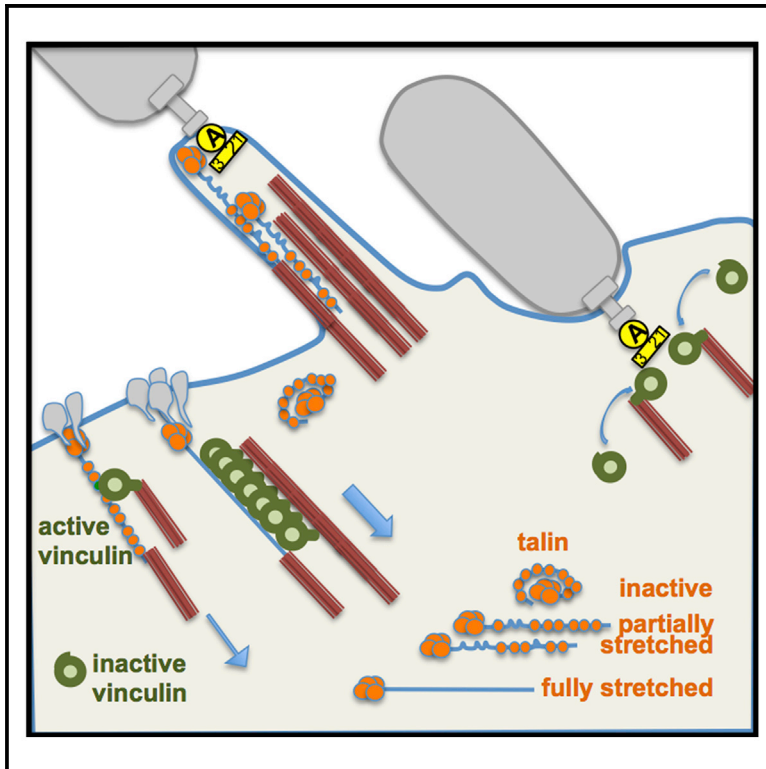
3.1 Overview

Talin was identified as a binding partner of IpaA by a two-hybrid approach. This was done by using an IpaA fragment (containing the residues 1-565 and lacking IpaA VBS1-2) as a bait against a human placental cDNA library. Further biochemical characterization identified IpaA VBS3 as the binding partner of talin H1-H4 helices, mimicking talin H5 helix. IpaA VBS3 was found to be structurally analogous to talin H5 helix, which, together with H1-H4, forms the R1 talin bundle. Functional analysis identified IpaA VBS3 is necessary for talin recruitment to *Shigella* entry foci. When expressed in human cells it also stimulates the formation of nascent adhesions and promotes filopodia. We found that IpaA VBS3 stimulates filopodial capture of bacteria and stabilizes cell adhesions in invaded cells. My contribution to this article was the conceiving and realization of experiments, generation of IpaA VBS3 and talin constructs, microscopy analysis of adhesion structures and filopodia and in bacterial adhesion assays.

Cell Reports

Shigella IpaA Binding to Talin Stimulates Filopodial Capture and Cell Adhesion

Graphical Abstract



Authors

Cesar Valencia-Gallardo,
Charles Bou-Nader,
Daniel-Isui Aguilar-Salvador, ...,
Marc Fontecave, Tina Izard,
Guy Tran Van Nhieu

Correspondence

guy.tran-van-nhieu@college-de-france.fr

In Brief

Vinculin binding sites (VBSs) present in the cytoskeletal linker talin and the *Shigella* type III effector of invasion IpaA strengthen cytoskeletal association through vinculin recruitment and activation. Here, Valencia-Gallardo et al. characterize the talin-binding property of *Shigella* IpaA VBS3 and show its relevance in filopodial adhesions and capture of bacteria.

Highlights

- *Shigella* IpaA vinculin-binding site (VBS) 3 binds to talin
- IpaA VBS3 forms a bundle with talin H1–H4 compatible with partially stretched talin
- Talin binding by IpaA VBS3 favors bacterial capture by filopodia and cell adhesions



Shigella IpaA Binding to Talin Stimulates Filopodial Capture and Cell Adhesion

Cesar Valencia-Gallardo,^{1,2,3,4} Charles Bou-Nader,^{5,6} Daniel-Isui Aguilar-Salvador,^{1,2,3,4} Nathalie Carayol,^{1,2,3,4} Nicole Quenech'Du,^{1,2,3,4} Ludovic Pecqueur,^{5,6} HaJeung Park,⁷ Marc Fontecave,^{5,6} Tina Izard,⁸ and Guy Tran Van Nhieu^{1,2,3,4,9,*}

¹Equipe Communication Intercellulaire et Infections Microbiennes, Centre de Recherche Interdisciplinaire en Biologie (CIRB), Collège de France, 75005 Paris, France

²INSERM U1050, 75005 Paris, France

³Centre National de la Recherche Scientifique UMR7241, 75005 Paris, France

⁴MEMOLIFE Laboratory of Excellence and Paris Science Lettres, 75005 Paris, France

⁵Laboratoire de Chimie des Processus Biologiques, Collège de France, 75005 Paris, France

⁶Centre National de la Recherche Scientifique UMR8229, 75005 Paris, France

⁷Macromolecular X-ray Crystallography Core, Department of Neuroscience, The Scripps Research Institute, Jupiter, FL 33458, USA

⁸Cell Adhesion Laboratory, Department of Integrative Structural & Computational Biology, The Scripps Research Institute, Jupiter, FL 33458, USA

⁹Lead Contact

*Correspondence: guy.tran-van-nhieu@college-de-france.fr

<https://doi.org/10.1016/j.celrep.2018.12.091>

SUMMARY

The *Shigella* type III effector IpaA contains three binding sites for the focal adhesion protein vinculin (VBSs), which are involved in bacterial invasion of host cells. Here, we report that IpaA VBS3 unexpectedly binds to talin. The 2.5 Å resolution crystal structure of IpaA VBS3 in complex with the talin H1–H4 helices shows a tightly folded α -helical bundle, which is in contrast to the bundle unraveling upon vinculin interaction. High-affinity binding to talin H1–H4 requires a core of hydrophobic residues and electrostatic interactions conserved in talin VBS H46. Remarkably, IpaA VBS3 localizes to filopodial distal adhesions enriched in talin, but not vinculin. In addition, IpaA VBS3 binding to talin was required for filopodial adhesions and efficient capture of *Shigella*. These results point to the functional diversity of VBSs and support a specific role for talin binding by a subset of VBSs in the formation of filopodial adhesions.

INTRODUCTION

The cytoskeletal linkers talin and vinculin play important and distinct roles in integrin-mediated cell adhesion (Atherton et al., 2016; Klapholz and Brown, 2017). Although vinculin strengthens adhesion and cytoskeletal anchorage, talin is critically required for the formation and maturation of adhesion structures (Lagarigue et al., 2016; Yan et al., 2015). Talin consists of an amino-terminal FERM domain connected to a large rod domain containing vinculin binding sites (VBSs) buried in helical bundles (Calderwood et al., 2013; Lagarigue et al., 2016; Yan et al., 2015). Upon activation, talin bridges the cytoplasmic tail of the integrin

β 1 subunit with actin filaments (Yan et al., 2015). Stretching of the talin molecule due to actomyosin-dependent contractility leads to the unveiling of VBSs buried in helical bundles along the talin rod domain (Yan et al., 2015). Upon exposure, talin VBSs activate vinculin that further tethers actin filaments to adjust adhesion strength in response to substrate stiffness (Gingras et al., 2005; Yan et al., 2015). *In vitro* measurements on single molecules indicate that unveiling of VBSs in various talin bundles occurs with a defined hierarchy, suggesting different talin activation states.

Bacterial pathogens have evolved remarkable strategies to invade host cells (Dunn and Valdivia, 2010; Pizarro-Cerdá et al., 2012). *Shigella*, the causative agent of bacillary dysentery, invades intestinal epithelial cells after being captured by filopodia using a type III secretion system (T3SS) that injects bacterial effectors into host cells (Dunn and Valdivia, 2010; Galán et al., 2014; Valencia-Gallardo et al., 2015). The *Shigella* IpaA type III effector contains three exposed VBSs located within its 145 C-terminal residues that act in concert to promote bacterial invasion (Izard et al., 2006; Park et al., 2011; Nhieu and Izard, 2007). Here, we show that in addition to vinculin, IpaA VBS3 also directly targets talin. IpaA VBS3 forms a folded globular structure with the H1–H4 helices in the talin R1 bundle, which differs from the stretched bundle structure expected during full talin activation. Our results suggest that binding of IpaA VBS3 to a semi-stretched talin conformer stabilizes filopodial adhesions and stimulates bacterial capture.

RESULTS

Talin Is Recruited by IpaA and Is Required for *Shigella* Invasion

IpaA recruits vinculin at *Shigella* invasion sites to trigger the formation of a transient adhesion required for bacterial internalization by epithelial cells (Tran Van Nhieu et al., 1997). Talin is also recruited at *Shigella* entry sites, but its role requires



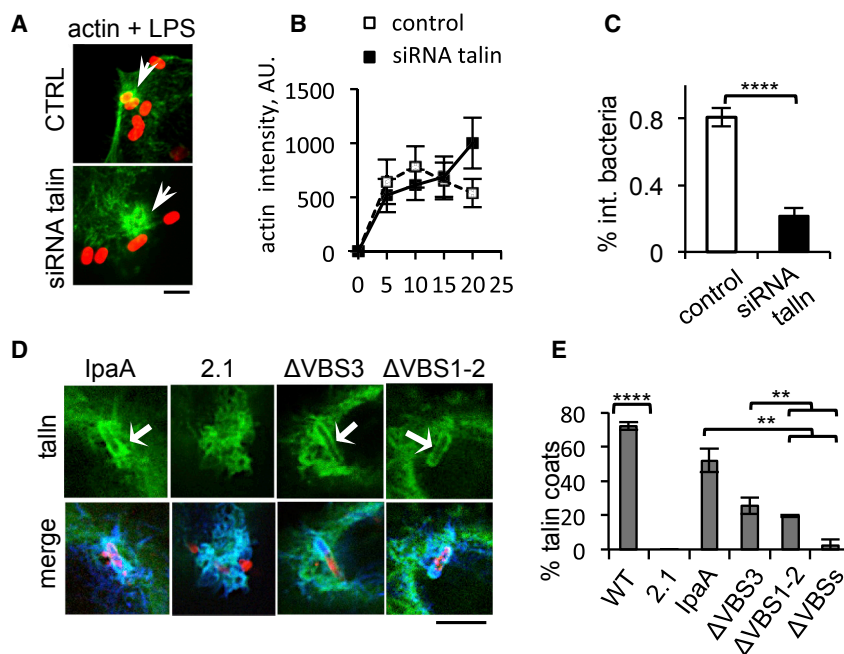


Figure 1. Talin Is Required for *Shigella* Invasion and Is Recruited in an IpaA-Dependent Manner

(A) Representative micrographs of control cells and cells treated with anti-talin siRNA prior to bacterial challenge at 37°C for 15 min. Green, actin; red, bacterial lipopolysaccharide (LPS). The arrows point to actin “cups” at bacterial cell contact (CTRL) or at the periphery of the foci (siRNA talin). Scale bar, 2 μm.

(B) The average intensity ± SEM of actin foci was determined at the indicated time points following bacterial challenge for control cells (empty squares) or anti-talin siRNA-treated cells (black squares). N = 3, >30 foci.

(C) Cells were treated with anti-talin siRNA prior to bacterial challenge at 37°C for 15 min. The percentage of internalized bacteria ± SEM after 30 min of infection with wild-type (WT) *Shigella* was determined (STAR Methods). For each sample, n > 35 foci in at least three independent experiments. ****p < 0.001, Wilcoxon test.

(D) Representative micrographs of cells were transfected with talin-GFP and challenged with *Shigella* strains for 30 min at 37°C. Red, bacterial; blue, actin; green, talin-GFP. Cells challenged with the IpaA mutant strain complemented with full-length IpaA

(Bricogne et al., 2011), vector alone (2.1), IpaA ΔVBS3, and IpaA ΔVBS1–2. The arrows point to talin coat structures surrounding invading bacteria. Scale bar, 5 μm.

(E) Average percentage of actin foci forming talin-coat structures induced by the indicated bacterial strain ± SD (STAR Methods). For each sample, n > 35 foci in at least three independent experiments. Chi-square test (χ^2) with post hoc comparison (false discovery rate [FDR] correction for p value).

clarification. When analyzed using immunofluorescence microscopy, talin was detected in coat structures around internalized bacteria as early as 10 min incubation at 37°C (Figures S1A and S1B, arrowhead). Talin recruitment and coalescing around internalized bacteria occurred concomitantly with the depolymerization of actin in membrane ruffles (Figures 1A, 1B, S1A, and S1B). Cell treatment with anti-talin small interfering RNA (siRNA) did not impair actin polymerization at *Shigella* invasion sites, but actin coat structures surrounding invading bacteria seldom formed, reminiscent of foci induced by an IpaA mutant (Figures 1A and 1B). Consistently, bacterial invasion was reduced by 4-fold in anti-talin siRNA-treated cells compared with control cells (Figure 1C). A *Shigella* IpaA mutant strain failed to form talin coats, suggesting a role for IpaA in talin recruitment at invasion sites (Figures 1D, 1E, and S1C–S1E).

To investigate the role of IpaA VBSs in the formation of talin coat structures, cells were challenged with IpaA mutant strains complemented with IpaA derivatives. Talin coat structures were not detected for the IpaA mutant complemented with vector alone or IpaA deleted for all its VBSs (Figures 1D and 1E). Complementation of the IpaA mutant with full-length IpaA, IpaA ΔVBS1–2, or IpaA ΔVBS3 restored the formation of foci with talin coat structures (Figure 1E). However, a significant decrease in the percentage of foci forming talin coat structures was observed for the IpaA mutant strains expressing IpaA ΔVBS1–2 or IpaA ΔVBS3 compared with full-length IpaA, with 19% ± 0.7% and 25% ± 5% relative to 52% ± 6.7%, respectively (Figure 1E). These results indicate that talin recruitment could

occur via IpaA VBS3 or via IpaA VBS1–2, possibly through vinculin-talin interactions.

These results indicate that talin is required for *Shigella* invasion and is recruited at entry sites in an IpaA-dependent manner to form actin coats surrounding invading bacteria.

IpaA VBS3 Binds to Talin

To confirm and further investigate how IpaA VBS3 recruited talin, we performed a yeast two-hybrid screen using an established human placental cDNA library corresponding to a total of 82.02 million prey clones and a bait containing IpaA1–565 containing the VBS3 but devoid of the VBS1–2 sites (559–633). This screen identified 150 clones representing 16 different genes. Among these, talin was identified with very high confidence in 95 prey clones, with clones corresponding to different open reading frames in talin (Table S1). As expected, vinculin was also identified as a prey (Table S1). To test whether IpaA VBS3 could directly bind to talin, we performed native gel shift assays using synthetic peptides (STAR Methods). As observed for vinculin, IpaA VBS3 did not bind to talin R1 (talin H1–H5) but formed a complex with talin H1–H4, suggesting that the targeting of active talin in which the inhibitory H5 helix is removed by mechanical stretching (Papagrigoriou et al., 2004) (Figures 2A and S4B). In contrast, even at high molar ratios, IpaA VBS1 and IpaA VBS2 did not form any detectable complex with talin H1–H4. Isothermal titration calorimetry (ITC) measurements indicated that IpaA VBS3 bound to talin H1–H4 with high affinity ($K_D = 174 \pm 19$ nM), whereas IpaA VBS2 did not show any detectable interaction with talin H1–H4 (Figure 2B; Table 1). IpaA VBS1

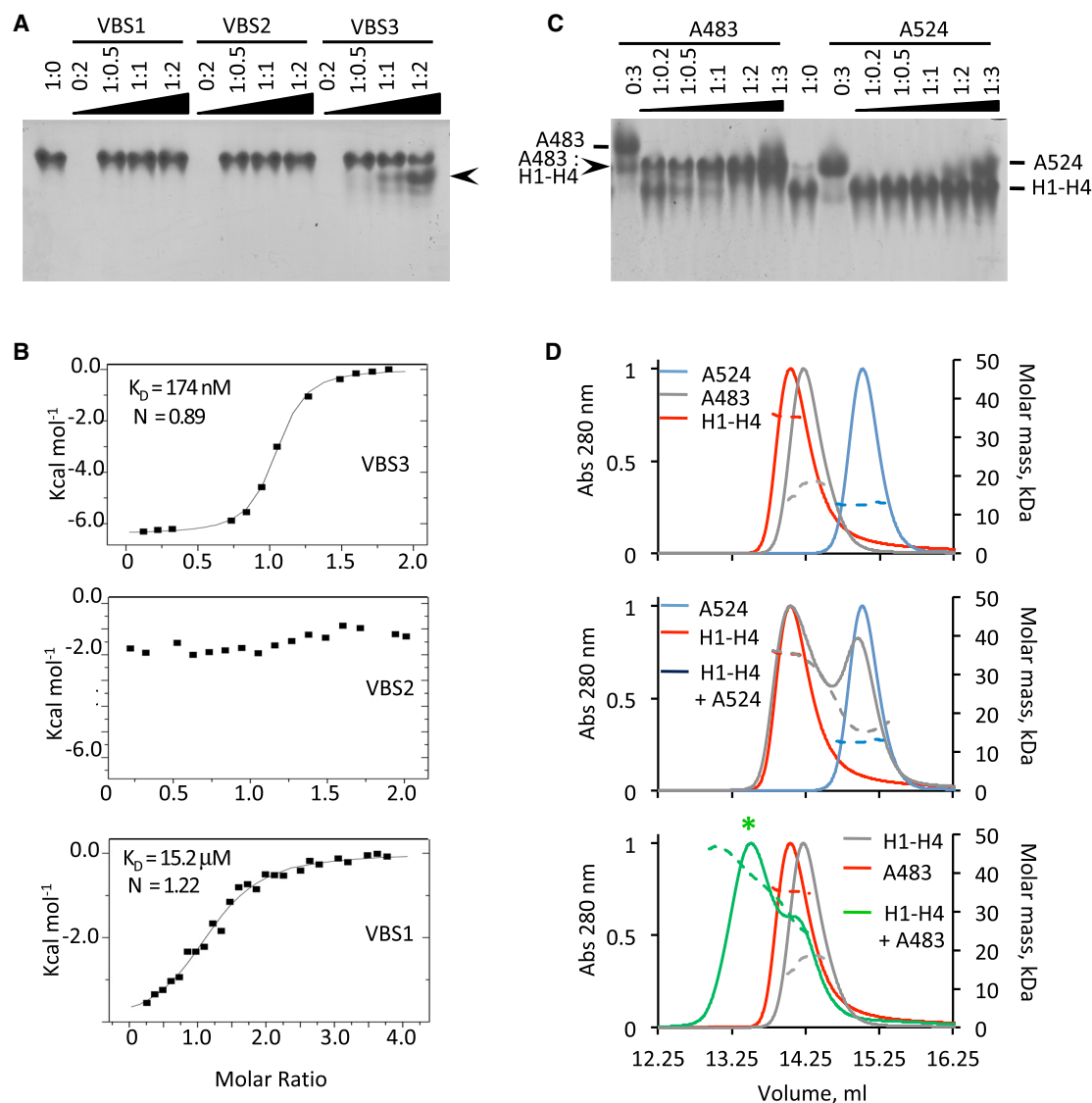


Figure 2. IpaA VBS3 Interacts with Talin

(A) Analysis of IpaA VBSs and talin H1-H4 interaction using 6%–18% gradient native PAGE. The talin H1-H4:IpaA VBS molar ratio is indicated, with 1 corresponding to a final concentration of 25 μ M. Arrowheads point to talin H1-H4 and talin H1-H4:IpaA VBS3.

(B) Isothermal titration calorimetry (ITC) analysis of the interaction between talin H1-H4 and the indicated IpaA VBSs. The estimated K_D values are indicated. IpaA VBS2 showed no binding to talin.

(C) Native PAGE analysis. The talin H1-H4:IpaA derivative molar ratios are indicated, with 1 corresponding to a final concentration of 25 μ M.

(D) SEC-MALS analysis. Indicated proteins were incubated for 60 min in column buffer prior to SEC analysis using a Superdex 200 10/300 GL increase column. Traces, normalized absorbance at 280 nm of the indicated proteins or complex species in the corresponding color. Dotted lines, molecular mass of the indicated proteins or complexes determined by MALS in the corresponding colors.

interacted with talin H1-H4 with much lower affinity than IpaA VBS3 ($K_D = 15.2 \pm 1.1$ μ M; Figure 2B; Table 1). When native gel shift assays using IpaA 483–633 containing all three VBS1–3 (A483) were performed, a clear migration shift corresponding to an A483-talin H1-H4 complex was observed with depletion of free talin H1-H4 (Figure 2C, arrowhead). In contrast, when IpaA 524–634 containing only IpaA VBS1–2 (A524) was incubated with talin H1-H4, no migration shift could be detected (Figure 2C, A524).

Size-exclusion chromatography coupled with multi-angle static light scattering (SEC-MALS) analysis indicated that A483 and A524 were monomers in solution, as indicated by the molecular mass determination (Figure 2D; Table S2). Of note, H1-H4 behaved as a globular dimer in SEC-MALS analysis (Figure 2D; Table S2), consistent with the crystal structure of talin rod 482–655 (Papagrigoriou et al., 2004). When mixed prior to analysis, only single species corresponding to the talin H1-H4 dimer or A524 monomer were recovered, consistent with the native gels

Table 1. Non-linear Fit Values for ITC Measurements

Cell	Titrant	K_D (Talin H1–H4)	N	DH (kcal/mol)	$-T\Delta S$ (kcal/mol)	ΔG (kcal/mol)	K_D (vD1)
Talin H1–H4	IpaA VBS1	$15.2 \pm 1.1 \mu\text{M}$	1.22	–4.10	–2.47	–6.57	110 pM
	IpaA VBS2	NA	NA	NA	NA	NA	6.6 nM
	IpaA VBS3	$174.5 \pm 18.9 \text{ nM}$	0.89	–6.65	–2.81	–9.47	54 pM
	IpaA VBS3 K498A	$163.1 \pm 1.1 \text{ nM}$	1.18	–6.28	–2.97	–9.26	n.d.
	IpaA VBS3 K498E	$300.3 \pm 2.8 \text{ nM}$	0.73	–12.1	3.25	–8.90	n.d.
	IpaA VBS3 R489A K498A	$328.9 \pm 1.9 \text{ nM}$	0.69	–8.68	–0.16	–8.84	n.d.
	IpaA VBS3 A495K	$2.93 \pm 0.2 \mu\text{M}$	1.05	–3.73	–3.81	–7.54	n.d.
	talin VBS46	$60 \pm 0.8 \text{ nM}$	0.92	–16.97	7.20	–9.77	3 nM
	talin VBS6	$21 \pm 3.4 \mu\text{M}$	1.26	–14.34	7.97	–6.37	n.d.
	talin VBS9	$1 \pm 0.1 \mu\text{M}$	1.29	–14.65	6.47	–8.18	n.d.
	talin VBS50	$45 \pm 7.5 \mu\text{M}$	1.02	–13.23	7.31	–5.92	99 nM
	talin VBS33	no binding	NA	NA	NA	NA	n.d.
	talin VBS36	no binding	NA	NA	NA	NA	n.d.
A483 (site 1)	talin H1–H4	$115.7 \pm 32.15 \text{ nM}$	1	–6.38	–3.07	–9.45	n.d.
A483 (site 2)		$4.6 \pm 0.6 \mu\text{M}$	1	–6.76	–5.01	–7.27	n.d.
A524 (sites 1 + 2)		$2.0 \pm 0.5 \mu\text{M}$	1.52	–3.97	–3.78	–7.76	n.d.

The affinity of synthetic peptides corresponding to talin VBS6, VBS9, VBS33, VBS36, VBS46, and VBS50 for talin H1–H4. Talin VBSs could be divided into four classes according to their affinity for talin H1–H4: whereas VBS33 and VBS36 did not show detectable binding, VBS6, VBS50, and VBS9 showed weak or moderate affinity for talin H1–H4. Talin VBS46, however, interacted with talin H1–H4 with an affinity comparable with that of IpaA VBS3, with an estimated K_D of 60 ± 0.8 (SD) nM. Although consistently displaying high affinity for vD1, IpaA and talin VBSs bound to talin H1–H4 with a broad range of K_D values. N, stoichiometry; K_D , affinity constant; DH (cal/mol), enthalpy; $-T\Delta S$ (cal/mol), entropic contribution; ΔG (cal/mol), free enthalpy; NA, not applicable; n.d., not determined. IpaA VBS3 and talin H46 binding to talin H1–H4 is exothermic ($\Delta G < 0$) and driven mainly by enthalpy ($\Delta H < 0$ and $\Delta H < -T\Delta S$). Talin H1–H4 binding to IpaA peptides VBS1 and VBS3 show an important enthalpic and minor entropic contribution. Talin H1–H4 binding to talin VBSs shows an important enthalpic contribution and an unfavorable entropic contribution to ΔG . The estimated K_D value of other talin VBSs for vinculin D1 (K_D vD1) was inferred from previous studies (Izard et al., 2006; Izard and Vornrhein, 2004; Park et al., 2011; Yogesha et al., 2012).

and ITC results (Figure 2D; Table S2). In contrast, a compact globular complex corresponding to one talin H1–H4 dimer bound to a single A483 molecule was observed (Figure 2D, talin H1–H4 + A483; Table S2). These results are in agreement with the ITC measurements and suggest that A483 strongly interacts with the talin H1–H4 via IpaA VBS3. These results indicate that in addition to vinculin, IpaA VBS3 also binds to talin with high affinity, a property not shared with other IpaA VBSs.

IpaA VBS3 Mimics Talin H5 to Form an α -Helix Bundle with Talin H1–H4

We solved the crystal structure of the IpaA VBS3–talin H1–H4 complex at 2.5 Å resolution (Table S3). The complex was purified using a strategy similar to that used for the IpaA VBS3–vD1 complex (Park et al., 2011). The asymmetric unit contains six molecules of talin H1–H4 organized into dimers as observed in SEC-MALS (Figure S2). Each talin H1–H4 molecule shows a clear additional density corresponding to the IpaA VBS3 peptide in vicinity of mainly the H2 and H4 helices (Figure S2B). All talin H1–H4 chains in the asymmetric unit were very similar with pairwise RMSDs in the range 0.28–0.64 Å over 140 C α . The interface area between IpaA VBS3 and talin H1–H4 is $849 \pm 26 \text{ Å}^2$ and involves mainly hydrophobic residues located in talin α helices H2, H3, and H4 (Figures 3A and 3B). In addition, electrostatic interactions, either direct, between K498 and E621, or indirect with R489 pointing within a negatively charged region, further

strengthen IpaA VBS3 binding and positioning in the talin H2–H4 groove (Figures 3A and 3B). Structural comparison of IpaA VBS3 in its talin-bound and vinculin-bound state (PDB: 3rf3; Figure 3B) indicates that the same IpaA VBS3 hydrophobic residues are involved in binding to talin H1–H4 and vD1. The IpaA VBS3–vinculin vD1 interaction surface area, however, is wider ($1,150 \text{ Å}^2$) than that of IpaA VBS3–talin H1–H4 and comprises IpaA residues F493, K497, and E490, which are not involved in talin H1–H4 recognition (Figure 3B). Strikingly, IpaA K498 specifically interacts with talin E621 and does not establish interaction with vD1 (Figure 3B).

Structural comparison with talin H1–H5 (Figures 3C–3E) reveals a remarkable superposition of VBS3 with H5. I492, A495, V499, L506, and I507 of IpaA VBS3 involved in hydrophobic interaction with talin H1–H4 are homologous to L637, A640, V644, L651, and L652 in the talin α -helix H5, nesting in the identical hydrophobic groove (Figures 3C–3E). Furthermore, a strong similarity in polarity is observed between talin H5 and IpaA VBS3, with IpaA R489 corresponding to talin R634 engaged in the same polar interaction with the talin H2–H3 loop.

Contact Residues in IpaA VBS3 Determining Binding Specificity for Talin

Synthetic peptides were generated to confirm the role of IpaA polar and hydrophobic residues in talin H1–H4 binding. Specifically, we tested the effects of charge at R489 and K498, and

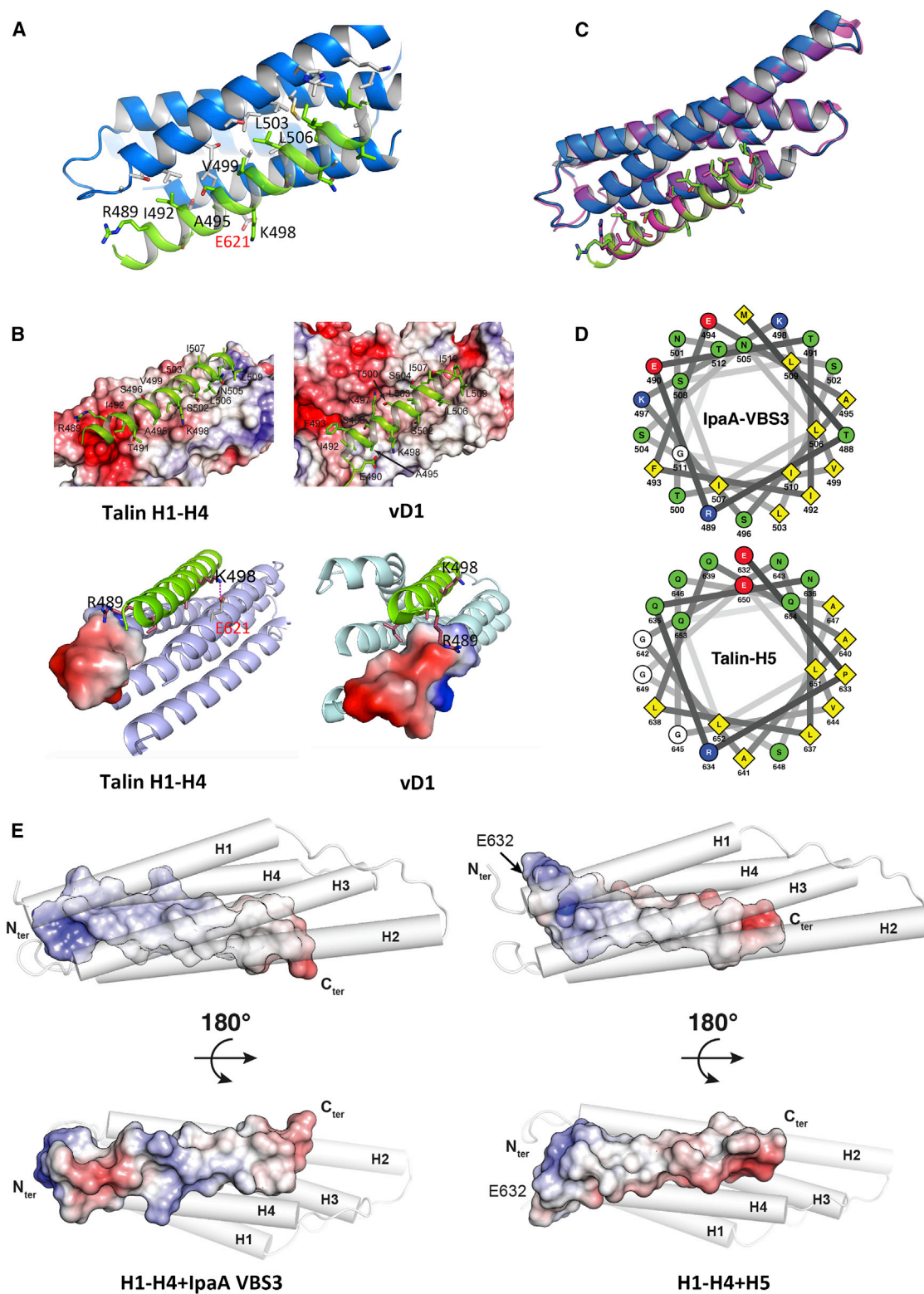


Figure 3. IpaA VBS3 Forms a Compact Fold with Talin H1–H4

(A) X-ray structure of the talin H1–H4:IpaA VBS3 complex. Blue, talin polypeptide chain; white, interacting residues; green, bound IpaA VBS3, with interacting residues in green. VBS3 residues are annotated according to full-length IpaA.

(legend continued on next page)

substitution of A495 rationalized by the structural alignment with IpaA and talin VBSs (Figure S3). ITC analysis indicated that the K498A substitution did not significantly decrease the talin-binding affinity of IpaA VBS3, possibly because of the complementary charge contribution by adjacent K497 (Table 1). The single charge inversion K498E, however, led to a 1.7-fold increase in the determined K_D ($K_D = 300 \pm 2.8$ nM) for talin H1–H4. A similar increase was observed for the charge suppressing double mutations R489A K498A with a K_D of 328 ± 1.9 nM. Consistent with a critical role for the hydrophobic interactions, the A495K substitution led to a drastic defect in IpaA VBS3 binding to talin, with a 17-fold increase in K_D ($K_D = 2.93 \pm 0.3$ μ M) (Table 1). These results were further confirmed in native gel shift experiments showing that as opposed to IpaA VBS3, IpaA VBS3 498E and IpaA VBS3 A495K did not induce any detectable shift of talin H1–H4 (Figure S4). In contrast, shifts were still observed in the presence of vD1, indicating that the mutations did not prevent complex formation with vinculin, although higher peptide concentrations were required for the A495K substitution consistent with a partial effect of this substitution on vinculin binding (Figure S4B).

Talin Binding by IpaA VBS3 Stimulates the Formation of Nascent Adhesions

Our evidence suggests that IpaA VBS3 targets an active conformer of talin containing a four-helix folded R1 bundle that differs from the “opened” configuration reported to interact with vinculin (del Rio et al., 2009; Papagrigoriou et al., 2004). To test the targeting of a specific talin conformer by IpaA VBS3, we took advantage of its high affinities for vinculin and talin and generated a GFP fusion as a probe to analyze its localization following cell transfection. As shown in Figure S5A, GFP-IpaA VBS3 labeled focal adhesions (FAs) of cells plated onto fibronectin-coated glass coverslips, showing a strict co-localization with talin and vinculin. As expected, siRNA-mediated depletion experiments showed that GFP-IpaA VBS3 labeling of adhesion structures was vinculin and talin dependent (Figure S5). When cells were plated on 15 kPa stiffness substrate, GFP-IpaA VBS3 labeled vinculin- and talin-containing adhesions at the cell periphery, including at the base of filopodia as well as at the edge of lamellae. Adhesion structures located toward the cell interior, however, were less enriched in IpaA VBS3, consistent with labeling of nascent adhesions (Figures S5E and S5F) (Benigno et al., 2001; van Hoorn et al., 2014).

In replating experiments, GFP-IpaA VBS3 labeled talin- and vinculin-containing peripheral adhesions, consistent with nascent adhesions, as well as prominent adhesions (Figures

4A–4C). As expected, control cells transfected with GFP alone showed a diffuse cytoplasmic labeling and virtually no recruitment in adhesion structures (Figures 4B and 4C). When cells were transfected with the mutated IpaA VBS3 variants, 6- and 7.8-fold reductions in the number of GFP-IpaA VBS3-positive adhesions per cell were observed for IpaA VBS3 A495K and K498E, respectively, compared with parental IpaA-VBS3 (Figures 4A–4C). In addition, the size of adhesions was significantly reduced in GFP-IpaA VBS3 A495K and K498E transfected cells compared with GFP-IpaA VBS3 transfectants (Figures 4D and 4E). Of note, while showing reduced stimulatory effects on adhesion formation, the talin-binding deficient variants A495K and K498E showed an increase in the size of FAs compared with GFP-transfected control cells, with a median \pm median absolute deviation (MAD) of 1.53 ± 0.51 and 1.21 ± 0.39 , respectively (Figures 4D and 4E), likely due to their residual vinculin-binding ability.

IpaA VBS3 Regulates Filopodial Extension through Its Talin- but Not Vinculin-Binding Activity

In replating experiments, talin was also enriched in adhesions in the filopodial shaft distal moiety, while vinculin preferentially localized at the filopodial shaft proximal moiety and base (Figure 5A), with median distances \pm MAD of 2.5 ± 1.8 and 1.7 ± 1.3 μ m, respectively (Figure 5B; STAR Methods). In addition, GFP-IpaA VBS3 was associated with distal filopodial talin adhesions, whereas association with vinculin was observed in more proximal filopodial adhesions, with a median distance of 2.8 ± 1.5 μ m compared with 1.4 ± 0.9 μ m, respectively (Figures 5C and S6). VBS3- and talin-labeled adhesions were located more distally than talin- and vinculin-labeled adhesions in filopodia, suggesting the formation of distinct complexes (Figure 5C). Consistent with different talin conformers, the canonical talin-binding domain of vinculin vD1 labeled filopodial clusters that were more proximal to the cell body than those labeled with VBS3, with median distances to the cell body of 2.5 ± 1.8 and 3.1 ± 2.2 μ m, respectively (Figure 5D). As expected, GFP alone did not label structures in filopodia (Figures 5E and S6).

To test the role of talin binding in the targeting of filopodial distal adhesions by IpaA VBS3, we analyzed the localization of the GFP-IpaA VBS3 A495K and K498E mutants. As opposed to GFP-IpaA VBS3, the mutated VBS3 variants impaired for talin binding showed a 2.7-fold decrease labeling of large filopodial adhesions (Figures 5A and 5E). Binding of vD1 to activated talin was shown to inhibit its refolding, thereby stabilizing FAs (Atherton et al., 2015; Yao et al., 2014). We therefore expected binding

(B) Molecular detail of the interaction between IpaA VBS3 with talin H1–H4 and vD1. Top: IpaA VBS3 is shown as a cartoon with its relevant interacting residues. Bottom: talin H1–H4 and vinculin D1 are illustrated by their vacuum electrostatic potential generated with APBS (Baker et al., 2001). Of note, the amino-terminal residues Thr 489 to Thr 487 of IpaA VBS3 form an additional helical turn when bound to talin H1–H4 as opposed to the vD1 complex, suggesting that this different fold further tunes recognition specificity.

(C) Superimposition of talin H1–H4:IpaA VBS3 and talin H1–H5 structures. Talin H1–H4 bound to IpaA VBS3 (green) and to talin H5 (pink) are shown as a cartoon in blue and magenta, respectively.

(D) Helical wheel analysis of IpaA VBS3 (top) and talin H5 (bottom) indicates that both are amphipathic α helices with conserved residues in their hydrophobic interphase. The hydrophobic residues, polar residues, and positively and negatively charged residues are colored yellow, green, blue, and red, respectively.

(E) Comparison of talin H1–H4 binding to IpaA VBS3 and talin H5. Talin H1–H4 is shown in white cylinder while the electrostatic surface of IpaA VBS3 and H5 are represented as calculated with APBS.

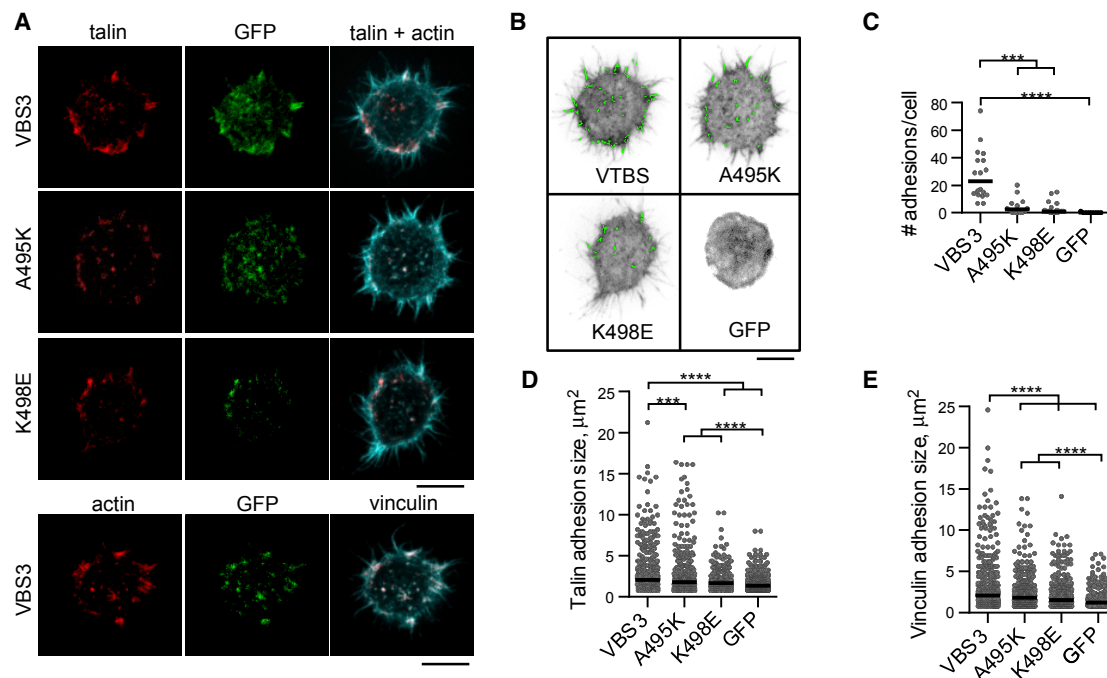


Figure 4. Talin Binding by IpaA VBS3 Promotes Focal Adhesion Formation

Cells were trypsinized and replated onto fibronectin-coated glass coverslip for 15 min prior to fixation and processing for fluorescence staining. Samples were analyzed by spinning disk microscopy. Cells were transfected with GFP: GFP-IpaA VBS3 (VBS3), A495K, or K498E variant and talin-mCherry (talin) or mCherry-vinculin (vinculin).

(A) Representative fluorescence micrographs of confocal basal planes. Scale bar, 5 μm .

(B) Wavelet spot detection (green) of adhesion structures in replated cells (STAR Methods).

(C) Distribution of cells as a function of the number of detected VBS3-labeled adhesions. Median \pm MAD: VBS3, 23 \pm 10.5 (18 cells, $n = 3$); A495K, 2.5 \pm 2.5 (14 cells, $N = 3$); K498E, 1 \pm 1 (17 cells, $N = 3$); GFP, 0 \pm 0 (9 cells, $N = 3$). *** $p < 0.005$ and **** $p < 0.001$ (Dunn's test).

(D) Size distribution of focal adhesions (FAs) for talin-mCherry transfected cells. Median \pm MAD: VBS3, 1.79 \pm 0.76 (774 FAs, $N = 3$); A495K, 1.53 \pm 0.51 (568 FAs, $N = 3$); K498E, 1.53 \pm 0.51 (383 FAs, $N = 3$); GFP, 1.29 \pm 0.39 (878 FAs, $N = 3$). *** $p < 0.005$ and **** $p < 0.001$ (Dunn's test).

(E) Size distribution of FAs for mCherry-vinculin-transfected cells. Median \pm MAD: VBS3, 2.04 \pm 0.76 (629 FAs, $N = 3$); A495K, 1.79 \pm 0.76 (595 FAs, $N = 3$); K498E, 1.53 \pm 0.51 (480 FAs, $N = 3$); GFP, 1.23 \pm 0.32 (482 FAs, $N = 3$). **** $p < 0.001$ (Dunn's test).

of IpaA VBS3 to favor filopodial extension by stabilizing filopodial adhesions. Consistently, quantification indicated that filopodia in GFP-IpaA VBS3 transfectants were longer than those observed in cells transfected with GFP-talin with median lengths \pm MAD of 4.1 \pm 1.9 and 3.4 \pm 1.9 μm , respectively (Figure 5F). Remarkably, cells transfected with GFP-IpaA VBS3 A495K and K498E showed filopodia that were significantly shorter than cells transfected with GFP-IpaA VBS3, with median lengths of 2.6 \pm 0.8 and 2.9 \pm 1 μm , respectively, and comparable with the filopodial length in cells transfected with vD1 (Figure 5F; median 2.5 \pm 1.8 μm). In control experiments, the filopodial length in cells co-transfected with GFP and mCherry-talin or vinculin-mCherry were comparable with those of GFP-talin alone or GFP-VBS3 K498E, with median lengths of 3.0 \pm 1.1 and 2.9 \pm 0.1 μm , respectively (Figure 5F).

Together, these results suggest that through talin binding, IpaA VBS3 stabilizes filopodial adhesions, thereby favoring their extension. The role of IpaA VBS3 in the regulation of both filopodial and nascent adhesions further supports the link reported between these adhesion structures (Hoffmann and Schäfer, 2010; Jacquemet et al., 2015; Partridge and Marcantonio, 2006).

Talin Binding by IpaA VBS3 Stimulates Filopodial Capture and *Shigella*-Induced Cell Adhesion Formation

Shigella invasion of epithelial cells is preceded by its capture by filopodia (Romero et al., 2011). We next analyzed the effects of GFP-IpaA VBS3 transfection in bacterial capture (Romero et al., 2011). As shown in Figure 6A, GFP-IpaA VBS3 and talin structures could be observed at the tip of 84.6% of filopodia-capturing bacteria (Figure 6A, arrowhead; 13 filopodia, $n = 3$), but only in 12.8% of filopodia devoid of bacteria (304 filopodia, $n = 3$). To test the relevance of talin binding by IpaA VBS3 during filopodial capture, cells were challenged with *ipaA* mutant strains complemented with various IpaA constructs. As shown in Figure 6B, deletion of all IpaA VBSs resulted in a 5-fold reduction in the number of bacterial capture compared with full-length IpaA. Although deletion of IpaA VBS1–2 containing VBS3 did not affect filopodial capture, deletion of IpaA VBS3 reduced filopodial capture by 2.4-fold (Figure 6B). The A495K or K498E mutations that impaired talin binding reduced filopodial capture to similar extent than IpaA Δ VBS3 (Figure 6B).

In addition to forming pseudo-adhesion structures in membrane ruffles during invasion, *Shigella* stabilizes FAs to prevent

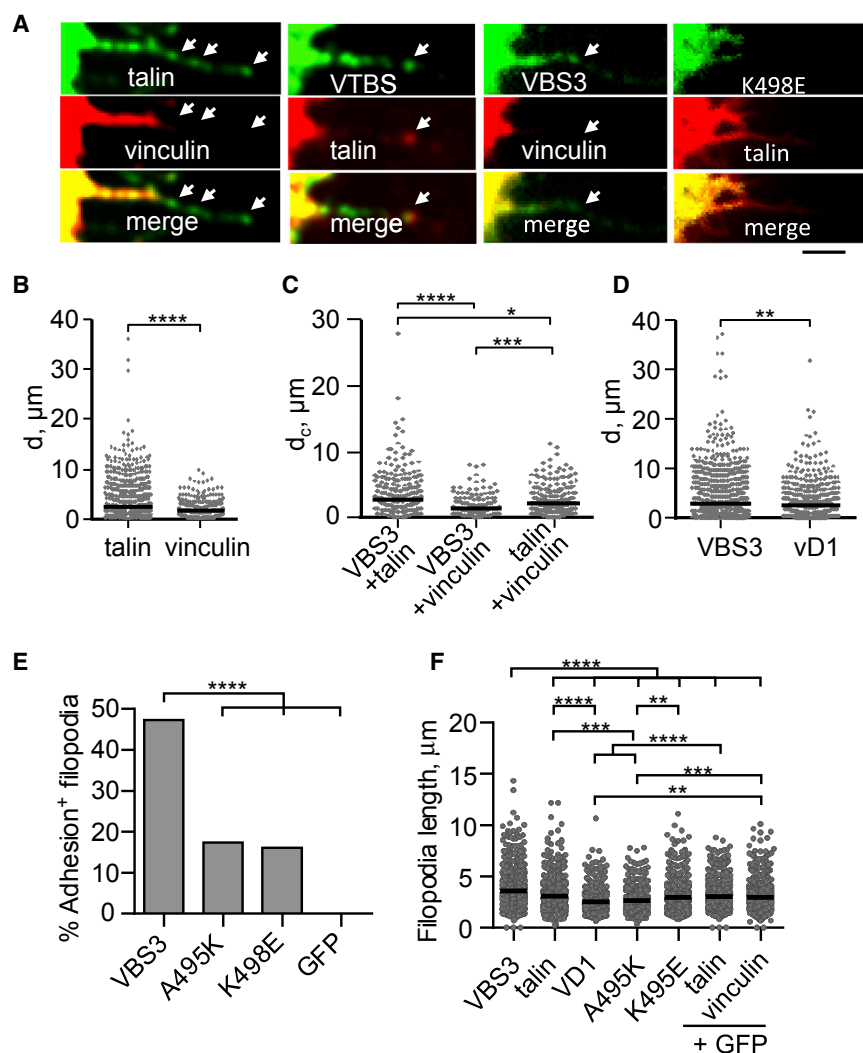


Figure 5. IpaA VBS3 Targets Talin-Containing Filopodial Adhesions

Cells transfected with vinculin-mCherry and talin-mCherry, GFP-IpaA VBS3, A495K, or K498E variants.

(A) Representative confocal micrographs. Scale bar, 5 μ m.

(B and D) Distribution of the distance relative to the cell body (d) of filopodial clusters labeled with the indicated marker in cells co-transfected with GFP-talin and vinculin-mCherry (B) and VBS3 or vD1 and vinculin-mCherry (D). Median \pm MAD: talin, 2.48 ± 1.81 (858 clusters, N = 3); vinculin, 1.71 ± 1.31 (252 clusters, N = 3); VBS3, 3.08 ± 2.22 (1,008 clusters, N = 3); vD1, 2.53 ± 1.79 (537 clusters, N = 3). **p < 0.01 and ****p < 0.001 (Mann-Whitney test).

(C) Distribution of the distance relative to the cell body (d) of filopodial clusters co-labeled with the indicated markers in co-transfected cells. Median \pm MAD: VBS3 + talin, 2.86 ± 1.49 (285 clusters, N = 3); VBS3 + vinculin, 1.43 ± 0.88 (128 clusters, N = 3); talin + vinculin, 2.32 ± 1.36 (209 clusters, N = 3). *p < 0.05, ***p < 0.005, and ****p < 0.001 (Dunn's test).

(E) Percentage of filopodia showing VBS3 clusters. VBS3 (563 filopodia, N = 3), A495K (375 filopodia, N = 3), K498E (332 filopodia, N = 3), GFP (495 filopodia, N = 3). ****p < 0.001 (Pearson's χ^2 test).

(F) Dot plot of filopodia lengths. Bar, median \pm MAD. VBS3, 34.5 ± 3.6 μ m (656 filopodia, N = 4); talin, 24.1 ± 4.4 μ m (435 filopodia, N = 4); vD1, 21.0 ± 3.6 μ m (336 filopodia, N = 3); A495K, 2.6 ± 0.9 μ m (345 filopodia, N = 3); K498E, 2.9 ± 1 μ m (434 filopodia, N = 3); GFP + talin, 3.04 ± 0.01 μ m (589 filopodia, N = 3); GFP + vinculin, 2.96 ± 0.01 μ m (516 filopodia, N = 3); **p < 0.01, ***p < 0.005, and ****p < 0.001 (Dunn's test).

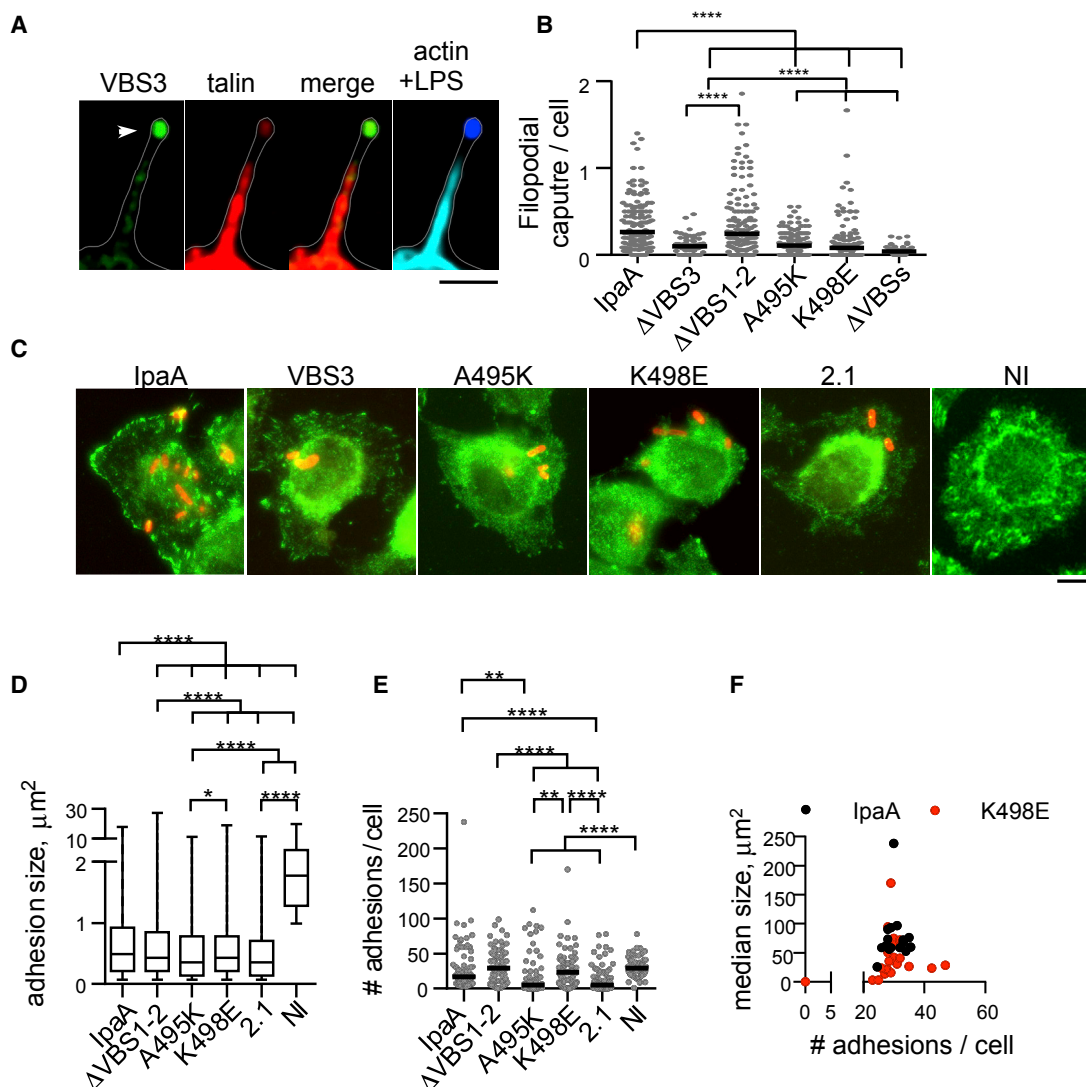
early detachment of infected cells (Sun et al., 2017). To investigate the role of IpaA VBS3 in this process, cells were challenged with bacteria for 30 min, and talin-containing adhesions were analyzed using immunofluorescence microscopy (STAR Methods). As shown in Figures 6C and 6D, while showing less FAs than uninfected cells, cells infected with the *ipaA* mutant complemented with full-length IpaA remained spread and showed large adhesion structures. In contrast, cells challenged with *ipaA* mutant complemented with vector alone showed a significant decrease in size and number of adhesions (Figures 6C and 6D). Complementation with IpaA Δ VBS1–2 containing VBS3 restored adhesion structures, although these latter were smaller than those observed for full-length IpaA (Figures 6C and 6D). Strikingly, the A495K and K498E mutations affected the IpaA VBS3-dependent formation of adhesion structures at different degrees. Cells infected with *ipaA* and IpaA Δ VBS1–2–A495K were similar to cells infected with *ipaA* complemented with vector alone, with smaller and fewer adhesion structures compared with *ipaA* and IpaA Δ VBS1–2 (Figures 6C and 6D). Complementation with IpaA Δ VBS1–2–K498E led to an intermediate phenotype with similar numbers of adhe-

sions per cell but a clear shift in the distribution toward cells showing smaller adhesions (Figures 6C–6F).

Together, these results indicate that talin binding by IpaA VBS3 plays an important role in bacterial capture by filopodia and stabilizes cell adhesions during *Shigella* infection.

DISCUSSION

Our work provides a mechanistic basis for how IpaA VBS3 acts as a dual talin-vinculin binder, a property not shared by IpaA VBS1 or IpaA VBS2. IpaA residues V499–L503–L507 are involved in interactions with talin or vinculin, suggesting that these constitute a common hydrophobic core essential for binding but not conferring specificity. Two other hydrophobic residues, IpaA I492–A495, however, appear to be specific for talin interaction. Also, electrostatic interactions involving residues IpaA R489 and K498 are important for talin specificity. Specifically, the lysine residue at position 498 in IpaA VBS3 is critical for specific and high-affinity binding to talin. The sequence alignment of IpaA and talin VBSs and ITC-based affinity measurements highlight that among the VBSs analyzed, only talin H46 share properties similar to IpaA VBS3 in binding to talin H1–H4 (Table 1;



Our structural and cell labeling data suggest that IpaA VBS3 targets an active talin conformer presenting a folded R1 bundle in filopodial distal adhesions that differs from fully active talin. Stretching experiments on purified talin bundles failed to detect intermediate steps during R1 unfolding (Yao et al., 2014, 2016). Current magnetic tweezer resolution limits, however, do not enable detection of displacement of a single helix, such as that of H5 expected to occur during IpaA VBS3 binding to R1. Recent single-molecule atomic force microscopy combined with steered molecular dynamics (SMDs), however, supported the existence of 3-helix intermediates during unfolding of the talin R9 and R11 five-helix bundles (Mykuliak et al., 2018). SMDs also predict that stronger hydrogen and salt bridge interactions between the talin H1 and H4 helices result in a torque leading to dissociation of talin H5 from H4 under applied force (Hytönen and Vogel, 2008; Lee et al., 2007), consistent with a talin conformer with a partially unfolded R1 bundle. Because of their structure, the talin R2 and R3 bundles are proposed to unfold first in response to stretching forces, leading to RIAM dissociation and vinculin binding (Goult et al., 2013b), while R1 and R10 unfold at intermediate forces (del Rio et al., 2009; Wang and Ha, 2013; Yao et al., 2014, 2016). Talin VBSs' exposure in cells, however, may be altered by ligands stabilizing talin bundles or in the talin auto-inhibited state (Goult et al., 2013a).

Early studies had pointed to a role for talin in controlling filopodial elongation and retraction (Sydor et al., 1996). In line with this, the functional analysis of mutated IpaA VBS3 indicated that talin binding is specifically required for filopodial adhesions and bacterial capture. Consistently, IpaA A495K, and K498E mutations that decrease talin-binding activity prevented the localization of IpaA VBS3 in filopodial shaft adhesions and its effects on filopodia elongation. We propose that in crawling filopodia, IpaA VBS3 favors filopodial protrusion by stabilizing talin-mediated cytoskeletal anchorage at filopodial shaft adhesions. Talin contains a C-terminal F-actin-binding domain involved in talin dimer formation (Gingras et al., 2008). It is possible that talin-talin interactions are favored during initial activation steps. Interactions between talin H1–H4 and IpaA VBS3 or talin H46 may stabilize and/or contribute to the formation of higher order talin oligomers devoid of vinculin in filopodial tip and distal adhesions, acting as a molecular clutch adapted to the low force range exerted by filopodia. Adhesions involving this talin-based clutch would serve as anchoring points favoring filopodial extension through actin polymerization at the tip of filopodia.

Unlike talin VBSs, IpaA VBSs are not buried within bundles and may bind to available ligands in an opportunistic manner. Following capture by swirling filopodia, IpaA VBS3 may bind to talin R1 to stabilize the filopodial tip adhesion. Because pathogens often mimic cellular processes, a similar role may be performed by talin H46 in the R10 bundle during filopodial sensing. Upon filopodial retraction IpaA VBS3 may cooperate with IpaA VBS1–2 to trigger vinculin activation and reinforce cytoskeletal tethering. IpaA could possibly also bridge activated vinculin through its VBS1, 2 and talin through its VBS3, thereby contributing in the cross-linking of cytoskeletal network at *Shigella* invasion sites. As force increases, further stretching of talin will lead to the dissociation of VBS3-talin recipient bundle interaction and subsequent VBS-vinculin interaction, in line with the enrichment of vinculin at proximal filopodial shaft and basal adhesions.

STAR★METHODS

Detailed methods are provided in the online version of this paper and include the following:

- KEY RESOURCES TABLE
- CONTACT FOR REAGENT AND RESOURCE SHARING
- EXPERIMENTAL MODEL AND SUBJECT DETAILS
 - Cell lines
 - Bacterial strains
- METHOD DETAILS
 - Antibodies
 - Generation of expression constructs
 - Yeast double hybrid analysis
 - Protein purification
 - Native-PAGE analysis
 - SEC-MALS
 - Crystallization, structure determination, and crystallographic refinement
 - Isothermal titration calorimetry
 - siRNA transfection
 - Cell challenge with *Shigella* strains
 - Immunofluorescence microscopy analysis
 - Image processing and analysis
- QUANTIFICATION AND STATISTICAL ANALYSIS
- DATA AND SOFTWARE AVAILABILITY

SUPPLEMENTAL INFORMATION

Supplemental Information includes three tables and seven figures and can be found with this article online at <https://doi.org/10.1016/j.celrep.2018.12.091>.

ACKNOWLEDGMENTS

We thank Dr. Olivera Francetic for careful reading of the manuscript and Dr. David Stroebel (IBENS) for his help with ITC measurements. This work benefited from the facilities of Plateforme de Mesures d'Interaction des Macromolécules (PIM), I2BC, and Plateforme de Proteomique (Ecole Normale Supérieure). We acknowledge SOLEIL for provision of synchrotron radiation facilities (proposal ID 20150780), and we would like to thank the Proxima 1 team for assistance in using the beamline. This work was supported by grants from INSERM, CNRS, and Collège de France to the CIRB, as well as a grant from PSL Idex project "Shigaforce." C.V.-G. is a recipient of a PhD fellowship from Memolife Labex and a post-doctoral fellowship from PSL Idex. N.C. is a recipient of an IRG Marie-Curie fellowship. D.-I.A.-S. is funded by CONACYT and the Labex Memolife international PhD program.

AUTHOR CONTRIBUTIONS

N.C., N.Q., L.P., and H.P. performed and analyzed experiments. M.F. and T.I. analyzed experiments. C.V.-G., C.B.-N., D.-I.A.-S., and G.T.V.N. performed and analyzed experiments and wrote the manuscript.

DECLARATION OF INTERESTS

The authors declare no competing interests.

Received: July 6, 2018

Revised: November 7, 2018

Accepted: December 20, 2018

Published: January 22, 2019

REFERENCES

- Atherton, P., Stutchbury, B., Wang, D.Y., Jethwa, D., Tsang, R., Meiler-Rodriguez, E., Wang, P., Bate, N., Zent, R., Barsukov, I.L., et al. (2015). Vinculin controls talin engagement with the actomyosin machinery. *Nat. Commun.* **6**, 10038.
- Atherton, P., Stutchbury, B., Jethwa, D., and Ballestrem, C. (2016). Mechano-sensitive components of integrin adhesions: Role of vinculin. *Exp. Cell Res.* **343**, 21–27.
- Baker, N.A., Sept, D., Joseph, S., Holst, M.J., and McCammon, J.A. (2001). Electrostatics of nanosystems: application to microtubules and the ribosome. *Proc. Natl. Acad. Sci. USA* **98**, 10037–10041.
- Beningo, K.A., Dembo, M., Kaverina, I., Small, J.V., and Wang, Y.L. (2001). Nascent focal adhesions are responsible for the generation of strong propulsive forces in migrating fibroblasts. *J. Cell Biol.* **153**, 881–888.
- Bricogne, G., Blanc, E., Brandl, M., Flensburg, C., Keller, P., Paciorek, P., Ro-versi, P., Sharff, A., Smart, O.S., Vornrhein, C., and Womack, T.O. (2011). BUSTER version 2.9 (Cambridge, UK: Global Phasing Ltd.). <https://www.globalphasing.com/buster/>.
- Calderwood, D.A., Campbell, I.D., and Critchley, D.R. (2013). Talins and kindlins: partners in integrin-mediated adhesion. *Nat. Rev. Mol. Cell Biol.* **14**, 503–517.
- de Chaumont, F., Dallongeville, S., Chenouard, N., Hervé, N., Pop, S., Provoost, T., Meas-Yedid, V., Pankajakshan, P., Lecomte, T., Le Montagner, Y., et al. (2012). Icy: an open bioimage informatics platform for extended reproducible research. *Nat. Methods* **9**, 690–696.
- del Rio, A., Perez-Jimenez, R., Liu, R., Roca-Cusachs, P., Fernandez, J.M., and Sheetz, M.P. (2009). Stretching single talin rod molecules activates vinculin binding. *Science* **323**, 638–641.
- Dunn, J.D., and Valdivia, R.H. (2010). Uncivil engineers: Chlamydia, Salmonella and Shigella alter cytoskeleton architecture to invade epithelial cells. *Future Microbiol.* **5**, 1219–1232.
- Emsley, P., Lohkamp, B., Scott, W.G., and Cowtan, K. (2010). Features and development of Coot. *Acta Crystallogr. D Biol. Crystallogr.* **66**, 486–501.
- Galán, J.E., Lara-Tejero, M., Marlovits, T.C., and Wagner, S. (2014). Bacterial type III secretion systems: specialized nanomachines for protein delivery into target cells. *Annu. Rev. Microbiol.* **68**, 415–438.
- Gingras, A.R., Ziegler, W.H., Frank, R., Barsukov, I.L., Roberts, G.C., Critchley, D.R., and Emsley, J. (2005). Mapping and consensus sequence identification for multiple vinculin binding sites within the talin rod. *J. Biol. Chem.* **280**, 37217–37224.
- Gingras, A.R., Bate, N., Goult, B.T., Hazelwood, L., Canestrelli, I., Grossmann, J.G., Liu, H., Putz, N.S., Roberts, G.C., Volkman, N., et al. (2008). The structure of the C-terminal actin-binding domain of talin. *EMBO J.* **27**, 458–469.
- Goult, B.T., Xu, X.P., Gingras, A.R., Swift, M., Patel, B., Bate, N., Kopp, P.M., Barsukov, I.L., Critchley, D.R., Volkman, N., and Hanein, D. (2013a). Structural studies on full-length talin1 reveal a compact auto-inhibited dimer: implications for talin activation. *J. Struct. Biol.* **184**, 21–32.
- Goult, B.T., Zacharchenko, T., Bate, N., Tsang, R., Hey, F., Gingras, A.R., Elliott, P.R., Roberts, G.C., Ballestrem, C., Critchley, D.R., and Barsukov, I.L. (2013b). RIAM and vinculin binding to talin are mutually exclusive and regulate adhesion assembly and turnover. *J. Biol. Chem.* **288**, 8238–8249.
- Hoffmann, B., and Schäfer, C. (2010). Filopodial focal complexes direct adhesion and force generation towards filopodia outgrowth. *Cell Adhes. Migr.* **4**, 190–193.
- Hytönen, V.P., and Vogel, V. (2008). How force might activate talin's vinculin binding sites: SMD reveals a structural mechanism. *PLoS Comput. Biol.* **4**, e24.
- Izard, T., and Vornrhein, C. (2004). Structural basis for amplifying vinculin activation by talin. *J. Biol. Chem.* **279**, 27667–27678.
- Izard, T., Tran Van Nhieu, G., and Bois, P.R. (2006). Shigella applies molecular mimicry to subvert vinculin and invade host cells. *J. Cell Biol.* **175**, 465–475.
- Jacquemet, G., Hamidi, H., and Ivaska, J. (2015). Filopodia in cell adhesion, 3D migration and cancer cell invasion. *Curr. Opin. Cell Biol.* **36**, 23–31.
- Kabsch, W. (2010). XDS. *Acta Crystallogr. D Biol. Crystallogr.* **66**, 125–132.
- Klapholz, B., and Brown, N.H. (2017). Talin—the master of integrin adhesions. *J. Cell Sci.* **130**, 2435–2446.
- Lagarrigue, F., Kim, C., and Ginsberg, M.H. (2016). The Rap1-RIAM-talin axis of integrin activation and blood cell function. *Blood* **128**, 479–487.
- Lee, S.E., Kamm, R.D., and Moirad, M.R. (2007). Force-induced activation of talin and its possible role in focal adhesion mechanotransduction. *J. Biomech.* **40**, 2096–2106.
- McCoy, A.J., Grosse-Kunstleve, R.W., Adams, P.D., Winn, M.D., Storoni, L.C., and Read, R.J. (2007). Phaser crystallographic software. *J. Appl. Cryst.* **40**, 658–674.
- Mykuliak, V.V., Haining, A.W.M., von Essen, M., Del Rio Hernández, A., and Hytönen, V.P. (2018). Mechanical unfolding reveals stable 3-helix intermediates in talin and α -catenin. *PLoS Comput. Biol.* **14**, e1006126.
- Nhieu, G.T., and Izard, T. (2007). Vinculin binding in its closed conformation by a helix addition mechanism. *EMBO J.* **26**, 4588–4596.
- Papagrigoriou, E., Gingras, A.R., Barsukov, I.L., Bate, N., Fillingham, I.J., Patel, B., Frank, R., Ziegler, W.H., Roberts, G.C., Critchley, D.R., and Emsley, J. (2004). Activation of a vinculin-binding site in the talin rod involves rearrangement of a five-helix bundle. *EMBO J.* **23**, 2942–2951.
- Park, H., Valencia-Gallardo, C., Sharff, A., Tran Van Nhieu, G., and Izard, T. (2011). Novel vinculin binding site of the IpaA invasin of Shigella. *J. Biol. Chem.* **286**, 23214–23221.
- Partridge, M.A., and Marcantonio, E.E. (2006). Initiation of attachment and generation of mature focal adhesions by integrin-containing filopodia in cell spreading. *Mol. Biol. Cell* **17**, 4237–4248.
- Pizarro-Cerdá, J., Kühbacher, A., and Cossart, P. (2012). Entry of *Listeria monocytogenes* in mammalian epithelial cells: an updated view. *Cold Spring Harb. Perspect. Med.* **2**, a010009.
- Ramarao, N., Le Clainche, C., Izard, T., Bourdet-Sicard, R., Ageron, E., Sansonetti, P.J., Carlier, M.F., and Tran Van Nhieu, G. (2007). Capping of actin filaments by vinculin activated by the Shigella IpaA carboxyl-terminal domain. *FEBS Lett.* **581**, 853–857.
- Romero, S., Grompone, G., Carayol, N., Mounier, J., Guadagnini, S., Prevost, M.C., Sansonetti, P.J., and Van Nhieu, G.T. (2011). ATP-mediated Erk1/2 activation stimulates bacterial capture by filopodia, which precedes Shigella invasion of epithelial cells. *Cell Host Microbe* **9**, 508–519.
- Romero, S., Quatela, A., Bornschlög, T., Guadagnini, S., Bassereau, P., and Tran Van Nhieu, G. (2012). Filopodium retraction is controlled by adhesion to its tip. *J. Cell Sci.* **125**, 4999–5004.
- Schägger, H., Cramer, W.A., and von Jagow, G. (1994). Analysis of molecular masses and oligomeric states of protein complexes by blue native electrophoresis and isolation of membrane protein complexes by two-dimensional native electrophoresis. *Anal. Biochem.* **217**, 220–230.
- Sun, C.H., Wacquier, B., Aguilar, D.I., Carayol, N., Denis, K., Boucherie, S., Valencia-Gallardo, C., Simsek, C., Erneux, C., Lehman, A., et al. (2017). The Shigella type III effector IpgD recodes Ca^{2+} signals during invasion of epithelial cells. *EMBO J.* **36**, 2567–2580.
- Sydney, A.M., Su, A.L., Wang, F.S., Xu, A., and Jay, D.G. (1996). Talin and vinculin play distinct roles in filopodial motility in the neuronal growth cone. *J. Cell Biol.* **134**, 1197–1207.
- Tran Van Nhieu, G., Ben-Ze'ev, A., and Sansonetti, P.J. (1997). Modulation of bacterial entry into epithelial cells by association between vinculin and the Shigella IpaA invasin. *EMBO J.* **16**, 2717–2729.
- Valencia-Gallardo, C.M., Carayol, N., and Tran Van Nhieu, G. (2015). Cytoskeletal mechanics during Shigella invasion and dissemination in epithelial cells. *Cell. Microbiol.* **17**, 174–182.
- van Hooft, H., Harkes, R., Spiesz, E.M., Storm, C., van Noort, D., Ladoux, B., and Schmidt, T. (2014). The nanoscale architecture of force-bearing focal adhesions. *Nano Lett.* **14**, 4257–4262.

- Wang, X., and Ha, T. (2013). Defining single molecular forces required to activate integrin and notch signaling. *Science* 340, 991–994.
- Yan, J., Yao, M., Goult, B.T., and Sheetz, M.P. (2015). Talin dependent mechanosensitivity of cell focal adhesions. *Cell. Mol. Bioeng.* 8, 151–159.
- Yao, M., Goult, B.T., Chen, H., Cong, P., Sheetz, M.P., and Yan, J. (2014). Mechanical activation of vinculin binding to talin locks talin in an unfolded conformation. *Sci. Rep.* 4, 4610.
- Yao, M., Goult, B.T., Klapholz, B., Hu, X., Toseland, C.P., Guo, Y., Cong, P., Sheetz, M.P., and Yan, J. (2016). The mechanical response of talin. *Nat. Commun.* 7, 11966.
- Yogesha, S.D., Rangarajan, E.S., Vonnrhein, C., Bricogne, G., and Izard, T. (2012). Crystal structure of vinculin in complex with vinculin binding site 50 (VBS50), the integrin binding site 2 (IBS2) of talin. *Protein Sci.* 21, 583–588.

STAR★METHODS

KEY RESOURCES TABLE

REAGENT or RESOURCE	SOURCE	IDENTIFIER
Antibodies		
anti- <i>Shigella</i> serotype V LPS rabbit antibody	Tran Van Nhieu et al., 1997	N/A
mouse monoclonal anti-talin clone 8d4 antibody	Sigma-Aldrich	Cat# T3287-2ML; RRID:AB_535866
DyLight 405 AffiniPure Goat Anti-Rabbit IgG	Jackson Immunoresearch	Cat# 111-475-045
Alexa Fluor® 488 AffiniPure Donkey Anti-Mouse IgG	Jackson Immunoresearch	Cat# 715-545-150
Alexa Fluor 647 Phalloidin	Invitrogen	Cat# A22287
Bacterial and Virus Strains		
<i>Shigella flexneri</i> M90T	Park et al., 2011	N/A
<i>Shigella flexneri</i> AfaE	Park et al., 2011	N/A
<i>Shigella flexneri</i> IpaA ⁻	Park et al., 2011	N/A
<i>Shigella flexneri</i> IpaA ⁻ :2.1	This paper	N/A
<i>Shigella flexneri</i> IpaA ⁻ : IpaA	This paper	N/A
<i>Shigella flexneri</i> IpaA ⁻ :ΔVTBS	This paper	N/A
<i>Shigella flexneri</i> IpaA ⁻ :ΔVBS 1-2	This paper	N/A
<i>Shigella flexneri</i> IpaA ⁻ ΔVBSs	This paper	N/A
Chemicals, Peptides, and Recombinant Proteins		
Talin H1-H4	This paper	N/A
IpaA483	This paper	N/A
IpaA524	This paper	N/A
IpaA VTBS (N-TRETIFEASKKVTNSLSNLISLIGT-C, 488-512)	This paper	N/A
VTBS variant K9498A (N-TRETIFEASKA VTNSLSNLISLIGT-C)	This paper	N/A
VTBS variant K498E (N-TRETIFEASKEVTN SLSNLISLIGT-C)	This paper	N/A
VTBS variant R489A K498A (N-TAETIFEASKAVTN SLSNLISLIGT-C)	This paper	N/A
VTBS variant A495K (N-TRETIFEKSKKVT NSLSNLISLIGT-C)	This paper	N/A
Talin peptide VBS46 (N-YTKKELIECARRVSE KVSHVLAALQ-C, 1945-1970)	This paper	N/A
Talin VBS6 (N-FQDVLMQLANAVAS AAAALVLKAKS-C, 664-689)	This paper	N/A
Talin VBS9 (N-RGVGAAATAVTQAL NELLQHVKAH-C, 765-789)	This paper	N/A
Talin (N-NLKSQLAAAAARAVTDSINQLITMCT-C, 1330-1357)	This paper	N/A
Talin VBS50 (N-QVVLINAVKDVAKALG DLISATKAA-C, 2077-2102)	This paper	N/A
Critical Commercial Assays		
Yeast two-hybrid assay IpaA1-565	Hybrigenics services	N/A
Deposited Data		
<i>Shigella</i> IpaA-VBS3/TBS in complex with the Talin VBS1 domain 488-512 (structure)	This paper	PDB: 5NL1

(Continued on next page)

Continued		
REAGENT or RESOURCE	SOURCE	IDENTIFIER
Experimental Models: Cell Lines		
HeLa cells	ATCC	CCL-2
Mouse Embryo Fibroblast cells	ATCC	N/A
Oligonucleotides		
Primers targeting Human vinculin Forward: CTGTGCGACTGATGCCAGTGTTCATACG Reverse: CTCCCGGGTCTGGTACCAGGG AGTCTTTC	This Paper	N/A
Primers targeting IpaA 483: Forward: GGCGAATTCGAGACACATATT TAACACG Reverse: GCCGTCGACTTAA TCCTTATTGATATTCT	This paper	N/A
Primers targeting IpaA 483: Forward: GCGAT ATCATGGCCAGCAAAGG Reverse: GCGC GGCCGCTTAATCCTTATTGATATTC	This paper	N/A
Primers targeting IpaAVTBS: Forward: ACCCGGGGATTAAGCGGCC Reverse: ACCCGGGATCCTGATTTAGTTCC	This paper	N/A
Primers for VTBS A495K mutation: Forward: CACGGGAAACGATATTTGAAAAATCAAAA AAGTAACAACTC Reverse: GAGTTTGTTA CTTTTTTGATTTTTCAAATATCGTTTCCCGTG	This paper	N/A
Primers for VTBS K498E mutation: Forward: CGATATTTGAAGCTTCAAAGAAGTAACA ACAACTCCCTAA Reverse: TTAGGG AGTTTGTTGTTACTTCTTTGAAGCTT CAAATATCG	This paper	N/A
Primers for pET28a-IpaA-VBS3/VTBS-talinH1-H4 bicistronic construction: Forward: CGAATTCAG GAGGACAGCTATGCACCGAGGACACATG Reverse: CGAGCTCGTTACTGACGGGGCT CAGCACTG	This paper	N/A
Stealth Select Anti-Talin1 siRNA	Invitrogen	Cat# 1299003
Stealth Select Anti-vinculin siRNA	Invitrogen	Cat# 1299001
Recombinant DNA		
Human Vinculin-mCherry	This paper	N/A
Human talin-GFP	Laboratory of Ken Yamada	N/A
A483-GST	This paper	N/A
GFP-A483-633	This paper	N/A
GFP-IpaAVTBS	This paper	N/A
talin VBS1 (H1-H4) 482-636	Izard et al., 2006	N/A
GST-IpaA 524-633	Izard et al., 2006	N/A
IpaA-VBS1 (611-633)	Izard et al., 2006	N/A
IpaA- VBS2 (565-586)	Izard et al., 2006	N/A
pET28a-IpaA-VBS3/VTBS-talinH1-H4	This paper	N/A
Software and Algorithms		
Icy Bioimaging Analysis software	de Chaumont et al., 2012	N/A
XDS	Kabsch 2010	http://xds.mpimf-heidelberg.mpg.de/

(Continued on next page)

Continued

REAGENT or RESOURCE	SOURCE	IDENTIFIER
STARANISO	Global Phasing Limited	http://staraniso.globalphasing.org/cgi-bin/staraniso.cgi
Phaser	McCoy et al., 2007	http://www.phaser.cimr.cam.ac.uk/index.php/Phaser_Crystallographic_Software
autoBuster	Global Phasing Limited	https://www.globalphasing.com/buster/
Coot	Emsley et al., 2010	https://www2.mrc-lmb.cam.ac.uk/personal/pemsley/coot/

CONTACT FOR REAGENT AND RESOURCE SHARING

Further information and requests for resources and reagents should be directed to and will be fulfilled by the Lead Contact, Guy Tran van Nhieu (guy.tran-van-nhieu@college-de-france.fr).

EXPERIMENTAL MODEL AND SUBJECT DETAILS

Cell lines

HeLa cells (ATCC CCL-2) were incubated in RPMI (Roswell Park Memorial Institute) medium containing 5% FCS (fetal calf serum, GIBCO®) in an incubator with 5% CO₂. Mouse Embryo Fibroblast (MEF) cells were incubated in DMEM (11965092, GIBCO) medium containing 10% FCS (fetal calf serum, GIBCO®) in an incubator with 5% CO₂.

Bacterial strains

The wild-type *Shigella flexneri*, isogenic mutants, and complemented *ipaA* mutant strains, as well as wild-type *Shigella* expressing the AfaE adhesin were previously described (Park et al., 2011). Bacterial strains were cultured in trypticase soy broth (TCS) medium at 37°C. When specified, antibiotics were added at the following concentrations: carbenicillin 100 µg/ml, kanamycin 20 µg/ml.

METHOD DETAILS

Antibodies

The anti-*Shigella* serotype V LPS rabbit antibody was described previously (Tran Van Nhieu et al., 1997). The mouse monoclonal anti-talin clone 8d4 antibody was from Sigma-Aldrich. Alexa 405 coupled anti-rabbit and Alexa 488 coupled anti-mouse IgGs were from Jackson ImmunoResearch. Alexa 647-coupled phalloidin was from Invitrogen.

Generation of expression constructs

Full-length human vinculin-mCherry (residues 1-1066) was generated by polymerase chain reaction using 5'-CTGTCGACTGATGC CAGTGTTCATACG-3' / 5'-CTCCCGGGTCTGGTACCAGGGAGTCTTTC-3' primers and cloned into the pmCherry-N1 (Clontech) vector using the Sall - Sma sites. Human talin-mCherry was from Addgene. Human talin-GFP was a gift from K. Yamada. The A483 construct was PCR amplified using 5'-GGCGAATCCCGGAGACACATATTTAACACG -3' / 5'-GCCGTCGACTTAATCCT TATTGATATTCT -3' primers and cloned into the EcoRI - Sall sites of pGEX-4T-2 (GE Lifesciences). The GFP-A483 plasmid was generated by PCR amplification using the 5'-GCGATATCATGGCCAGCAAAGG-3' and 5'-GCGCGGCCGCTTAATCCTTATTGA TATTC-3' primers and cloned into a pcDNA3.1 NT-GFP Topo (Invitrogen). The GFP-IpaAVBS3 plasmid was generated by PCR amplification using the 5'-ACCCGGGGATTAAGCGGCC-3' and 5'-ACCCGGGATCCTGATTTAGTTCC-3' primers and the GFP-A483 plasmid as matrix. The amplicon was digested with SmaI and ligated using a T4 DNA Ligase. Mutagenesis to generate the GFP-IpaA VBS3 A495K and K498E variants was performed using the following pairs of primers 5'-CACGGGAAACGATATTTGAAAAAT CAAAAAAGTAACAACTC-3'; 5'-GAGTTTGTTACTTTTTTGTATTTTCAAATATCGTTTCCCGTG-3', and 5'-CGATATTTGAAGCTT CAAAAGAAGTAACAACAACTCCCTAA-3' and 5'-TTAGGGAGTTTGTGTTACTTCTTTGAAGCTTCAAATATCG-3', respectively, using the Quickchange II site-directed mutagenesis procedure (Stratagene). All other enzymes were from New England Biolabs. Plasmids containing talin VBS1 (H1-H4) residues 482-636 and GST-IpaA 524-633, as well as peptides IpaA-VBS1 (611-633) and VBS2 (565-586) were previously described (Izard et al., 2006; Papagrigoriou et al., 2004; Ramarao et al., 2007; Tran Van Nhieu and Izard, 2007). IpaA VBS3 (N-TRETIFEASKKVTNSLSNLSLIGT-C, 488-512), and VBS3 variant peptides K9498A (N-TRETIFEAS KAVTNSLSNLSLIGT-C), K498E (N-TRETIFEASKEVTNSLSNLSLIGT-C), R489A K498A (N-TAETIFEASKAVTNSLSNLSLIGT-C) and A495K (N-TRETIFEKSKKVTNSLSNLSLIGT-C) were synthesized by Genscript USA Inc. Talin peptides VBS46 (N-YTKKELIE CARRVSEKVVSHVLAALQ-C, 1945-1970), Talin VBS6 (N-FQDVLMQLANAVASAAAALVLAKS-C, 664-689), Talin VBS9 (N-RGVGAAATAVTQALNELLQHVKAH-C, 765-789), Talin (N-NLKSQAAAAAARAVTDSINQLITMCT-C, 1330-1357) and Talin VBS50

(N- QVVLINAVKDVAKALGDLISATKAA-C, 2077-2102) were synthesized at the Scripps Institute proteomics facility (Jupiter Florida, USA). For crystallographic studies, the human talin H1-H4 domain (residues 481-636) preceded by an internal ribosome-binding site and a start codon was PCR-amplified and cloned into the EcoRI/SacI sites of pET28a-IpaA-VBS3 (Park et al., 2011) using the following pairs of primers 5-CGAATTCAGGAGGACAGCTATGCACCGAGGACACATG-3 and 5-CGAGCTCGTTACTGACGGGGCT CAGCACTG-3 to generate the bicistronic expression vector pET28a-IpaA-VBS3/VTBS-talinH1-H4. Plasmids were transformed into the *E. coli* BL21 (DE3) strain (Invitrogen).

Yeast double hybrid analysis

The yeast two-hybrid analysis was performed using IpaA1-565 as bait to screen a human placental RP1 library, according to standard procedures and the Y2H protocole (Hybrigenics services).

Protein purification

The talin H1-H4 derivative was purified by affinity chromatography in 25 mM Tris-HCl pH 7.4, 0.5 M NaCl and 30 mM imidazole using a HisTrap HP 5ml affinity column (GE Healthcare). For crystallographic studies, the binary complex of IpaA-VBS3 / talinH1-H4 was purified by passage over a HisTrap HP 5 mL affinity column (GE Healthcare) in 25 mM Tris-HCl pH 7.4, 0.5 M NaCl and 30 mM imidazole. The elution fractions were pooled and concentrated with a 3 kDa cut-off ultrafiltration unit (Amicon), and the buffer was exchanged to phosphate-buffered saline (PBS) and digested by thrombin digestion. The complex was loaded onto a Superdex 200 size chromatography column and fractions containing IpaA-VBS3 / talinH1-H4 complex concentrated up to 30 mg/ml.

IpaA derivatives were purified by affinity chromatography in PBS (Phosphate Buffer Saline) using a GStrap HP affinity column (GE Healthcare), cleaved with thrombin to remove the GST moiety, followed by size exclusion chromatography (HiLoad S200, GE Healthcare). For crystallographic studies, talin H1-H4-IpaA-VBS3 binary complex was purified as described (Park et al., 2011). Protein concentration was determined using the BCA assay (Thermo Scientific). Samples were dialyzed in binding buffer and stored at -80°C at concentrations ranging from 1 to 10 mg/ml.

Native-PAGE analysis

Talin H1-H4 and IpaA peptides were incubated in binding buffer (25 mM Tris-HCl pH 7.0, 100 mM NaCl and 1 mM β -Mercaptoethanol) for 1 hr at 4°C . After incubation, samples were resuspended in 2 x Native loading buffer (62,5mM Tris pH 6,8 containing 25% Glycerol) and separated by Tris-Glycine Native-PAGE electrophoresis (Schägger et al., 1994). Gels were stained using standard colloidal Coomassie stain.

SEC-MALS

The purified proteins IpaA483-633, IpaA524-633 and talin H1-H4 were used at 20 μM equimolar concentrations and incubated at 4°C for one hour in binding buffer (25 mM Tris-HCl pH 7.0, 100 mM NaCl and 1 mM β -Mercaptoethanol). 200 μL s of the protein mixtures were analyzed by size-exclusion chromatography (SEC) on a Superdex 200 10/300 GL (GE Healthcare) using a Shimadzu Prominence HPLC. Multi-angle laser light scattering (MALS) was measured with a MiniDAWN TREOS equipped with a quasi-elastic light scattering module and a refractometer Optilab T-REX (Wyatt Technology). Protein concentration was determined using a specific refractive index (dn/dc) of 0.183 at 658 nm.

Crystallization, structure determination, and crystallographic refinement

Crystals of the IpaA-VBS3 / talin H1-H4 complex were obtained by mixing 1 μL of protein complex at 7 mg/ml in buffer 25 mM Tris pH 7.4 and 150 mM NaCl with 1 μL of 0.2 mM ammonium sulfate, 0.1 mM sodium acetate pH 4.6 and 30% PEG 4000 by vapor diffusion at 292 K. Crystals were cryoprotected with a solution consisting of the reservoir supplemented with 20% v/v ethylene glycol and flash frozen. X-ray diffraction data were collected at 100 K on a single crystal at PROXIMA-1 beamline at the SOLEIL synchrotron (Saint-Aubin, France). Data were indexed and processed using XDS (Kabsch, 2010) and corrected for anisotropy with the STARANISO server (staraniso.globalphasing.org). Structure solution was obtained by molecular replacement with Phaser (McCoy et al., 2007) using as search template a monomer of talin-H1-H4 derived from the pdb entry 1sj8 lacking residues 515 to 538. A clear solution was obtained (TFZ = 28.5; LLG = 2105.5) Refinement was done with autoBUSTER (Bricogne et al., 2011) using NCS and alternating with manual building in Coot (Emsley et al., 2010). One TLS group per chain was used at the end of the refinement. Final structure is deposited on ProteinDataBank (PDB ID: 5NL1).

Isothermal titration calorimetry

Protein interaction was analyzed by microcalorimetry using an ITC200 calorimeter (MicroCal) at 25°C . 200 μL s of 20-100 μM of talin H1-H4 protein in binding buffer (25 mM Tris-HCl pH 7.0, 100 mM NaCl and 1 mM β -mercaptoethanol) were added to the cell and binding was measured in the presence of different concentrations of IpaA / talin VBSs peptides. In other experiments, A483 or A524 were added to the cell and binding of talin H1-H4 (100 μM) was measured. Typically 20-40 injections of 2 μL s of ligand were made with intervals of 320 s between each addition, with a reference power of 12 μcal / sec. Data was analyzed using the MicroCal software provided by manufacturer.

siRNA transfection

HeLa cells were seeded at a density of 10^5 cells in wells containing a 22 × 22 mm coverslip in a 6-well plate. The following day, cells were transfected with of anti-talin 1 siRNA (Stealth Select RNAi, catalog no. 1299003, Invitrogen, oligo 804; sequence: 5'-CCA AGAACGGAAACCUGCCAGAGUU-3') or anti-vinculin siRNA (Stealth Select RNAi, catalog no. 1299001, Invitrogen, oligo VCLH55111259) duplex at the indicated concentrations and time periods.

Cell challenge with *Shigella* strains

HeLa cells seeded at 2×10^5 cells in coverslip-containing 33 mm-diameter wells the day before, were transfected with the indicated constructs using the JetPei® transfection reagent. After 16 hours, cells were challenged with *Shigella* strains coated with poly-L-lysine, as follows. Bacteria grown to an $OD_{600\text{ nm}}$ of 0.6 - 0.8 were washed three-times by successive centrifugation at 13 Kg for 30 s and resuspension in EM buffer (120 mM NaCl, 7 mM KCl, 1.8 mM $CaCl_2$, 0.8 mM $MgCl_2$, 5 mM glucose, and 25 mM HEPES, pH = 7.3). Samples were resuspended in EM buffer containing 50 μ g/ml poly-L-lysine and incubated for 15 min at 21°C, washed three times in EM bufer and resuspended in the same buffer at a final OD of $OD_{600\text{ nm}} = 0.2$. Cell samples were washed three times in EM buffer and challenged with 1 mL of the bacterial suspension and incubated at 37°C. Samples were fixed with PBS containing 3.7% PFA after 15 min incubation for the analysis of filopodial capture. Alternatively, for the analysis of FAs in infected cells, a similar procedure was used except that cells were seeded at a density of 400 000 cells / well and challenged after 16H for 60 min with poly-L-lysine coated bacteria prior to fixation with a 1:1 ethanol-acetone solution for 5 min at -20°C. Samples were processed for immunofluorescence microscopy.

Immunofluorescence microscopy analysis

For GFP-IpaA VBS3, GFP and talin / vinculin co-localization experiments MEF cells were seeded at a density of 1×10^4 cells in a μ -Dish 35 mm 15 kPa stiffness chamber (Cat #81391, ibidi) coated with 10 μ g / ml of Fibronectin (Calbiochem). Cells were transfected with plasmids encoding human talin-mCherry, vinculin-mCherry, GFP-IpaA VBS3 and GFP using the Lipofectamine 2000 transfection reagent (Life Technologies). For replating experiments HeLa cells co-transfected with vinculin-mCherry and talin-GFP, were resuspended by trypsinization and replated on glass coverslips. After 20 minutes the samples were fixed, processed for immunofluorescence microscopy, and mounted on slides using Dako mounting medium (Dako, Agilent Technologies), as described (Romero et al., 2012).

Samples were analyzed using an Eclipse Ti microscope (Nikon) equipped with a 100x objective, a CSU-X1 spinning disk confocal head (Yokogawa), and a Coolsnap HQ2 camera (Roper Scientific Instruments), controlled by the Metamorph 7.7 software. The percent of internalized bacteria was scored as one if the number of internalized bacteria per foci was at least the 50% of the total number of bacteria in the foci or zero if below, in three independent experiments ($n_{\text{control}} = 27$, $n_{\text{siRNATalin}} = 23$). For control and anti-talin siRNA transfected cells, the percent of internalized bacteria was compared using a Chi-square test (R Statistical Software).

Image processing and analysis

Analysis was performed in Icy Bioimaging Analysis software (de Chaumont et al., 2012). Scans of GFP-IpaA VBS3, Vinculin-mCherry and Talin-mCherry were performed as follows. Defined ROIs in median projections of basal in-focus planes were segmented in concentric areas from the edge of the cell. Average values of intensities were normalized to the maximum and minimum average intensities of the ROI. For talin-GFP and vinculin-mCherry filopodial distribution, saturated sum projections of images from 20 minutes-replated cells were used for Concentric Area Scan analysis. For the quantification of the number of FAs, a semi-automated protocol was developed using Icy software (de Chaumont et al., 2012). Spinning-disk fluorescent microscopy planes were used to detect GFP-IpaA VBS3 structures using HK means thresholding and overlaid binary masks obtained from the threshold projections of F-actin labeled images (Max-entropy method). FAs were detected as spots positive for both GFP-IpaA VBS3 and actin structures using Wavelet Spot Detector. FAs were detected as spots positive for both GFP- IpaA VBS3 above background intensity levels. Filopodia length and number were determined manually from actin-labeled projections. IpaA VBS3, talin, vinculin and vD1 filopodial clusters were identified using Wavelet Spot Detector in Saturated sum projections. Co-localizing clusters were determined by overlaying the separate detections. Distance to cell body was determined using ROI Inclusion analysis plugin.

QUANTIFICATION AND STATISTICAL ANALYSIS

Bacterial internalization and talin coat-structure formation were analyzed a contingency table using in a Pearson Chi-square test (R Statistical Software). A Post hoc pairwise Chi-square test (NCStats package, R Statistical Software) with FDR p value correction was further used to compare the distribution between the various strains. $n > 35$ foci, $N = 3$. The correlation of the intensity of talin and vinculin labeling was analyzed using a Wilcoxon rank sum test (R Statistical software).

For all statistical tests a D'Agostino-Pearson normality test was performed in order to decide if performing a parametric or a non-parametric test. Applied statistical test, number of datapoints (n) and number of experimental replicates (N) are indicated in the figure legends; as well as mean \pm SEM, for normally-distributed data, and median \pm MAD, otherwise.

DATA AND SOFTWARE AVAILABILITY

Crystallographic structure of the IpaA-VBS3 / talin H1-H4 complex was deposited on the Protein Data Bank, with PDB ID: 5NL1.

4 Article 2

4.1 Overview

IpaA injection during invasion leads to the recruitment of Vinculin to bacterial entry sites, a process mediated by the presence of Vinculin Binding Sites at the C-terminal end of IpaA. SEC-MALS and native gels were used to characterize the interaction between IpaA VBS1-3 and vinculin. Analysis of cross-linked complexes by Mass-spectrometry allowed the obtention of structural models for IpaA VBSs/Vinculin interactions. We also characterized the functional effects of IpaA VBSs constructs in cell adhesions combining microscopy analysis, microfluidics and migration assays to evaluate the effects of VBSs in cell adhesion and affinity. My contribution to this article was the conception and realization of experiments, generation of vinculin constructs, microscopy analysis of adhesion structures, and implementation of the microfluidics-based adhesion assay.

**Vinculin targeting by *Shigella* IpaA promotes stable cell adhesion independent of
mechanotransduction**

Cesar Valencia-Gallardo^{1-4*}, Daniel-Isui Aguilar-Salvador^{1-4*}, Hamed Khakzad^{5, 7§}, Charles Bou-
Nader^{8, 9§}, Christian Malosse¹⁰, Diogo Borges Lima¹⁰, Chakir Bello¹⁻⁴, Benjamin Cocom-Chan¹⁻⁴, Nicole
Quenech'Du¹⁻⁴, Bilal Mazhar¹⁻⁴, Delphine Javelaud¹¹⁻¹³, Jacques Fattaccioli^{14, 15}, Alain Mauviel¹¹⁻¹³, Marc
Fontecave^{8, 9}, Atef Asnacios¹⁶, Julia Chamot-Rooke¹⁰, Lars Malmström^{5, 7, 17}, Guy Tran Van Nhieu^{1-4¶*}

¹Equipe Communication Intercellulaire et Infections Microbiennes, Centre de Recherche
Interdisciplinaire en Biologie (CIRB), Collège de France, 75005 Paris, France

²Institut National de la Santé et de la Recherche Médicale U1050, 75005 Paris, France

³Centre National de la Recherche Scientifique UMR7241, 75005 Paris, France

⁴MEMOLIFE Laboratory of excellence and Paris Science Lettre

⁵Institute for Computational Science, University of Zürich, Zürich, Switzerland.

⁶S3IT, University of Zürich, Zürich, Switzerland.

⁷Swiss Institute of Bioinformatics, Lausanne, Switzerland.

⁸Laboratoire de Chimie des Processus Biologiques, Collège De France, 75005 Paris, France.

⁹Centre National de la Recherche Scientifique UMR8229, 75005 Paris, France

¹⁰ Mass Spectrometry for Biology Utechs, Institut Pasteur, USR 2000, CNRS, 75015 Paris, France

¹¹Institut Curie, PSL Research University, INSERM U1021, CNRS UMR3347, Team "TGF- β and
Oncogenesis", Equipe Labellisée LIGUE 2016, F-91400, Orsay, France.

¹²Université Paris-Sud, F-91400, Orsay, France.

¹³Centre National de la Recherche Scientifique UMR 3347, 91400 Orsay, France

¹⁴PASTEUR, Département de Chimie, École Normale Supérieure, PSL University, Sorbonne Université,
CNRS, 75005 Paris, France

¹⁵Institut Pierre-Gilles de Gennes pour la Microfluidique, 75005 Paris, France

¹⁶Laboratoire Matière et Systèmes Complexes, UMR 7057 CNRS & Université Paris Diderot, Sorbonne
Paris Cité, Paris, France

¹⁷Division of Infection Medicine, Department of Clinical Sciences, Lund University, Lund, Sweden.

^{*}, [§]equal contribution

[¶]For correspondence:

E-mail: guy.tran-van-nhieu@college-de-france.fr. Tel: 33-1-44-27-14-89. FAX: 33-1-44-27-14-19

***Shigella*, the causative agent of bacillary dysentery, invades epithelial cells by injecting type III effectors that locally reorganize the actin cytoskeleton¹. The type III effector IpaA targets the focal adhesion protein vinculin to induce bacterial adhesion associated with the recruitment of mature focal adhesion markers, despite the inability of bacteria to exert significant counter-forces², ³. Here, we show that three vinculin-binding sites (VBSs) exposed at the IpaA C-terminus act in a cooperative manner to trigger a yet unreported mode of vinculin activation through specific interactions with sites in the vinculin head sub-domain D2. Structural modeling based on the mass spectrometry identification of interacting residues by cross-linking indicated that upon IpaA binding to vinculin D2, vinculin head sub-domains undergo major conformational changes leading to higher order heterocomplexes and vinculin homo-trimers. IpaA-mediated vinculin activation induces the formation of large and stable focal adhesions resisting the action of actin relaxing drugs. This property enables IpaA to rapidly elicit strong cell adhesion to fibronectin-coated substrates. While *Shigella* IpaA promotes strong adhesion in the absence of mechanotransduction,**

its mode of vinculin activation likely reflects a key step during maturation of cell adhesions driven by acto-myosin contractility.

Integrin-mediated cell adhesion critically depends on the cytoskeletal linkers talin and vinculin⁴⁻⁶. During mechanotransduction, talin acts as a mechanosensor by exposing its VBSs as a function of the stretching force generated by acto-myosin and dependent on substrate stiffness⁷. Talin exposed VBSs recruit and activate vinculin, reinforcing anchorage to the actin cytoskeleton in response to mechanical load^{8, 9}. Vinculin contains three repetitions (D1-D3) of a conserved domain consisting of two bundles of four helices, and a fourth D4 domain containing only one helical bundle connected to a proline-rich unstructured region and the carboxyterminal F-actin binding domain¹⁰. Under its inactive folded form, intramolecular interactions between the vinculin head and tail domains prevent ligand binding.

The *Shigella* type III invasion effector IpaA contains 3 VBSs located in its carboxyterminal moiety¹¹⁻¹³. IpaA VBS1, as for all VBSs described to date to promote vinculin activation, interacts with the first helical bundle of the D1 domain, promoting major conformational changes that disrupt the D1-tail intramolecular interactions and free the vinculin F-actin binding region¹¹ (Fig. 1a). IpaA VBS2, in contrast, interacts with the second helical bundle of D1¹² (Fig. 1a) and its association with IpaA VBS1 results in a very high affinity and stable IpaA VBS1-2:D1 complex, with an estimated K_D in the femtoM range¹². While functional evidence indicates that IpaA VBS3 cooperates with IpaA VBS1-2 to stimulate bacterial invasion, the isolated peptide acts as IpaA VBS1 in promoting vinculin activation through interaction with the vinculin D1 first helical bundle and also forms a folded bundle with the talin H1-H4 helices^{13, 14}.

Here, we studied the effects of the IpaA subdomains containing VBS1-2 (A524) or VBS1-3 (A483) on vinculin activation (Fig. 1b). We performed SEC-MALS (Size Exclusion Chromatography-Multi-Angle Light Scattering) to analyze complexes formed upon incubation of A483 with HV₁₋₈₃₄ containing the D1-D4 domains, corresponding to full-length human vinculin (HV) devoid of the

carboxyterminal F-actin binding domain (Fig. 1b). In addition to the 1:1 D1D4: A483 complex, larger complexes were observed corresponding to a 2:1 heterocomplex and a 3:0 D1-D4 homo-trimer (Fig. 1c). Similar 2:1 and 3:0 complexes were observed when A483 was incubated with HV₁₋₄₈₄ containing only the vinculin D1 and D2 domains (D1D2) (Fig. 1d), indicating that vinculin homo-trimerization occurs exclusively through these vinculin head sub-domains. By contrast, when A524 was incubated with D1D2, 1:1 and 2:1 D1D2:A524 complexes were detected, but not the D1D2 homo-trimer suggesting a role for IpaA VBS3 in vinculin trimerization (Fig. 1d). Consistently, higher order D1D2 homo-complexes devoid of A483 and D1D2:A524 hetero-complexes were visualized by native PAGE (Fig. 1e and Suppl. Figs. 3c, d). These results suggest that binding of IpaA VBSs to vinculin triggers conformational changes in vinculin leading to the formation of an IpaA VBS3-dependent vinculin homo-trimer.

To further investigate initial interactions responsible for vinculin trimer formation, we performed binding assays with HV derivatives immobilized onto a solid phase to restrict conformational changes. These assays indicated that A483 and A524 bound to HV with a similar affinity, as estimated by their EC₅₀ (95% confidence interval) of 6.1 (4.2-9.0) and 3.7 (1.7-8.1) nM, respectively (Suppl. Fig. 1a). Strikingly, a large difference was observed in the binding plateau, indicating that HV presented more binding sites for A483 than for A524 (Suppl. Fig. 1a). Also, D1D2 presented more binding sites for HV₁₋₂₅₈ containing the D1 domain only, suggesting the presence of additional sites on the D2 domain (Suppl. Fig. 1b). Consistently, BN-PAGE showed the formation of 1:1, as well as a 1:2 D1D2:A483 complex, observed with increasing A483 molar ratio (Suppl. Fig. 1c). In contrast, single 1:1 complexes were observed for D1:A483, D1:A524 or D1D2-A524 (Suppl. Figs. 1c-h), indicating that IpaA VBS3 was required to reveal additional sites on the D2 domain. Of note, D1D2 homo-trimers observed in the SEC-MALS and native gel analysis (Figs. 1d, e and Ext Data Figs. 3c, d) were not detected in BN-PAGE, suggesting that Coomassie brilliant blue interfered with the formation of higher order D1D2 complexes. Together, these results suggested that the formation of vinculin trimers triggered by A483 required the IpaA VBS3 dependent exposure of binding sites on D2. These findings were

unexpected, since vinculin activating ligands have been described to bind to a single site on the D1 domain of vinculin.

To map interactions of A524 and A483 with D1D2, complexes were cross-linked, subjected to proteolysis and analyzed using Liquid Chromatography coupled to Mass Spectrometry (LC-MS) (Methods). Intermolecular links were identified from the characterization of cross-linked peptides (Suppl. Tables 1-3; Methods) and along with identified intramolecular links, used to produce structural models (Methods). The A524:D1 complex showed links consistent with a "canonical" conformer expected from established structures^{11, 12, 15} (Suppl. Fig. 2). Similar links were identified for the A524:D1D2 complex, with a majority of links observed with the D1 domain (Fig. 2a). For both complexes, the structure shows interactions between IpaA VBS1 and VBS2 with the D1 first and second bundles, respectively, leading to helical bundle reorganization of D1 associated with vinculin activation (Figs. 2c, d; Suppl. Fig. 2 and Suppl. Tables 1, 2). For the A483:D1D2 complex, structural modeling shows 2 major conformers accounting for the majority of links. In a first "closed" conformer, IpaA VBS1 and VBS2 interact with the D1 bundles in a similar manner as for A524, where the relative positioning of D1 and D2 is globally conserved compared to apo D1D2 in the A524-D1D2 complex (compare Figs. 2d and 2e). In this "closed" conformer, IpaA VBS3 interacts with an interface formed by the H5 (residues 128-149) and H8 (residues 222-250) helices in the second bundle of D1 and the H13 (residues 373-397) helix in the second bundle of the D2 domain (Figs. 2e and f). The second "open" conformer, however, shows a major re-orientation of D1 and D2 subdomains with their major axis forming an angle value of ca 82° compared to the 25° observed in the native vinculin structure or the first conformer (Fig. 2g), with IpaA VBS3 docking sidewise through extensive interaction with the H5 (residues 128-149) and H8 (residues 222-250) helices of the vinculin D1 domain. Because this latter conformer leads to major changes in bundle exposure in D1 and D2, we posit that it is involved in the formation of higher order D1D2 complexes and trimer induced by A483. To test this, we engineered a structural clamp by substituting residue Q68 in the first D1 bundle and A396 in the second D2 bundle for cysteine residues, expected to prevent the formation of the open

conformer upon disulfide bridge formation (Suppl. Figs. 3a, b). Consistently, cysteine clamped D1D2-Q68C A396C did not prevent the exposure of additional sites on D2 or 1:1 complex formation induced by A524 or A483, but prevented the formation of higher order complexes (Fig. 1 e and Suppl. Figs. 3c-e). We coined "supra-activation" the mode of vinculin activation induced by A483 involving major conformational changes in the vinculin head, to distinguish it from the canonical activation associated with the dissociation of vinculin head-tail domains.

We then characterized the effects of A524 and A483 expression by performing immunofluorescence staining of vinculin-containing adhesion structures. As shown in Figs 3a-c, C2.7 cells transfected with GFP-A524 formed more numerous and larger peripheral adhesions as well as actin-rich ruffles compared to control cells (Figs. 3a-d). Strikingly, GFP-A483 transfected cells formed even larger and more numerous adhesions than GFP-A524 transfected cells, but significantly less actin ruffles than GFP-A524 transfectants (Figs. 3a-d). These observations were confirmed by live TIRF microscopy showing the extreme stability of adhesions in GFP-A483 transfectants, with a median duration of at least 84 min, while GFP-A524 and control cells showed adhesions with a comparable median duration of less than 25 min (Fig. 3e; Suppl. movie 1). GFP-A524 and GFP-A483 transfectants showed slightly slower median instant rates of adhesion assembly than control cells (Suppl. Fig. 4; Suppl. movie 1) but significant 1.6-fold and 2-fold decrease in median instant rates of disassembly relative to control cells, respectively (Suppl. Fig. 4). The stability of GFP-A483-induced FAs was independent of acto-myosin contraction. Indeed, GFP-A483-induced FAs resisted the action of the Rho-kinase inhibitor Y27632 relaxing actin-myosin, with a five- and four-times slower median rate of disassembly of adhesions relative to control cells and GFP-A524 transfectants, respectively (Figs. 3f-i; Suppl. movie 2). Furthermore, large adhesions formed in GFP-A483 transfectants following addition of the inhibitor (Figs. 3f, h), a process that was not observed for the other samples, including cells transfected with GFP-A524 or GFP fused to the vinculin D1 domain (vD1) reported to delay talin refolding following stretching¹⁶⁻¹⁸ (Figs. 3g-i; Suppl. movie 2). In line with the stabilization of mature FAs through vinculin supra-activation, GFP-A483 but not GFP-vD1 also delayed the Y27632-induced

removal of the late adhesion marker VASP (Suppl. Fig. 5; Suppl. movie 3). Consistent with A483 bypassing mechanotransduction, GFP-A483 expression induced 5- and 1.6-fold higher yield of short term (≤ 10 min) cell adhesion to fibronectin substrates compared to control GFP and GFP-A524 transfectants, respectively (Suppl. Fig. 6a). By contrast, little difference in adhesion yield was detected at 15 min suggesting that canonical activation of vinculin also resulted in its supra-activation during mechanotransduction (Suppl. Fig. 6a). In line with this, MEF vinculin-null cells transfected with the clamped vinculin version formed fewer and smaller FAs than cells transfected with wild-type vinculin but more than mock-transfected cells (Suppl. Figs. 6b-d).

To confirm and extend these findings, cell adhesion strength was assessed measuring their detachment upon application of a controlled shear stress in a microfluidic chamber. When 1205Lu melanoma cells were allowed to adhere to fibronectin-coated surfaces for more than 25 min, little difference in resistance to shear stress could be detected among samples (Suppl. Fig. 7a). In contrast, when shear stress was applied less than 20 min following cell incubation, GFP-A483-transfected cells showed significantly higher resistance to shear stress up to $22.2 \text{ dynes.cm}^{-2}$ than GFP-A524- or GFP-transfected cells, with 1.7 ± 0.2 - and 0.9 ± 0.14 -fold enrichment \pm SD of adherent cells for GFP-A483 and GFP-A524-transfected cells versus control GFP-transfected cells, respectively (Fig. 4b; Suppl. movie 4). In addition, similar to melanoma cells depleted for by siRNA treatment, cells transfected with the clamped vinculin version showed a decreased ability to adhere in comparison to WT vinculin-transfected cells (Suppl. Figs. 7a, b). These results are in full agreement with effects observed on adhesion structures and suggest that A483 interaction with vinculin leads to the bypass of mechanotransducing steps to promote strong adhesion.

Vinculin is paradoxically described as a prognostic marker favoring the migration of cancer cells or as a tumor suppressor stimulating cell anchorage¹⁹⁻²¹. These contradictory findings reflect its complex and poorly understood regulation, as well as different roles in 2D or 3D systems^{22, 23}. Also, an increase of the total pool of vinculin may not correlate with increased vinculin activation. We took advantage of the unique property of A483 to study the effects of vinculin supra-activation on the

motility and invasion of melanoma cells. In time-lapse microscopy experiments in 2D-chambers, GFP-A524 inhibited melanocyte motility compared to control cells, with a rate of Root Median Square Displacement (rMSD) of 3.16 and 15.6 $\mu\text{m}.\text{min}$, respectively (Figs. 4c, d). An even stronger inhibition was observed for GFP-A483-transfected cells (rMSD = 2.3 $\mu\text{m}.\text{min}$) (Figs. 4c, d). Transmigration of melanocytes in 3D-matrigels was similarly inhibited by A524 and A483 (Fig. 4e).

Bacteria invading through a triggering mode rely on a discrete number of T3SS-dependent contacts for which cytoskeletal tethering is likely critical for invasion². As opposed to physiological substrates, bacteria cannot sustain the range of counter-forces associated with integrin-mediated adhesion to the substrate. The *Shigella* type III effector IpaA provides an elegant solution to this problem by promoting strong adhesion without requirement for mechanotransduction. Through the joint action of its VBSs, IpaA induces major conformational changes of the vinculin head sub-domains. Understanding how these major vinculin conformational changes regulate the composition and properties of cell adhesions will bring important insights into cell adhesion processes and will be the focus of future investigations.

REFERENCES

- 1 Ogawa, M., Handa, Y., Ashida, H., Suzuki, M. & Sasakawa, C. The versatility of *Shigella* effectors. *Nat Rev Microbiol* **6**, 11-16, doi:10.1038/nrmicro1814 (2008).
- 2 Valencia-Gallardo, C. M., Carayol, N. & Tran Van Nhieu, G. Cytoskeletal mechanics during *Shigella* invasion and dissemination in epithelial cells. *Cellular microbiology* **17**, 174-182, doi:10.1111/cmi.12400 (2015).
- 3 Tran Van Nhieu, G., Ben-Ze'ev, A. & Sansonetti, P. J. Modulation of bacterial entry into epithelial cells by association between vinculin and the *Shigella* IpaA invasin. *The EMBO journal* **16**, 2717-2729, doi:10.1093/emboj/16.10.2717 (1997).
- 4 Atherton, P., Stutchbury, B., Jethwa, D. & Ballestrem, C. Mechanosensitive components of integrin adhesions: Role of vinculin. *Exp Cell Res*, doi:10.1016/j.yexcr.2015.11.017 (2015).

199 5 Yan, J., Yao, M., Goult, B. T. & Sheetz, M. P. Talin Dependent Mechanosensitivity of Cell Focal
200 Adhesions. *Cellular and molecular bioengineering* **8**, 151-159, doi:10.1007/s12195-014-0364-5
201 (2015).

202 6 Burridge, K. & Guilluy, C. Focal adhesions, stress fibers and mechanical tension. *Exp Cell Res*,
203 doi:10.1016/j.yexcr.2015.10.029 (2015).

204 7 Parsons, J. T., Horwitz, A. R. & Schwartz, M. A. Cell adhesion: integrating cytoskeletal dynamics
205 and cellular tension. *Nat Rev Mol Cell Biol* **11**, 633-643, doi:10.1038/nrm2957 (2010).

206 8 Humphries, J. D. *et al.* Vinculin controls focal adhesion formation by direct interactions with talin
207 and actin. *J Cell Biol* **179**, 1043-1057, doi:10.1083/jcb.200703036 (2007).

208 9 Lavelin, I., Wolfenson, H., Patla, I., Henis, Y. I., Medalia, O., Volberg, T., Livne, A., Kam, Z., Geiger,
209 B. Differential effect of actomyosin relaxation on the dynamic properties of focal adhesion
210 proteins. *PLoS One*. 8:e73549 (2013).

211 10 Bakolitsa, C. *et al.* Structural basis for vinculin activation at sites of cell adhesion. *Nature* **430**,
212 583-586, doi:10.1038/nature02610 (2004).

213 11 Izard, T., Tran Van Nhieu, G. & Bois, P. R. Shigella applies molecular mimicry to subvert vinculin
214 and invade host cells. *J Cell Biol* **175**, 465-475, doi:10.1083/jcb.200605091 (2006).

215 12 Tran Van Nhieu, G. & Izard, T. Vinculin binding in its closed conformation by a helix addition
216 mechanism. *The EMBO journal* **26**, 4588-4596, doi:10.1038/sj.emboj.7601863 (2007).

217 13 Park, H., Valencia-Gallardo, C., Sharff, A., Tran Van Nhieu, G. & Izard, T. Novel vinculin binding
218 site of the IpaA invasin of *Shigella*. *J Biol Chem* **286**, 23214-23221, doi:10.1074/jbc.M110.184283
219 (2011).

220 14 Valencia-Gallardo C, Bou-Nader C, Aguilar D, Carayol N, Quenech'Du N, Pecqueur L, Park HJ,
221 Fontecave M, Izard T, Tran Van Nhieu G. *Shigella* IpaA binding to talin stimulates filopodial
222 capture and cell adhesion. *Cell Reports* **26**, 921-932. doi: 10.1016/j.celrep.2018.12.091 (2019).

223 15 Izard, T. *et al.* Vinculin activation by talin through helical bundle conversion. *Nature* **427**, 171-
224 175, doi:10.1038/nature02281 (2004).

- 225 16 del Rio, A. *et al.* Stretching single talin rod molecules activates vinculin binding. *Science* **323**, 638-
226 641, doi:10.1126/science.1162912 (2009).
- 227 17 Margadant, F. *et al.* Mechanotransduction in vivo by repeated talin stretch-relaxation events
228 depends upon vinculin. *PLoS Biol* **9**, e1001223, doi:10.1371/journal.pbio.1001223 (2011).
- 229 18 Carisey, A. *et al.* Vinculin regulates the recruitment and release of core focal adhesion proteins in
230 a force-dependent manner. *Curr Biol* **23**, 271-281, doi:10.1016/j.cub.2013.01.009 (2013).
- 231 19 Goldmann, W. H. Role of vinculin in cellular mechanotransduction. *Cell Biol Int* **40**, 241-256,
232 doi:10.1002/cbin.10563 (2016).
- 233 20 Labernadie, A. *et al.* A mechanically active heterotypic E-cadherin/N-cadherin adhesion enables
234 fibroblasts to drive cancer cell invasion. *Nat Cell Biol* **19**, 224-237, doi:10.1038/ncb3478 (2017).
- 235 21 Hamidi, H. & Ivaska, J. Every step of the way: integrins in cancer progression and metastasis. *Nat*
236 *Rev Cancer*, doi:10.1038/s41568-018-0038-z (2018).
- 237 22 Mierke, C. T. *et al.* Vinculin facilitates cell invasion into three-dimensional collagen matrices. *J*
238 *Biol Chem* **285**, 13121-13130, doi:10.1074/jbc.M109.087171 (2010).
- 239 23 Gulvady, A. C., Dubois, F., Deakin, N. O., Goreczny, G. J. & Turner, C. E. Hic-5 expression is a
240 major indicator of cancer cell morphology, migration, and plasticity in three-dimensional
241 matrices. *Mol Biol Cell* **29**, 1704-1717, doi:10.1091/mbc.E18-02-0092 (2018).

242

243 ACKNOWLEDGEMENTS

244 The authors thank Gauthier Mercante for technical help, Philippe Mailly for help with image
245 analysis and René-Marc Mège for insightful discussions and reading of the manuscript. This work was
246 supported by grants from Inserm, CNRS and Collège de France to the CIRB, as well as grant from the
247 PSL Idex project “Shigaforce”. DIAS and BCC are recipients of a PhD fellowship from a CONACYT
248 scholarship. CV-G and DIAS also received support from the Memolife Labex. HK and LM were
249 supported by Swiss National Science Foundation (grant no. SNF 200021 160188) and LM by the Knut
250 And Alice Wallenberg Foundation (grant no. KAW 2016.0023).

251

AUTHOR CONTRIBUTIONS

252

253

254

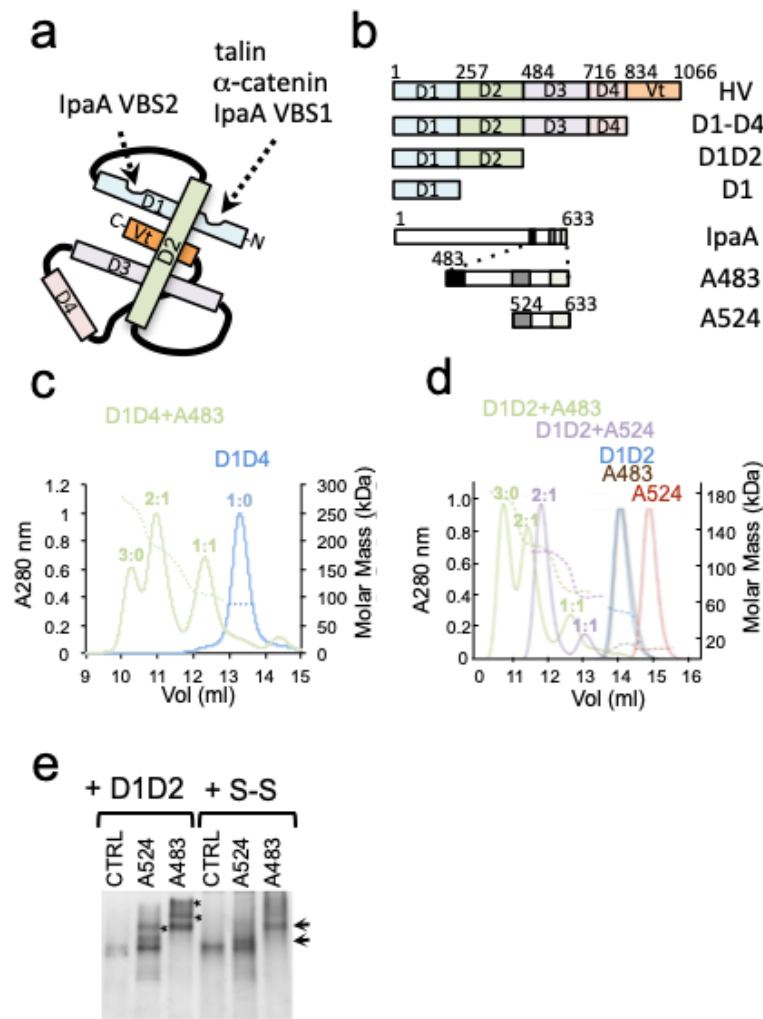
255

256

257

258

CV-G and DIAS conceived and performed most of the experimental works, data analysis and wrote the manuscript. BCC and BM analyzed TIRF experiments. CB-N performed the SEC-MALS analysis. CB and NQD performed and analyzed experiments with melanocytes with the help of DJ and AM. BCC, AA and JF provided technical help for cell adhesion and microfluidics experiments. CM and JCR designed and performed the LC-MS analysis. DBL analyzed the cross-linked mass spectrometry data. HK and LM generated structural models. GTVN designed the project and wrote the manuscript.



260

261

Figure 1 – IpaA reveals binding sites in vinculin head subdomains

262

a

Scheme of folded vinculin (HV). The binding sites and corresponding ligands are indicated.

263

b

Scheme of HV and IpaA constructs. HV domains and IpaA VBSs are depicted as boxes. The numbers

264

c, d

SEC elution profiles of complexes formed between A483 (green) or A524 (purple) and vinculin D1D4 (c) or D1D2 (d). The indicated complex stoichiometry was

265

inferred from the molecular weight estimated by MALS.

266

e

native gel analysis of vinculin D1D2 and IpaA derivatives. D1D2 or cysteine-clamped D1D2 (S-S) were incubated with the indicated IpaA derivatives

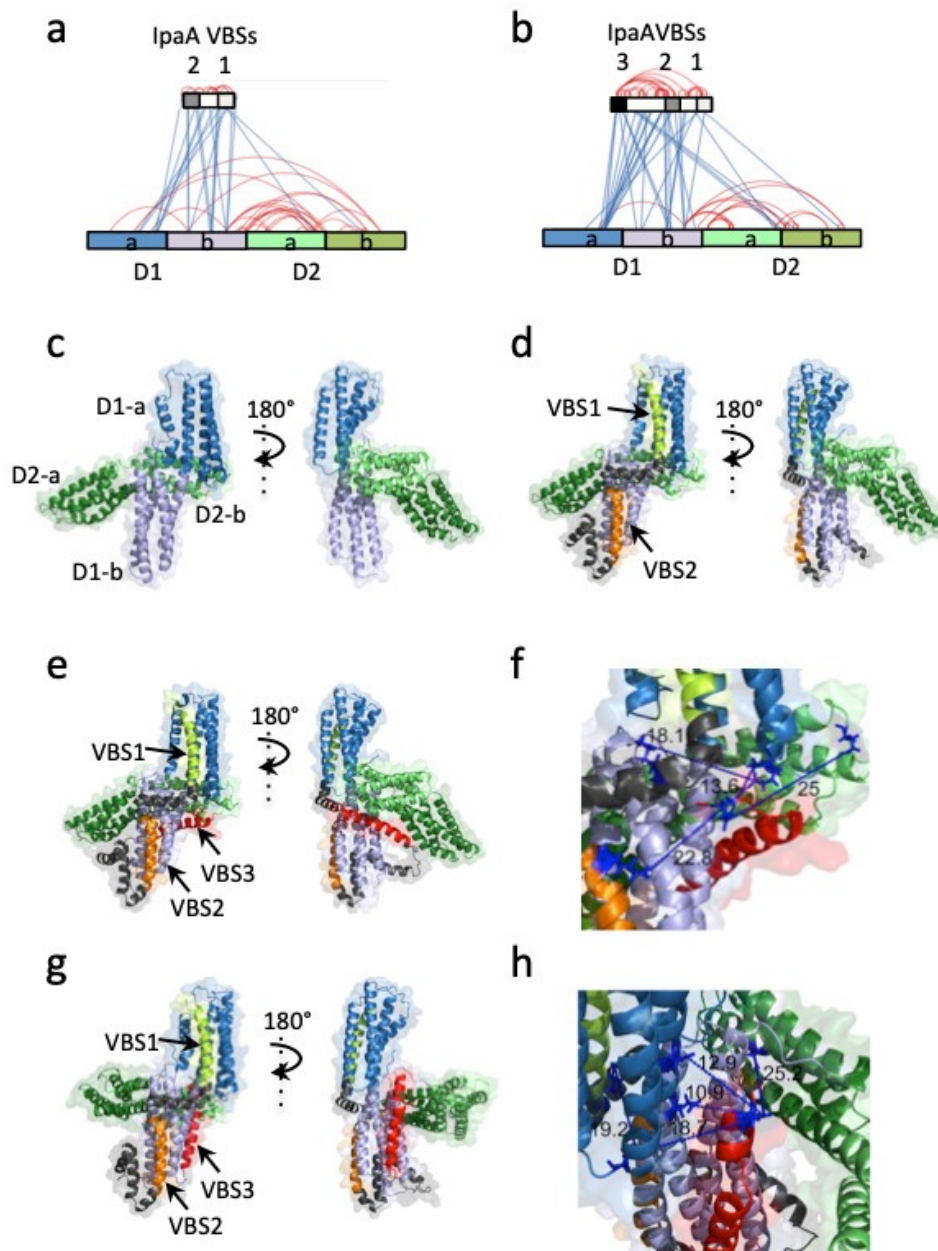
267

and analyzed by native PAGE followed by Coomassie staining. Arrows: 1:1 complexes. *: higher order

268

complexes. Note the absence of higher order complexes for cysteine-clamped D1D2.

269



271

272 **Figure 2 – Characterization of IpaA contact sites on vinculin.**

273 **a, b**, EDC cross-link map from mass spectrometry analysis (LC-MS/MS) of vinculin D1D2-A524 (**a**) and
 274 D1D2-A483 (**b**) following extraction of 1:1 complexes from BN-PAGE. Blue lines: inter-molecular links.
 275 Red lines: intra-molecular links. Note the links between IpaA VBS3 and the D2 second bundle. Cross-
 276 linked residues are detailed in Suppl. Table 1. **c-e**) Structural models of D1D2 (**c**), D1D2-A524 (**d**), D1D2-
 277 A483 “closed” conformer (**e**), D1D2-A483 “open” conformer (**g**). **f, h**, higher magnification of the IpaA

VBS3-D1D2 interaction in (e) and (g) showing the distance between residues in Å. IpaA VBS1-3 were docked on the surface of Vinculin D1D2 using MS cross-link constraints. TX-MS protocol in combination with MS constraints was used to unify and adjust the final model, which justifies over 100 cross-links.

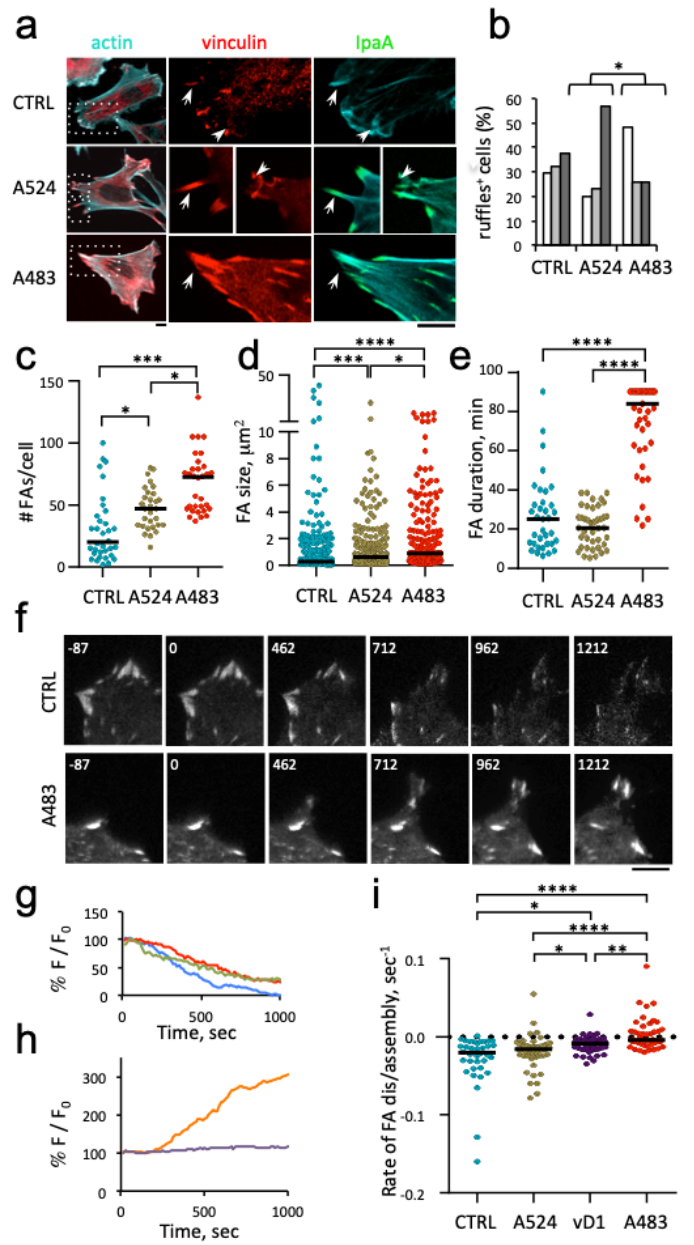


Figure 3 – A483 stabilizes vinculin in cell adhesions in the absence of mechanotransduction

a-c, Immunofluorescence analysis of vinculin adhesions. CTRL: C2.7 cells. A524: GFP-A524 transfectants. A483: GFP-A483 transfectants. **a**, representative fluorescence micrographs. Arrows: adhesions; arrowheads: ruffles. Green: GFP; red: vinculin; cyan: actin. **b**, percent of cells with ruffles \pm

SEM. Cells with: no ruffles (empty bars); small ruffles (light grey bars); large ruffles (dark grey bars). *: Pearson's Chi-squared test (N=3, n > 30, p = 0.036). **c**, **d**, vinculin containing FAs were detected using a semi-automated program. **c**, median number of FAs per cell; **d**, FA size. (N=3, n > 30). Dunn's multiple comparisons test. *: p < 0.05;***: p < 0.005. **e**, TIRF microscopy of C2.7 cells transfected with mCherry-vinculin alone (CTRL) or co-transfected with GFP-A524 (A524), GFP-vD1 (vD1), or GFP-A483 (A483). The duration of vinculin-containing adhesions was determined from time-lapse acquisitions. **f-i**, TIRF microscopy analysis of cells treated with 100 μ M Y-27632. **f**, Representative time series acquisitions. Numbers indicate the elapsed time in seconds, with the inhibitor added at t = 0. Scale bar = 5 μ m. **g**, **h**, F/F₀: normalized average fluorescence intensity of adhesions as a function of time. Representative traces corresponding to single adhesions for: **h**, control cells: blue, A524: red, vD1: green; **g**, A483: purple and orange. **i**, initial rates of adhesion disassembly inferred from linear fits. N = 5. Number of adhesions analyzed: CTRL: 84; vD1: 75; A524: 140; A483: 97. Dunn's multiple comparisons test. *: p < 0.05; **: p < 0.01;***: p < 0.005; ****: p < 0.001.

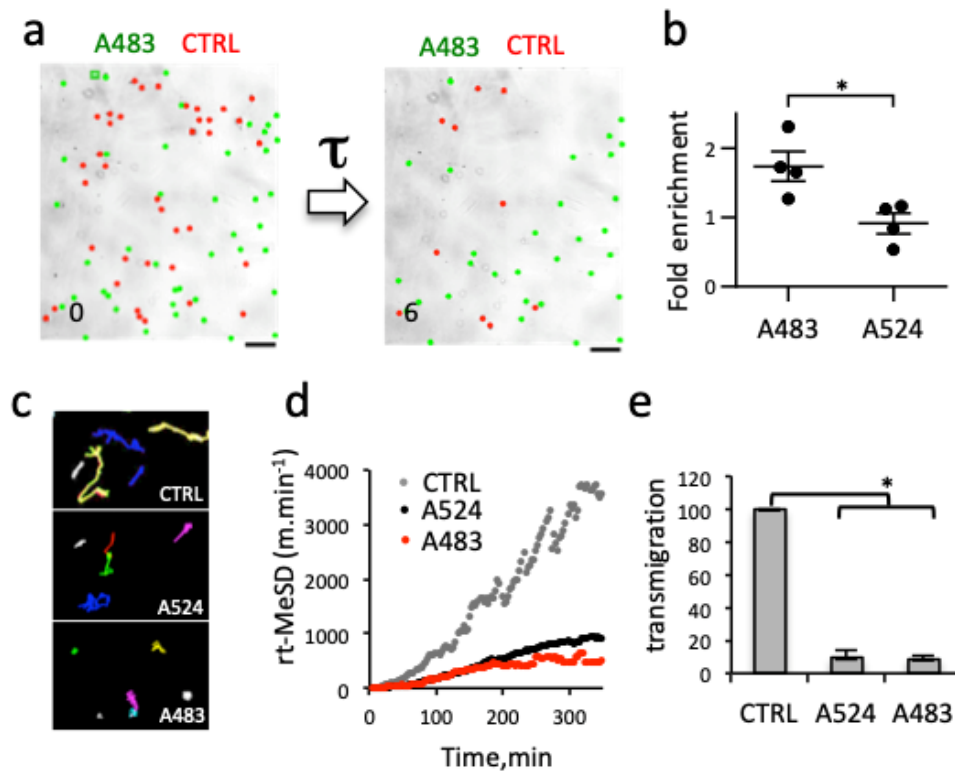


Figure 4. A483-mediated vinculin supra-activation stimulates strong cell adhesion and inhibits tumor cell invasion.

a, b, 1205Lu melanoma cells were transfected with the indicated constructs, labeled with calcein (methods) and mixed with the same ratio of control cells. Cells were perfused in a microfluidic chamber and allowed to adhere for 20 min prior to shear stress application. **a**, representative fields. The number indicates the elapsed time after shear stress application. **b**, Scatterplot of fold enrichment of: A483 (N = 4, n = 610) or A524 (N = 4, n = 433) transfected cells vs control cells (1594 cells, N = 4). Unpaired t test. *: p = 0.0229. **c, d**, cells were transfected with the indicated constructs, and analyzed by time-lapse videomicroscopy. **c**, representative single cell migration 20-hour tracks for indicated samples. **d**, Root of Median Square of displacement over time for control- (61 cells, N = 3), GFP-A524- (61 cells, N = 3) and GFP-A483 transfectants (64 cells, N = 3). ***p = 0.0007. The slopes were analyzed using a covariance test and found to be statistically different (ANCOVA, p < 2x10⁻¹⁶). **e**, 5 × 10⁴ cells were seeded in matrigel

314 chambers. The percent of transmigrated cells is indicated. (N = 3). Kruskal-Wallis test with Dunn's
315 multiple comparisons test. *: $p < 0.05$.
316

METHODS

Generation of constructs

Human vinculin constructs were generated by polymerase chain reaction using the forward primer 5' GCGCATATGCCAGTGTTCATACG-3' and reverse primer 5'-CGTCGACTCACCAGGCATCTTCATCGGC-3' for D1 (residues 1-258) or 5'-CGTCGACTCAGTGTACAGCTGCTTTG-3' for D2 (residues 1-492) using a plasmid containing full-length octahistidine-tagged human vinculin (residues 1–1,066), as template¹⁰, and cloned into the NdeI-Sall sites of pet15b (Novagen). The IpaA constructs GFP-A524 and GFP-A483 were generated by polymerase chain reaction (PCR) and cloning into pcDNA3.1 NT-GFP Topo TA (Invitrogen) using the 5'-TCAAAGGACATTACAAAATCC-3' and 5'-GCGATATCATGGCCAGCAAAGG-3' forward primers, respectively, and the 5'-GCGCGGCCGCTTAATCCTTATTGATATTC-3' reverse primer. The GST-A483A construct was generated by PCR using 5'-GGCGAATCCCCGAGACACATATTTAACACG-3' forward and 5'-GCCGTCGACTTAATCCTTATTGATATTCT-3' reverse primers and cloning into the *EcoRI-Sall* of pGEX-4T-2 (GE Lifesciences). pGST-A524 was previously described²⁴. The pGFP-vD1 plasmid was generated by polymerase chain reaction using the forward primer 5'-ACCCGGGATCCCGCC-3' and reverse primer 5'-ACCCGGGACCAGGCA-3', and cloned into pEGFP. The pmCherry-human vinculin (HV) and pmCherry-VASP plasmids were from Addgene. Stealth siRNA anti-human vinculin was from Invitrogen (reference number 1299001).

Protein purification

BL21 (DE3) chemically competent *E. coli* (Life Technologies) was transformed with the expression constructs. D1 and D1D2 were purified essentially as described^{11, 25}. For the IpaA derivatives, bacteria grown until OD_{600nm} = 1.0 were induced with 0.5 mM IPTG and incubated for another 3 hrs. Bacteria were pelleted and washed in binding buffer 25 mM Tris PH 7.4, 100 mM NaCl and 1 mM beta-mercaptoethanol, containing CompleteTM protease inhibitor. Bacterial pellets were resuspended in

1/50th of the original culture volume and lyzed using a cell disruptor (One shot model, Constant System Inc.). Proteins were purified by affinity chromatography using a GSTrap HP affinity column (GE Healthcare) and size exclusion chromatography (HiLoad S200, GE Healthcare). Samples were stored aliquoted at -80°C at concentrations ranging from 1 to 10 mg/ml.

Protein complex formation analysis

Proteins were incubated at a concentration of 30 µM in binding buffer for 60 min at 4°C. Samples were analyzed by SEC-MALS (Wyatt Technology Europe) using a 24 ml Superdex 200 Increase 10/300 GL filtration column and a MiniDAWN TREOS equipped with a quasi-elastic light scattering module and a refractometer Optilab T-rEX (Wyatt Technology). Data were analyzed using the ASTRA 6.1.7.17 software (Wyatt Technology Europe). Protein complex formation was visualized by PAGE under non-denaturing conditions using a 7.5% polyacrylamide gel, followed by Coomassie blue staining.

Solid-phase binding assay

96-well Maxisorp (Nunc) ELISA plates were coated with 30 nM of full-length vinculin, vinculin constructs or IpaA proteins at the indicated concentrations in binding buffer (25 mM Tris pH 7.4, 100 mM NaCl and 1 mM β-mercaptoethanol). Samples were blocked with PBS-BSA 2%, washed and incubated with IpaA or vinculin proteins in binding buffer containing 0.2% BSA at room temperature for one hour. After incubation, the plates were washed and incubated with an anti-IpaA (dilution 1/2000^e) polyclonal primary antibody³ or anti-vinculin (dilution 1/2000^e) Vin11Vin.5 monoclonal antibody (Sigma-Aldrich) in binding buffer containing 0.2% BSA for one hour at room temperature. Plates were washed and incubated with an HRP-coupled secondary anti-rabbit or anti-mouse IgG antibody (1/32000^e) (Jackson ImmunoResearch) for one hour. The reaction was revealed by adding 100 µl of tetramethylbenzidine (Sigma-Aldrich) for 15 min, stopped by adding 50 µl of 0.66N H₂SO₄ and the absorbance was read at 450 nm (Dynatech MR400).

BN-PAGE (Blue Native – Polyacrylamide Gel Electrophoresis) protein native gel analysis and complex cross-linking

25 μ M of vinculin constructs were incubated with different molar ratios of IpaA proteins in a 1X BN-PAGE buffer (250 mM ϵ -aminocaproic acid and 25mM Bis-Tris PH 7,0) at 4°C for one hour. The protein mixtures were separated in a one-dimension native BN-PAGE electrophoresis as described²⁶. For vinculin-IpaA protein ratio assay, vinculin-IpaA bands containing the complexes separated by BN-PAGE were cut, sliced and boiled in 2 x Laemmli SDS buffer followed by SDS-PAGE. The second dimension SDS-PAGE gels were stained (colloidal Coomassie staining) and the density of the bands was determined using Image J. The normalized vinculin:IpaA ratio of the complexes was compared using a non-parametric Kruskal-Wallis rank sum test (R statistical software).

For crosslinking vinculin-IpaA complex, bands containing the complexes were cut, sliced and electroeluted in native conditions (15 mM Bis-Tris pH 7.0 and 50 mM Tricine) inside a closed dialysis membrane (SpectraPor). The soluble complexes were recovered and their buffer exchanged twice into an amine-free cross-link buffer in 25 mM HEPES pH 7.0 containing 100 mM NaCl using 10MWCO ZEBA desalting columns (Thermo Scientific). The fractions containing the complexes were incubated for 1 hr at 4°C with 10 mM N-hydroxysulfosuccinimide and 5 mM EDC (Sigma-Aldrich) following the manufacturer's recommendations. The cross-linking reaction was stopped by adding 50 mM Tris pH 7.4 and incubating for 20 minutes. Samples were denaturated in 2x SDS Laemmli buffer for 5 min at 95°C and complexes were eluted from gel slices following SDS-PAGE.

Liquid Chromatography Mass spectrometry (LC-MS)

Complexes obtained after the cross-linking step were loaded onto a 4-20% polyacrylamide gradient gels and Coomassie stained. The bands containing the complexes were cut and submitted to tryptic digestion²⁷. The experiments were performed in duplicates for the 3 complexes D1:A524, D1D2:A524 and D1D2:A483. Peptides obtained after tryptic digestion were analyzed on a Q Exactive Plus instrument (Thermo Fisher Scientific, Bremen) coupled with an EASY nLC 1 000 chromatography system (Thermo

Fisher Scientific, Bremen). Sample was loaded on an in-house packed 50 cm nano-HPLC column (75 μm inner diameter) with C18 resin (1.9 μm particles, 100 Å pore size, Reprosil-Pur Basic C18-HD resin, Dr. Maisch GmbH, Ammerbuch-Entringen, Germany) and equilibrated in 98 % solvent A (H_2O , 0.1 % FA) and 2 % solvent B (ACN, 0.1 % FA). A 120 minute-gradient of solvent B at 250 nL.min⁻¹ flow rate was applied to separate peptides. The instrument method for the Q Exactive Plus was set up in DDA mode (Data Dependent Acquisition). After a survey scan in the Orbitrap (resolution 70 000), the 10 most intense precursor ions were selected for HCD fragmentation with a normalized collision energy set up to 28. Charge state screening was enabled, and precursors with unknown charge state or a charge state of 1 and >7 were excluded. Dynamic exclusion was enabled for 35 or 45 seconds respectively.

Data analysis

The identification of cross-linked peptides from LC-MS data was performed using SIM-XL v. 1.3²⁸, with the following search parameters: EDC as cross-linker, a tolerance of 20 ppm for precursor and fragment ions, trypsin fully specific digestion with up to three missed cleavages. Carbamidomethylation of cysteines was considered as a fixed modification. All initial identification of cross-linked peptides required a primary score of SIM-XL greater than 2.5 for inter-links and 2.0 for intra-links or loop-links. As single incorrect cross-link identification might lead to a different model, a manual post-validation of the search engine results at the MS2 level was thus performed. A 2D-map showing the protein-protein interaction was generated as an output (Figs. 2a,b). Only peptides present in the 2 replicates are gathered in Supplementary Tables 1-3 and were used for the modeling.

Modeling

We used the constraints obtained from the cross-linking MS data (Suppl. Tables 1-3) to guide the protein structure modeling using the TX-MS protocol as described by Hauri, Khakzad et al.²⁹. In short, TX-MS uses the Rosetta comparative modeling protocol (RosettaCM)³⁰, and the flexible backbone docking protocol (RosettaDock)³¹ to generate models and evaluate how well each model explains the MS constraints using a novel scoring function. Here, a total of 100,000 models was generated, of which the

highest-scoring model is displayed in (Fig2e), supported by a total of 100 inter and intra-molecular cross-links.

Cell lines

C2.7 myoblasts³² and MEF vinculin null cells⁸ were routinely grown in DMEM 1 g / L glucose containing 10 % FCS in a 37°C incubator containing 10 % CO₂. 1205Lu melanoma cells³³ were grown in RPMI + Glutamax medium (RPMI1640) supplemented with 10 % fetal calf serum (FCS) and non-essential aminoacids in a 37°C incubator with 5 % CO₂.

Immunofluorescence staining

C2.7 mice myoblasts cells were seeded at 2.5×10^4 cells in 25 mm-diameter coverslips. Cells were transfected with 3 µg of pGFP-A524 or pGFP-A483 plasmids with 6 µl JetPEI transfection reagent (Polyplus) for 16 hours following the manufacturer's recommendations. Cells were fixed in PBS containing 3.7% paraformaldehyde for 20 min at 21°C and permeabilized with 0.1% Triton X-100 for 4 min at 21°C. Cells were processed for immunofluorescence staining using the Vin11.5 anti-vinculin monoclonal antibody (ref. V4505, Sigma-Aldrich) and anti-mouse IgG antibody coupled to Alexa 546 (Jackson Research) and Phalloidin-Alexa 633 (Invitrogen), as described previously³. Samples were analyzed using an Eclipse Ti inverted microscope (Nikon) equipped with a 60 x objective, a CSU-X1 spinning disk confocal head (Yokogawa), and a Coolsnap HQ2 camera (Roper Scientific Instruments), controlled by the Metamorph 7.7 software.

TIRF (Total Internal Reflection Microscopy) analysis

C2.7 cells were transfected with pmCherry-HV or pmCherry-VASP and the indicated plasmids as described above. Samples were mounted onto a TIRF microscopy chamber on a stage of an Eclipse Ti inverted microscope (Nikon) equipped with an Apo TIRF 100 x N.A. 1.49 oil objective heated at 37°C. TIRF analysis was performed using the Roper ILAS module and an Evolve EM-CCD camera (Roper Scientific

Instruments). When mentioned, Y-27632 was used at 100 μ M. Image acquisition was performed every 12.5 seconds for 30 to 90 minutes.

Live cell tracking

1205Lu melanoma cells were transfected with IpaA constructs or GFP alone (control) and transferred in microscopy chamber on a 37°C 5%-CO₂ stage in RPMI1640 medium containing 25 mM HEPES. For cell tracking, samples were analyzed using an inverted Leica DMiBe microscope and a 20 X phase contrast objective. Image acquisitions were performed every 3 min for 200 hrs. The mean velocity of migration was measured for all tracks followed for at least 5 hours. The root square of MdSD over time was plotted over time and fitted by linear regression. The slopes of the linear fit were compared using an ANCOVA test (linear model). The median cell surface was quantified as the mean of the surface for three time points (25%, 50% and 75%) of the whole cell track and dispersion measured by the Median absolute dispersion (MAD).

Invasion assays

Tissue culture Transwell inserts (8 μ m pore size; Falcon, Franklin Lakes, NJ) were coated for 3 hours with 10 μ g of Matrigel following the manufacturer's instructions (Biocoat, BD Biosciences, San Jose, CA). Inserts were placed into 24-well dishes containing 500 μ l of RPMI medium supplemented with 1% fetal calf serum. 5×10^4 melanoma cells were added to the upper chamber in 250 μ l of serum-free RPMI medium. After 24 hours, transmigrated cells were scored by bright field microscopy. Experiments were performed at least three times, each with duplicate samples.

Image processing and statistical analysis

For the quantification of the number of adhesion structures in C2.7 cells, a semi-automated protocol was developed using Icy software³⁴. Spinning-disk fluorescent microscopy planes were used to detect vinculin structures using HK means thresholding and overlaid binary masks obtained from the threshold projections of F-actin labeled images (Max-entropy method). FAs were detected as spots

positive for both vinculin mCherry and actin structures using Wavelet Spot Detector. The number of adhesions was analyzed using Dunn's multiple comparisons test. The statistical analysis of cell motility was performed in the R software. Medians were compared using a Wilcoxon rank sum test and dispersion by Median absolute dispersion (MAD) parameter.

Microfluidics cell adhesion assay

Analysis of cell detachment under shear stress was based on previous works³⁵. 1205Lu melanocytes were transfected with the indicated constructs, then labeled with 2 μM calcein-AM (Life Technologies) in serum-free DMEM for 20 minutes. Cells were detached by incubation with 2 μM Cytochalasin D (Sigma-Aldrich) for 40 minutes to disassemble FAs, followed by incubation in PBS containing 10 mM EDTA for 20 minutes. Cells were washed in EM buffer (120 mM NaCl, 7 mM KCl, 1.8 mM CaCl_2 , 0.8 mM MgCl_2 , 5 mM glucose and 25 mM HEPES at pH 7.3) by centrifugation and resuspended in the same buffer at a density of 1.5×10^6 cells/ml. Calcein-labeled transfected cells and control unlabeled cells were mixed at a 1:1 ratio and perfused onto a 25 mm-diameter glass coverslips (Marienfeld) previously coated with 20 $\mu\text{g/ml}$ fibronectin and blocked with PBS containing 2% BSA (Sigma-Aldrich) in a microfluidic chamber on a microscope stage at 37°C. We used a commercial microfluidic setup (Flow chamber system 1C, Provitro) and a Miniplus3 peristaltic pump (Gilson) to adjust the flow rate in the chamber. Microscopy analysis was performed using a LEICA DMRIBe inverted microscope equipped with a Cascade 512B camera and LED source lights (Roper Instruments), driven by the Metamorph 7.7 software (Universal imaging). Cells were allowed to settle for the indicated time prior to application of a 4 ml/min, flow corresponding to a wall shear stress of 22.2 dyn/cm^2 (2.22 Pa). Acquisition was performed using a 20 X objective using phase contrast and fluorescence illumination (excitation $480 \pm 20 \text{ nm}$, emission $527 \pm 30 \text{ nm}$). Fluorescent images were acquired before and after flushing to differentiate between target and control cells. Phase contrast images were acquired every 200 ms. Fold enrichment was defined as the ratio between of attached labeled and unlabeled cells.

REFERENCES TO METHODS

486 24 Ramarao, N. *et al.* Capping of actin filaments by vinculin activated by the Shigella IpaA carboxyl-
487 terminal domain. *FEBS letters* **581**, 853-857, doi:10.1016/j.febslet.2007.01.057 (2007).

488 25 Papagrigoriou, E. *et al.* Activation of a vinculin-binding site in the talin rod involves
489 rearrangement of a five-helix bundle. *The EMBO journal* **23**, 2942-2951,
490 doi:10.1038/sj.emboj.7600285 (2004).

491 26 Eubel, H. & Millar, A. H. Systematic monitoring of protein complex composition and abundance
492 by blue-native PAGE. *Cold Spring Harb Protoc*, pdb prot5221, doi:10.1101/pdb.prot5221 (2009).

493 27 Shevchenko A, Tomas H, Havlis J, Olsen JV, Mann M. Nat Protoc. In-gel digestion for mass
494 spectrometric characterization of proteins and proteomes. **1**(6):2856-60 (2006).

495 28 Lima, D. B. *et al.* SIM-XL: A powerful and user-friendly tool for peptide cross-linking analysis. *J*
496 *Proteomics* **129**, 51-55, doi:10.1016/j.jprot.2015.01.013 (2015).

497 29 Hauri, S., Khakzad, H., Happonen, L., Teleman, J., Malmström, J., & Malmström, L. Rapid
498 determination of quaternary protein structures in complex biological samples. *Nature*
499 *communications*, **10**(1), 192. doi:10.1038/s41467-018-07986-1 (2019).

500 30 Song, Y. *et al.* High-resolution comparative modeling with RosettaCM. *Structure* **21**, 1735-1742,
501 doi:10.1016/j.str.2013.08.005 (2013).

502 31 Gray, J. J. High-resolution protein-protein docking. *Current opinion in structural biology* **16**, 183-
503 193, doi:10.1016/j.sbi.2006.03.003 (2006).

504 32 Mitrossilis, D. *et al.* Single-cell response to stiffness exhibits muscle-like behavior. *Proc. Nat.*
505 *Acad. Sci USA*. **106**(43), 18243-18248; <https://doi.org/10.1073/pnas.0903994106> (2009).

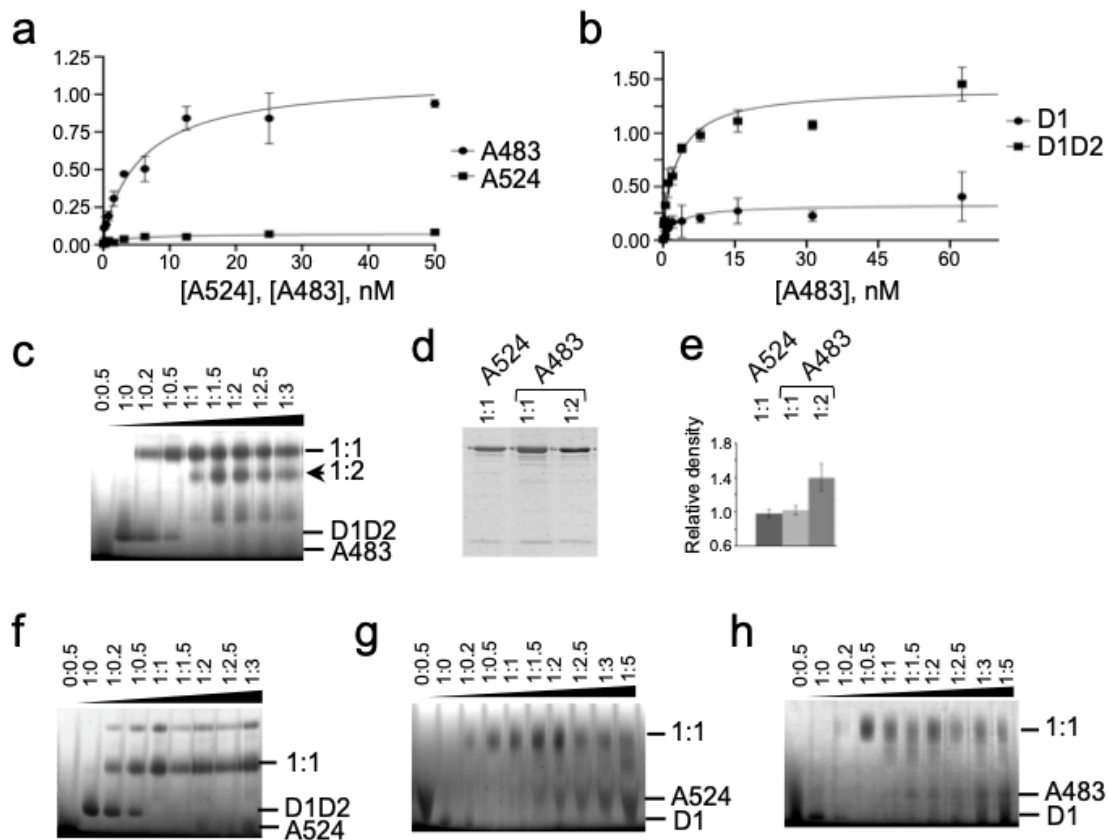
506 33 Smalley, K. S., *et al.* Increased cyclin D1 expression can mediate BRAF inhibitor resistance in
507 BRAF V600E-mutated melanomas. *Mol Cancer Ther.*, **7**(9):2876-83. doi: 10.1158/1535-
508 7163.MCT-08-0431 (2008).

509 34 de Chaumont, F. *et al.* Icy: an open bioimage informatics platform for extended reproducible
510 research. *Nat Methods* **9**, 690-696, doi:10.1038/nmeth.2075 (2012).

511 35 Gutierrez, E. *et al.* Microfluidic devices for studies of shear-dependent platelet adhesion. *Lab*
512 *Chip* **8**, 1486-1495, doi:10.1039/b804795b (2008).

513

514

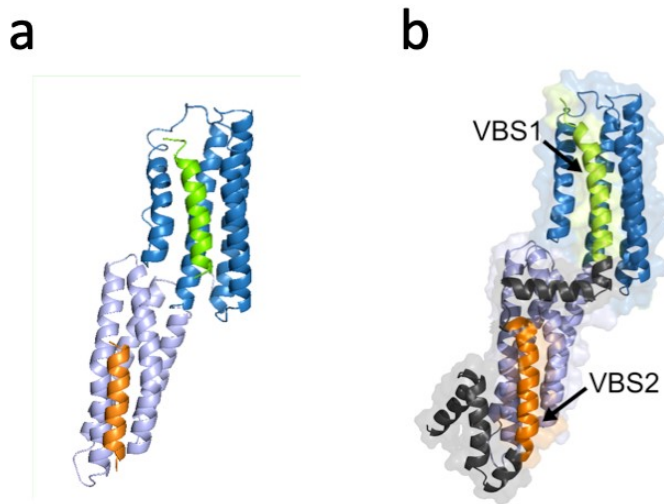


Supplementary Fig. 1. IpaA VBS3 reveals multiple binding sites on vinculin.

a, b, Solid phase binding assays. **a**, coating: HV; ligands: A483 (solid circles); A524 (solid squares). **b**, coating: D1 (solid circles) or HVD1D2 (solid squares); ligand: A483. **c, f-h**, BN-PAGE in 6-18% polyacrylamide gradient gels and Coomassie staining analysis of D1D2:A483 (**c**), D1D2:A524 (**f**), D1:A524 (**g**) or D1:A483 (**h**) complexes. The molar ratio is indicated above each lane. Arrowheads indicate protein alone, or complex migration at the indicated molar ratio. **d**, bands were recovered from BN-PAGE and analyzed in a second dimension SDS-PAGE in a 15% polyacrylamide gel and Coomassie staining. Bands were analyzed by densitometry. **e**, ratio of density values for the A524-D1D2 complex (empty bar) and A483-D1D2 complexes corresponding to the upper (light grey bar) or lower (dark grey bar) shifts.

528

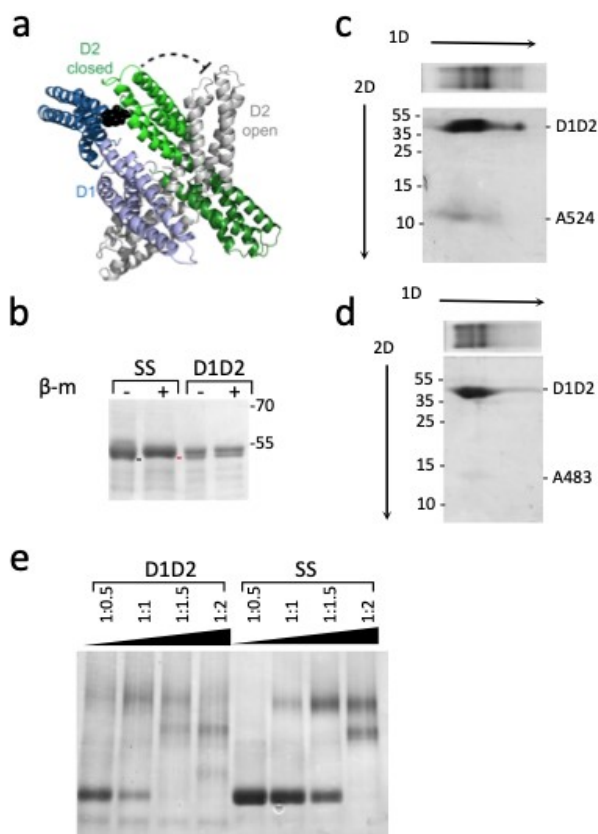
529



530

Supplementary Figure 2. Structural models of vD1:A524. **a**, Structure predicted from the resolved vD1: IpaA VBS1: and vD1:IpaA VBS2 crystal structures^{11, 12}. **b**, Structural model of vD1:A524. The model was established using RosettaCM protocol and accounts for 19 inter and intra-molecular cross-links out of 24 identified (Suppl. Table 1).

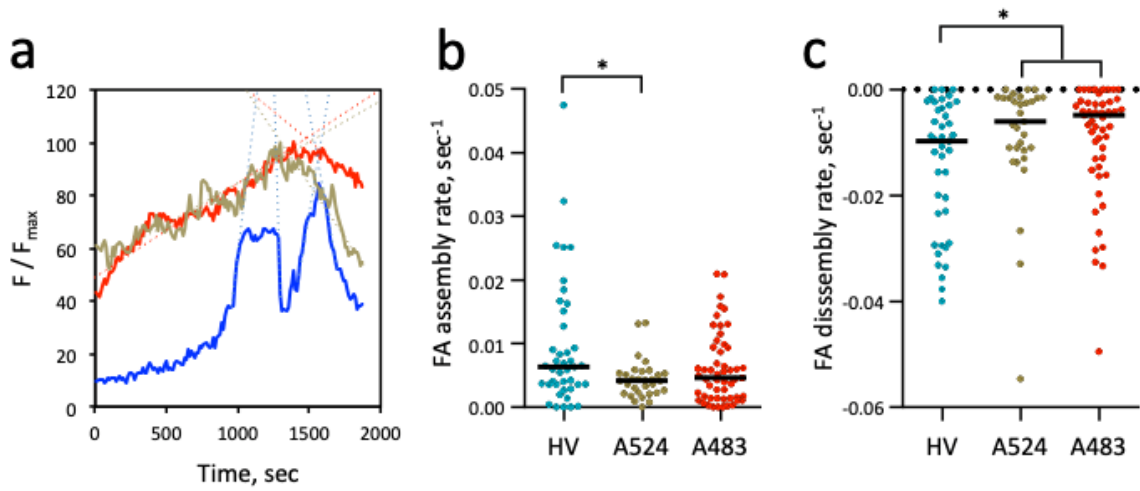
535



Supplementary Figure 3. Cysteine-clamped vinculin D1D2 does not form high order complexes. **a**, Structural model of cystein-clamped vinculin. Blue: D1 domain. Green: D2 domain in the closed conformer. Grey: D2 domain in the open conformer. Black: C68-C396 cystein clamp preventing the switch from closed to open conformers. **b-e**, Coomassie blue staining. **b**, Disulfide bridge formation in D1D2. D1D2: wild-type sequence. SS: D1D2 Q68C A396C. SDS-PAGE analysis using a 10 % polyacrylamide gel. + β -metOH: samples were boiled in Laemmli sample loading buffer containing 5 mM beta-mercaptoethanol prior to SDS-PAGE. The molecular weight markers in kDa are indicated. The black and red bars point the respective migration of unreduced and reduced D1D2 Q68C A396C, respectively. **c**, **d**, gel strips of the native-PAGE corresponding to the A524 + D1D2 (**c**) or A483 + D1D2 (**d**) as shown in **Fig. 1e** were analyzed in a second dimension by SDS-PAGE using a 10 % polyacrylamide gel as depicted. D1D2, SS, A483 and A524 are indicated. **e**, BN-PAGE analysis in a 6-18% polyacrylamide gradient gel of

D1D2:A483 (D1D2) and SS:A483 (SS) complexes. The molar ratio is indicated above each lane.

Arrowheads indicate protein alone, or complex migration



Supplementary Figure 4. TIRF analysis of FA dynamics. C2. 7 cells were transfected with HV-mCherry (HV), HV-mCherry and GFP-A524 (A524) or HV and GFP-A483 (A483). The dynamics of HV-mCherry-labeled FAs were analyzed by TIRF microscopy. **a**, traces correspond to the variations of average fluorescence intensity of a representative single FA (F) normalized to its maximal average fluorescence intensity over the analyzed period in seconds (F_{max}). Blue: HV; green: HV+A524; red: HV+A483. **b**, **c**, instant assembly (**b**) or disassembly (**c**) rates were inferred from the slopes of linear fits as depicted in **a**), with a Pearson correlation value > 0.85 . HV: $n = 41$, $N = 3$; HV+A524: $n = 31$, $N = 2$; HV+A483: $n = 55$, $N = 3$. Mann-Whitney U test. *: $p < 0.05$

566

567

568

569

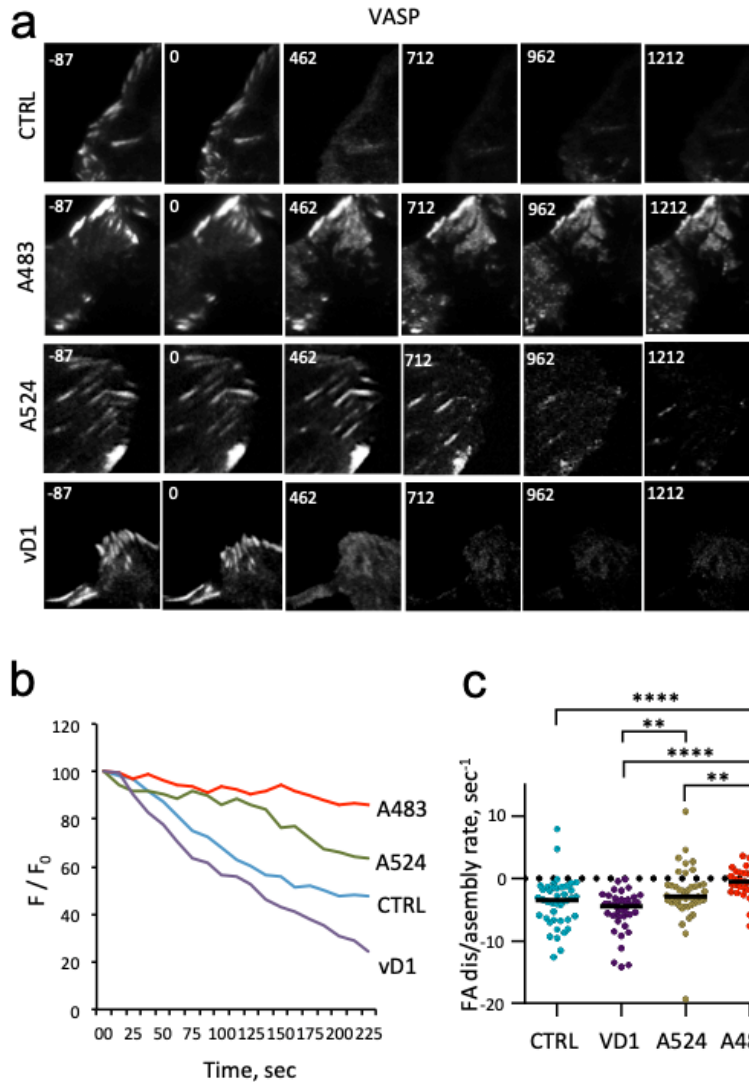
570

571

572

573

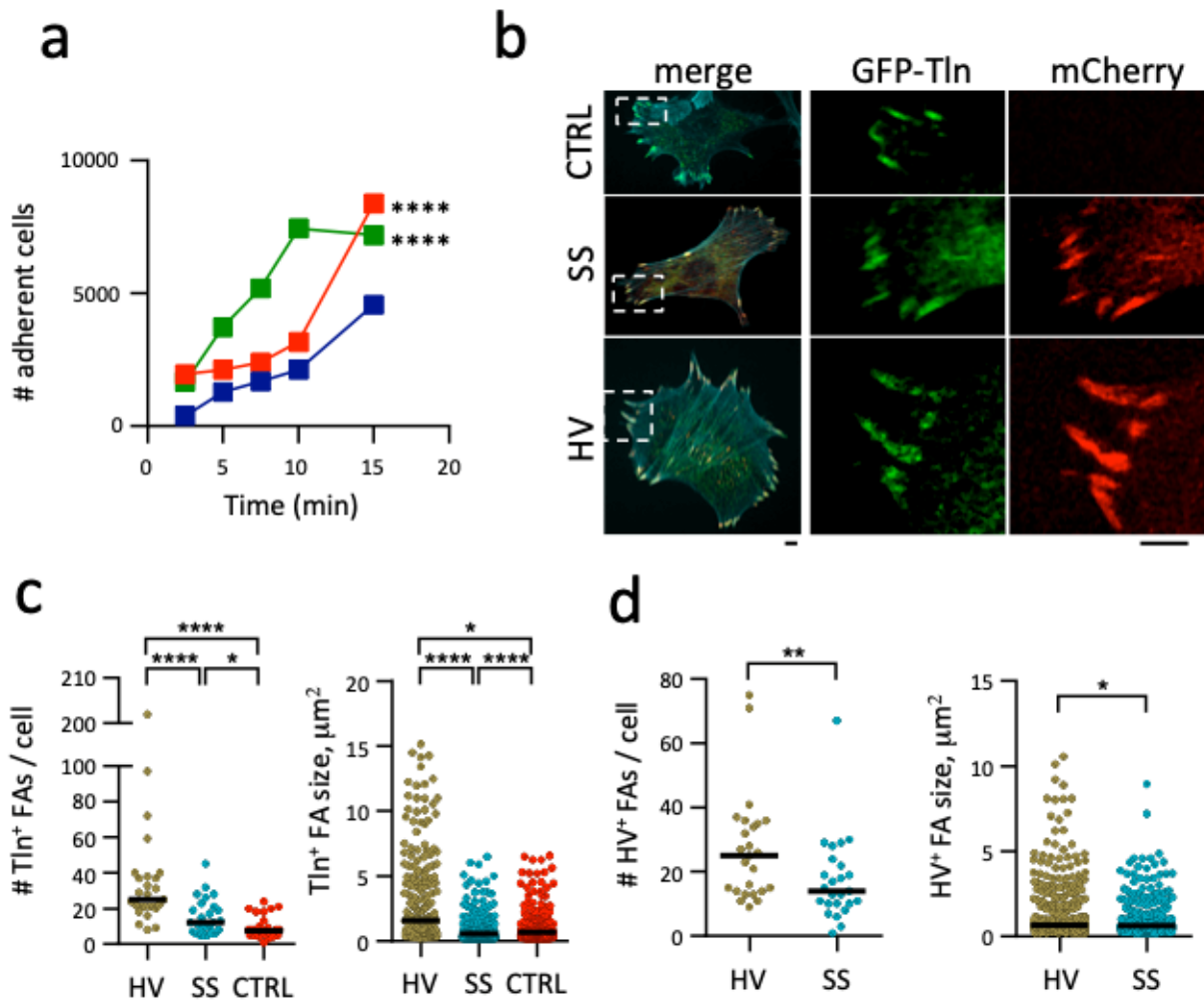
574



Supplementary Figure 5. A483 stabilizes VASP-containing cell adhesions in the absence of mechanotransduction

TIRF microscopy of C2.7 cells transfected with mCherry-VASP alone (CTRL) or co-transfected with GFP-A524 (A524), GFP-vD1 (vD1), or GFP-A483 (A483). Adhesion kinetic parameters were determined from time-lapse acquisitions of cells co-transfected with mCherry-VASP and the indicated construct following treatment with 100 μ M Y-27632. **a**) Representative time series acquisitions. Numbers indicated the elapsed time in seconds, with the inhibitor added at $t = 0$. Scale bar = 5 μ m. **b**, $\Delta F/F_0$: normalized average fluorescence intensity of adhesions as a function of time. Representative traces corresponding to single adhesions for the indicate samples. **c**, initial rates of adhesion disassembly inferred from linear

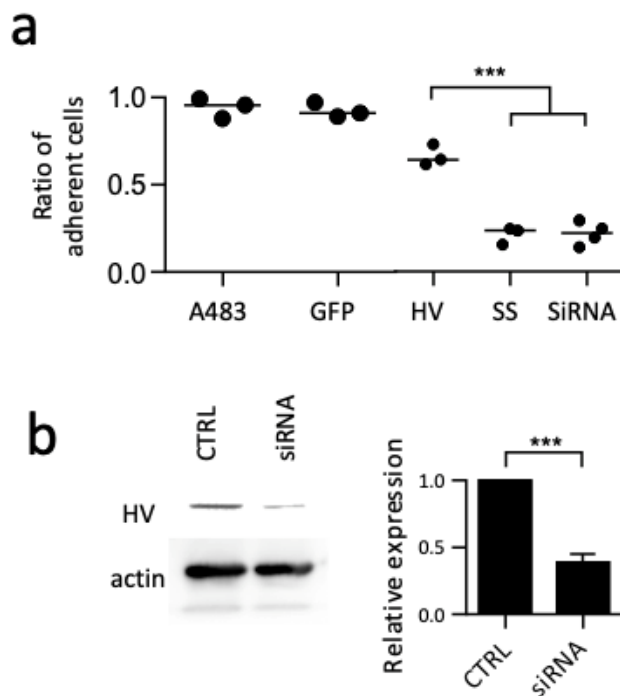
fits. N = 4. Number of adhesions analyzed: CTRL: 42; A483: 43; A524: 40; vD1: 40. Dunn's multiple
comparisons test. *: $p < 0.05$; ****: $p < 0.001$.



Supplementary Figure 6. Effects of A483 and vinculin supra-activation on cell adhesion kinetics

a, 1205Lu melanoma cells were transfected with GFP alone (blue), GFP-A524 (red) or GFP-A483 (green), lifted up by trypsinization and plated for the indicated time on Fn-coated coverslips. Samples were washed, fixed and adherent cells were scored microscopically. The total number of adherent cells scored is indicated. GFP: 3223 cells, N = 4; GFP-A524: n=7418, N = 4; GFP-A483: n = 5668, N = 4. Chi square corrected with Bonferroni multiple comparison correction. ****: $p < 0.001$. **b-d**, MEF vinculin null cells were co-transfected with GFP-talin (CTRL) and full length vinculin-mCherry (HV) or HV Q68C A396C-mCherry (SS). Samples were fixed and processed for fluorescence staining of F-actin. **b**, Representative fluorescence micrographs. Red: Vinculin-mCherry; green:

GFP-talin; cyan: F-actin. Scale bar = 1 μ m. **c, d**, FAs were scored using a semi-automatic detection program (Methods) and their number per cell (left) and size (right) are shown. Bar: median size. FAs labeled with: **c**, GFP-talin; **d**, HV or SS. CTRL: n=28, N=3; HV: n = 25 , N = 3; SS: n = 25, N = 3. Mann-Whitney test with Bonferroni multiple comparison correction. * p<0.05; ** p<0.01; *** p<0.005; **** p<0.001.



Supplementary Figure 7. Role of vinculin supra-activation on cell adhesion.

a, 1205Lu melanoma cells were transfected with the indicated constructs, labeled with calcein (methods) and mixed with the same ratio of control cells. Cells were perfused in a microfluidic chamber and allowed to adhere for 30 min (large solid circles) or 15 min (small solid circles) prior to shear stress application. Scatterplot of the ratio of adherent cells: A483 (N = 3, n = 557); GFP (N = 3, n = 490); HV: vinculin mCherry (N = 3, n = 481);

610 SS: vinculin Q68C A396C-mCherry (N = 3, n = 259); siRNA: cells treated with anti-vinculin siRNA (N = 3, n =
611 395). Unpaired t test. ***: $p < 0.005$. **b**, 1205Lu melanoma cells were mock-transfected (CTRL) or treated with
612 anti-vinculin siRNA (siRNA, Methods). Right: anti-vinculin Western blot analysis. Left: average HV band intensity
613 normalized to that of control cells. Unpaired t test. ***: $p = 0.005$.

614

#	Exp. MH ⁺	Primary Score	Peptide Sequence	A524	Hv D1
32670	4457.1	3.28	IDDTSAELLTDDISDLKNNNDITAENNNIYK - MAKMIDER	D604	K173
32798	1924.16	2.61	INNKLK - ELLPVLISAMK	K540	E200
33042	4613.23	3.70	IDDTSAELLTDDISDLKNNNDITAENNNIYK - NLGPGMTKMAK	D594	K170
33042	4613.23	3.70	IDDTSAELLTDDISDLKNNNDITAENNNIYK - NLGPGMTKMAK	D595	K170
33042	4613.23	4.11	IDDTSAELLTDDISDLKNNNDITAENNNIYK - NLGPGMTKMAK	D604	K170
33322	5310.64	4.48	IDDTSAELLTDDISDLKNNNDITAENNNIYK - VGKETVQTTEQILKR	K600	D67
33334	2347.28	2.51	DVTTSLSKVLK - MSAEINEIIR	K625	E240
33432	2138.26	2.88	VLKNINKD - ELLPVLISAMK	K628	E200
33496	2315.32	3.09	AAKDVTTSLSK - ELLPVLISAMK	K617	E200
34822	2642.55	2.68	AKEVSSALSQVLSK - ELLPVLISAMK	K579	E200
38218	3685.86	3.87	NINKD - TIESILEPVAQQISHLVIMHEEGEVDGK	K632	E31
38218	3685.86	3.66	NINKD - TIESILEPVAQQISHLVIMHEEGEVDGK	K632	E28
#	Exp. MH ⁺	Primary Score	Peptide Sequence	Hv D1	
34075	2342.29	3	ELLPVLISAMK - NLGPGMTKMAK	E200	K170

36135	3088.67	2.62	NFTVE K MSAEINEIR - ELLPVLISAMK	K236	E200
#	Exp. MH ⁺	Primary Score	Peptide Sequence	A524	
14281	3051.56	3.52	NYVTETNADTIDKNHAIYEK - INN K LK	E554	K540
15477	3342.67	2.74	NYVTETNADTIDKNHAIYEK - AKEVSSAL S K	E554	K571
17603	3141.54	2.71	NYVTETNADTIDKNHAIYEK - EVSSAL S K	K562	K572
31359	4483.2	2.64	IDDTSAELLTDDISDLKNNNDITAENNNIYK - AKEVSSAL S K	E590	K571
31996	2965.5	2.94	IDDTSAELLTDDIS D LK - AAKDVTTSLSK	D598	K617
31996	2965.5	2.51	IDDTSAELLT D DISDLK - AAKDVTTSLSK	D594	K617
32705	4586.24	4.1	IDDTSAELLTDDISDLKNNNDITAENNNIYK - AAKDVTTSLS K	E608	K617
33253	3291.74	3.81	IDDTSAELLTDDIS D LK - AKEVSSALS K VLSK	D595	K579
33997	5328.54	4.76	IDDTSAELLTDDISDLKNNNDITAENNNIYK - ID D TSAELLTDDISDLK	K600	D586
34007	4655.33	4.78	IDDTSAELLT D DISDLKNNNDITAENNNIYK - DVTTSLS K VLK	D594	K625

Suppl. Table 1. Cross-linked residues characterized in the D1:A524 complex (XL-amino acids of each protein are bolded in the sequences).

#	Exp. MH ⁺	Primary	Peptide Sequence	A524	Hv D1D2
---	----------------------	---------	------------------	------	---------

		Score			
20480	3470.68	3.86	NYVTETNADTIDKNHAIYEK - NLGPGMTKMAK	E554	K170
23021	3883.92	3.71	NYVTETNADTIDKNHAIYEK - ETVQTTEDQILKR	K562	E60
24707	3117.73	5.00	AKEVSSALSKVLSK - VGKETVQTTEDQILK	K579	E66
36724	4612.22	4.82	IDDTSAELLTDDISDLKNNNDITAENNNIYK - NLGPGMTKMAK	D604	K170
39712	5255.49	3.79	IDDTSAELLTDDISDLKNNNDITAENNNIYK - NLGPGMTKMAKMIDER	D598	K173
39893	5162.6	4.51	IDDTSAELLTDDISDLKNNNDITAENNNIYK - ALAKQVATALQNLQTK	E590	K464
40011	2641.56	4.45	AKEVSSALSKVLSK - ELLPVLISAMK	K579	E200
41002	3047.64	3.99	LKVT DANIR - GILSGTSDLLTFDEAEVR	K542	E128
41440	3944.01	3.86	IDDTSAELLTDDISDLK - AQQVSQGLDVLTA KVENAAR	D598	K366
42699	3685.87	4.03	NINKD -TIESILEPVAQQISHLVIMHEEGEVDGK	K632	E31
#	Exp. MH⁺	Primary Score	Peptide Sequence	Hv D1D2	
25162	3323.71	4.54	LNQAKGWLRDPSASPGDAGEQAIR - ALASIDSK	K281	D274
30025	3169.64	4.03	GQGSSPVAMQKAQQVSQGLDVLTA K - VENAAR	K352	E368
30045	3278.66	3.69	VLQLTSWDEDAWASK - KLEAMTNSKQSIK	D275	K381
30201	3695.87	3.82	LNQAKGWLRDPSASPGDAGEQAIR - MSAEINEIIR	K281	E240
31264	3251.77	5.03	ALAKQVATALQNLQTKTNR - RQGKGDSPEAR	K464	E458
31264	3251.77	4.50	ALAKQVATALQNLQTKTNR - RQGKGDSPEAR	K464	D455

31620	2516.36	3.44	ALASIDSKLNQAK - MSAEINEIR	K295	E240
35256	3787.88	4.12	GILSGTSDLLLTDFDEAEVR - GSSHHHHHHSSGLVPR	E128	G12
38115	3310.75	4.29	GILSGTSDLLLTDFDEAEVR - AVANSRPAKAAVH	E147	K507
39508	3685.90	3.56	GQGSSPVAMQKAQQVSQGLDVLTA - MSAEINEIR	K352	E240
40134	3129.61	2.19	NQGIEEALKNRNFTVEKMMSAEINEIR	E224	K236
40285	3184.71	4.81	AQQVSQGLDVLTAKEVENAAR - SLGEISALTSK	K366	E437
40296	2280.32	3.69	ELLPVLISAMK - LNQAKGWLR	E200	K281
40351	3255.72	4.00	AQQVSQGLDVLTAKEVENAAR - MSAEINEIR	K366	E240
40571	4536.51	4.44	GDSPEARALAKQVATALQNLQTK - SLGEISALTSKLADLRRQ GK	D455	K444
40881	3704.92	4.32	KIDAAQNW LADPN GGPEGEEQIR - ELLPVLISAMK	K387	E200
40923	3100.63	3.94	AQQVSQGLDVLTAKEVENAAR - KLEAMTNSK	E368	K373
41473	3723.01	4.34	GQGSSPVAMQKAQQVSQGLDVLTA - ELLPVLISAMK	K352	E200
41482	4633.41	3.54	TIESILEPVAQQISHLVIMHEEGEVDGK - KLEAMTNSKQSI AK	E28	K381
42201	3294.83	3.66	AQQVSQGLDVLTAKEVENAAR - ELLPVLISAMK	K366	E200
#	Exp. MH ⁺	Primary Score	Peptide Sequence	A524	
15424	3050.56	3.57	NYVTETNADTIDKNHAIYEK - INNKLK	E554	K540
16531	3340.67	3.55	NYVTETNADTIDKNHAIYEK - AKEVSSALSK	E558	K571

16865	3341.67	4.11	NYVT E TNADTIDKNHAIYEK - AKEVSSALSK	E554	K571
34602	4584.25	4.05	IDDTSAELLTDDISDLKNNNDITAENNNIYK - AAKDVTTSLSK	E590	K617
35202	4586.25	5.2	IDDTSAELLTDDISDLKNNNDITAENNNIYK - AAKDVTTSLSK	D594	K617
35824	4583.26	3.43	IDDTSAELLTDDISDLKNNNDITAENNNIYK - AAKDVTTSLSK	E608	K617
39340	4911.48	4.37	IDDTSAELLTDDISDLKNNNDITAENNNIYK - AKEVSSALSKVLSK	D595	K579
39340	4911.48	4.06	IDDTSAELLTDDISDLKNNNDITAENNNIYK - AKEVSSALSKVLSK	D598	K579
39340	4911.48	3.83	IDDTSAELLTDDISDLKNNNDITAENNNIYK - AKEVSSALSKVLSK	E590	K579
39730	3291.74	3.64	IDDTSAELLTDDISDLK - AKEVSSALSKVLSK	D595	K571
40244	4655.32	4.35	IDDTSAELLTDDISDLKNNNDITAENNNIYK - DVTTSLSKVLK	D594	K625
40244	4655.32	4.35	IDDTSAELLTDDISDLKNNNDITAENNNIYK - DVTTSLSKVLK	D595	K625

Suppl. Table 2. Cross-linked residues characterized in the D1D2:A524 complex (XL-amino acids of each protein are bolded in the sequences).

632

633

634

#	Exp. MH ⁺	Primary Score	Peptide Sequence	A483	Hv D1D2
13237	3014.59	3.29	DITKSTTEHR - VGKETVQTTEQILKR	K530	E66
14671	2518.38	2.49	SKDITK - VGKETVQTTEQILKR	K526	E66
14791	2556.44	2.35	INNKLK - VGKETVQTTEQILKR	K540	E66
17806	2621.29	3.10	GSPGIPGDTYLTR - QQELTHQEHR	G517	E181
20039	2571.40	3.08	LKVTANIR - ETVQTTEQILKR	K542	E66
20526	3651.79	3.37	NYVTETNADTIDKNHAIYEK - NSKNQGIEEALK	E554	K219
20985	3469.67	3.01	NYVTETNADTIDKNHAIYEK - NLGPGMTKMAK	D558	K170
22936	3468.66	2.62	NYVTETNADTIDKNHAIYEK - NLGPGMTKMAK	E554	K170
23137	4011	3.29	NYVTETNADTIDKNHAIYEK - VGKETVQTTEQILK	D561	K59
25418	3725.82	3.27	NYVTETNADTIDKNHAIYEK - ETVQTTEQILK	K562	E66
25418	3725.82	3.72	NYVTETNADTIDKNHAIYEK - ETVQTTEQILK	K562	E60
27618	3161.66	3.21	GSPGIPGDTYLTR - VGKETVQTTEQILKR	G517	E60
27618	3161.66	3.61	GSPGIPGDTYLTR - VGKETVQTTEQILKR	G517	D67
28366	2918.61	3.18	EVSSALSKVLSK - VGKETVQTTEQILK -	K579	E66
29996	1977.96	3.06	GSPGIPGDTYLTR - MIDER	G517	D176
36497	2772.45	3.78	GSPGIPGDTYLTR - AQQVSQGLDVLTA	G517	D361
36615	4613.23	3.68	IDDTSAELLTDIDSLKNNNDITAENNNIYK - NLGPGMTKMAK	D594	K170
36632	2214.27	3.22	AKVSSALSK - ELLPVLISAMK -	K571	E200
37536	3824.86	2.64	GSPGIPGDTYLTR - KIDAAQNLADPNNGGPEGEEQIR	G517	D389

40263	3413.78	3.79	GSPGIPGDTYLTR - AQQVSQGLDVLTA K VENAAR	D484	K366
40432	5992.94	5.1	IDDTSAELLTDDISDLKNNNDITAENNNIYK - GQGSSPVAMQKAQQVSQGLDVLTA K	E590	K362
40679	2708.42	3.25	S KDITK - GILSGTSDLLLT F DEAEVR	K526	E128
40994	3074.69	3.12	KVTNSLSNLISLIGTK - ETVQT T EDQILK	K498	E66
41187	4612.22	2.86	IDDTSAELLTDDISDLKNNNDITAENNNIYK - NLGPGMT K MAK	E590	K170
41816	2387.41	3.65	DVTTSLS K VLK - ELLPVLISAMK	K625	E200
43326	3137.65	3.41	AAKDVTTSLSK - GILSGTSDLLLT F DEAEVR	K625	E128
43537	3542.88	3.63	IDDTSAELLT D DISDLK - ALAKQVATALQNLQTK	D594	K464
43612	3604.91	3.34	VTNSLSNLISLIGTKSGTQER - ETVQT T EDQILK	K513	E66
45081	3350.71	3.48	GSPGIPGDTYLTR - GILSGTSD L LLTFDEAEVR	G517	D121
53474	5745.03	4.09	NINKD - TIESILEPVAQQISHLVIMHEEGEV D GKAIPDLTAPV AAVQAAVSNLVR	K632	E31
#	Exp. MH ⁺	Primary Score	Peptide Sequence	Hv D1D2	
17582	1670.89	3.51	VGKETVQT T EDQILK	K59	E66
17582	1670.89	3.38	VGKETVQT D QILK	K59	D67
26000	3322.71	4.03	LNQAKGWL R DPSASPGDAGEQAIR - ALAS I DSK	K281	D374
30901	3169.64	3.79	GQGSSPVAMQKAQQVSQGLDVLTA K - VENAAR	K352	E368
31031	3695.87	3.81	LNQAKGWL R DPSASPGDAGEQAIR - MSAEINE I IR	K281	E240
35827	3665.8	3.75	KIDAAQNWLADPNGG P EGEEQIR - MSAEINE I IR	K387	E240

38215	3040.71	3.43	VGKETVQTTEQILKR - ELLPVLISAMK	K59	K200
39734	3614.9	4.15	GQGSSPVAMQKAQQVSQGLDVLTA - SLGEISALTSK	K352	E437
40218	3580.72	3.88	VLQLTSWDEDAWASKDTEAMK - MSAEINEIIR	K261	E240
40418	2881.63	3.77	QVATALQNLQTKTNR - ELLPVLISAMK	K476	E200
40559	3184.71	4.71	AQQVSQGLDVLTAKEVENAAR - SLGEISALTSK	K366	E437
40560	2280.32	3.35	ELLPVLISAMK - LNQAKGWLR	E200	K281
40604	2553.46	3.78	ALASIDSKLNQAK - ELLPVLISAMK	K276	E200
41140	2892.69	3.97	ALAKQVATALQNLQTK - ELLPVLISAMK	K464	E200
41598	4173.16	5.49	GQGSSPVAMQKAQQVSQGLDVLTAKEVENAAR - KLEAMTNSK	K366	E375
41598	4173.16	5.8	GQGSSPVAMQKAQQVSQGLDVLTAKEVENAAR - KLEAMTNSK	E368	K373
41598	4173.16	4.98	GQGSSPVAMQKAQQVSQGLDVLTAKEVENAAR - KLEAMTNSK	D361	K373
41682	3726.02	3.87	GQGSSPVAMQKAQQVSQGLDVLTAKEVENAAR - ELLPVLISAMK	K352	E200
42387	3293.83	4.63	AQQVSQGLDVLTAKEVENAAR - ELLPVLISAMK	K366	E200
42387	3293.83	3.3	AQQVSQGLDVLTAKEVENAARK - LNQAKGWLR	E368	K281
#	Exp. MH ⁺	Primary Score	Peptide Sequence	A483	
17398	3339.66	3.31	NYVTETNADTIDKNHAIYEK - AKEVSSALSK	D561	K571
17630	3341.68	3.44	NYVTETNADTIDKNHAIYEK - AKEVSSALSK	D558	K571
17630	3341.68	4.19	NYVTETNADTIDKNHAIYEK - AKEVSSALSK	E554	K571

20071	3141.53	3.53	NYVTETNADTIDKNHAIYEK - AKEVSSALSK	K562	E572
20150	3349.69	4.44	NYVTETNADTIDKNHAIYEK - LKVTDANIR	D558	K542
20150	3349.69	4.03	NYVTETNADTIDKNHAIYEK - LKVTDANIR	D561	K542
35163	4584.24	3.59	IDDTSAELLTDDISDLKNNNDITAENNNIYK - AAKDVTTSLSK	D594	K617
35163	4584.24	3.49	IDDTSAELLTDDISDLKNNNDITAENNNIYK - AAKDVTTSLSK	D595	K617
35382	4586.24	3.35	IDDTSAELLTDDISDLKNNNDITAENNNIYK - AAKDVTTSLSK	E590	K617
35967	4584.24	4.42	IDDTSAELLTDDISDLKNNNDITAENNNIYK - AAKDVTTSLSK	D598	K617
35967	4584.24	4.95	IDDTSAELLTDDISDLKNNNDITAENNNIYK - AAKDVTTSLSK	E608	K617
35967	4584.24	4.52	IDDTSAELLTDDISDLKNNNDITAENNNIYK - AAKDVTTSLSK	K600	D618
35967	4584.24	4.22	IDDTSAELLTDDISDLKNNNDITAENNNIYK - AAKDVTTSLSK	K614	D618
35967	4584.24	4.94	IDDTSAELLTDDISDLKNNNDITAENNNIYK - AAKDVTTSLSK	D604	K617
39881	2845.52	4.73	VTNSLSNLISLIGTKSGTQER - ELQEK	K513	E520
39881	2845.52	4.62	VTNSLSNLISLIGTKSGTQER - ELQEK	K513	E523
40044	4655.33	5.07	IDDTSAELLTDDISDLKNNNDITAENNNIYK - DVTTSLSKVLK	D594	K625
40044	4655.33	4.86	IDDTSAELLTDDISDLKNNNDITAENNNIYK - DVTTSLSKVLK	D595	K625

40044	4655.33	4.45	IDDTSAELLTDDIS DL KNNNDITAENNNIYK - DVTTSLSKVL K	D598	K625
40044	4655.33	4.44	IDDTSAELLTDDISDLKNNNDITAENNNIYK - DVTTSLSKVL K	E590	K625
40065	3092.6	3.51	IDDTSAELLTDDISDLK - EVSSALS KVLSK	D594	K579
40065	3092.6	3.38	IDDTSAELLTDDISDLK - EVSSALS KVLSK	D594	K579
40069	3093.61	3.36	IDDTSAELLTDDISDLK - EVSSALS KVLSK	D598	K579
40095	2988.61	4.48	VTNSLSNLISLIGTKSGTQER - VT D ANIR	K513	D545
40448	3252.74	3.81	VTNSLSNLISLIGTKSGTQER - ETIFE A SKK	K513	E494
40603	5153.62	4.36	IDDTSAELLTDDISDLKNNNDITAENNNIYK - KVTNSLSNLISLIGTK	D594	K498
40603	5153.62	4.46	IDDTSAELLTDDISDLKNNNDITAENNNIYK - KVTNSLSNLISLIGTK	D595	K498
40603	5153.62	4.56	IDDTSAELLTDDIS DL KNNNDITAENNNIYK - KVTNSLSNLISLIGTK	D598	K498
40603	5153.62	3.99	IDDTSAELLTDDISDLKNNNDITAENNNIYK - KVTNSLSNLISLIGTK	D604	K498
40606	5153.62	3.53	IDDTSAELLTDDISDLKNNNDITAENNNIYK - KVTNSLSNLISLIGTK	E590	K498
41116	2593.44	3.85	KVTNSLSNLISLIGTK - ETIFE A SK	K498	E490
41142	3909.09	4	ETIFEASKKVTNSLSNLISLIGTK - G SPGIPGDTYLTR	E490	G477

Suppl. Table 3. Cross-linked residues characterized in the D1D2 -A483 1:1 complex (XL-amino acids of each protein are bolded in the sequences)

642

643

Suppl. movie 1. TIRF analysis of HV-mCherry expressing C2.7 cells co-transfected with a GFP fusion to the indicated construct. The time is indicated in seconds.

Suppl. movie 2. TIRF analysis of HV-mCherry expressing C2.7 cells co-transfected with a GFP fusion to the indicated construct. The time is indicated in seconds. At time "0", addition of the Rho kinase inhibitor Y-27632 was added at 100 μ M final concentration.

Suppl. movie3. TIRF analysis of VASP-mCherry expressing C2.7 cells co-transfected with a GFP fusion to the indicated construct. The time is indicated in seconds. At time "0", addition of the Rho kinase inhibitor Y-27632 was added at 100 μ M final concentration.

Suppl. Movie 4. 1205Lu melanoma cells 1205Lu melanoma cells were transfected with the indicated constructs. Cells were perfused in a microfluidic chamber and allowed to adhere for 20 min prior to application of shear stress reaching 22.2 dynes.cm⁻². The elapsed time is indicated in seconds.

5 Article 3

5.1 Overview

The aim of the Article 3 is to look into the functional role of IpaA in the context of *Shigella* invasion. In order to track the localization of IpaA during invasion we developed a *Shigella* strain expressing a tetracysteine-tagged IpaA, allowing its labeling with the FIAsh reagent. Detection of injection-only events led us to further characterize the priming effects on bacterial adhesion induced by kiss-and-run bacteria. Potential clustering of lipid rafts and receptors was further assessed by the presence of active integrin in the host cell surface and microfluidics-based timelapse microscopy. My contribution to this article was the conception and realization of experiments, generation of IpaA tetracystein construct, microscopy analysis and implementation of the microfluidics-based adhesion assay, as well as writing of the manuscript. However, the manuscript here presented is a draft and requires the performance of further experiments.

"Kiss-and-run" priming of host cell invasion by the *Shigella* type III effector IpaA

Daniel Isui Aguilar Salvador^{1,2,3,4}, Guy Tran Van Nhieu^{1,2,3,4*}

¹Equipe Communication Intercellulaire et Infections Microbiennes, Centre de Recherche Interdisciplinaire en Biologie (CIRB), Collège de France, 75005 Paris, France

²Institut National de la Santé et de la Recherche Médicale U1050, 75005 Paris, France

³Centre National de la Recherche Scientifique UMR7241, 75005 Paris, France

⁴MEMOLIFE Laboratory of excellence and Paris Science Lettres.

* For correspondence:

E-mail: guy.tran-van-nhieu@college-de-france.fr

Tel: 33-1-44-27-14-89

FAX: 33-1-44-27-14-19

Keywords: *Shigella*, Type III secretion, invasion, IpaA, vinculin

Abstract

Shigella invades cells of the intestinal epithelium by injecting effector proteins through a Type III Secretion System (T3SS). The type III effector IpaA binds to talin and vinculin through three Vinculin Binding Sites (VBSs), promoting cytoskeletal anchorage to promote bacterial internalization. As opposed to other invasive bacteria, *Shigella* does not show constitutive cell binding activity but triggers transient adhesion through T3SS activation. Here, we show that *Shigella* primes host cells by IpaA injection not resulting in cell invasion. IpaA injected by "kissing-and-running" *Shigella* facilitated additional bacterial binding and invasion events. This IpaA-dependent priming was dependent on IpaA VBS3 but not on IpaA VBS1-2. Injected IpaA was observed to form clusters apposed to the cell apical side and to induce integrin clustering. The results indicate that IpaA triggers general changes in cell adhesive properties and a cooperative mechanism of *Shigella* invasion.

Introduction

Shigella is a highly specialized bacteria that causes bacillary dysentery. Humans are its only known natural host and a very low bacterial load is sufficient to trigger disease (DuPont et al. 1989). All *Shigella* species harbor a large virulence plasmid of ~200 kb that encodes key virulence factors (Sansonetti et al. 1983), including a Type III Secretion System (T3SS) and a set of effector proteins that are translocated into the host cytosol. Unlike other pathogenic bacteria, *Shigella* does not express any known

constitutive adhesin. However, adhesion is induced through the activity of the T3SS that activates binding of the bacterial surface protein IcsA to host cell receptors (Brotcke Zumsteg et al. 2014; Skoudy et al. 2000). Prior to contact with the cell body, *Shigella* is first captured by filopodia, a process mediated by the T3SS tip complex components (Romero et al. 2012). Upon contact with the host membrane, bacterial effector proteins are injected into the host cytoplasm (van der Goot et al. 2004). This initial contact depends on the IpaB-CD44 interaction (Skoudy et al. 2000) and on lipid rafts (Lafont et al. 2002). Once the translocon is formed, injection of first wave of effector proteins that remodel the cytoskeleton takes place within minutes, leading to the formation of actin-rich foci (Enninga et al. 2005). IpaA, one of these *Shigella* type III effectors, is involved in bacterial invasion through its interaction with the focal adhesion proteins vinculin (Tran Van Nhieu, Ben-Ze'ev, and Sansonetti 1997) and talin (Valencia-Gallardo et al. 2019). This interaction is mediated by the presence of three Vinculin Binding Sites (VBS) at the IpaA C-terminal end (Park et al. 2011; Izard, Tran Van Nhieu, and Bois 2006). Recent evidence indicates that IpaA VBS3 also interacts with a partially unfolded conformer of talin (Valencia-Gallardo et al. 2019). Since talin is known to mediate integrin inside-out activation (Changade et al. 2015), IpaA may trigger integrin activation through its interaction with talin.

It has been reported that injection of *Shigella* type III effector proteins in intestinal cells leads to downregulation of antimicrobial peptides in the absence of bacterial invasion (Sperandio et al. 2008). Also, T3S apparatus contact and / or injection of effector proteins in lymphocytes dampens the immune response (Pinaud et al. 2017a; Konradt et al. 2011a). Here, we describe how injection of IpaA by bacteria that transiently

interact with host cells enhances *Shigella* capture associated with inside-out integrin activation. Priming of cells by IpaA injection in a "kiss-and-run" mechanism provides new insights into the *Shigella* invasion process.

Results

Construction of functional 4-Cys-tagged IpaA

To track the injection of IpaA into host cells, we generated a construct corresponding to full length IpaA fused to a teracystein motif (IpaA-4C; Figure 1A; Experimental procedures). This construction allows IpaA-4C detection based on fluorescein-based biarsenical dye (FIAsh) labeling, as previously reported for other *Shigella* and *Salmonella* T3SS effectors (Enninga et al. 2005; Van Engelenburg and Palmer 2008). We first confirmed expression of IpaA-4C in an *ipaA* mutant strain by fluorescence microscopy analysis. As observed for the translocon components IpaB and IpaC prior to secretion, IpaA-4C showed a predominant localization at one bacterial pole (Figure 1B; Enninga et al., 2005; Collet et al., 2018). To determine if IpaA-4C was functional, we performed cell invasion assays. *Shigella ipaA* mutant expressing IpaA-4C showed the same invasion levels of a WT strain, indicating full complementation (Figure 1C).

IpaA injection in host cells in the absence of bacterial invasion

To track IpaA during bacterial early capture and invasion steps, *Shigella* expressing IpaA-4C was incubated with HeLa cells. Because of the low levels of *Shigella* invasivity *in vitro*, invasion assays were performed at high multiplicity of infection (MOI ~1000,

Exp. procedures). As expected from previous immunofluorescence localization studies, IpaA-4C was observed to localize in membrane ruffles at bacterial entry foci (Figure 2A (Tran Van Nhieu 1997)). Surprisingly, all cells, including cells devoid of bacteria, showed increased levels of IpaA-4C signal, as compared to cells incubated with a *mxiD* mutant strain (Figure 2B), indicating that IpaA translocation occurred in the absence of bacterial invasion by "kissing-and-running" bacteria. IpaA-4C showed a diffuse labeling in the cell cytosol and also formed clusters at the cell apical side (Figure 2C). These IpaA clusters were consistently observed in all cells challenged with ipaA / IpaA-4C but not in cells incubated with the *mxiD* / IpaA-4C strain (Figure 2C). The median size of the clusters observed was of 0.34 μm^2 (Figure 2D). These observations indicate that IpaA persists in host cells following injection and suggest its association with a cell component, triggering its clustering at the cell apical membrane.

Injected IpaA promotes inside-out integrin activation

Talin interaction with integrin leads to integrin inside-out activation associated with the formation of integrin nano-clusters (Changade et al. 2015). Since IpaA was shown to bind to talin, presumably stabilizing a partially-unfolded talin conformer (Valencia-Gallardo et al. 2019), we reasoned that the IpaA clusters observed at the apical membrane could be linked to integrin clusters following IpaA- and talin-mediated inside-out activation. To test this, we used an antibody that binds to activated integrin following cell challenge with *Shigella* strains expressing various fragments of IpaA.

As shown in Figure 3, in non-infected cells and cells incubated with the T3S-deficient *mxiD* mutant strain, active integrins showed a diffuse distribution, with clusters usually

detected at one cell edge but not overall the cell body (Figure 3; NT; *mxiD*). In cells challenged with WT *Shigella*, however, clusters were consistently observed throughout the apical cell surface, resembling those present in cells with manganese-induced integrin activation (Figure 3; WT, Mn^{2+}). This change in active integrin distribution was dependent on IpaA, since no such integrin redistribution could be detected when cells were challenged with an *ipaA* mutant strain (Figure 3). We next evaluated the contributions of IpaA VBSs in integrin activation. Neither bacteria lacking all three VBSs nor VBS3 showed increased clustering at the cell body, (Figure 3; dVBS1-3, dVBS3). VBS3 alone was shown to be sufficient to restore active integrin redistribution (Figure 3; dVBS1-2).

Although a qualitative change in active integrin distribution was observed, the overall levels of active integrin were not significantly different between cells challenged with an *ipaA* mutant strain and a wild-type strain, when analyzed by immunofluorescence microscopy (Figure 4A). The lack of significant differences might be due to the detection limits of the procedure used to detect active integrins with respect to the low amounts of IpaA injected by bacteria. To overcome this limitation and further confirm that intracellular IpaA triggered integrin inside-out activation, cells were transfected with constructs containing various IpaA subdomains and analyzed integrin activation. Consistent with previous observations, cells expressing all three VBSs had an increased level of active integrins, reaching overall levels similar to manganese-activated cells (Figure 4B; VBS1-3, $+\text{Mn}^{2+}$). In contrast, cells lacking VBS3 had levels of active integrin similar to non-transfected cells (Figure 4B; VBS1-2; NT). These results indicate that VBS3 mediates integrin activation and clustering.

Priming of epithelial cells by injected IpaA-4C facilitates *de novo* *Shigella* invasion

Previous reports have shown the important role of IpaA in bacterial invasion and the contribution of IpaA VBSs. Given that *Shigella* injection of IpaA into host cells leads to the general activation of integrins on the cell surface, including cells devoid of bacteria, we tested whether "kiss-and-run" injection of IpaA primes cells for *de novo* invasion by extracellular bacteria. A microfluidics setup was implemented to assess *de novo* bacterial capture by primed cells. HeLa cells plated inside the microfluidic chamber were incubated with bacteria for 30 mins to allow for T3 effector injection (priming). Then, samples were washed with buffer to remove bacteria that were not associated with cells and a bacterial suspension was perfused under a constant flow into the chamber. Using this procedure, few rare events of bacterial capture were observed in primed HeLa cells (Figure 5A). In contrast, such capture events were not observed in not-primed cells. This suggests that bacterial capture was promoted by prior bacterial priming.

To better quantify *de novo* bacterial capture, we performed a high-throughput two-wave invasion assay. In the first, priming wave, cells were incubated in 6-well plates with *Shigella ipaA* mutant expressing different IpaA constructs. After washing, cells were challenged with a second wave of wild-type *Shigella*. Samples were fixed and invasion levels were quantified by immunostaining. We used GFP-expressing *Shigella* in the second wave challenge to differentiate bacteria from the two infection waves.

As shown in Fig.5B, priming with *Shigella* WT resulted in a 3-fold increase in *de novo* bacterial capture over cells primed with the T3 secretion-deficient *mxiD* strain. However, when cells were primed with an *ipaA* mutant strain, no increase in bacterial capture was observed indicating that IpaA was required for priming. Bacteria expressing IpaA constructs lacking all three VBSs or VBS3 alone failed to restore *de novo* capture. Remarkably, priming of bacteria expressing IpaA VBS3 alone was sufficient to restore the capture levels (Figure 5B). These results indicate that IpaA VBS3 mediates host cell priming to increase *de novo* bacterial capture and invasion.

Discussion

Here, we report that *Shigella* is able to prime epithelial cells for invasion through a kiss-and-run mechanism. While the effects of injected T3 effectors on immune function of lymphocytes and the downregulation of antimicrobial peptides production were previously observed in the absence of bacterial association (Konradt et al. 2011b; Pinaud et al. 2017b; Sperandio et al. 2008), the impact on bacterial invasion of epithelial cells has not been reported previously.

We show here that IpaA VBS3 is crucial for an efficient integrin clustering and priming of epithelial cells. Since no such effects were observed with IpaA VBS1-2, the IpaA VBS3-dependent priming is likely be due to its unique ability to bind to talin (Valencia-Gallardo et al. 2019). Our results suggest that VBS3 mediates integrin inside-out activation, which might in turn affect integrin clustering and concomitant membrane lipid composition. Indeed, integrins and focal adhesion proteins are associated with lipid rafts

in adhesion structures (Head, Patel, and Insel 2014). These lipid rafts coalesce after integrins engage with fibronectin, permitting the rapid recruitment of talin at FAs (Fuentes and Butler 2012). This process is mediated by integrin-dependent Src-RhoA signaling, leading to activation of formins and consequent actin nucleation (Kalappurakkal et al. 2019), implicating signaling pathways also involved in *Shigella* invasion (Dumenil et al., 1999; Alto et al., 2006; Mounier et al., 2009). Inside-out integrin activation could represent a strategy exploited by *Shigella* to promote capture of additional bacteria, since the association of the T3SS and translocation of protein effectors depends on the presence of lipid rafts enriched in cholesterol and sphingolipids (van der Goot et al. 2004). Furthermore, these membrane domains are also enriched in the hyaluronan receptor CD44, which associates with the T3SS tip complex protein IpaB (Oliferenko et al. 1999). The clustering of integrins might also directly play a role, since IpaB, together with IpaC and IpaD, have also been reported to associate with integrins (Watarai, Funato, and Sasakawa 1996).

Talin and vinculin recruitment at entry sites mediated by IpaA VBSs, together with vinculin activation, could promote the coalescence of lipid rafts at bacterial injection sites. Such process could explain the formation of IpaA clusters at the host cell surface (Park et al. 2011; Izard, Tran Van Nhieu, and Bois 2006; Valencia-Gallardo et al. 2019). Additionally, IpaA activity as RhoA activator could also play a role in promoting integrin clustering (Demali, Jue, and Burridge 2006).

A similar mechanism of cooperative invasion has been reported in *Salmonella* and was shown to be dependent on the presence of *Salmonella*-induced membrane ruffles, (Lorkowski et al. 2014; Misselwitz et al. 2012). Lorkowski et al. showed that additional

bacteria invaded preferentially at sites where an initial invasion event took place. In the present study, although bacteria was observed to bind to *Shigella*-induced ruffles, binding of additional bacteria elsewhere in the cell body was also observed, indicating that membrane ruffling is not necessary to induce *de novo* bacterial capture by kiss-and-run bacteria.

Shigella priming of host cells might also have a favorable impact on other pathogens, such as *Yersinia* spp (Martens, Neumann, and Desai 2018). The intestinal milieu is densely populated by bacteria, and bacterial capture is unlikely to be restricted to *Shigella*. Thus, the promotion of generalized bacterial capture might contribute to co-infections involving *Shigella* and other enteric pathogens, as is evidenced by the high rate of co-infections in dysentery-endemic areas (Andersson et al. 2018).

Experimental procedures

Generation of IpaA-tetracysteine *Shigella* strain

IpaA tetracystein construction (IpaA-4C) was generated by polymerase chain reaction using the 5'-TGCCCGGGCTGCTGCATGGAACCGTAAAAGGGCGAATTCTGCAGA-3', 5'-AGCCCGGGGCACGAGTTCAGGAAATCCTTATTGATATTCTTTA-3' primers and cloned the plasmid pCR2.1 IpaA (Valencia-Gallardo et al. 2019), digested with *Sma*I. All the VBS mutants *S. flexneri* strains were previously reported (Valencia-Gallardo et al. 2019).

Priming assays

All *S. flexneri* strains were cultivated in TCS medium at 37°C under agitation (200 rpm). A fresh culture was grown to mid-exponential phase ($OD_{600}=1$) from an overnight preculture. Bacteria were washed three times on PBS and resuspended on EM buffer (120 mM NaCl, 7 mM KCl, 1.8 mM $CaCl_2$, 0.8 mM $MgCl_2$, 5 mM glucose and 25 mM HEPES at pH 7.3). HeLa cells were plated on coverslips the day before at 300,000 cells per well. Before infection, HeLa cells were washed 3 times in EM buffer and incubated with bacterial suspensions for 45 min. Cells were washed thoroughly three times and the second wave of *Shigella* strains was incubated with the cells for 45 min. Cells were washed and fixed using 3.7% PFA and processed for immunofluorescence staining as previously described (Izard, Tran Van Nhieu, and Bois 2006) .

FIAsh Bacterial imaging

Bacteria grown to mid-exponential phase were washed three times with PBS, and incubated in TCS with the FIAsh reagent at 2 μ M final concentration (Invitrogen). Prior to contact with HeLa cells, bacteria were washed three times in PBS and resuspended in EM buffer. HeLa cells were incubated with suspensions of FIAsh-labeled bacteria for 30 min followed by washing with PBS. After incubation, cells were fixed with PFA 3.7% and washed for 30 min at 37°C in PBS-BAL wash buffer (Invitrogen), permeabilized and stained with anti-LPS and Alexa647-phalloidin.

Flow cytometry

HeLa cells were plated on 6-well plates at 200,000 cell/well a day before transfection with plasmids encoding GFP-IpaA VBS1-2 (A524) or GFP-IpaA VBS1-3 (A483) using JetPRIME (Invitrogen). On the day of transfection, cells were trypsinized, washed and fixed using PFA 4%. Cells were blocked with PBS+FCS 1% and incubated with antibody anti-activated β 1 integrin clone HUTS-4 conjugated with Alexa-647 (Merck-Milipore). Cells were washed and analyzed using a FACS Aria.

Timelapse adhesion video

We used a commercial microfluidic setup (Flow chamber system 1C, Provitro) and a Miniplus3 peristaltic pump (Gilson) to adjust the flow rate in the chamber. Microscopy analysis was performed using a LEICA DMRIBe inverted microscope equipped with a Cascade 512B camera and LED source lights (Roper Instruments), driven by the Metamorph 7.7 software (Universal imaging). Bacteria were grown as described above and injected into the microfluidics setup, followed by an incubation of 15 minutes, followed by washing with EM buffer. The second wave of bacteria was injected into the chamber at a flowrate of 1ml/min and images were acquired at a 100ms interval.

References

- Andersson, Maria, Jean-Claude Kabayiza, Kristina Elfving, Staffan Nilsson, Mwinyi I. Msellem, Andreas Mårtensson, Anders Björkman, Tomas Bergström, and Magnus Lindh. 2018. "Coinfection with Enteric Pathogens in East African Children with Acute Gastroenteritis-Associations and Interpretations." *The American Journal of Tropical Medicine and Hygiene* 98 (6): 1566–70.
- Brotcke Zumsteg, Anna, Christian Goosmann, Volker Brinkmann, Renato Morona, and Arturo Zychlinsky. 2014. "IcsA Is a *Shigella Flexneri* Adhesin Regulated by the Type III Secretion System and Required for Pathogenesis." *Cell Host & Microbe* 15 (4): 435–45.
- Changede, Rishita, Xiaochun Xu, Felix Margadant, and Michael P. Sheetz. 2015. "Nascent Integrin Adhesions Form on All Matrix Rigidities after Integrin Activation." *Developmental Cell* 35 (5): 614–21.
- Demali, Kris A., April L. Jue, and Keith Burridge. 2006. "IpaA Targets beta1 Integrins and Rho to Promote Actin Cytoskeleton Rearrangements Necessary for *Shigella* Entry." *The Journal of Biological Chemistry* 281 (51): 39534–41.
- DuPont, H. L., M. M. Levine, R. B. Hornick, and S. B. Formal. 1989. "Inoculum Size in Shigellosis and Implications for Expected Mode of Transmission." *The Journal of Infectious Diseases* 159 (6): 1126–28.
- Enninga, Jost, Joëlle Mounier, Philippe Sansonetti, and Guy Tran Van Nhieu. 2005. "Secretion of Type III Effectors into Host Cells in Real Time." *Nature Methods* 2 (12): 959–65.
- Fuentes, Daniela E., and Peter J. Butler. 2012. "Coordinated Mechanosensitivity of Membrane Rafts and Focal Adhesions." *Cellular and Molecular Bioengineering* 5 (2): 143–54.
- Goot, Françoise G. van der, Guy Tran van Nhieu, Abdelmounaaim Allaoui, Phillipe Sansonetti, and Frank Lafont. 2004. "Rafts Can Trigger Contact-Mediated Secretion of Bacterial Effectors via a Lipid-Based Mechanism." *The Journal of Biological Chemistry* 279 (46): 47792–98.
- Head, Brian P., Hemal H. Patel, and Paul A. Insel. 2014. "Interaction of Membrane/lipid Rafts with the Cytoskeleton: Impact on Signaling and Function: Membrane/lipid Rafts, Mediators of Cytoskeletal Arrangement and Cell Signaling." *Biochimica et Biophysica Acta* 1838 (2): 532–45.
- Izard, Tina, Guy Tran Van Nhieu, and Philippe R. J. Bois. 2006. "*Shigella* Applies Molecular Mimicry to Subvert Vinculin and Invade Host Cells." *The Journal of Cell Biology* 175 (3): 465–75.
- Kalappurakkal, Joseph Mathew, Anupama Ambika Anilkumar, Chandrima Patra, Thomas S. van Zanten, Michael P. Sheetz, and Satyajit Mayor. 2019. "Integrin Mechano-Chemical Signaling Generates Plasma Membrane Nanodomains That Promote Cell Spreading." *Cell* 177 (7): 1738–56.e23.
- Konradt, Christoph, Elisabetta Frigimelica, Katharina Nothelfer, Andrea Puhar, Wilmara Salgado-Pabon, Vincenzo di Bartolo, Daniel Scott-Algara, Cristina D. Rodrigues, Philippe J. Sansonetti, and Armelle Phalipon. 2011a. "The *Shigella Flexneri* Type Three Secretion System Effector IpgD Inhibits T Cell Migration by Manipulating Host Phosphoinositide Metabolism." *Cell Host & Microbe* 9 (4): 263–72.
- . 2011b. "The *Shigella Flexneri* Type Three Secretion System Effector IpgD Inhibits T Cell Migration by Manipulating Host Phosphoinositide Metabolism." *Cell Host & Microbe* 9 (4): 263–72.
- Lafont, Frank, Guy Tran Van Nhieu, Kentaro Hanada, Philippe Sansonetti, and F. Gisou van der Goot. 2002. "Initial Steps of *Shigella* Infection Depend on the Cholesterol/sphingolipid Raft-Mediated CD44-IpaB Interaction." *The EMBO Journal* 21 (17): 4449–57.

- Lorkowski, Martin, Alfonso Felipe-López, Claudia A. Danzer, Nicole Hansmeier, and Michael Hensel. 2014. "Salmonella Enterica Invasion of Polarized Epithelial Cells Is a Highly Cooperative Effort." *Infection and Immunity* 82 (6): 2657–67.
- Martens, Eric C., Mareike Neumann, and Mahesh S. Desai. 2018. "Interactions of Commensal and Pathogenic Microorganisms with the Intestinal Mucosal Barrier." *Nature Reviews. Microbiology* 16 (8): 457–70.
- Misselwitz, Benjamin, Naomi Barrett, Saskia Kreibich, Pascale Vonaesch, Daniel Andritschke, Samuel Rout, Kerstin Weidner, et al. 2012. "Near Surface Swimming of Salmonella Typhimurium Explains Target-Site Selection and Cooperative Invasion." *PLoS Pathogens* 8 (7): e1002810.
- Oliferenko, S., K. Paiha, T. Harder, V. Gerke, C. Schwärzler, H. Schwarz, H. Beug, U. Günthert, and L. A. Huber. 1999. "Analysis of CD44-Containing Lipid Rafts: Recruitment of Annexin II and Stabilization by the Actin Cytoskeleton." *The Journal of Cell Biology* 146 (4): 843–54.
- Park, Hajeung, Cesar Valencia-Gallardo, Andrew Sharff, Guy Tran Van Nhieu, and Tina Izard. 2011. "Novel Vinculin Binding Site of the IpaA Invasin of *Shigella*." *The Journal of Biological Chemistry* 286 (26): 23214–21.
- Pinaud, Laurie, Fatoumata Samassa, Ziv Porat, Mariana L. Ferrari, Ilia Belotserkovsky, Claude Parsot, Philippe J. Sansonetti, François-Xavier Campbell-Valois, and Armelle Phalipon. 2017a. "Injection of T3SS Effectors Not Resulting in Invasion Is the Main Targeting Mechanism of *Shigella* toward Human Lymphocytes." *Proceedings of the National Academy of Sciences*. <https://doi.org/10.1073/pnas.1707098114>.
- . 2017b. "Injection of T3SS Effectors Not Resulting in Invasion Is the Main Targeting Mechanism of *Shigella* toward Human Lymphocytes." *Proceedings of the National Academy of Sciences*. <https://doi.org/10.1073/pnas.1707098114>.
- Romero, Stephane, Alessia Quatela, Thomas Bornschlögl, Stéphanie Guadagnini, Patricia Bassereau, and Guy Tran Van Nhieu. 2012. "Filopodium Retraction Is Controlled by Adhesion to Its Tip." *Journal of Cell Science* 125 (Pt 21): 4999–5004.
- Sansonetti, P. J., T. L. Hale, G. J. Dammin, C. Kapfer, H. H. Collins Jr, and S. B. Formal. 1983. "Alterations in the Pathogenicity of *Escherichia Coli* K-12 after Transfer of Plasmid and Chromosomal Genes from *Shigella Flexneri*." *Infection and Immunity* 39 (3): 1392–1402.
- Skoudy, A., J. Mounier, A. Aruffo, H. Ohayon, P. Gounon, P. Sansonetti, and G. Tran Van Nhieu. 2000. "CD44 Binds to the *Shigella* IpaB Protein and Participates in Bacterial Invasion of Epithelial Cells." *Cellular Microbiology* 2 (1): 19–33.
- Sperandio, Brice, Béatrice Regnault, Jianhua Guo, Zhi Zhang, Samuel L. Stanley Jr, Philippe J. Sansonetti, and Thierry Pédrón. 2008. "Virulent *Shigella Flexneri* Subverts the Host Innate Immune Response through Manipulation of Antimicrobial Peptide Gene Expression." *The Journal of Experimental Medicine* 205 (5): 1121–32.
- Tran Van Nhieu, G., A. Ben-Ze'ev, and P. J. Sansonetti. 1997. "Modulation of Bacterial Entry into Epithelial Cells by Association between Vinculin and the *Shigella* IpaA Invasin." *The EMBO Journal* 16 (10): 2717–29.
- Valencia-Gallardo, Cesar, Charles Bou-Nader, Daniel-Isui Aguilar-Salvador, Nathalie Carayol, Nicole Quenech'Du, Ludovic Pecqueur, Hajeung Park, Marc Fontecave, Tina Izard, and Guy Tran Van Nhieu. 2019. "*Shigella* IpaA Binding to Talin Stimulates Filopodial Capture and Cell Adhesion." *Cell Reports* 26 (4): 921–32.e6.
- Van Engelenburg, Schuyler B., and Amy E. Palmer. 2008. "Quantification of Real-Time Salmonella Effector Type III Secretion Kinetics Reveals Differential Secretion Rates for SopE2 and SptP." *Chemistry & Biology* 15 (6): 619–28.
- Van Nhieu, G. T. 1997. "Modulation of Bacterial Entry into Epithelial Cells by Association between Vinculin and the *Shigella* IpaA Invasin." *The EMBO Journal*. <https://doi.org/10.1093/emboj/16.10.2717>.
- Watarai, M., S. Funato, and C. Sasakawa. 1996. "Interaction of Ipa Proteins of *Shigella Flexneri*

with alpha5beta1 Integrin Promotes Entry of the Bacteria into Mammalian Cells.” *The Journal of Experimental Medicine* 183 (3): 991–99.

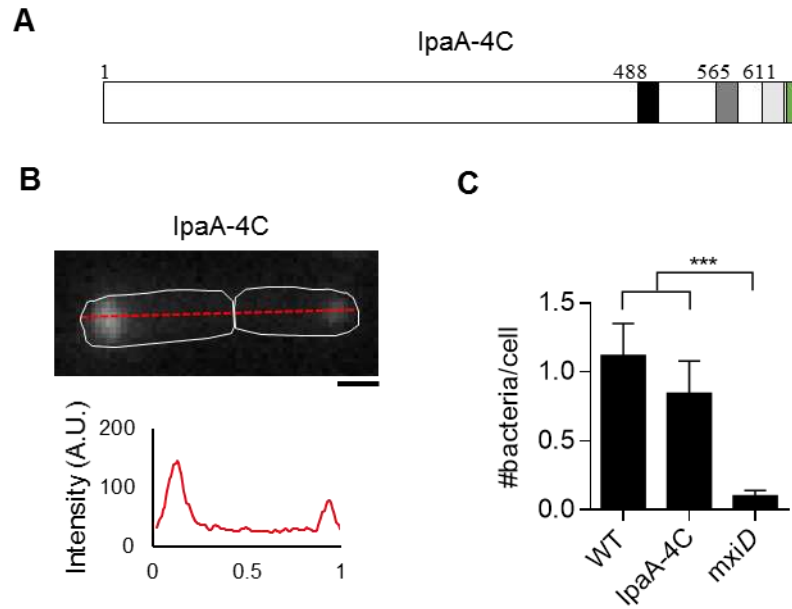


Figure 1. Construction of IpaA-4C. A. Scheme of IpaA-4C construct. VBS are indicated by gray boxes. Tetra-cysteine tag is indicated in green. Numbers indicate aminoacid residue positions. B. Fluorescent image of IpaA-4C-expressing *Shigella* stained with FIAsH reagent and line-scan across dotted line. C. HeLa invasion assays of WT, IpaA-4C-expressing and *mxiD* mutant *Shigella* strains. **** $p < 0.0001$ Unpaired t test.

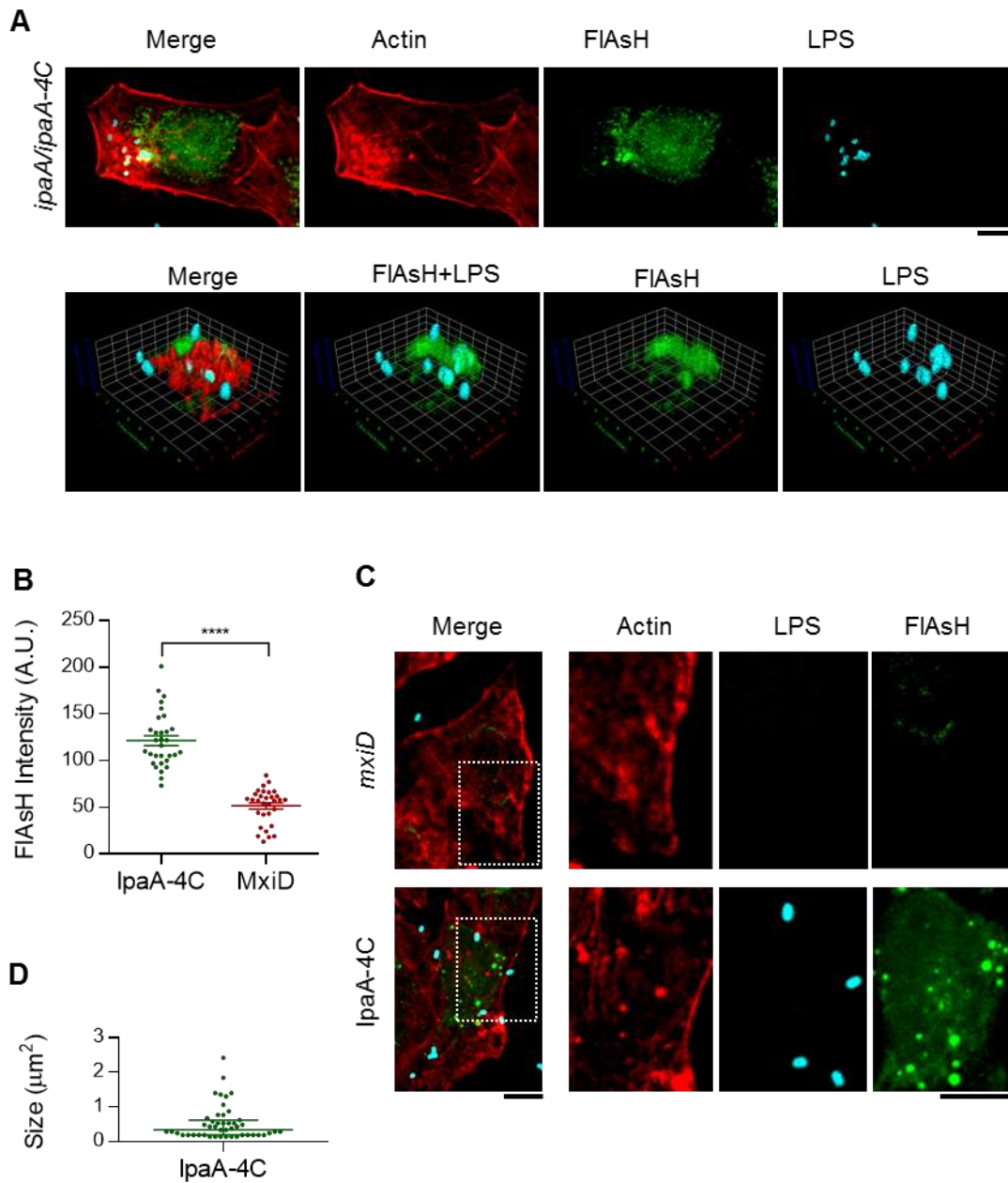


Figure 2. IpaA-4C is injected by kiss-and-run bacteria. A. 2D projections (Top) and 3D renderings (Bottom) of 3D stacks from HeLa challenged with *Shigella* IpaA-4C. B. Quantification of FIAsH fluorescent intensity of HeLa cells challenged with *Shigella* IpaA-4C of *mxiD* strains. C. Fluorescent micrographs of HeLa cells challenged with

Shigella lpaA-4C of *mxiD* strains. Note the presence of FIAsh clusters. D.

Quantification of the size of FIAsh clusters in HeLa cells challenged with *Shigella*

lpaA-4C. **** $p < 0.0001$ Unpaired t test.

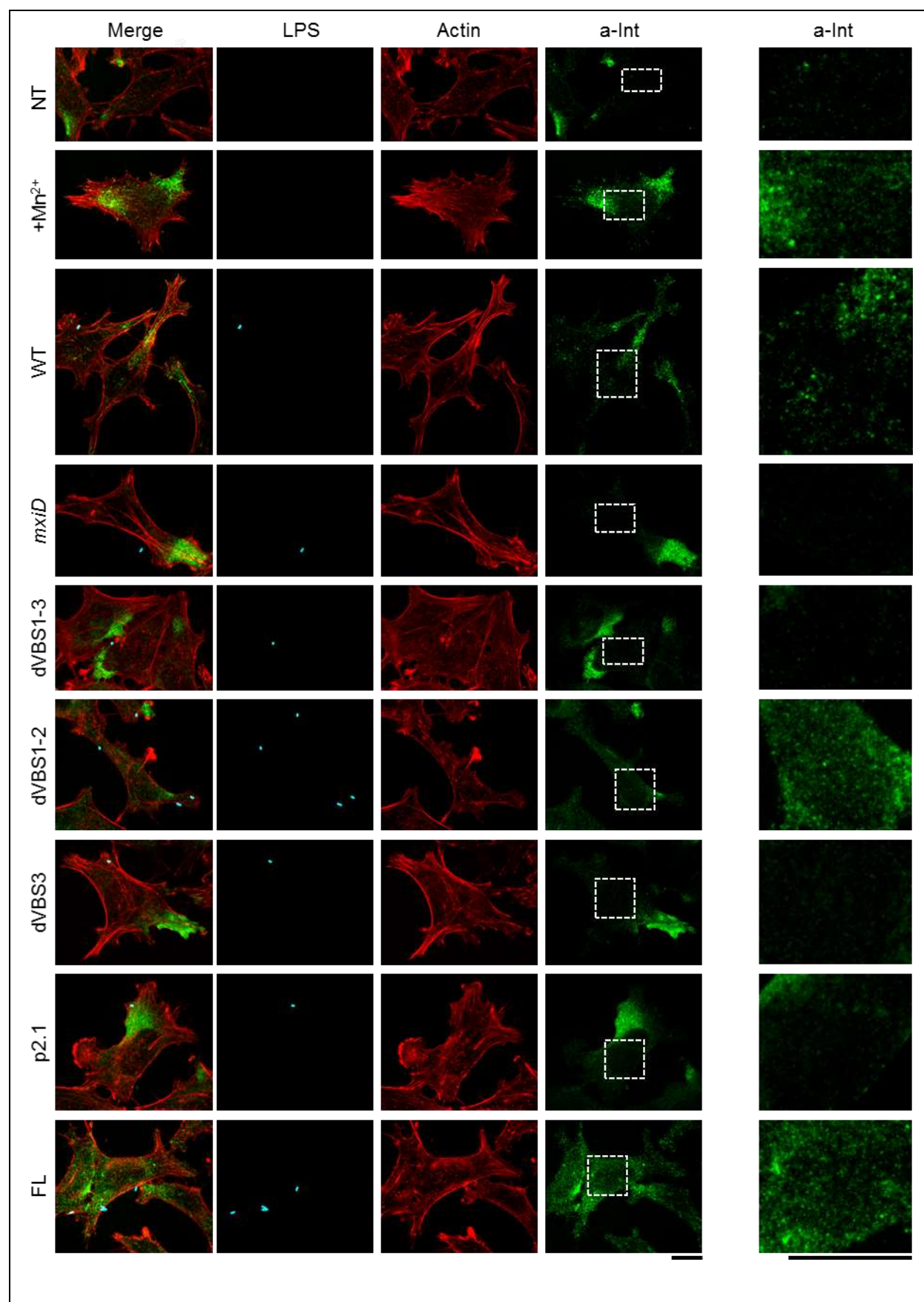


Figure 3. . *Shigella* IpaA VBS3 mediates integrin clustering. HeLa cells were challenged with *Shigella* expressing IpaA constructs lacking the indicated fragments (NT: non-treated; +Mn²⁺: cells incubated with manganese; WT: *Shigella* WT; dVBS1-3; dVBS1-2; dVBS3; p2.1: expression plasmid only; FL: Full-length IpaA).

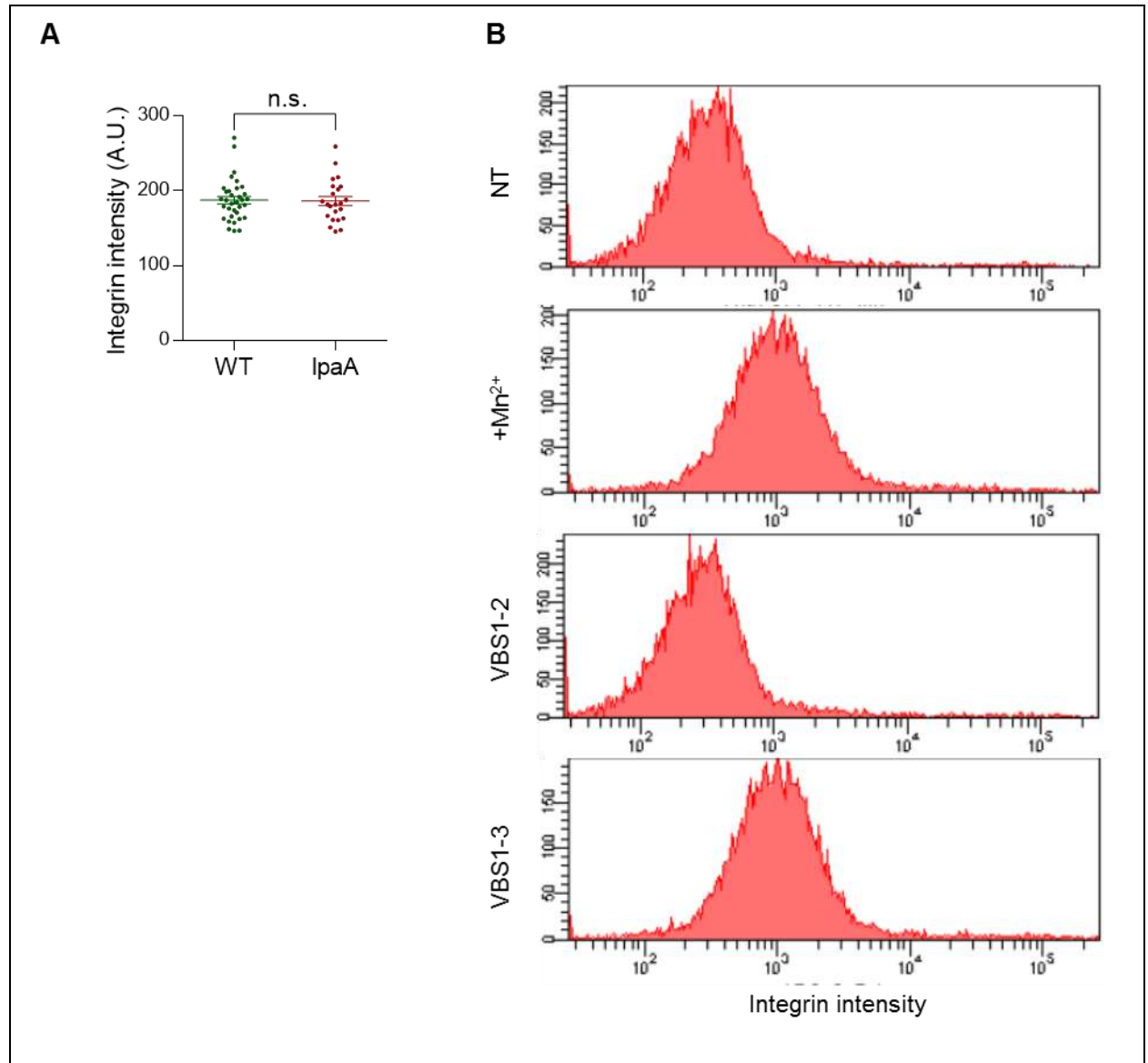


Figure 4. IpaA VBSs lead to integrin activation. A. HeLa cells incubated with the indicated strains. a-Int (Activated integrin). B. HeLa cells were transfected with the indicated IpaA constructs (NT: Non-treated; +Mn²⁺: incubated with manganese), trypsinized, fixed and stained with fluorescently-labeled antibody specific for activated integrin. Histograms are depicted. n.s: non significant. Unpaired t test.

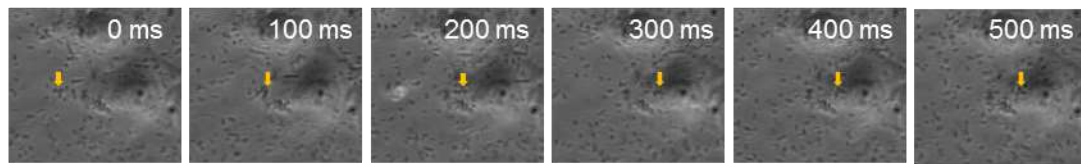
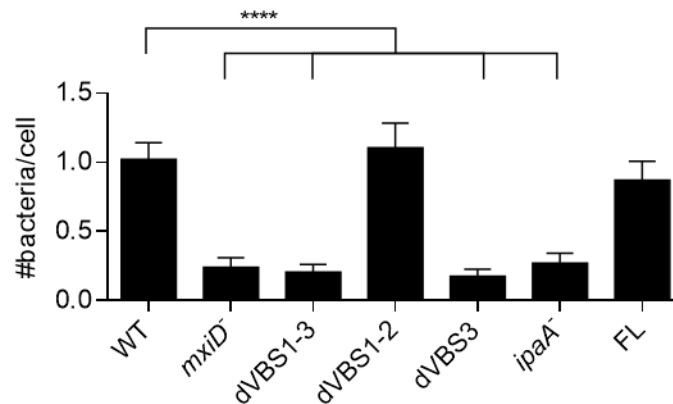
A**B**

Figure 4. *Shigella* cell priming increases bacterial capture. A. Timelapse of microfluidics experiment. Arrow indicates bacteria under flow being captured at the cell body. B. HeLa cells were primed with indicated *Shigella* expressing IpaA constructs lacking the indicated domains (WT: Wild Type; FL: Full-length IpaA), washed and incubated with a second wave of GFP-expressing *Shigella* WT. Number of GFP-bacteria per cell was quantified. **** $p < 0.0001$. Kruskal-Wallis with Dunn's multiple comparison test. Only statistically-significant differences are indicated.

6 Discussion

Shigella is a highly efficient pathogen, despite being non-motile and lacking “conventional” adhesion mechanisms, ingestion of a very low dose is sufficient to trigger dysentery symptoms. The fact that the acquisition of the pINV plasmid allows *E. coli* strains to become invasive and that a convergent loss of motility is observed in different strains, suggest that advantages conferred by motility and constitutive adhesion are fully compensated by proteins carried in the pINV plasmid.

IpaA is a highly conserved protein and strains lacking this protein, and specifically its VBSs, are highly deficient for invasion. Identification of the mechanisms through which this protein exerts its function can lead to a better understanding of invasion strategies not only in *Shigella*, but also in other pathogens, since pathogens often target similar processes.

Because of their biochemical similarity to talin VBSs (i.e. being amphipathic helices with some functionally homologous residues at their contact sites and binding to vinculin in their VD1 domain in a similar fashion), previous studies of isolated IpaA VBS1 and VBS3 have attributed their functional activity to disruption of vinculin head-tail interactions, leading to its activation. VBS2 role was thought to act in conjunction with VBS1 to lock IpaA to vinculin. This would suggest a functional redundancy for IpaA VBS1-2 and VBS3, which seems to be unlikely. It is therefore logical to speculate that IpaA VBSs convey additional functionalities.

In search for novel functions for VBS3, the host laboratory performed a screening for unknown binding partners through a double-hybrid assay, yielding talin as a potential candidate.

Previous studies have shown that IpaA VBS2 binds to the second bundle of VD1, suggesting a binding model where IpaA VBS1 binds to the first bundle of VD1 and IpaA VBS2 to the second bundle, stabilizing the interaction. However, under this scheme a binding site for VBS3 would have to be somewhere else in the vinculin molecule. Solid-phase assays also suggested the unveiling of additional binding sites outside the VD1 vinculin domain when it is incubated with IpaA VBS 1-3, a finding that has not been previously reported for any vinculin-interacting molecule.

6.1 IpaA VBS3 binding to talin

First described as a Vinculin Binding Site, IpaA VBS3 binding to talin is unexpected, as no amphipathic α -helices have been reported to be hybrid talin/vinculin binders. Comparison with other VBSs and residue substitution analysis indicate that hydrophobic interactions are relevant for targeting hydrophobic grooves of both vinculin and talin. However, the residues K498 and R489 account for talin-specific interactions, as suggested by VBSs alignment and affinity analysis. This analysis also suggests that talin and vinculin hybrid binding properties could be a more general property of VBSs, as the same surface is involved in binding to both targets. Furthermore, Talin VBSs 46, 9, 6 and 50; as well as IpaA VBS1 were observed to bind to talin H1-H4 with varying affinity degrees. It is unlikely that this functional similarity is the result of domain duplication, since their aminoacid sequences are remarkably different and their relative positions inside their respective helical bundles is different in some cases. Talin H5, the helix that is replaced by IpaA VBS3, is the fifth helix of a 5-helix bundle and so it is H46. However, talin VBSs 9 and 6 are part of a 4-helix bundle, whilst talin H50 is the fourth helix of a 5-helix bundle.

The fact that hybrid talin-binding VBSs target talin H1-H4 fragment but are unable to bind to the 5-helix bundle indicates hybrid VBSs are unable to displace H5 helix. This would make a partially-unfolded talin conformer the target of these hybrid VBSs. As it is described in the introduction, talin rod unfolds upon force application and there is evidence that talin bundles that contain H1-H4 (Bundle R1) and H46 (Bundle R10) unfold under a similar force range (Yao et al. 2016). In addition, there is modeling and experimental evidence suggesting that some talin bundles have stable intermediates before becoming completely unfolded (Mykuliak et al. 2018), which supports the existence of an R1 bundle with a displaced H5 helix. However, most of the experimental studies performed so far have explored only complete unfolding of helical bundles and lack the sensitivity to detect single-helix displacements. If a talin conformer with its fifth helix is displaced exists, it would most likely be located in cell regions where force exertion is low. In agreement with this hypothesis, we detected the presence of GFP-labeled VBS3 along filopodia. Along filopodia, retraction forces

are driven by actin fibers' retrograde flow and are driven by cortical actin dynamics (Bornschlöggl et al. 2013), thus generating low-range forces on protein linkers such as talin. It is important to note that this labeling was located in talin-enriched regions devoid of vinculin, whereas vinculin signal was detected towards the cell interior, a region where force exertion would be higher.

Based on the high structural similarity between IpaA VBS3 and talin H46 and on the high affinity at which both of them bind to talin H1-H4, we propose talin H46 and perhaps other talin VBSs mediate talin-talin interactions that might result in talin oligomers. The role of these hypothetical talin oligomers requires further studies. It has been reported that the amount of force that can be transmitted by filopodia is limited by the strength of the link between actin fibers and the membrane at the filopodia tip. Talin is recruited at filopodial tips by myosin X and connects actin fibers to integrin (Lagarrigue et al. 2015). It is therefore possible that under a specific force range at which partially-unfolded talin conformers exist, endogenous hybrid VBSs stabilize talin-talin interactions to increase the linkage strength between actin fibers and integrins at the filopodial tips, thus modulating the force exerted by filopodia. Application of increasing forces along the filopodia might disrupt the partially-unfolded conformation and lead to a full exposure of VBSs and to vinculin recruitment towards the cell body (Figure 18A).

GFP tagged IpaA VBS3 localizes to filopodial tip and shaft adhesions and its enriched in nascent adhesions. During *Shigella* invasion, it is likely that its role involves the stabilization of early and low force adhesions. In particular, targeting of nascent and filopodial adhesion structures by *Shigella* is relevant for bacterial invasion for a number of reasons. Being *Shigella*'s first contact with host cells through filopodia, it would be relevant for it to promote its adhesion once the initial contact is established through the T3S apparatus. Indeed, GFP-tagged IpaA VBS3 was detected at bacterial contact sites with filopodial tips. As mentioned before, the limiting factor during in filopodial retraction force lies in the linkage between actin fibers and the membrane. VBS3 stabilization of low-force adhesions at initial contact sites might strengthen this linkage.

6.2 Vinculin supra-activation: a novel interaction mode

All the previously reported VBSs interact with the first domain of vinculin, as has been described for talin, α -actinin (Philippe R. J. Bois et al. 2005, 2006), α -catenin (Peng et al. 2012) and isolated IpaA VBSs (Van Nhieu and Izard 2007; Park, Valencia-Gallardo, et al. 2011; Izard, Tran Van Nhieu, and Bois 2006). Moreover, the classical mode of activation by talin requires mechanical stretching of talin to reveal its cryptic VBSs and it does not involve vinculin oligomerization. This is why the generation of vinculin trimers upon incubation with an IpaA subdomain containing VBSs 1-3 is unexpected. The only mechanism described so far involving vinculin multimerization is by vinculin binding to phosphatidylinositol 4,5 - bisphosphate, which induces homotypic and heterotypic interactions through the vinculin tail domain. This interaction is proposed to contribute to vinculin activation and turnover at focal adhesions (Chinthalapudi et al. 2015, 2016).

Structural modeling of vinculin/IpaA VBS1-3 equimolar complex, based on this cross-link data, suggest the existence of two conformers. In one model IpaA VBS3 binds to the interface between vinculin subdomains VD1 and VD2. This finding alone is outstanding, since no binding sites have been reported to target this region. The second conformer, in addition to contain a VBS3 binding site at the interdomain interface, importantly involves the rearrangement of a conformational change in the orientation between both domains. This finding is also highly relevant, since no rearrangements induced by VBSs in vinculin head domain have ever been reported. This suggests a novel mechanism of action by IpaA VBSs when forming part of the same polypeptide, as opposed to the apparent functional redundancy previously reported when studied separately.

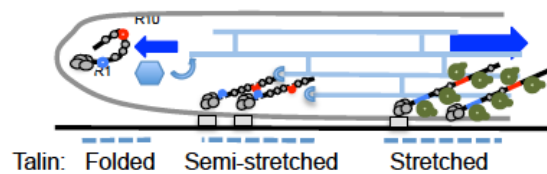
On the other hand, modelling of vinculin interacting with a construct devoid of IpaA VBS3, IpaA VBS1-2, yielded no significant difference in the conformation of vinculin domains VD1 and VD2. IpaA VBS1-2 was also unable to generate high-order vinculin trimers. Thus, vinculin trimer formation and conformational changes require the presence of VBS3 as part of the subdomain.

It is likely that the vinculin/IpaA VBS1-3 modeled structures represent intermediate states between inactive vinculin and the formation of vinculin trimers devoid of IpaA VBS1-3. Under this hypothesis, binding of IpaA would not only disrupt head-tail interactions, but would also trigger conformational changes in vinculin head, unveiling novel binding sites that mediate vinculin-vinculin interactions, perhaps by disrupting interactions between VD1 and VD2 domains. It is reasonable to assume that vinculin multimerization domains are located in the first two vinculin head domains, since trimer formation of full-length vinculin is recapitulated when using vinculin fragments containing only VD1 and VD2. Although no structural modeling of vinculin trimers were generated, it is likely that IpaA VBSs binding pockets become either unavailable or are allosterically modified by vinculin head rearrangement, since no IpaA VBS1-3 was detected in complex with vinculin trimers. If this is the case, it is also likely that affinities for VBSs (e.g. talin, α -actinin, vinexin) from other proteins change when trimers are formed, as they also bind to VD1. This would lead to a force-dependent differential scaffolding of adhesion proteins. This mechanism of regulation is completely different from the “classical” activation described so far, which is why we propose the new term “supra-activation” when referring to this process (Figure 19B).

IpaA-induced conformational changes in vinculin could be proxies of an endogenous process. It is important to remember that vinculin, like talin, lies at the core of adhesion structures, a mechanosensitive structure (Case and Waterman 2015). Both talin and vinculin share also an α -helical bundle structure and both are tethered at their extremes: talin to integrin and F-actin, and vinculin to VBSs and F-actin. Being its tail domain tethered to the fibers, the physical stress could be transmitted to the head domain and lead to conformational changes in the rest of the molecule, in an analogous manner to talin unfolding. This could result in the unveiling of cryptic binding sites, perhaps not only to other vinculin molecules, but also to other proteins. The fact that the trimer is devoid of VBSs might also mirror a physiological process. Supra-activation might induce a change in binding affinities for binding partners under the canonical active state. This might contribute to regulate the scaffolding of adhesions proteins at different levels of tension. Indeed, there is evidence that other proteins involved in adhesions can experience conformational changes (X. Hu et al. 2017). However, direct evidence for trimer formation in vivo and under physiological conditions is still required.

Modelling of vinculin interacting with a construct devoid of IpaA VBS3, IpaA VBS1-2, yielded no significant difference in the conformation of vinculin domains VD1 and VD2. IpaA VBS1-2 was also unable to generate high-order vinculin trimers. Thus, vinculin trimer formation and conformational changes require the presence of VBS3 as part of the subdomain. It is likely that the interaction of VBS3 with the VD1-VD2 interface is crucial to trigger vinculin trimer formation.

A



B

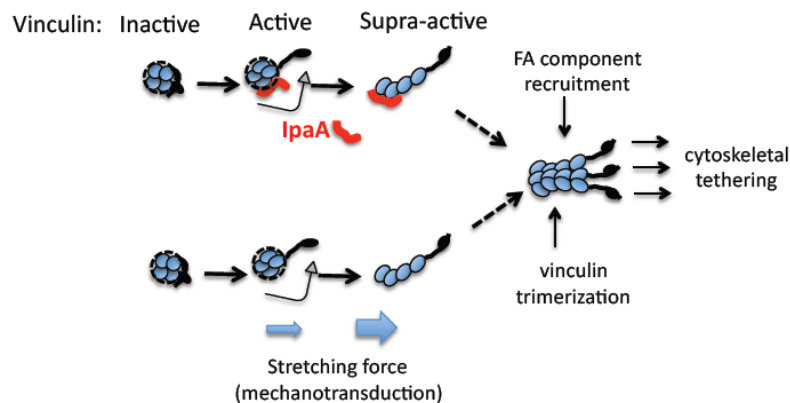


Figure 19. Model of IpaA VBSs interaction with focal adhesion proteins. A. Hybrid vinculin/talin VBS in talin mediates talin oligomers in semi-stretched talin molecules. B. IpaA VBSs lead to supra-activation and vinculin trimerization in the absence of force

Figure 19. Model of IpaA VBSs interaction with focal adhesion proteins

6.3 Functional implications of vinculin supra-activation on cell adhesion

Despite the precise mechanistic details of vinculin-IpaA interaction require further experimental work, there is a marked effect of IpaA VBSs on cell adhesion. Focal adhesions are known to be structures dependent on force exertion, and relaxation of the actomyosin cytoskeleton leads to vinculin disappearance from focal adhesions due to talin refolding (Carisey et al. 2013). Although it is known that constitutively active vinculin and VD1 domains retard talin refolding due to stabilization of unfolded talin VBSs, they also eventually disappear. It is remarkable that adhesion structures in cells transfected with IpaA VBS1-3 resist the effect of actomyosin relaxation by Rho kinase inhibitor, and in some cases adhesions even increase in size, a phenomenon that surpasses the effect of constitutively-active vinculin. This observation further supports a novel force-independent vinculin activation mechanism by IpaA VBSs.

IpaA VBSs effects on focal adhesion increase of stability also impact cell adhesion strength. Microfluidic-adhesion assay also indicates that cell adhesion is enhanced in cells transfected with IpaA VBS1-3 and this effect is dependent on its effects through vinculin. Notably, the difference in resistance to cell detachment between control cells and IpaA VBS1-3 transfected cells is more marked at early time points after initial contact with the substrate. Both cell populations have similar detachment levels at later time points. This would suggest that IpaA VBS1-3 does not have an effect on the adhesion strength that the cell can exert, but it rather triggers force-independent maturation of adhesion structures. These observations suggest IpaA VBS1-3 decreases the amount of force required to trigger adhesion formation by bypassing steps that normally require actomyosin contraction.

It is important to note that neither conformational changes nor the striking cell adhesion effects take place when IpaA VBS 1-2 constructs were analyzed. The results observed for this construct were more in accordance with the canonical activation of vinculin. This stresses the role of IpaA VBS3 in supra-activation and

further supports *in vivo* effects of conformational changes induced by IpaA VBS1-3 on vinculin head observed *in vitro*.

Although there is no direct evidence of trimer formation *in vivo*, the hypothesis that IpaA-mediated supra-activation of vinculin bypasses the requirements of force application is strongly supported by the experimental results.

6.4 IpaA VBSs role during *Shigella* invasion

IpaA VBSs mutants have a low invasion ability, thus highlighting the importance of recruiting vinculin and talin to bacterial entry sites. *Shigella* is first captured by filopodia (Romero et al. 2011), mediated by the interaction between T3 apparatus and filopodial tips. After contact, injection of IpaA might contribute to the stabilization of semi-stretched talin through IpaA VBS3 for an efficient filopodial capture to take place. After filopodial retraction and engagement of increasing forces, talin might completely stretch, leading to IpaA VBS3 release and allowing IpaA interaction with vinculin (Figure 20).

Bacterial anchoring to cytoskeleton is highly important, since in parallel to IpaA secretion T3SS effector proteins IpgB1 and IpgB2 promote the formation of membrane ruffling and bacteria could ultimately be pushed outwards. However, *Shigella* requires to do this in the absence of a counterforce. IpaA induction of conformational changes on vinculin (supra-activation) that would otherwise require force is thus an elegant solution to this problem.

On the other hand, the observation of injection-only events and the presence of IpaA clusters at the cell surface devoid of bacteria suggest a cooperative invasion process, similar to the one reported for *Salmonella*, where additional bacteria are captured by ruffles induced by previous bacteria (Lorkowski et al. 2014). However, it is likely that bacteria undergoing this kiss-and run mechanism result in a priming of the cell surface, rendering competent the host surface for bacterial invasion or

stimulating the formation of filopodia to increase filopodial capture, as *Shigella* IpaA VBSs do.

Bacterial adhesins and flagella are often the target of immune response. In the intestinal lumen the constant shedding of antibodies that target bacterial surface proteins can prevent the adhesion of both commensal and pathogenic bacteria (Kline et al. 2009). Although *Shigella* infections do induce serum and mucosal antibody responses, protection against reinfections is not always conferred (Mani, Wierzba, and Walker 2016). In addition to bacterial effector proteins that dampen the immune response, the lack of bacterial targets such as adhesins and flagella might be part of *Shigella* pathogenic strategy. In order to compensate this, targeting the natural host adhesion machinery to promote bacterial uptake is an elegant strategy.

As evidenced in previous studies, *Shigella* depends on a cholesterol- and sphingolipid-enriched membrane composition to trigger T3S interaction and translocation (van der Goot et al. 2004). This composition is also present in lipid rafts enriched at cellular adhesions (Head, Patel, and Insel 2014). It is thus plausible that IpaA-mediated induction of adhesion-like structures at invasion sites is a strategy to also locally modify membrane composition to promote bacterial contact through T3S apparatus. It is known that talin interaction with integrins can lead to integrin inside-out activation, and activated integrins are associated with lipid rafts, and so are several of the molecules involved in adhesion formation (Changade and Sheetz 2017). This strategy would result in the double function of promoting bacterial adhesion to cell surface and anchoring to host cytoskeleton.

The observation of increase in integrin activation levels in cells transfected with IpaA VBS1-3 supports the hypothesis that IpaA interaction with vinculin and talin promotes inside-out activation. Also, the observation of integrin clustering on the surface of cells injected with kiss-and-run bacteria suggests that *Shigella* injection-only strategy might have an impact in the sensitivity of cells to bacterial capture. Of note, similar strategy of cooperative invasion has been reported in *Salmonella* (Lorkowski et al. 2014),

Furthermore, *Shigella* sensitization of host cells might also have a favorable impact in other pathogens. The intestinal milieu is densely populated by bacteria, and bacterial capture is unlikely to be restricted to *Shigella*. The promotion of unrelated bacterial

capture by *Shigella* might explain the high rate of coinfections of enteric pathogens observed in areas of endemic disease, where coinfection reaches 65% of the cases (Andersson et al. 2018).

Finally, other pathogens might trigger similar vinculin and talin targeting. *Rickettsia* protein Cell Antigen 4, has been described to harbor two VBSs (Park, Lee, et al. 2011), and *Chlamydia* protein TarP contains a segment with three VBSs in a similar spatial arrangement to that of IpaA (Thwaites et al. 2015). However, their mechanism of action remains to be further explored.

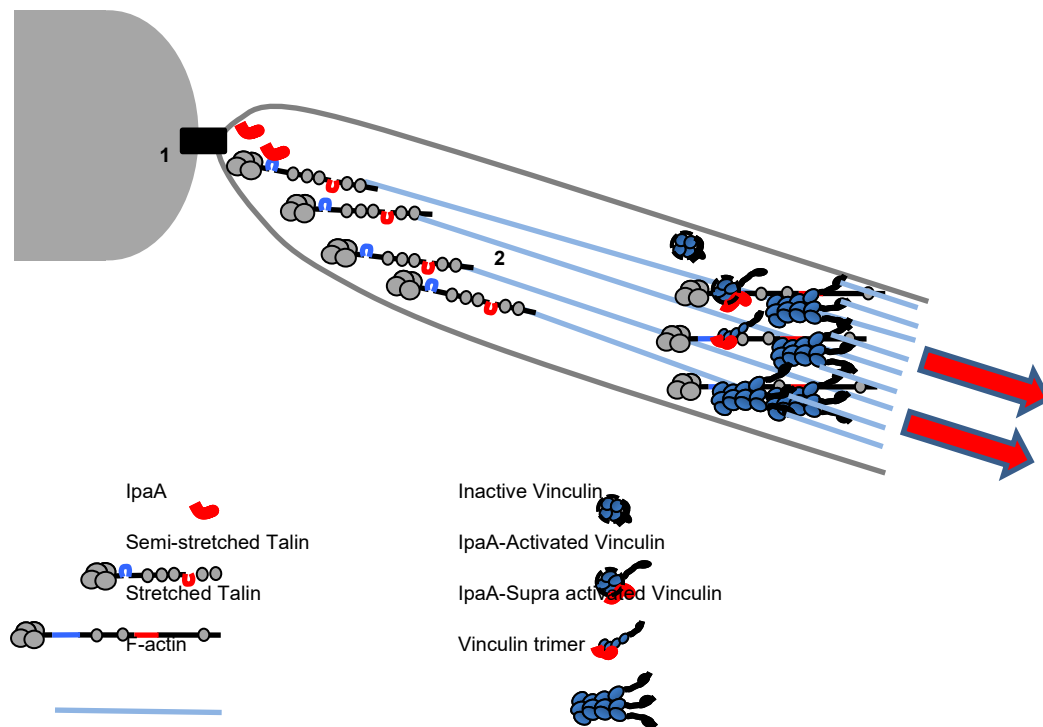


Figure 20. Model for IpaA action on talin and vinculin. 1, IpaA stabilization of semi-stretched talin by IpaA stabilizes initial contact. 2, Activation and supra-activation of vinculin leads to vinculin trimer formation and promotes bacterial anchoring.

Figure 20. Model for IpaA action on talin and vinculin

6.5 General conclusion

This work explored the biochemical and microbiological mechanisms behind IpaA substantial role for *Shigella* invasion. Being a non-motile, constitutively non-adhesive

bacteria, and yet being able to cause disease at a very low inoculum dose, requires *Shigella* to efficiently hijack the host system.

On the biochemical side, we describe a new role of IpaA VBS3 in targeting a semi-stretched talin conformer. We also show a novel mechanism of vinculin activation and induction of conformational changes in vinculin head, pointing towards a potentially unreported physiological mode of action for vinculin on adhesion structures, to which *Shigella* has evolved to take advantage of. This “supra-activation” mechanism, mediated by IpaA VBS1-3, would have the particularity of not requiring the exertion of force to form adhesion-like structures around bacterial foci, This aspect is key for a free-floating bacteria to anchor to its host cytoskeleton, while at the same time inducing membrane ruffling.

On the last part of this work, we show that kiss-and-run injection of effector proteins, and particularly of IpaA, promotes a cooperative invasion. Although IcsA has been reported to act as an inducible adhesin upon bile salt contact, no constitutive receptor has been identified. On the contrary, interaction between the tip complex proteins and lipid rafts components (cholesterol and sphingolipids) and enriched proteins (CD44 and integrins), has been shown to be essential for invasion. Both the recruitment of focal adhesion proteins to bacterial entry sites and the stimulation of RhoA activity induced by IpaA might contribute to the priming of the host surface, enriching it with lipid rafts, and promoting the adhesion and invasion of additional bacteria.

Altogether, IpaA highjacking molecular mechanisms reveal a highly adapted strategy for invasion. First, priming of cells to promote the capture of additional bacteria by talin recruitment to the host membrane and triggering inside-out activation and modifying membrane lipid composition. And second, its ability to take advantage of focal adhesion proteins' mechanosensing properties to promote bacterial anchoring in the absence of counterforces. Functionally, IpaA would first bind to partially-unfolded talin in order to stabilize filopodial adhesions upon bacterial contact. As filopodia retract and the amount of force increases, IpaA would be released from talin due to further talin unfolding and would be free to supra-activate vinculin, leading to the formation of force-independent adhesion-like structures.

It is likely that other pathogens take advantage of similar mechanisms, being cytoskeleton and membrane components common virulence targets. Of note, *Salmonella* can also promote a cooperative invasion dependent on the formation of membrane ruffles (Lorkowski et al. 2014). However, the mechanism behind this phenomenon is different, since the homolog of IpaA in *Salmonella*, SipA, has a low degree of homology with IpaA at its C-terminus and does not possess VBSs (Kaniga, Trollinger, and Galán 1995).

However, other pathogens also harbor VBSs in their effector proteins. Such is the case of Rickettsia protein Cell Antigen 4, where two VBSs have been reported (Park, Lee, et al. 2011) and of Chlamydia protein TarP, which also harbors three VBSs in a highly similar arrangement to Shigella VBSs (Thwaites et al. 2015). Although reported to bind to and activate vinculin, no studies have been done to analyze non-canonical vinculin activation. However, filopodial capture and formation of adhesion-like structures have been observed at entry sites (Ford et al. 2018), which suggest a similar mechanism might take place.

Altogether, IpaA VBS interaction with talin and a novel mechanism of vinculin activation open possibilities for unexpected regulatory processes in cell adhesion. It also points to novel ways in which other pathogens can take advantage of cell adhesion mechanisms.

7 References

- Albuschies, Jörg, and Viola Vogel. 2013. "The Role of Filopodia in the Recognition of Nanotopographies." *Scientific Reports* 3: 1658.
- Al-Hasani, Keith, Fernando Navarro-Garcia, Jazmin Huerta, Harry Sakellaris, and Ben Adler. 2009. "The Immunogenic SigA Enterotoxin of *Shigella Flexneri* 2a Binds to HEp-2 Cells and Induces Fodrin Redistribution in Intoxicated Epithelial Cells." *PloS One* 4 (12): e8223.
- Allison, G. E., and N. K. Verma. 2000. "Serotype-Converting Bacteriophages and O-Antigen Modification in *Shigella Flexneri*." *Trends in Microbiology* 8 (1): 17–23.
- Al Mamun, A. A., A. Tominaga, and M. Enomoto. 1997. "Cloning and Characterization of the Region III Flagellar Operons of the Four *Shigella* Subgroups: Genetic Defects That Cause Loss of Flagella of *Shigella* *Boydii* and *Shigella* *Sonnei*." *Journal of Bacteriology* 179 (14): 4493–4500.
- Alto, Neal M., Feng Shao, Cheri S. Lazar, Renee L. Brost, Gordon Chua, Seema Mattoo, Stephen A. McMahon, et al. 2006. "Identification of a Bacterial Type III Effector Family with G Protein Mimicry Functions." *Cell*. <https://doi.org/10.1016/j.cell.2005.10.031>.
- Amann, K. J., and T. D. Pollard. 2001. "Direct Real-Time Observation of Actin Filament Branching Mediated by Arp2/3 Complex Using Total Internal Reflection Fluorescence Microscopy." *Proceedings of the National Academy of Sciences of the United States of America* 98 (26): 15009–13.
- Anderson, Mark C., Pascale Vonaesch, Azadeh Saffarian, Benoit S. Marteyn, and Philippe J. Sansonetti. 2017. "Shigella *Sonnei* Encodes a Functional T6SS Used for Interbacterial Competition and Niche Occupancy." *Cell Host & Microbe* 21 (6): 769–76.e3.
- Andersson, Maria, Jean-Claude Kabayiza, Kristina Elfving, Staffan Nilsson, Mwinyi I. Msellem, Andreas Mårtensson, Anders Björkman, Tomas Bergström, and Magnus Lindh. 2018. "Coinfection with Enteric Pathogens in East African Children with Acute Gastroenteritis-Associations and Interpretations." *The American Journal of Tropical Medicine and Hygiene* 98 (6): 1566–70.
- Anthis, Nicholas J., Kate L. Wegener, Feng Ye, Chungho Kim, Benjamin T. Goult, Edward D. Lowe, Ioannis Vakonakis, et al. 2009. "The Structure of an Integrin/talin Complex Reveals the Basis of inside-out Signal Transduction." *The EMBO Journal* 28 (22): 3623–32.
- Arena, Ellen T., Francois-Xavier Campbell-Valois, Jean-Yves Tinevez, Giulia Nigro, Martin Sachse, Maryse Moya-Nilges, Katharina Nothelfer, Benoit Marteyn, Spencer L. Shorte, and Philippe J. Sansonetti. 2015. "Bioimage Analysis of Shigella Infection Reveals Targeting of Colonic Crypts." *Proceedings of the National Academy of Sciences*. <https://doi.org/10.1073/pnas.1509091112>.
- Ashida, Hiroshi, Minsoo Kim, Marc Schmidt-Supprian, Averil Ma, Michinaga Ogawa, and Chihiro Sasakawa. 2010. "A Bacterial E3 Ubiquitin Ligase IpaH9.8 Targets NEMO/IKKgamma to Dampen the Host NF-kappaB-Mediated Inflammatory Response." *Nature Cell Biology* 12 (1): 66–73; sup pp 1–9.
- Ashida, Hiroshi, Hiroyasu Nakano, and Chihiro Sasakawa. 2013. "Shigella IpaH0722 E3 Ubiquitin Ligase Effector Targets TRAF2 to Inhibit PKC–NF-κB Activity in Invaded Epithelial Cells." *PLoS Pathogens*. <https://doi.org/10.1371/journal.ppat.1003409>.
- Auernheimer, Vera, Lena A. Lautscham, Maria Leidenberger, Oliver Friedrich, Barbara Kappes, Ben Fabry, and Wolfgang H. Goldmann. 2015. "Vinculin Phosphorylation at Residues Y100 and Y1065 Is Required for Cellular Force Transmission." *Journal of Cell Science* 128 (18): 3435–43.
- Baker, Kate S., Timothy J. Dallman, Philip M. Ashton, Martin Day, Gwenda Hughes, Paul D. Crook, Victoria L. Gilbert, et al. 2015. "Intercontinental Dissemination of Azithromycin-Resistant Shigellosis through Sexual Transmission: A Cross-Sectional Study." *The Lancet Infectious Diseases* 15 (8): 913–21.

- Bakolitsa, Constantina, Daniel M. Cohen, Laurie A. Bankston, Andrey A. Bobkov, Gregory W. Cadwell, Lisa Jennings, David R. Critchley, Susan W. Craig, and Robert C. Liddington. 2004. "Structural Basis for Vinculin Activation at Sites of Cell Adhesion." *Nature*. <https://doi.org/10.1038/nature02610>.
- Barbara W. Bernstein, James R. Bamburg. 2010. "ADF/Cofilin: A Functional Node in Cell Biology." *Trends in Cell Biology* 20 (4): 187.
- Bergounioux, Jean, Ruben Elisee, Anne-Laure Prunier, Françoise Donnadieu, Brice Sperandio, Philippe Sansonetti, and Laurence Arbibe. 2012. "Calpain Activation by the Shigella Flexneri Effector VirA Regulates Key Steps in the Formation and Life of the Bacterium's Epithelial Niche." *Cell Host & Microbe* 11 (3): 240–52.
- Bhunja, Arun K. 2018. "Foodborne Microbial Pathogens." *Food Science Text Series*. <https://doi.org/10.1007/978-1-4939-7349-1>.
- Bishai, Ellen A., Gurjit S. Sidhu, Wei Li, Jess Dhillon, Aparna B. Bohil, Richard E. Cheney, John H. Hartwig, and Frederick S. Southwick. 2013. "Myosin-X Facilitates Shigella-Induced Membrane Protrusions and Cell-to-Cell Spread." *Cellular Microbiology* 15 (3): 353–67.
- Blocker, A., N. Jouihri, E. Larquet, P. Gounon, F. Ebel, C. Parsot, P. Sansonetti, and A. Allaoui. 2001. "Structure and Composition of the Shigella Flexneri 'Needle Complex', a Part of Its Type III Secretion." *Molecular Microbiology* 39 (3): 652–63.
- Bois, Philippe R. J., Robert A. Borgon, Clemens Vornrhein, and Tina Izard. 2005. "Structural Dynamics of Alpha-Actinin-Vinculin Interactions." *Molecular and Cellular Biology* 25 (14): 6112–22.
- Bois, Philippe R. J., Brendan P. O'Hara, Daniel Nietlispach, John Kirkpatrick, and Tina Izard. 2006. "The Vinculin Binding Sites of Talin and α -Actinin Are Sufficient to Activate Vinculin." *Journal of Biological Chemistry*. <https://doi.org/10.1074/jbc.m510397200>.
- Bois, P. R. J., R. A. Borgon, C. Vornrhein, and T. Izard. 2005. "Structural Dynamics of - Actinin-Vinculin Interactions." *Molecular and Cellular Biology*. <https://doi.org/10.1128/mcb.25.14.6112-6122.2005>.
- Bonazzi, Matteo, Esteban Veiga, Javier Pizarro-Cerdá, and Pascale Cossart. 2008. "Successive Post-Translational Modifications of E-Cadherin Are Required for InlA-Mediated Internalization of Listeria Monocytogenes." *Cellular Microbiology* 10 (11): 2208–22.
- Borgon, Robert A., Clemens Vornrhein, Gerard Bricogne, Philippe R. J. Bois, and Tina Izard. 2004. "Crystal Structure of Human Vinculin." *Structure* 12 (7): 1189–97.
- Bornschlöggl, Thomas, Stéphane Romero, Christian L. Vestergaard, Jean-François Joanny, Guy Tran Van Nhieu, and Patricia Bassereau. 2013. "Filopodial Retraction Force Is Generated by Cortical Actin Dynamics and Controlled by Reversible Tethering at the Tip." *Proceedings of the National Academy of Sciences of the United States of America* 110 (47): 18928–33.
- Botteaux, Anne, Christian A. Kayath, Anne-Laure Page, Nouredine Jouihri, Musa Sani, Egbert Boekema, Latéfa Biskri, Claude Parsot, and Abdelmounaaim Allaoui. 2010. "The 33 Carboxyl-Terminal Residues of Spa40 Orchestrate the Multi-Step Assembly Process of the Type III Secretion Needle Complex in Shigella Flexneri." *Microbiology* 156 (Pt 9): 2807–17.
- Bourdet-Sicard, R., M. Rüdiger, B. M. Jockusch, P. Gounon, P. J. Sansonetti, and G. T. Nhieu. 1999. "Binding of the Shigella Protein IpaA to Vinculin Induces F-Actin Depolymerization." *The EMBO Journal* 18 (21): 5853–62.
- Boyd, J. S. 1938. "The Antigenic Structure of the Mannitol-Fermenting Group of Dysentery Bacilli." *The Journal of Hygiene* 38 (4): 477–99.
- Brotcke Zumsteg, Anna, Christian Goosmann, Volker Brinkmann, Renato Morona, and Arturo Zychlinsky. 2014. "IcsA Is a Shigella Flexneri Adhesin Regulated by the Type III Secretion System and Required for Pathogenesis." *Cell Host & Microbe* 15 (4): 435–45.
- Buckley, Craig D., Jiongqi Tan, Karen L. Anderson, Dorit Hanein, Niels Volkmann, William I. Weis, W. James Nelson, and Alexander R. Dunn. 2014. "Cell Adhesion. The Minimal Cadherin-Catenin Complex Binds to Actin Filaments under Force." *Science* 346 (6209):

1254211.

- Burgess, Jamie L., R. Alan Burgess, Yalemi Morales, Jenna M. Bouvang, Sean J. Johnson, and Nicholas E. Dickenson. 2016. "Structural and Biochemical Characterization of Spa47 Provides Mechanistic Insight into Type III Secretion System ATPase Activation and Shigella Virulence Regulation." *The Journal of Biological Chemistry* 291 (50): 25837–52.
- Calcuttawala, Fatema, Chellaram Hariharan, Gururaja P. Pazhani, Santanu Ghosh, and Thandavarayan Ramamurthy. 2015. "Activity Spectrum of Colicins Produced by Shigella Sonnei and Genetic Mechanism of Colicin Resistance in Conspecific S. Sonnei Strains and Escherichia Coli." *Antimicrobial Agents and Chemotherapy* 59 (1): 152–58.
- Campbell-Valois, F-X, and Stéphanie M. Pontier. 2016. "Implications of Spatiotemporal Regulation of Shigella Flexneri Type Three Secretion Activity on Effector Functions: Think Globally, Act Locally." *Frontiers in Cellular and Infection Microbiology* 6 (March): 28.
- Campellone, Kenneth G., Hui-Chun Cheng, Douglas Robbins, Anosha D. Siripala, Emma J. McGhie, Richard D. Hayward, Matthew D. Welch, Michael K. Rosen, Vassilis Koronakis, and John M. Leong. 2008. "Repetitive N-WASP-Binding Elements of the Enterohemorrhagic Escherichia Coli Effector EspF(U) Synergistically Activate Actin Assembly." *PLoS Pathogens* 4 (10): e1000191.
- Campellone, Kenneth G., Douglas Robbins, and John M. Leong. 2004. "EspFU Is a Translocated EHEC Effector That Interacts with Tir and N-WASP and Promotes Nck-Independent Actin Assembly." *Developmental Cell* 7 (2): 217–28.
- Carisey, Alex, Ricky Tsang, Alexandra M. Greiner, Nadja Nijenhuis, Nikki Heath, Alicja Nazgiewicz, Ralf Kemkemer, Brian Derby, Joachim Spatz, and Christoph Ballestrem. 2013. "Vinculin Regulates the Recruitment and Release of Core Focal Adhesion Proteins in a Force-Dependent Manner." *Current Biology*.
<https://doi.org/10.1016/j.cub.2013.01.009>.
- Case, Lindsay B., and Clare M. Waterman. 2015. "Integration of Actin Dynamics and Cell Adhesion by a Three-Dimensional, Mechanosensitive Molecular Clutch." *Nature Cell Biology* 17 (8): 955–63.
- Changade, Rishita, and Michael Sheetz. 2017. "Integrin and Cadherin Clusters: A Robust Way to Organize Adhesions for Cell Mechanics." *BioEssays: News and Reviews in Molecular, Cellular and Developmental Biology* 39 (1): 1–12.
- Chen, Hui, Dilshad M. Choudhury, and Susan W. Craig. 2006. "Coincidence of Actin Filaments and Talin Is Required to Activate Vinculin." *The Journal of Biological Chemistry* 281 (52): 40389–98.
- Chen, Wei, Jizhong Lou, and Cheng Zhu. 2010. "Forcing Switch from Short- to Intermediate- and Long-Lived States of the alphaA Domain Generates LFA-1/ICAM-1 Catch Bonds." *The Journal of Biological Chemistry* 285 (46): 35967–78.
- Cherradi, Youness, Lionel Schiavolin, Simon Moussa, Alaeddine Meghraoui, Ahmed Meksem, Latéfa Biskri, Mohamed Azarkan, Abdelmounaïm Allaoui, and Anne Botteaux. 2013. "Interplay between Predicted Inner-Rod and Gatekeeper in Controlling Substrate Specificity of the Type III Secretion System." *Molecular Microbiology*.
<https://doi.org/10.1111/mmi.12158>.
- Cheung, Martin, Da-Kang Shen, Fumiaki Makino, Takayuki Kato, A. Dorothea Roehrich, Isabel Martinez-Argudo, Matthew L. Walker, et al. 2015. "Three-Dimensional Electron Microscopy Reconstruction and Cysteine-Mediated Crosslinking Provide a Model of the Type III Secretion System Needle Tip Complex." *Molecular Microbiology* 95 (1): 31–50.
- Chinthalapudi, Krishna, Dipak N. Patil, Erumbi S. Rangarajan, Christoph Rader, and Tina Izard. 2015. "Lipid-Directed Vinculin Dimerization." *Biochemistry* 54 (17): 2758–68.
- Chinthalapudi, Krishna, Erumbi S. Rangarajan, David T. Brown, and Tina Izard. 2016. "Differential Lipid Binding of Vinculin Isoforms Promotes Quasi-Equivalent Dimerization." *Proceedings of the National Academy of Sciences*.
<https://doi.org/10.1073/pnas.1600702113>.
- Chinthalapudi, Krishna, Erumbi S. Rangarajan, Dipak N. Patil, Eric M. George, David T.

- Brown, and Tina Izard. 2014. "Lipid Binding Promotes Oligomerization and Focal Adhesion Activity of Vinculin." *The Journal of Cell Biology* 207 (5): 643–56.
- Choi, Young I., Jonathan S. Duke-Cohan, Wei Chen, Baoyu Liu, Jérémie Rossy, Thibault Tabarin, Lining Ju, et al. 2014. "Dynamic Control of $\beta 1$ Integrin Adhesion by the plexinD1-sema3E Axis." *Proceedings of the National Academy of Sciences of the United States of America* 111 (1): 379–84.
- Cilia, V., B. Lafay, and R. Christen. 1996. "Sequence Heterogeneities among 16S Ribosomal RNA Sequences, and Their Effect on Phylogenetic Analyses at the Species Level." *Molecular Biology and Evolution* 13 (3): 451–61.
- Cohen, Daniel M., Hui Chen, Robert P. Johnson, Begum Choudhury, and Susan W. Craig. 2005. "Two Distinct Head-Tail Interfaces Cooperate to Suppress Activation of Vinculin by Talin." *The Journal of Biological Chemistry* 280 (17): 17109–17.
- Cornes, J. S. 1965. "Number, Size, and Distribution of Peyer's Patches in the Human Small Intestine: Part I The Development of Peyer's Patches." *Gut*.
<https://doi.org/10.1136/gut.6.3.225>.
- Crosnier, Cécile, Despina Stamatakis, and Julian Lewis. 2006. "Organizing Cell Renewal in the Intestine: Stem Cells, Signals and Combinatorial Control." *Nature Reviews. Genetics* 7 (5): 349–59.
- Defilippi, P., M. Venturino, D. Gulino, A. Duperray, P. Boquet, C. Fiorentini, G. Volpe, M. Palmieri, L. Silengo, and G. Tarone. 1997. "Dissection of Pathways Implicated in Integrin-Mediated Actin Cytoskeleton Assembly. Involvement of Protein Kinase C, Rho GTPase, and Tyrosine Phosphorylation." *The Journal of Biological Chemistry* 272 (35): 21726–34.
- Demali, Kris A., April L. Jue, and Keith Burrridge. 2006. "IpaA Targets beta1 Integrins and Rho to Promote Actin Cytoskeleton Rearrangements Necessary for Shigella Entry." *The Journal of Biological Chemistry* 281 (51): 39534–41.
- Dobbs, Nicole, Nikolay Burnaevskiy, Didi Chen, Vijay K. Gonugunta, Neal M. Alto, and Nan Yan. 2015. "STING Activation by Translocation from the ER Is Associated with Infection and Autoinflammatory Disease." *Cell Host & Microbe* 18 (2): 157–68.
- Dominguez, Roberto, and Kenneth C. Holmes. 2011. "Actin Structure and Function." *Annual Review of Biophysics* 40: 169–86.
- Dougan, Gordon, and Stephen Baker. 2014. "Salmonella Enterica Seroovar Typhi and the Pathogenesis of Typhoid Fever." *Annual Review of Microbiology* 68: 317–36.
- Du, Juan, Analise Z. Reeves, Jessica A. Klein, Donna J. Twedt, Leigh A. Knodler, and Cammie F. Lesser. 2016. "The Type III Secretion System Apparatus Determines the Intracellular Niche of Bacterial Pathogens." *Proceedings of the National Academy of Sciences of the United States of America* 113 (17): 4794–99.
- DuPont, H. L., M. M. Levine, R. B. Hornick, and S. B. Formal. 1989. "Inoculum Size in Shigellosis and Implications for Expected Mode of Transmission." *The Journal of Infectious Diseases* 159 (6): 1126–28.
- Edwards, Marc, Adam Zwolak, Dorothy A. Schafer, David Sept, Roberto Dominguez, and John A. Cooper. 2014. "Capping Protein Regulators Fine-Tune Actin Assembly Dynamics." *Nature Reviews. Molecular Cell Biology* 15 (10): 677–89.
- Edwards, Philip R., and William Howell Ewing. 1986. *Edwards and Ewing's Identification of Enterobacteriaceae*. Elsevier Publishing Company.
- Egile, C., T. P. Loisel, V. Laurent, R. Li, D. Pantaloni, P. J. Sansonetti, and M. F. Carlier. 1999. "Activation of the CDC42 Effector N-WASP by the Shigella Flexneri IcsA Protein Promotes Actin Nucleation by Arp2/3 Complex and Bacterial Actin-Based Motility." *The Journal of Cell Biology* 146 (6): 1319–32.
- El Hajjami, Nargisse, Simon Moussa, Jonathan Houssa, Daniel Monteyne, David Perez-Morga, and Anne Botteaux. 2018. "The Inner-Rod Component of Shigella Flexneri Type 3 Secretion System, MxiI, Is Involved in the Transmission of the Secretion Activation Signal by Its Interaction with MxiC." *MicrobiologyOpen* 7 (1).
<https://doi.org/10.1002/mbo3.520>.
- Enninga, Jost, Joëlle Mounier, Philippe Sansonetti, and Guy Tran Van Nhieu. 2005.

- “Secretion of Type III Effectors into Host Cells in Real Time.” *Nature Methods* 2 (12): 959–65.
- Epler, Chelsea R., Nicholas E. Dickenson, Esther Bullitt, and Wendy L. Picking. 2012. “Ultrastructural Analysis of IpaD at the Tip of the Nascent MxiH Type III Secretion Apparatus of *Shigella Flexneri*.” *Journal of Molecular Biology* 420 (1-2): 29–39.
- Ewing, W. H. 1949. “SHIGELLA NOMENCLATURE.” *Journal of Bacteriology* 57 (6): 633–38.
- Farag, Tamer H., Abu S. Faruque, Yukun Wu, Sumon K. Das, Anowar Hossain, Shahnawaz Ahmed, Dilruba Ahmed, et al. 2013. “Housefly Population Density Correlates with Shigellosis among Children in Mirzapur, Bangladesh: A Time Series Analysis.” *PLoS Neglected Tropical Diseases* 7 (6): e2280.
- Fasano, A., F. R. Noriega, D. R. Maneval Jr, S. Chanasongcram, R. Russell, S. Guandalini, and M. M. Levine. 1995. “Shigella Enterotoxin 1: An Enterotoxin of *Shigella Flexneri* 2a Active in Rabbit Small Intestine in Vivo and in Vitro.” *The Journal of Clinical Investigation* 95 (6): 2853–61.
- Friebel, A., H. Ilchmann, M. Aepfelbacher, K. Ehrbar, W. Machleidt, and W. D. Hardt. 2001. “SopE and SopE2 from *Salmonella Typhimurium* Activate Different Sets of RhoGTPases of the Host Cell.” *The Journal of Biological Chemistry* 276 (36): 34035–40.
- Gaillard, J. L., P. Berche, C. Frehel, E. Gouin, and P. Cossart. 1991. “Entry of *L. Monocytogenes* into Cells Is Mediated by Internalin, a Repeat Protein Reminiscent of Surface Antigens from Gram-Positive Cocci.” *Cell* 65 (7): 1127–41.
- Garza-Mayers, Anna Cristina, Kelly A. Miller, Brian C. Russo, Dipal V. Nagda, and Marcia B. Goldberg. 2015. “*Shigella Flexneri* Regulation of ARF6 Activation during Bacterial Entry via an IpgD-Mediated Positive Feedback Loop.” *mBio* 6 (2): e02584.
- Georgakopoulou, T., G. Mandilara, K. Mellou, K. Tryfinopoulou, A. Chrisostomou, H. Lillakou, C. Hadjichristodoulou, and A. Vatopoulos. 2016. “Resistant *Shigella* Strains in Refugees, August-October 2015, Greece.” *Epidemiology and Infection* 144 (11): 2415–19.
- Gerbe, François, Emmanuelle Sidot, Danielle J. Smyth, Makoto Ohmoto, Ichiro Matsumoto, Valérie Dardalhon, Pierre Cesses, et al. 2016. “Intestinal Epithelial Tuft Cells Initiate Type 2 Mucosal Immunity to Helminth Parasites.” *Nature* 529 (7585): 226–30.
- Gingras, Alexandre R., Wolfgang H. Ziegler, Ronald Frank, Igor L. Barsukov, Gordon C. K. Roberts, David R. Critchley, and Jonas Emsley. 2005. “Mapping and Consensus Sequence Identification for Multiple Vinculin Binding Sites within the Talin Rod.” *The Journal of Biological Chemistry* 280 (44): 37217–24.
- Goot, Françoise G. van der, Françoise G. van der Goot, Guy Tran van Nhieu, Abdelmounaaim Allaoui, Phillipe Sansonetti, and Frank Lafont. 2004. “Rafts Can Trigger Contact-Mediated Secretion of Bacterial Effectors via a Lipid-Based Mechanism.” *Journal of Biological Chemistry*. <https://doi.org/10.1074/jbc.m406824200>.
- Goot, Françoise G. van der, Guy Tran van Nhieu, Abdelmounaaim Allaoui, Phillipe Sansonetti, and Frank Lafont. 2004. “Rafts Can Trigger Contact-Mediated Secretion of Bacterial Effectors via a Lipid-Based Mechanism.” *The Journal of Biological Chemistry* 279 (46): 47792–98.
- Gruenheid, S., R. DeVinney, F. Bladt, D. Goosney, S. Gelkop, G. D. Gish, T. Pawson, and B. B. Finlay. 2001. “Enteropathogenic *E. Coli* Tir Binds Nck to Initiate Actin Pedestal Formation in Host Cells.” *Nature Cell Biology* 3 (9): 856–59.
- Gu, Bing, Yan Cao, Shiyang Pan, Ling Zhuang, Rongbin Yu, Zhihang Peng, Huimin Qian, et al. 2012. “Comparison of the Prevalence and Changing Resistance to Nalidixic Acid and Ciprofloxacin of *Shigella* between Europe-America and Asia-Africa from 1998 to 2009.” *International Journal of Antimicrobial Agents* 40 (1): 9–17.
- Gupton, Stephanie L., and Frank B. Gertler. 2007. “Filopodia: The Fingers That Do the Walking.” *Science’s STKE: Signal Transduction Knowledge Environment* 2007 (400): re5.
- Haider, K., A. Hossain, C. Wanke, F. Qadri, S. Ali, and S. Nahar. 1993. “Production of Mucinase and Neuraminidase and Binding of *Shigella* to Intestinal Mucin.” *Journal of Diarrhoeal Diseases Research* 11 (2): 88–92.
- Haining, Alexander William M., Magdaléna von Essen, Simon J. Attwood, Vesa P. Hytönen,

- and Armando Del Río Hernández. 2016. "All Subdomains of the Talin Rod Are Mechanically Vulnerable and May Contribute To Cellular Mechanosensing." *ACS Nano* 10 (7): 6648–58.
- Hardt, W. D., L. M. Chen, K. E. Schuebel, X. R. Bustelo, and J. E. Galán. 1998. "S. Typhimurium Encodes an Activator of Rho GTPases That Induces Membrane Ruffling and Nuclear Responses in Host Cells." *Cell* 93 (5): 815–26.
- Hayward, R. D., and V. Koronakis. 1999. "Direct Nucleation and Bundling of Actin by the SipC Protein of Invasive Salmonella." *The EMBO Journal* 18 (18): 4926–34.
- Head, Brian P., Hemal H. Patel, and Paul A. Insel. 2014. "Interaction of Membrane/lipid Rafts with the Cytoskeleton: Impact on Signaling and Function: Membrane/lipid Rafts, Mediators of Cytoskeletal Arrangement and Cell Signaling." *Biochimica et Biophysica Acta* 1838 (2): 532–45.
- Heindl, Jason E., Indrani Saran, Chae-Ryun Yi, Cammie F. Lesser, and Marcia B. Goldberg. 2010. "Requirement for Formin-Induced Actin Polymerization during Spread of Shigella Flexneri." *Infection and Immunity* 78 (1): 193–203.
- Henderson, I. R., J. Czczulin, C. Eslava, F. Noriega, and J. P. Nataro. 1999. "Characterization of Pic, a Secreted Protease of Shigella Flexneri and Enteroaggregative Escherichia Coli." *Infection and Immunity* 67 (11): 5587–96.
- Holt, Kathryn E., Stephen Baker, François-Xavier Weill, Edward C. Holmes, Andrew Kitchen, Jun Yu, Vartul Sangal, et al. 2012. "Shigella Sonnei Genome Sequencing and Phylogenetic Analysis Indicate Recent Global Dissemination from Europe." *Nature Genetics* 44 (9): 1056–59.
- Huang, Derek L., Nicolas A. Bax, Craig D. Buckley, William I. Weis, and Alexander R. Dunn. 2017. "Vinculin Forms a Directionally Asymmetric Catch Bond with F-Actin." *Science* 357 (6352): 703–6.
- Huang, Zhiwei, Sarah E. Sutton, Adam J. Wallenfang, Robert C. Orchard, Xiaojing Wu, Yingcai Feng, Jijie Chai, and Neal M. Alto. 2009. "Structural Insights into Host GTPase Isoform Selection by a Family of Bacterial GEF Mimics." *Nature Structural & Molecular Biology* 16 (8): 853–60.
- Hu, Bo, Dustin R. Morado, William Margolin, John R. Rohde, Olivia Arizmendi, Wendy L. Picking, William D. Picking, and Jun Liu. 2015. "Visualization of the Type III Secretion Sorting Platform of Shigella Flexneri." *Proceedings of the National Academy of Sciences of the United States of America* 112 (4): 1047–52.
- Hu, Xian, Felix Martin Margadant, Mingxi Yao, and Michael Patrick Sheetz. 2017. "Molecular Stretching Modulates Mechanosensing Pathways." *Protein Science: A Publication of the Protein Society* 26 (7): 1337–51.
- Hynes, Richard O. 2002. "Integrins: Bidirectional, Allosteric Signaling Machines." *Cell* 110 (6): 673–87.
- Hytönen, Vesa P., and Viola Vogel. 2008. "How Force Might Activate Talin's Vinculin Binding Sites: SMD Reveals a Structural Mechanism." *PLoS Computational Biology* 4 (2): e24.
- Isenberg, G., U. Aebi, and T. D. Pollard. 1980. "An Actin-Binding Protein from Acanthamoeba Regulates Actin Filament Polymerization and Interactions." *Nature* 288 (5790): 455–59.
- Ito, H., N. Kido, Y. Arakawa, M. Ohta, T. Sugiyama, and N. Kato. 1991. "Possible Mechanisms Underlying the Slow Lactose Fermentation Phenotype in Shigella Spp." *Applied and Environmental Microbiology* 57 (10): 2912–17.
- Izard, Tina, Gwyndaf Evans, Robert A. Borgon, Christina L. Rush, Gerard Bricogne, and Philippe R. J. Bois. 2004. "Vinculin Activation by Talin through Helical Bundle Conversion." *Nature* 427 (6970): 171–75.
- Izard, Tina, Guy Tran Van Nhieu, and Philippe R. J. Bois. 2006. "Shigella Applies Molecular Mimicry to Subvert Vinculin and Invade Host Cells." *The Journal of Cell Biology* 175 (3): 465–75.
- Jacquemet, Guillaume, Hellyeh Hamidi, and Johanna Ivaska. 2015. "Filopodia in Cell Adhesion, 3D Migration and Cancer Cell Invasion." *Current Opinion in Cell Biology* 36 (October): 23–31.
- Jennison, Amy V., and Naresh K. Verma. 2007. "The Acid-Resistance Pathways of Shigella

- Flexneri 2457T." *Microbiology* 153 (Pt 8): 2593–2602.
- Johannes, Ludger, and Winfried Römer. 2010. "Shiga Toxins — from Cell Biology to Biomedical Applications." *Nature Reviews Microbiology*.
<https://doi.org/10.1038/nrmicro2279>.
- Jong, Maarten F. de, Zixu Liu, Didi Chen, and Neal M. Alto. 2016. "Shigella Flexneri Suppresses NF- κ B Activation by Inhibiting Linear Ubiquitin Chain Ligation." *Nature Microbiology* 1 (7): 16084.
- Kalman, D., O. D. Weiner, D. L. Goosney, J. W. Sedat, B. B. Finlay, A. Abo, and J. M. Bishop. 1999. "Enteropathogenic E. Coli Acts through WASP and Arp2/3 Complex to Form Actin Pedestals." *Nature Cell Biology* 1 (6): 389–91.
- Kane, C. D., R. Schuch, W. A. Day, and A. T. Maurelli. 2002. "MxiE Regulates Intracellular Expression of Factors Secreted by the Shigella Flexneri 2a Type III Secretion System." *Journal of Bacteriology*. <https://doi.org/10.1128/jb.184.16.4409-4419.2002>.
- Kaniga, K., D. Trollinger, and J. E. Galán. 1995. "Identification of Two Targets of the Type III Protein Secretion System Encoded by the Inv and Spa Loci of Salmonella Typhimurium That Have Homology to the Shigella IpaD and IpaA Proteins." *Journal of Bacteriology* 177 (24): 7078–85.
- Karaolis, D. K., R. Lan, and P. R. Reeves. 1994. "Sequence Variation in Shigella Sonnei (Sonnei), a Pathogenic Clone of Escherichia Coli, over Four Continents and 41 Years." *Journal of Clinical Microbiology* 32 (3): 796–802.
- Kayath, Christian Aimé, Seamus Hussey, Nargisse El hajjami, Karan Nagra, Dana Philpott, and Abdelmounaaim Allaoui. 2010. "Escape of Intracellular Shigella from Autophagy Requires Binding to Cholesterol through the Type III Effector, IcsB." *Microbes and Infection / Institut Pasteur* 12 (12-13): 956–66.
- Kechagia, Jenny Z., Johanna Ivaska, and Pere Roca-Cusachs. 2019. "Integrins as Biomechanical Sensors of the Microenvironment." *Nature Reviews. Molecular Cell Biology*, June. <https://doi.org/10.1038/s41580-019-0134-2>.
- Kenny, B. 1999. "Phosphorylation of Tyrosine 474 of the Enteropathogenic Escherichia Coli (EPEC) Tir Receptor Molecule Is Essential for Actin Nucleating Activity and Is Preceded by Additional Host Modifications." *Molecular Microbiology* 31 (4): 1229–41.
- Kenny, B., R. DeVinney, M. Stein, D. J. Reinscheid, E. A. Frey, and B. B. Finlay. 1997. "Enteropathogenic E. Coli (EPEC) Transfers Its Receptor for Intimate Adherence into Mammalian Cells." *Cell* 91 (4): 511–20.
- Khalil, Ibrahim A., Christopher Troeger, Brigitte F. Blacker, Puja C. Rao, Alexandria Brown, Deborah E. Atherly, Thomas G. Brewer, et al. 2018. "Morbidity and Mortality due to Shigella and Enterotoxigenic Escherichia Coli Diarrhoea: The Global Burden of Disease Study 1990–2016." *The Lancet Infectious Diseases*. [https://doi.org/10.1016/s1473-3099\(18\)30475-4](https://doi.org/10.1016/s1473-3099(18)30475-4).
- Killackey, Samuel A., Matthew T. Sorbara, and Stephen E. Girardin. 2016. "Cellular Aspects of Shigella Pathogenesis: Focus on the Manipulation of Host Cell Processes." *Frontiers in Cellular and Infection Microbiology* 6 (March): 38.
- Kim, Dong Wook, Gerlinde Lenzen, Anne-Laure Page, Pierre Legrain, Philippe J. Sansonetti, and Claude Parsot. 2005. "The Shigella Flexneri Effector OspG Interferes with Innate Immune Responses by Targeting Ubiquitin-Conjugating Enzymes." *Proceedings of the National Academy of Sciences of the United States of America* 102 (39): 14046–51.
- Kline, Kimberly A., Stefan Fölker, Sofia Dahlberg, Staffan Normark, and Birgitta Henriques-Normark. 2009. "Bacterial Adhesins in Host-Microbe Interactions." *Cell Host & Microbe*. <https://doi.org/10.1016/j.chom.2009.05.011>.
- Kobayashi, Taira, Michinaga Ogawa, Takahito Sanada, Hitomi Mimuro, Minsoo Kim, Hiroshi Ashida, Reiko Akakura, et al. 2013. "The Shigella OspC3 Effector Inhibits Caspase-4, Antagonizes Inflammatory Cell Death, and Promotes Epithelial Infection." *Cell Host & Microbe* 13 (5): 570–83.
- Kong, Fang, Andrés J. García, A. Paul Mould, Martin J. Humphries, and Cheng Zhu. 2009. "Demonstration of Catch Bonds between an Integrin and Its Ligand." *The Journal of Cell Biology* 185 (7): 1275–84.

- Kopecko, D. J., O. Washington, and S. B. Formal. 1980. "Genetic and Physical Evidence for Plasmid Control of Shigella Sonnei Form I Cell Surface Antigen." *Infection and Immunity* 29 (1): 207–14.
- Koronakis, V., P. J. Hume, D. Humphreys, T. Liu, O. Horning, O. N. Jensen, and E. J. McGhie. 2011. "WAVE Regulatory Complex Activation by Cooperating GTPases Arp and Rac1." *Proceedings of the National Academy of Sciences*. <https://doi.org/10.1073/pnas.1107666108>.
- Kotloff, Karen L., Mark S. Riddle, James A. Platts-Mills, Patricia Pavlinac, and Anita K. M. Zaidi. 2018. "Shigellosis." *The Lancet*. [https://doi.org/10.1016/s0140-6736\(17\)33296-8](https://doi.org/10.1016/s0140-6736(17)33296-8).
- Kovar, David R., Elizabeth S. Harris, Rachel Mahaffy, Henry N. Higgs, and Thomas D. Pollard. 2006. "Control of the Assembly of ATP- and ADP-Actin by Formins and Profilin." *Cell* 124 (2): 423–35.
- Lafont, Frank, Guy Tran Van Nhieu, Kentaro Hanada, Philippe Sansonetti, and F. Gisou van der Goot. 2002. "Initial Steps of Shigella Infection Depend on the Cholesterol/sphingolipid Raft-Mediated CD44-IpaB Interaction." *The EMBO Journal* 21 (17): 4449–57.
- Lagarrigue, Frederic, Praju Vikas Anekal, Ho-Sup Lee, Alexia I. Bachir, Jailal N. Ablack, Alan F. Horwitz, and Mark H. Ginsberg. 2015. "A RIAM/lamellipodin–talin–integrin Complex Forms the Tip of Sticky Fingers That Guide Cell Migration." *Nature Communications*. <https://doi.org/10.1038/ncomms9492>.
- Lebrand, Cecile, Erik W. Dent, Geraldine A. Strasser, Lorene M. Lanier, Matthias Krause, Tatyana M. Svitkina, Gary G. Borisy, and Frank B. Gertler. 2004. "Critical Role of Ena/VASP Proteins for Filopodia Formation in Neurons and in Function Downstream of Netrin-1." *Neuron* 42 (1): 37–49.
- Lecuit, M., R. Hurme, J. Pizarro-Cerda, H. Ohayon, B. Geiger, and P. Cossart. 2000. "A Role for Alpha - and Beta -Catenins in Bacterial Uptake." *Proceedings of the National Academy of Sciences*. <https://doi.org/10.1073/pnas.97.18.10008>.
- Lecuit, M., H. Ohayon, L. Braun, J. Mengaud, and P. Cossart. 1997. "Internalin of Listeria Monocytogenes with an Intact Leucine-Rich Repeat Region Is Sufficient to Promote Internalization." *Infection and Immunity* 65 (12): 5309–19.
- Lee, Ho-Sup, Chinten James Lim, Wilma Puzon-McLaughlin, Sanford J. Shattil, and Mark H. Ginsberg. 2009. "RIAM Activates Integrins by Linking Talin to Ras GTPase Membrane-Targeting Sequences." *The Journal of Biological Chemistry* 284 (8): 5119–27.
- Leung, Yiuka, Shabeen Ally, and Marcia B. Goldberg. 2008. "Bacterial Actin Assembly Requires Toca-1 to Relieve N-Wasp Autoinhibition." *Cell Host & Microbe* 3 (1): 39–47.
- Levine, M. M., H. L. DuPont, M. Khodabandelou, and R. B. Hornick. 1973. "Long-Term Shigella-Carrier State." *The New England Journal of Medicine* 288 (22): 1169–71.
- Lorkowski, Martin, Alfonso Felipe-López, Claudia A. Danzer, Nicole Hansmeier, and Michael Hensel. 2014. "Salmonella Enterica Invasion of Polarized Epithelial Cells Is a Highly Cooperative Effort." *Infection and Immunity* 82 (6): 2657–67.
- Lu, Richard, Bobby Brooke Herrera, Heather D. Eshleman, Yang Fu, Alexander Bloom, Zhigang Li, David B. Sacks, and Marcia B. Goldberg. 2015. "Shigella Effector OspB Activates mTORC1 in a Manner That Depends on IQGAP1 and Promotes Cell Proliferation." *PLOS Pathogens*. <https://doi.org/10.1371/journal.ppat.1005200>.
- Mallo, Gustavo V., Marianela Espina, Adam C. Smith, Mauricio R. Terebiznik, Ainel Alemán, B. Brett Finlay, Lucia E. Rameh, Sergio Grinstein, and John H. Brumell. 2008. "SopB Promotes Phosphatidylinositol 3-Phosphate Formation on Salmonella Vacuoles by Recruiting Rab5 and Vps34." *The Journal of Cell Biology* 182 (4): 741–52.
- Mani, Sachin, Thomas Wierzbza, and Richard I. Walker. 2016. "Status of Vaccine Research and Development for Shigella." *Vaccine* 34 (26): 2887–94.
- Mathan, Minnie M., and V. I. Mathan. 1991. "Morphology of Rectal Mucosa of Patients with Shigellosis." *Clinical Infectious Diseases*. https://doi.org/10.1093/clinids/13.supplement_4.s314.
- Mattock, Emily, and Ariel J. Blocker. 2017. "How Do the Virulence Factors of Shigella Work Together to Cause Disease?" *Frontiers in Cellular and Infection Microbiology*.

- <https://doi.org/10.3389/fcimb.2017.00064>.
- Maurelli, A. T., B. Blackmon, and R. Curtiss 3rd. 1984. "Temperature-Dependent Expression of Virulence Genes in *Shigella* Species." *Infection and Immunity* 43 (1): 195–201.
- Maurelli, A. T., and P. J. Sansonetti. 1988. "Identification of a Chromosomal Gene Controlling Temperature-Regulated Expression of *Shigella* Virulence." *Proceedings of the National Academy of Sciences*. <https://doi.org/10.1073/pnas.85.8.2820>.
- McGhie, Emma J., Richard D. Hayward, and Vassilis Koronakis. 2004. "Control of Actin Turnover by a *Salmonella* Invasion Protein." *Molecular Cell* 13 (4): 497–510.
- Mellouk, Nora, Allon Weiner, Nathalie Aulner, Christine Schmitt, Michael Elbaum, Spencer L. Shorte, Anne Danckaert, and Jost Enninga. 2014. "Shigella Subverts the Host Recycling Compartment to Rupture Its Vacuole." *Cell Host & Microbe* 16 (4): 517–30.
- Mengaud, J., H. Ohayon, P. Gounon, Mege R-M, and P. Cossart. 1996. "E-Cadherin Is the Receptor for Internalin, a Surface Protein Required for Entry of *L. Monocytogenes* into Epithelial Cells." *Cell* 84 (6): 923–32.
- Morita-Ishihara, Tomoko, Michinaga Ogawa, Hiroshi Sagara, Mitutaka Yoshida, Eisaku Katayama, and Chihiro Sasakawa. 2006. "Shigella Spa33 Is an Essential C-Ring Component of Type III Secretion Machinery." *The Journal of Biological Chemistry* 281 (1): 599–607.
- Mortezaei, Narges, Chelsea R. Epler, Paul P. Shao, Mariam Shirdel, Bhupender Singh, Annette McVeigh, Bernt Eric Uhlin, Stephen J. Savarino, Magnus Andersson, and Esther Bullitt. 2015. "Structure and Function of Enterotoxigenic *Escherichia Coli* Fimbriae from Differing Assembly Pathways." *Molecular Microbiology* 95 (1): 116–26.
- Moss, J. E., T. J. Cardozo, A. Zychlinsky, and E. A. Groisman. 1999. "The selC-Associated SHI-2 Pathogenicity Island of *Shigella Flexneri*." *Molecular Microbiology* 33 (1): 74–83.
- Mounier, Joëlle, Gaëlle Boncompain, Lidija Senerovic, Thibault Lagache, Fabrice Chrétien, Franck Perez, Michael Kolbe, Jean-Christophe Olivo-Marin, Philippe J. Sansonetti, and Nathalie Sauvonnet. 2012. "Shigella Effector IpaB-Induced Cholesterol Relocation Disrupts the Golgi Complex and Recycling Network to Inhibit Host Cell Secretion." *Cell Host & Microbe* 12 (3): 381–89.
- Mounier, Joëlle, Michel R. Popoff, Jost Enninga, Margaret C. Frame, Philippe J. Sansonetti, and Guy Tran Van Nhieu. 2009. "The IpaC Carboxyterminal Effector Domain Mediates Src-Dependent Actin Polymerization during *Shigella* Invasion of Epithelial Cells." *PLoS Pathogens* 5 (1): e1000271.
- Mowat, Allan M., and William W. Agace. 2014. "Regional Specialization within the Intestinal Immune System." *Nature Reviews. Immunology* 14 (10): 667–85.
- Mykuliak, Vasyl V., Alexander William M. Haining, Magdaléna von Essen, Armando Del Río Hernández, and Vesa P. Hytönen. 2018. "Mechanical Unfolding Reveals Stable 3-Helix Intermediates in Talin and α -Catenin." *PLoS Computational Biology* 14 (4): e1006126.
- Nakayama, S., and H. Watanabe. 1995. "Involvement of cpxA, a Sensor of a Two-Component Regulatory System, in the pH-Dependent Regulation of Expression of *Shigella Sonnei* virF Gene." *Journal of Bacteriology* 177 (17): 5062–69.
- Nassif, X., M. C. Mazert, J. Mounier, and P. J. Sansonetti. 1987. "Evaluation with an iuc::Tn10 Mutant of the Role of Aerobactin Production in the Virulence of *Shigella Flexneri*." *Infection and Immunity* 55 (9): 1963–69.
- Newton, Hayley J., Jaclyn S. Pearson, Luminita Badea, Michelle Kelly, Mark Lucas, Gavan Holloway, Kylie M. Wagstaff, et al. 2010. "The Type III Effectors NleE and NleB from Enteropathogenic *E. Coli* and OspZ from *Shigella* Block Nuclear Translocation of NF- κ B p65." *PLoS Pathogens*. <https://doi.org/10.1371/journal.ppat.1000898>.
- Niebuhr, Kirsten, Sylvie Giuriato, Thierry Pedron, Dana J. Philpott, Frédérique Gaits, Julia Sable, Michael P. Sheetz, Claude Parsot, Philippe J. Sansonetti, and Bernard Payrastre. 2002. "Conversion of PtdIns(4,5)P₂ into PtdIns(5)P by the *S. flexneri* Effector IpgD Reorganizes Host Cell Morphology." *The EMBO Journal*. <https://doi.org/10.1093/emboj/cdf522>.
- Oakes, Patrick W., Yvonne Beckham, Jonathan Stricker, and Margaret L. Gardel. 2012. "Tension Is Required but Not Sufficient for Focal Adhesion Maturation without a Stress

- Fiber Template.” *The Journal of Cell Biology*. <https://doi.org/10.1083/jcb.201107042>.
- Ochman, H., T. S. Whittam, D. A. Caugant, and R. K. Selander. 1983. “Enzyme Polymorphism and Genetic Population Structure in *Escherichia Coli* and *Shigella*.” *Journal of General Microbiology* 129 (9): 2715–26.
- Ogawa, Michinaga, Tamotsu Yoshimori, Toshihiko Suzuki, Hiroshi Sagara, Noboru Mizushima, and Chihiro Sasakawa. 2005. “Escape of Intracellular *Shigella* from Autophagy.” *Science* 307 (5710): 727–31.
- Ohno, Hiroshi. 2016. “Intestinal M Cells.” *Journal of Biochemistry* 159 (2): 151–60.
- Owen, R. L., A. J. Piazza, and T. H. Ermak. 1991. “Ultrastructural and Cytoarchitectural Features of Lymphoreticular Organs in the Colon and Rectum of Adult BALB/c Mice.” *The American Journal of Anatomy* 190 (1): 10–18.
- Pantaloni, D., and M. F. Carlier. 1993. “How Profilin Promotes Actin Filament Assembly in the Presence of Thymosin Beta 4.” *Cell* 75 (5): 1007–14.
- Park, Hajeung, Jun Hyuck Lee, Edith Gouin, Pascale Cossart, and Tina Izard. 2011. “The *Rickettsia* Surface Cell Antigen 4 Applies Mimicry to Bind to and Activate Vinculin.” *The Journal of Biological Chemistry* 286 (40): 35096–103.
- Park, Hajeung, Cesar Valencia-Gallardo, Andrew Sharff, Guy Tran Van Nhieu, and Tina Izard. 2011. “Novel Vinculin Binding Site of the IpaA Invasin of *Shigella*.” *The Journal of Biological Chemistry* 286 (26): 23214–21.
- Parsot, C. 2003. “The Various and Varying Roles of Specific Chaperones in Type III Secretion Systems.” *Current Opinion in Microbiology*. [https://doi.org/10.1016/s1369-5274\(02\)00002-4](https://doi.org/10.1016/s1369-5274(02)00002-4).
- Patel, Jayesh C., and Jorge E. Galán. 2006. “Differential Activation and Function of Rho GTPases during *Salmonella*-Host Cell Interactions.” *The Journal of Cell Biology* 175 (3): 453–63.
- Pendaries, Caroline, Hélène Tronchère, Laurence Arbibe, Joelle Mounier, Or Gozani, Lewis Cantley, Michael J. Fry, Frédérique Gaits-Iacovoni, Philippe J. Sansonetti, and Bernard Payrastre. 2006. “PtdIns5P Activates the Host Cell PI3-kinase/Akt Pathway during *Shigella Flexneri* Infection.” *The EMBO Journal* 25 (5): 1024–34.
- Peng, Xiao, Jessica L. Maiers, Dilshad Choudhury, Susan W. Craig, and Kris A. DeMali. 2012. “ α -Catenin Uses a Novel Mechanism to Activate Vinculin.” *The Journal of Biological Chemistry* 287 (10): 7728–37.
- Pentecost, Mickey, Jyothi Kumaran, Partho Ghosh, and Manuel R. Amieva. 2010. “*Listeria Monocytogenes* Internalin B Activates Junctional Endocytosis to Accelerate Intestinal Invasion.” *PLoS Pathogens* 6 (5): e1000900.
- Pilonieta, M. Carolina, and George P. Munson. 2008. “The Chaperone IpgC Copurifies with the Virulence Regulator MxiE.” *Journal of Bacteriology* 190 (6): 2249–51.
- Pollard, Thomas D. 2007. “Regulation of Actin Filament Assembly by Arp2/3 Complex and Formins.” *Annual Review of Biophysics and Biomolecular Structure* 36: 451–77.
- Porter, M. E., and C. J. Dorman. 1994. “A Role for H-NS in the Thermo-Osmotic Regulation of Virulence Gene Expression in *Shigella Flexneri*.” *Journal of Bacteriology* 176 (13): 4187–91.
- Pupo, G. M., R. Lan, and P. R. Reeves. 2000. “Multiple Independent Origins of *Shigella* Clones of *Escherichia Coli* and Convergent Evolution of Many of Their Characteristics.” *Proceedings of the National Academy of Sciences of the United States of America* 97 (19): 10567–72.
- Radoshevich, Lilliana, and Pascale Cossart. 2018. “*Listeria Monocytogenes*: Towards a Complete Picture of Its Physiology and Pathogenesis.” *Nature Reviews. Microbiology* 16 (1): 32–46.
- Rajakumar, K., C. Sasakawa, and B. Adler. 1997. “Use of a Novel Approach, Termed Island Probing, Identifies the *Shigella Flexneri* She Pathogenicity Island Which Encodes a Homolog of the Immunoglobulin A Protease-like Family of Proteins.” *Infection and Immunity* 65 (11): 4606–14.
- Rakshit, Sabyasachi, and Sanjeevi Sivasankar. 2014. “Biomechanics of Cell Adhesion: How Force Regulates the Lifetime of Adhesive Bonds at the Single Molecule Level.” *Physical*

- Chemistry Chemical Physics: PCCP* 16 (6): 2211–23.
- Rakshit, Sabyasachi, Yunxiang Zhang, Kristine Manibog, Omer Shafraz, and Sanjeevi Sivasankar. 2012. “Ideal, Catch, and Slip Bonds in Cadherin Adhesion.” *Proceedings of the National Academy of Sciences of the United States of America* 109 (46): 18815–20.
- Ramarao, Nalini, Christophe Le Clainche, Tina Izard, Raphaëlle Bourdet-Sicard, Elisabeth Ageron, Philippe J. Sansonetti, Marie-France Carlier, and Guy Tran Van Nhieu. 2007. “Capping of Actin Filaments by Vinculin Activated by the Shigella IpaA Carboxyl-Terminal Domain.” *FEBS Letters* 581 (5): 853–57.
- Reiterer, Veronika, Lars Grossniklaus, Therese Tschon, Christoph Alexander Kasper, Isabel Sorg, and Cécile Arrieumerlou. 2011. “Shigella Flexneri Type III Secreted Effector OspF Reveals New Crosstalks of Proinflammatory Signaling Pathways during Bacterial Infection.” *Cellular Signalling* 23 (7): 1188–96.
- Rio, Armando del, Raul Perez-Jimenez, Ruchuan Liu, Pere Roca-Cusachs, Julio M. Fernandez, and Michael P. Sheetz. 2009. “Stretching Single Talin Rod Molecules Activates Vinculin Binding.” *Science* 323 (5914): 638–41.
- Romero, Stéphane, Gianfranco Grompone, Nathalie Carayol, Joëlle Mounier, Stéphanie Guadagnini, Marie-Christine Prevost, Philippe J. Sansonetti, and Guy Tran Van Nhieu. 2011. “ATP-Mediated Erk1/2 Activation Stimulates Bacterial Capture by Filopodia, Which Precedes Shigella Invasion of Epithelial Cells.” *Cell Host & Microbe* 9 (6): 508–19.
- Romero, Stéphane, Christophe Le Clainche, Dominique Didry, Coumaran Egile, Dominique Pantaloni, and Marie-France Carlier. 2004. “Formin Is a Processive Motor That Requires Profilin to Accelerate Actin Assembly and Associated ATP Hydrolysis.” *Cell* 119 (3): 419–29.
- Romero, Stephane, Alessia Quatela, Thomas Bornschlöggl, Stéphanie Guadagnini, Patricia Bassereau, and Guy Tran Van Nhieu. 2012. “Filopodium Retraction Is Controlled by Adhesion to Its Tip.” *Journal of Cell Science*. <https://doi.org/10.1242/jcs.126540>.
- Sahl, Jason W., Carolyn R. Morris, Jennifer Emberger, Claire M. Fraser, John Benjamin Ochieng, Jane Juma, Barry Fields, et al. 2015. “Defining the Phylogenomics of Shigella Species: A Pathway to Diagnostics.” *Journal of Clinical Microbiology* 53 (3): 951–60.
- Sanada, Takahito, Minsoo Kim, Hitomi Mimuro, Masato Suzuki, Michinaga Ogawa, Akiho Oyama, Hiroshi Ashida, et al. 2012. “The Shigella Flexneri Effector OspI Deamidates UBC13 to Dampen the Inflammatory Response.” *Nature* 483 (7391): 623–26.
- Sansonetti, P. J., J. Arondel, J. R. Cantey, M. C. Prévost, and M. Huerre. 1996. “Infection of Rabbit Peyer’s Patches by Shigella Flexneri: Effect of Adhesive or Invasive Bacterial Phenotypes on Follicle-Associated Epithelium.” *Infection and Immunity* 64 (7): 2752–64.
- Sansonetti, P. J., T. L. Hale, G. J. Dammin, C. Kapfer, H. H. Collins Jr, and S. B. Formal. 1983. “Alterations in the Pathogenicity of Escherichia Coli K-12 after Transfer of Plasmid and Chromosomal Genes from Shigella Flexneri.” *Infection and Immunity* 39 (3): 1392–1402.
- Sauer, Maximilian M., Roman P. Jakob, Jonathan Eras, Sefer Baday, Deniz Eriş, Giulio Navarra, Simon Bernèche, Beat Ernst, Timm Maier, and Rudi Glockshuber. 2016. “Catch-Bond Mechanism of the Bacterial Adhesin FimH.” *Nature Communications* 7 (March): 10738.
- Schroeder, G. N., and H. Hilbi. 2008. “Molecular Pathogenesis of Shigella Spp.: Controlling Host Cell Signaling, Invasion, and Death by Type III Secretion.” *Clinical Microbiology Reviews*. <https://doi.org/10.1128/cmr.00032-07>.
- Selyunin, Andrey S., Lovett Evan Reddick, Bethany A. Weigele, and Neal M. Alto. 2014. “Selective Protection of an ARF1-GTP Signaling Axis by a Bacterial Scaffold Induces Bidirectional Trafficking Arrest.” *Cell Reports* 6 (5): 878–91.
- Shah, Nipam, David J. Ramsey, and Herbert L. DuPont. 2009. “Global Etiology of Travelers’ Diarrhea: Systematic Review from 1973 to the Present.” *The American Journal of Tropical Medicine and Hygiene*. <https://doi.org/10.4269/ajtmh.2009.80.609>.
- Shashikanth, Nitesh, Yuliya I. Petrova, Seongjin Park, Jillian Chekan, Stephanie Maiden, Martha Spano, Taekjip Ha, Barry M. Gumbiner, and Deborah E. Leckband. 2015.

- “Allosteric Regulation of E-Cadherin Adhesion.” *The Journal of Biological Chemistry* 290 (35): 21749–61.
- Shiga, K. 1901. “Studien über Die Epidemische Dysenterie in Japan, Unter Besonderer Berücksichtigung Des Bacillus Dysenteriae.” *DMW - Deutsche Medizinische Wochenschrift*. <https://doi.org/10.1055/s-0029-1187128>.
- Shim, Doo-Hee, Toshihiko Suzuki, Sun-Young Chang, Sung-Moo Park, Philippe J. Sansonetti, Chihiro Sasakawa, and Mi-Na Kweon. 2007. “New Animal Model of Shigellosis in the Guinea Pig: Its Usefulness for Protective Efficacy Studies.” *Journal of Immunology* 178 (4): 2476–82.
- Simmons, D. A. R., and E. Romanowska. 1987. “Structure and Biology of Shigella Flexneri O Antigens.” *Journal of Medical Microbiology*. <https://doi.org/10.1099/00222615-23-4-289>.
- Sjöblom, B., A. Salmazo, and K. Djinić-Carugo. 2008. “ α -Actinin Structure and Regulation.” *Cellular and Molecular Life Sciences*. <https://doi.org/10.1007/s00018-008-8080-8>.
- Skoudy, A., J. Mounier, A. Aruffo, H. Ohayon, P. Gounon, P. Sansonetti, and G. Tran Van Nhieu. 2000. “CD44 Binds to the Shigella IpaB Protein and Participates in Bacterial Invasion of Epithelial Cells.” *Cellular Microbiology* 2 (1): 19–33.
- Solanki, Vandana, Monalisa Tiwari, and Vishvanath Tiwari. 2018. “Host-Bacteria Interaction and Adhesin Study for Development of Therapeutics.” *International Journal of Biological Macromolecules* 112 (June): 54–64.
- Sousa, Sandra, Didier Cabanes, Laurence Bougnères, Marc Lecuit, Philippe Sansonetti, Guy Tran-Van-Nhieu, and Pascale Cossart. 2007. “Src, Cortactin and Arp2/3 Complex Are Required for E-Cadherin-Mediated Internalization of Listeria into Cells.” *Cellular Microbiology*. <https://doi.org/10.1111/j.1462-5822.2007.00984.x>.
- Sousa, Sandra, Didier Cabanes, Aziz El-Amraoui, Christine Petit, Marc Lecuit, and Pascale Cossart. 2004. “Unconventional Myosin VIIa and Vezatin, Two Proteins Crucial for Listeria Entry into Epithelial Cells.” *Journal of Cell Science* 117 (Pt 10): 2121–30.
- Stender, S., A. Friebel, S. Linder, M. Rohde, S. Mirolid, and W. D. Hardt. 2000. “Identification of SopE2 from Salmonella Typhimurium, a Conserved Guanine Nucleotide Exchange Factor for Cdc42 of the Host Cell.” *Molecular Microbiology* 36 (6): 1206–21.
- Stoebel, Daniel M., Andrew Free, and Charles J. Dorman. 2008. “Anti-Silencing: Overcoming H-NS-Mediated Repression of Transcription in Gram-Negative Enteric Bacteria.” *Microbiology* 154 (Pt 9): 2533–45.
- Strockbine, Nancy A., and Anthony T. Maurelli. 2015. “Shigella.” *Bergey’s Manual of Systematics of Archaea and Bacteria*. <https://doi.org/10.1002/9781118960608.gbm01168>.
- Sun, Chun Hui, Benjamin Wacquier, Daniel I. Aguilar, Nathalie Carayol, Kevin Denis, Sylviane Boucherie, Cesar Valencia-Gallardo, et al. 2017. “The Shigella Type III Effector IpgD Recodes Ca²⁺ Signals during Invasion of Epithelial Cells.” *The EMBO Journal*. <https://doi.org/10.15252/embj.201696272>.
- Suzuki, Takuya. 2013. “Regulation of Intestinal Epithelial Permeability by Tight Junctions.” *Cellular and Molecular Life Sciences*. <https://doi.org/10.1007/s00018-012-1070-x>.
- Suzuki, T., H. Mimuro, H. Miki, T. Takenawa, T. Sasaki, H. Nakanishi, Y. Takai, and C. Sasakawa. 2000. “Rho Family GTPase Cdc42 Is Essential for the Actin-Based Motility of Shigella in Mammalian Cells.” *The Journal of Experimental Medicine* 191 (11): 1905–20.
- Svitkina, Tatyana. 2018. “The Actin Cytoskeleton and Actin-Based Motility.” *Cold Spring Harbor Perspectives in Biology* 10 (1). <https://doi.org/10.1101/cshperspect.a018267>.
- Sweeney, H. Lee, and Erika L. F. Holzbaur. 2018. “Motor Proteins.” *Cold Spring Harbor Perspectives in Biology* 10 (5). <https://doi.org/10.1101/cshperspect.a021931>.
- Tamano, Koichi, Eisaku Katayama, Takahito Toyotome, and Chihiro Sasakawa. 2002. “Shigella Spa32 Is an Essential Secretory Protein for Functional Type III Secretion Machinery and Uniformity of Its Needle Length.” *Journal of Bacteriology* 184 (5): 1244–52.
- The, Hao Chung, Duy Pham Thanh, Kathryn E. Holt, Nicholas R. Thomson, and Stephen Baker. 2016. “The Genomic Signatures of Shigella Evolution, Adaptation and Geographical Spread.” *Nature Reviews. Microbiology* 14 (4): 235–50.

- Thomas, Wendy E., Elena Trintchina, Manu Forero, Viola Vogel, and Evgeni V. Sokurenko. 2002. "Bacterial Adhesion to Target Cells Enhanced by Shear Force." *Cell* 109 (7): 913–23.
- Thwaites, Tristan R., Antonio T. Pedrosa, Thomas P. Peacock, and Rey A. Carabeo. 2015. "Vinculin Interacts with the Chlamydia Effector TarP Via a Tripartite Vinculin Binding Domain to Mediate Actin Recruitment and Assembly at the Plasma Membrane." *Frontiers in Cellular and Infection Microbiology*. <https://doi.org/10.3389/fcimb.2015.00088>.
- Tran Van Nhieu, G., A. Ben-Ze'ev, and P. J. Sansonetti. 1997. "Modulation of Bacterial Entry into Epithelial Cells by Association between Vinculin and the Shigella IpaA Invasin." *The EMBO Journal* 16 (10): 2717–29.
- Tran Van Nhieu, G., E. Caron, A. Hall, and P. J. Sansonetti. 1999. "IpaC Induces Actin Polymerization and Filopodia Formation during Shigella Entry into Epithelial Cells." *The EMBO Journal* 18 (12): 3249–62.
- Valencia-Gallardo, Cesar, Charles Bou-Nader, Daniel-Isui Aguilar-Salvador, Nathalie Carayol, Nicole Quenech'Du, Ludovic Pecqueur, Hajeung Park, Marc Fontecave, Tina Izard, and Guy Tran Van Nhieu. 2019. "Shigella IpaA Binding to Talin Stimulates Filopodial Capture and Cell Adhesion." *Cell Reports* 26 (4): 921–32.e6.
- Valencia-Gallardo, Cesar M., Nathalie Carayol, and Guy Tran Van Nhieu. 2015. "Cytoskeletal Mechanics during Shigella Invasion and Dissemination in Epithelial Cells." *Cellular Microbiology*. <https://doi.org/10.1111/cmi.12400>.
- Van Nhieu, Guy Tran, and Tina Izard. 2007. "Vinculin Binding in Its Closed Conformation by a Helix Addition Mechanism." *The EMBO Journal* 26 (21): 4588–96.
- Veenendaal, Andreas K. J., Julie L. Hodgkinson, Lynn Schwarzer, David Stabat, Sebastian F. Zenk, and Ariel J. Blocker. 2007. "The Type III Secretion System Needle Tip Complex Mediates Host Cell Sensing and Translocon Insertion." *Molecular Microbiology* 63 (6): 1719–30.
- Venkatesan, M. M., and J. M. Buysse. 1990. "Nucleotide Sequence of Invasion Plasmid Antigen Gene ipaA from Shigella Flexneri 5." *Nucleic Acids Research* 18 (6): 1648.
- Venkatesan, M. M., M. B. Goldberg, D. J. Rose, E. J. Grotbeck, V. Burland, and F. R. Blattner. 2001. "Complete DNA Sequence and Analysis of the Large Virulence Plasmid of Shigella Flexneri." *Infection and Immunity* 69 (5): 3271–85.
- Vokes, S. A., S. A. Reeves, A. G. Torres, and S. M. Payne. 1999. "The Aerobactin Iron Transport System Genes in Shigella Flexneri Are Present within a Pathogenicity Island." *Molecular Microbiology* 33 (1): 63–73.
- Wang, Fang, Zheng Jiang, Yan Li, Xiang He, Jiangli Zhao, Xinlong Yang, Li Zhu, et al. 2013. "Shigella Flexneri T3SS Effector IpaH4.5 Modulates the Host Inflammatory Response via Interaction with NF- κ B p65 Protein." *Cellular Microbiology* 15 (3): 474–85.
- Wassef, J. S., D. F. Keren, and J. L. Mailloux. 1989. "Role of M Cells in Initial Antigen Uptake and in Ulcer Formation in the Rabbit Intestinal Loop Model of Shigellosis." *Infection and Immunity* 57 (3): 858–63.
- Weiner, Allon, Nora Mellouk, Noelia Lopez-Montero, Yuen-Yan Chang, Célia Souque, Christine Schmitt, and Jost Enninga. 2016. "Macropinosomes Are Key Players in Early Shigella Invasion and Vacuolar Escape in Epithelial Cells." *PLoS Pathogens* 12 (5): e1005602.
- "WHO | Dysentery." 2010, December. <https://www.who.int/topics/dysentery/en/>.
- Wollert, T., D. W. Heinz, and W. -D. Schubert. 2007. "Thermodynamically Reengineering the Listerial Invasion Complex InlA/E-Cadherin." *Proceedings of the National Academy of Sciences*. <https://doi.org/10.1073/pnas.0702199104>.
- Wong, Stephanie, Wei-Hui Guo, and Yu-Li Wang. 2014. "Fibroblasts Probe Substrate Rigidity with Filopodia Extensions before Occupying an Area." *Proceedings of the National Academy of Sciences*. <https://doi.org/10.1073/pnas.1412285111>.
- Wu, Congying, Sreeja B. Asokan, Matthew E. Berginski, Elizabeth M. Haynes, Norman E. Sharpless, Jack D. Griffith, Shawn M. Gomez, and James E. Bear. 2012. "Arp2/3 Is Critical for Lamellipodia and Response to Extracellular Matrix Cues but Is Dispensable

- for Chemotaxis." *Cell* 148 (5): 973–87.
- Xu, Dan, Chongbing Liao, Bing Zhang, W. David Tolbert, Wangxiao He, Zhijun Dai, Wei Zhang, et al. 2018. "Human Enteric α -Defensin 5 Promotes Shigella Infection by Enhancing Bacterial Adhesion and Invasion." *Immunity* 48 (6): 1233–44.e6.
- Xue, Bo, Cedric Leyrat, Jonathan M. Grimes, and Robert C. Robinson. 2014. "Structural Basis of Thymosin- β 4/profilin Exchange Leading to Actin Filament Polymerization." *Proceedings of the National Academy of Sciences of the United States of America* 111 (43): E4596–4605.
- Xu, J., J. F. Casella, and T. D. Pollard. 1999. "Effect of Capping Protein, CapZ, on the Length of Actin Filaments and Mechanical Properties of Actin Filament Networks." *Cell Motility and the Cytoskeleton* 42 (1): 73–81.
- Yao, Mingxi, Benjamin T. Gault, Hu Chen, Peiwen Cong, Michael P. Sheetz, and Jie Yan. 2015. "Mechanical Activation of Vinculin Binding to Talin Locks Talin in an Unfolded Conformation." *Scientific Reports*. <https://doi.org/10.1038/srep04610>.
- Yao, Mingxi, Benjamin T. Gault, Benjamin Klapholz, Xian Hu, Christopher P. Toseland, Yingjian Guo, Peiwen Cong, Michael P. Sheetz, and Jie Yan. 2016. "The Mechanical Response of Talin." *Nature Communications* 7 (July): 11966.
- Yi, Chae-Ryun, John E. Allen, Brian Russo, Soo Young Lee, Jason E. Heindl, Leigh A. Baxt, Bobby Brooke Herrera, Emily Kahoud, Gavin MacBeath, and Marcia B. Goldberg. 2014. "Systematic Analysis of Bacterial Effector-Postsynaptic Density 95/disc Large/zonula Occludens-1 (PDZ) Domain Interactions Demonstrates Shigella OspE Protein Promotes Protein Kinase C Activation via PDLIM Proteins." *The Journal of Biological Chemistry* 289 (43): 30101–13.
- Zheng, Zirui, Congwen Wei, Kai Guan, Yuan Yuan, Yanhong Zhang, Shengli Ma, Ye Cao, Fang Wang, Hui Zhong, and Xiang He. 2016. "Bacterial E3 Ubiquitin Ligase IpaH4.5 of Shigella Flexneri Targets TBK1 To Dampen the Host Antibacterial Response." *Journal of Immunology* 196 (3): 1199–1208.
- Zhou, D., L. M. Chen, L. Hernandez, S. B. Shears, and J. E. Galán. 2001. "A Salmonella Inositol Polyphosphatase Acts in Conjunction with Other Bacterial Effectors to Promote Host Cell Actin Cytoskeleton Rearrangements and Bacterial Internalization." *Molecular Microbiology* 39 (2): 248–59.
- Zimmerman, Baruch, Tova Volberg, and Benjamin Geiger. 2004. "Early Molecular Events in the Assembly of the Focal Adhesion-Stress Fiber Complex during Fibroblast Spreading." *Cell Motility and the Cytoskeleton* 58 (3): 143–59.